Institute of Automatic Control
Faculty of Automatic Control, Electronics and Computer Science
Silesian University of Technology

Control of Semiactive Vehicle Suspension System Using Magnetorheological Dampers

Doctoral Thesis

by

Piotr Krauze

Supervisor
dr hab. inż. Jerzy Kasprzyk, prof. nzw. w Pol. Śl.

September 2015
Gliwice, POLAND

To my parents Dorota and Jerzy,

and my wife Oliwia

Abstract

Control of Semiactive Vehicle Suspension System Using Magnetorheological Dampers

by Piotr Krauze

Vibrations have critical influence on objects which are transported in road vehicles; among these, human bodies of the driver and passengers need to be especially concerned. A vehicle suspension system was introduced as a vibro-isolation which separates vehicle wheels from the vehicle body. Magnetorheological (MR) damper is an example of a semiactive device applied in the suspension system for which the ride comfort versus road holding and suspension deflection trade-offs can be solved at significantly low cost during vehicle ride. Presented dissertation is dedicated to still challenging control of ride comfort using automotive MR dampers. The dissertation presents simulation-based studies as well as experimental results obtained using an off-road vehicle in which original shock-absorbers were replaced with MR dampers.

Road-induced excitations were divided into two groups, i.e. continuous and single road bumps. Resonance frequencies of the vehicle and human body have dominant influence on response to the road irregularities. In the case of continuous excitation the analysis is commonly performed in frequency domain using transmissibility characteristics. It was shown that ride comfort is commonly related to vibration power estimated based on vertical acceleration within frequency band from 0 to 25 Hz while driving safety and condition of the vehicle suspension are assessed within frequency band from 0 to 30 Hz. A bump excitation was defined taking into account dimensions of the experimental vehicle and a road obstacle, and was commonly validated using standard deviation and maximum values of vehicle body acceleration.

MR dampers of type RD-8040-1 and RD-8041-1 manufactured by Lord Corporation are key elements of the presented experimental set-up. They were modelled performing identification experiments using MTS (Material Testing System) for different excitation frequencies, amplitudes and varying current values controlling MR dampers. A model of hysteretic behaviour in velocity-force characteristics was proposed based on a transfer function with the desired characteristics. Finally, different classes of MR damper models, like Bouc-Wen, Spencer-Dyke and tanh-based models were analysed and identified for a reference excitation frequency equal to 1.5 Hz. Advantages of Spencer-Dyke and tanh-based models were indicated and analysed in details.

Simulation-based studies were conducted using a model of vehicle vibrations which consists of a linear 4-DOF half-car and Spencer-Dyke models. Dynamics of the vehicle model with MR dampers was analysed for different classes of continuous sinusoidal excitation. Vehicle vibrations were analysed using quality indices which are based on an averaged vehicle body acceleration as well as on suspension and tyre deflections. MR damper dissipative domain significantly restricts possibility of semiactive vibration control.

Suspension control schemes can be organised in a hierarchical topology. In vibration control layer, LQ algorithm and the different types of Skyhook control were analysed. The force control layer was used for generation of an appropriate control current using the continuous or on/off control approach and the inverse Tanh model. LQ and Skyhook control schemes were optimized and compared with the passive suspension for both continuous sinusoidal and single-road-bump excitation. Furthermore, significant influence of excitation type on a vehicle response was indicated.

All road vehicles exhibit changes in parameters during their exploitation. Thus, it is recommended for a suspension control to include algorithms which are responsible for online observation of vehicle dynamics as well as for adaptive control. The research was carried out for the modified multichannel FxLMS algorithm including leakage mechanism, where nominal characteristics of the MR damper was applied. Simulation-based studies indicated that the proposed algorithm gives simultaneous improvement of ride comfort, road holding and suspension deflection for greater amplitudes of road excitation in comparison to classical non-adaptive control. Additionally, an online tuning of the inverse tanh-based model was proposed for improvement of vibration control. Such tuning algorithm requires no force sensors but it is based on kinematic quantities only, i.e. vehicle body velocities and accelerations, which significantly limits the number of required sensors.

Selected non-adaptive semiactive control schemes were implemented in the suspension controller installed in the experimental off-road vehicle. Experimental validation of the adaptive FxLMS based control was omitted since it requires a dedicated test route for generation of the continuous excitation which was not available. Several types of the Skyhook control were validated including separate control of each suspension quarter as well as control of vehicle body pitch vibrations. Furthermore, it was stated that the continuous approach appears to be more efficient in comparison to on/off approach. The vehicle was traversing a single road obstacle for each experiment. Improvement of vibration control was indicated for semiactive control in comparison to the suspension controlled only with a constant current. Finally, results presented in the dissertation were concluded and discussed as well as perspectives were drawn.

Acknowledgements

The author would like to thank Professor Jerzy Kasprzyk for his supervision, support, encouragement and invaluable assistance in research studies.

Major thanks are also directed to Professor Marek Pawełczyk for his valuable tips and advices, and to members of the Measurement and Control Systems Group for their useful comments on work and friendly atmosphere. The author would like to thank to Łukasz Maliński and Krzysztof Mazur for long and fruitful scientific discussions.

The financial support of this research by the National Science Centre, decision no. DEC-2011/01/B/ST7/06027 is gratefully acknowledged. Thanks are also addressed to all members participating in that grant, i.e. Jerzy Kasprzyk, Sebastian Budzan, Krzysztof Plaza, Janusz Wyrwał and Sebastian Kurczyk for their support and suggestions.

The author would also like to thank for the scholarship received under the project "DoktoRIS - Scholarship Program for Innovative Silesia" co-financed by the European Union under the European Social Fund.

Contributions

The author believes that main contributions of the dissertation are as follows:

- Developing the idea of vibration control using MR dampers in road vehicles.
- Application of the modified FxLMS algorithm in adaptive control of automotive MR damper model including utilization of road profile obtained in advance.
- Synthesis of the estimation procedures for online identification of the MR damper using only kinematic quantities.
- Synthesis, implementation and validation of the selected vibration control algorithms, including different types of the Skyhook algorithm, using the vehicle vibration model and the semiactive suspension system installed in the experimental off-road vehicle.
- Modelling the MR damper velocity-force hysteretic behaviour using the transfer function with desired phase characteristics.
- Analysis of the different approaches to modelling the MR damper behaviour.

Furthermore, the author believes that the main and innovative technical contribution of the dissertation was to develop the fully functional suspension control system for an experimental off-road vehicle with MR dampers. In order to create the experimental set-up the following tasks had to be succeeded:

- Model of the vehicle vibration was developed including the Spencer-Dyke MR damper model which was evaluated in identification experiments.
- Simulator of the vehicle dynamics was implemented.
- Selected non-adaptive and adaptive vibration control algorithms were synthesized, implemented, optimized and validated in the simulation environment.
- Non-adaptive vibration control algorithms were implemented in the suspension controller and validated experimentally using the off-road vehicle with MR dampers while the results demonstrated improvement of ride comfort in comparison to the passive suspension.

Thesis outline

The dissertation is divided into eight chapters. Introduction to the control of the vehicle suspension system with MR dampers related to ride comfort and driving safety issues is presented in Chapter 1. The most important features of MR dampers and their applications in both scientific and commercial vehicles were shown. The introduction is summarized by main thesis and particular goals of the dissertation.

In Chapter 2 different types of road-induced excitation are referred. Herein, continuous stochastic and deterministic excitation can be distinguished while, finally, single-road-bump excitation is defined. Quality indices related to ride comfort and driving safety including those defined in time and frequency domain are shown in the second part of Chapter 2.

Chapter 3 presents a procedure of MR damper model identification. Series of identification experiments were performed where both frequency and amplitude of the sinusoidal excitation were varying. Identified Spencer-Dyke model was used as a reference model while Tanh model was reformulated into an inverse model. Reference model was included in the 4-DOF half-car vehicle model presented in Chapter 4. Furthermore, a decoupled half-car model was derived. Finally, the simulation environment was validated and dynamics of the resultant vehicle model was tested for different road excitation and control currents.

Semiactive control is introduced in Chapter 5. Presented analysis is initiated by a description of MR damper dissipative domain. Next, synthesis and validation of feedback control, strictly LQ and Skyhook algorithms for different types of road excitation is described. Analysis of semiactive control schemes is extended to adaptive control in Chapter 6. Direct and indirect adaptive approaches are presented including application of modified FxLMS and online identification of MR damper model, respectively. Results for both inadaptive and adaptive control algorithms are analysed with respect to ride comfort and driving safety in time and frequency domains.

Chapter 7 reports results obtained for an experimental off-road vehicle traversing an obstacle. Description of a suspension control system installed in the vehicle is presented including elements of the measurement and control parts of the system. Road experiments were performed for passive suspension and classical semiactive control while results were compared using ride comfort related quality indices.

Conclusions of the dissertation and future perspectives are drawn in Chapter 8.

Contents

Abbreviations

ARE	**A**lgebraic **R**iccati **E**quation
BH	**B**ing**H**am MR damper model
BW	**B**ouc-**W**en MR damper model
COG	**C**entre **O**f **G**ravity
DOF	**D**egree **O**f **F**reedom
ER	**E**lectro**R**heological
FxLMS	**F**iltered reference **LMS** algorithm
HC	**H**alf-**C**ar vehicle model
IMU	**I**nertial **M**easurement **U**nit
ISO	**I**nternational **O**rganization for **S**tandardization
LMS	**L**east **M**ean **S**quares algorithm
LQ	**L**inear-**Q**uadratic control
MR	**M**agneto**R**heological
MS	**M**otion **S**ickness
MSE	**M**ean **S**quared **E**rror
MTS	**M**aterial **T**esting **S**ystem
PN	**P**oly**N**omial model
PSD	**P**ower **S**pectral **D**ensity
RC	**R**ide **C**omfort
RMS	**R**oot **M**ean **S**quare
RH	**R**oad **H**olding
SC	**S**pen**C**er-Dyke MR damper model
SD	**S**uspension **D**eflection
SH1	**S**kyhook control for quarter-car model
SH2	**S**kyhook control for half-car model

SMA	**S**mart **M**emory **A**lloy
SVD	**S**ervo-**V**alve **D**amper
TH	**H**yperbolic **T**angent MR damper model

Symbols

		Units
a	linear acceleration	ms^{-2}
$\boldsymbol{A_{hc}}$, $\boldsymbol{B_{hc}}$	matrices of state differential equations of the half-car model	
$\widehat{A}_{a_s}$	performance index based on maximum amplitude of vertical acceleration of the vehicle body in the centre of gravity a_s for the single-road-bump excitation $\widehat{z}_r$	m
$\boldsymbol{B_{hc,F}}$, $\boldsymbol{B_{hc,r}}$	matrices of state differential equations of the half-car model related to forces desired by the control algorithm F and the road-induced excitation z_r	
$\boldsymbol{C}$	matrix of viscous damping parameters	Nsm^{-1}
c_{avg}	the MR damper nominal damping	Nsm^{-1}
$\boldsymbol{C_{hc}}$, $\boldsymbol{D_{hc}}$	matrices of output equations of the half-car model	
c_{sf}, c_{sr}	viscous damping parameters of the front and the rear suspension	Nsm^{-1}
c_{uf}, c_{ur}	viscous damping parameters of the front and the rear wheel tyre	Nsm^{-1}
$\boldsymbol{D_{hc,F}}$, $\boldsymbol{D_{hc,r}}$	matrices of output equations of the half-car model related to forces desired by the control algorithm F and the road-induced excitation z_r	
f	temporal frequency	Hz
f_n	damped natural frequency	Hz
$\boldsymbol{F_{hc}}$	vector of generalized forces for the half-car model	
F_{alg}	force that should be generated by the MR damper according to the control algorithm	N

F_{avg}	force generated according to the nominal damping c_{avg} of the MR damper	N
F_{mr}	force generated by the MR damper	N
F^*_{mr}	F_{mr} modified by the transfer function of the output signal path $H_{F_{mr}}$ related to the MR damper	N
$F_{mr,bw}$	F_{mr} for the Bouc-Wen model	N
$F_{mr,sc}$	F_{mr} for the Spencer-Dyke model	N
$F_{mr,th}$	F_{mr} for the Hyperbolic Tangent model	N
$\boldsymbol{G_{LQ}}$	matrix of gains in the LQ control	
$\boldsymbol{g_{SH1}}$	vector of gains in the Skyhook control for the quarter-car model	
$\boldsymbol{G_{SH2}}$	matrix of gains in the Skyhook control for the half-car model	
$g_{v_s,f}$, $g_{v_s,r}$	gains in the Skyhook control for the half-car model related to the vertical velocity of the vehicle body in the centre of gravity v_s for the front and the rear suspension	
$g_{v_{sf},f}$, $g_{v_{sr},r}$	gains in the Skyhook control for the quarter-car model related to vertical velocities v_{sf} and v_{sr} of the front and the rear part of the vehicle body	
$g_{\omega_{sp},f}$, $g_{\omega_{sp},r}$	gains in the Skyhook control for the half-car model related to the pitch velocity of the vehicle body ω_{sp} for the front and the rear suspension	
$H_{F_{mr}}$	the transfer function of the output signal path related to F_{mr}	
$\boldsymbol{h_f}$, $\boldsymbol{h_r}$	vectors of parameters of H_f and H_r	
H_f, H_r	adaptive filters for the front and the rear vehicle part in the FxLMS algorithm	
H_i	the transfer function of the input signal path related to i_{mr}	
H_v	the transfer function of the input signal path related to v_{mr}	
i_{mr}	the MR damper control current	A

I_{sL}	pitch moment of inertia of the vehicle body for the half-car model	kg m^2
$I_{y_{hc}}$	absolute root mean square performance index evaluated for an output variable of the half-car model y_{hc}	m
$\widetilde{J}_{RC}$	ride comfort performance criterion for the sinusoidal road-induced excitation $\widetilde{z}_{r,f}$	
$\widetilde{J}_{RH}$	road holding performance criterion for the sinusoidal road-induced excitation $\widetilde{z}_{r,f}$	
$\widetilde{J}_{SD}$	suspension deflection performance criterion for the sinusoidal road-induced excitation $\widetilde{z}_{r,f}$	
$\boldsymbol{K}$	matrix of stiffness parameters	Nm^{-1}
k_{sf}, k_{sr}	stiffness parameters of the front and the rear suspension	Nm^{-1}
k_{uf}, k_{ur}	stiffness parameters of the front and the rear wheel tyre	Nm^{-1}
l	spatial domain	m
L_f, L_r	distances between the centre of gravity of the vehicle body and its front or rear end for the half-car model	m
L	length of the vehicle body for the half-car model	m
$\boldsymbol{M}$	matrix including masses and the moment of inertia for the half-car model	kg, kg m^2
m^*_{COG}	coupling mass of the decoupled half-car model	kg
m_s	mass of the vehicle body for the half-car model	kg
m^*_{sf}, m^*_{sr}	front and rear masses of the decoupled half-car model	kg
m_{uf}, m_{ur}	masses of the front and the rear vehicle wheel for the half-car model	kg
n	discrete-time	
p	spatial frequency	cycle m^{-1}
NA_{a_s}	normalized maximum amplitude performance index $\widehat{A}_{a_s}$ for the single-road-bump excitation $\widehat{z}_r$	m
$NI_{y_{hc}}$	normalized absolute root mean square performance index $I_{y_{hc}}$ for the single-road-bump excitation $\widehat{z}_r$	m
NJ_{RC}	normalized ride comfort performance criterion $\widetilde{J}_{RC}$ for the sinusoidal road-induced excitation $\widetilde{z}_{r,f}$	

NJ_{RH}	normalized road holding performance criterion $\widetilde{J}_{RH}$ for the sinusoidal road-induced excitation $\widetilde{z}_{r,f}$	
NJ_{SD}	normalized suspension deflection performance criterion $\widetilde{J}_{SD}$ for the sinusoidal road-induced excitation $\widetilde{z}_{r,f}$	
$\boldsymbol{q_{hc}}$	vector of generalised coordinates for the half-car model	
$\boldsymbol{Q_F}$	weighting matrix for control forces in the LQ control	
$\boldsymbol{Q_x}$	weighting matrix for state variables in the LQ control	
$\boldsymbol{S_F}$	constraint matrix for control forces in the LQ control	
$\boldsymbol{s_{F_{mr}}}$	vector of diagonal elements of S_F for MR damper forces	
$\boldsymbol{S_x}$	constraint matrix for state variables in the LQ control	
s_{v_s}	diagonal element of $\boldsymbol{S_x}$ related to the vertical velocity of the vehicle body in the centre of gravity v_s	
$s_{\omega_{sp}}$	diagonal element of $\boldsymbol{S_x}$ related to the pitch velocity of the vehicle body ω_{sp}	
t	continuous-time	s
T_s	sampling period for the suspension controller	s
$T_{u,y}$	transmissibility estimated from an excitation u to a response y	
$\boldsymbol{u_{hc}}$	vector of general excitations of the half-car model	
v	linear velocity	ms^{-1}
v_p	progressive velocity of vehicle	ms^{-1}
x	an arbitrary measured or estimated signal	
$\boldsymbol{x_{hc}}$	vector of state variables of the half-car model	
$\boldsymbol{y_{hc}}$	vector of output variables of the half-car model	
z	linear displacement	m
z_{mr}	linear relative displacement of the MR damper piston	m
z_{pv}	preview displacement of z_r	m
z_r	general road-induced excitation	m
$\widehat{z}_r$	single-road-bump excitation	m
$\widetilde{z}_{r,f}$	sinusoidal road-induced excitation of frequency f	m
z_s	vertical motion of the vehicle body in the centre of gravity	m

z_{sf}, z_{sr}	vertical motion of the front and the rear part of the vehicle body	m
z_{uf}, z_{ur}	vertical motion of the front and the rear vehicle wheel	m
z^{-1}	delay operator	
$\alpha_{mr,f}$, $\alpha_{mr,r}$	inclination angles of the front and the rear MR damper in the half-car model	rad
α_{v_s}, $\alpha_{\omega_{sp}}$	weighting parameters related to the heave v_s and the pitch ω_{sp} velocities in the FxLMS algorithm	rad
γ	leakage parameter in the FxLMS algorithm	
ϵ	angular acceleration	rad s^{-2}
μ	adaptation step in the FxLMS algorithm	
ξ	damping ratio	
φ	angle	rad
φ_{sp}	pitch of the vehicle body	rad
$\Phi(n)$	spatial PSD with respect to n	m^3
$\Psi(f)$	temporal PSD with respect to f	m^2s
ω	angular velocity	rad s^{-1}

Chapter 1

Introduction

Mechanical vibrations are an inherent feature of a moving road vehicle. Mechanical vibrations are defined as a phenomenon in which continuous oscillations in mechanical system occur around its equilibrium point [7]. Vehicle vibrations are commonly induced by vertically oriented road unevenness. Vibrations have critical influence on objects which are transported in road vehicles; among these, human bodies of the driver and passengers need to be especially concerned [38]. The harmful influence of vibrations is especially indicated if they occur at frequencies related to resonances of road vehicle or human body [17].

A vehicle suspension system was introduced as a vibro-isolation which separates vehicle body parts and passengers from vehicle wheels [60]. Parameters of the suspension influence both the vehicle ride comfort criterion related to vehicle body [86] and driving safety criterion related to wheels [98]. Ride comfort and driving safety criteria are contradictory in road vehicles [126]. Thus, the comfort versus safety trade-off needs to be solved depending on a target vehicle application and its target road conditions.

Semi-active suspension system which includes varying parameter suspension elements was proposed to adaptively solve the ride comfort versus driving safety trade-off [40, 122, 126]. MR dampers [137], ER dampers [139], SVD [64, 126] or pneumatic suspension springs [116, 157] are examples of semi-active elements applied in road vehicles. The main advantage of semiactive devices is their low energy consumption. Herein, MR dampers are especially favoured for their short time response of about 20 ms [72].

Nowadays, comprehensive studies on semiactive suspension systems and vehicle vibration control are being carried out over the world by numerous research institutes. Moreover, most known commercial applications of MR dampers are being developed by BWI Group (previously Delphi company) and Lord Corporation company. Additionally, representatives of automotive industry such as Audi, BMW or Mercedes-Benz are developing and improving their own suspension control systems. However, due to the complex nonlinear behaviour of semiactive devices, especially MR dampers, control of vehicle vibrations using MR dampers is still challenging and requires further research.

1.1 Passengers and vehicles subjected to road unevenness

Vehicle vibrations, which are vertically induced by road unevenness, propagate into the vehicle parts and influence the vehicle passengers. Two types of road-induced excitation can be distinguished, i.e. single road bumps or continuous excitation as presented in Figure 1.1. Both types of excitation need to be applied for validation of control algorithms [48]. Single road bumps induce vibrations in a wide frequency band. They result in free vibrations of passengers and a vehicle at their resonance frequencies. For continuous excitation, vehicle response is described as forced vibrations of frequency band determined by a road profile.

Continuous road-induced excitation is divided in the literature into deterministic and stochastic road profiles. Multiple road bump excitation is an example of deterministic excitation which induces vehicle vibration at certain harmonic frequencies. Stochastic road excitation model is a more general case which is based on analysis of typical road profiles. Such analysis performed in frequency domain leads to a conclusion that the amplitude of a frequency component of the wideband continuous stochastic road excitation is recommended to be inversely proportional to its frequency [142]. Such observations were reported in ISO 8606:1995(E) standard [58] and different road profiles were classified within a range of road classes denoted from A to F.

Road-induced excitation can deteriorate both the vehicle ride comfort and driving safety. Vibrations of the vehicle are commonly related to resonance frequencies of the vehicle body and underbody parts (see Figure 1.2). Vehicle body vibrations modes, i.e. heave, pitch and roll are defined at frequencies typically around 1-2 Hz [53, 99]. Vertical

(a) (b)

Figure 1.1: Examples of road-induced excitation of vehicle vibrations: a) single-road-bump excitation; b) continuous excitation

vibration modes of vehicle wheels usually referred to as the "wheel-hop" mode exhibit resonance frequencies in the range from 8 Hz to 16 Hz [99]. Moreover, other components of the vehicle also exhibit resonance frequencies, e.g. engine suspension or passengers seats.

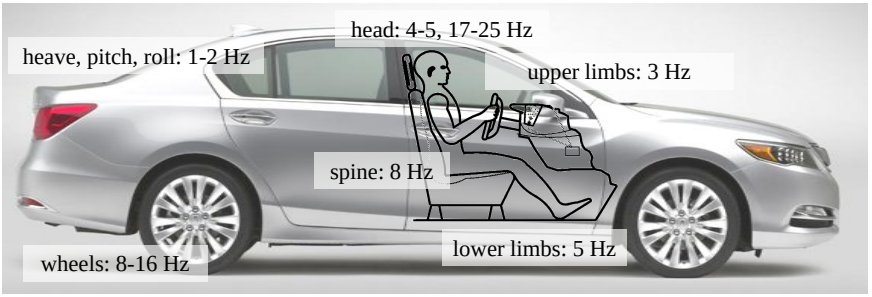

Figure 1.2: Dominant resonance frequencies of human body parts and a road vehicle

Road-induced excitation indirectly influences all objects transported by a vehicle, especially human bodies of passengers which significantly deteriorates ride comfort. Generally, in the case of objects which are strongly sensitive to vibrations, the control algorithms need to take into account additional frequency bands related to resonance frequencies of such objects. Analysis of passengers vibrations is particularly important. Low frequency vibrations, commonly of about 0.2 Hz, influence the human labyrinth and cause motion sickness [87, 95]. High frequency vibrations within the range from 1 Hz to 25 Hz cover resonance frequencies of human body parts. In extreme cases for high level vibrations the occurrence of resonance can cause organ damage [38]. Generally, standing human body exhibits resonance frequency of 4-6 Hz, selected human body parts exhibit resonance frequencies of e.g.: 3 Hz for upper limbs, 5 Hz for lower limbs, 4-5 Hz for head

or 8 Hz for spine. Extended list of resonance frequencies for human body and a general road vehicle is presented in Table 1.1.

Table 1.1: Selected resonance frequencies of human body [17] and vehicle parts [53, 99]

Road vehicle	
vehicle wheels	8 – 16 Hz
vehicle body heave, pitch and roll	1 – 2 Hz
Human body	
human standing	4 – 6 Hz
human sitting	5 – 12 Hz
head	4 – 5 Hz, 17 – 25 Hz
jaw	6 – 8 Hz
spine	8 Hz
liver	3 – 4 Hz
upper limbs	3 Hz
lower limbs	5 Hz

Driving safety can be deteriorated by multiple phenomena including vibrations of wheels covered by road holding performance index, range of suspension travel covered by suspension deflection performance index or pitching and rolling of the vehicle body which is covered by vehicle handling performance index. High amplitudes of wheels vertical vibrations mostly occur at resonance frequency and can cause temporary loss of traction. The suspension controller needs to minimize such wheels vibrations especially for heavy vehicles for which their heavy load is a significant source of vibrations [138]. Suspension system which is excessively extended or deflected can be worn out and damaged, which requires its continuous monitoring using suspension deflection performance indices. Pitching and rolling of the vehicle body can lead to the vehicle roll-over. Moreover, vehicle vibrations, which influence ride comfort, can cause driver fatigue and indirectly degrade the driving safety. Numerous automotive systems analyse condition of the driver and try to detect driver's fatigue [4, 131]. Additional higher-level algorithms included in the suspension control system can be dedicated to on-line identification of the psychological driver model and its sensitivity to traffic events related to the ride comfort and driving safety.

1.2 Ride comfort versus driving safety

Design of a vehicle suspension system is directly related to its application. Vibration mitigation can be focused on a whole vehicle or certain vehicle parts (see Figure 1.3). Generally, vehicle engine is suspended and isolated from other vehicle parts since it generates vibrations of high amplitude and deteriorates the quality of measurements taken in the vehicle. In order to focus on isolation of passengers and the driver only the seats may be suspended. Application of seat suspension is commonly used in the case of off-road vehicles and working machines [124]. However, the most convenient but complex design of vibro-isolation in vehicles is the full vehicle suspension which isolates the vehicle body part from vehicle wheels.

(a) (b)

Figure 1.3: Examples of suspension systems in vehicles: a) suspension of passenger seat [155], b) vehicle suspension system [156]

Parameters of the suspension system need to be defined during the design process and typically in the case of passive suspension it cannot be modified during further exploitation. The ride comfort versus driving safety trade-off can be shown in the form of diagram of a ride comfort and road holding where an example was estimated for a reference quarter-car model in [126] (see Figure 1.4). Results indicated that the higher damping is applied in vehicle suspension, the better road holding and the worse ride comfort. Generally, softer suspension makes the vehicle comfortable; unfortunately, at the same time its wheels tend to lose of traction. On the other hand, racing cars require the suspension to be hard in order to improve road holding. Similarly, ride comfort and suspension deflection performance criteria can be compared which also confirms the trade-off occurring between them, which is unavoidable in road vehicles.

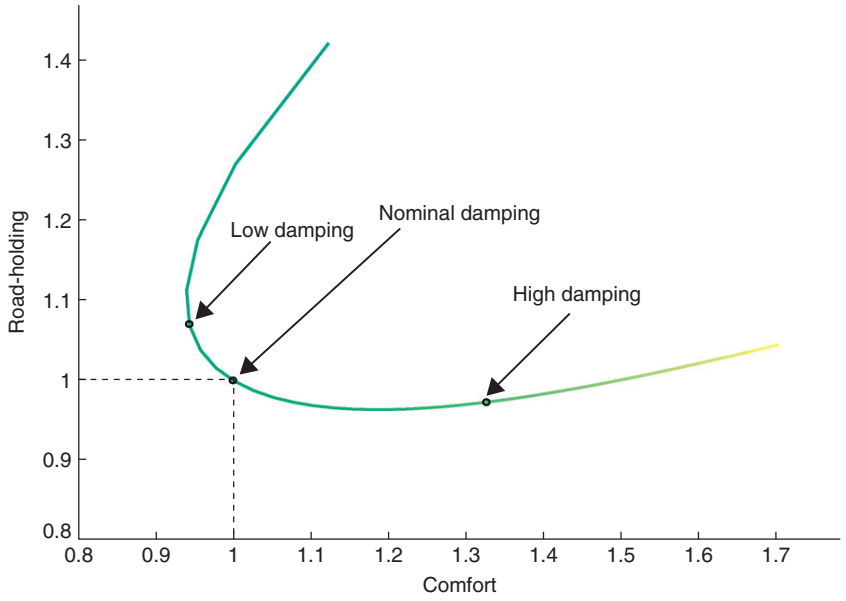

Figure 1.4: Trade-off between the normalized ride comfort and road holding performance criteria for a passive suspension system [126]

Response of a suspension system strictly depends on its damping ratio defined as the relation between its current damping and its critical damping. Critical damping indicates the borderline between non-oscillating and oscillating response of the system. Usually, suspension systems are designed to be described by 0.3 or 0.7 damping ratio values [56]. The former value corresponds to a configuration of a comfortable road vehicle, the latter is related to a racing car with improved road holding.

An alternative solution is offered in the market and can be found in literature. It is based on slow changes of suspension stiffness and viscous damping parameters. Load levelling elements change stiffness of the suspension within frequency bandwidth of 0.5 Hz [126]. Suspension damping can be modulated by specific adaptive devices within the bandwidth of a few Hz. Both configurations offer relatively long time response comparing to resonance frequencies of road vehicles and human body which are defined within the frequency band up to 25 Hz.

1.3 Semiactive vibration control systems in vehicles

Semiactive elements are being applied as a compromise between energy-consuming active elements and invariant passive elements. The low energy consumption feature is especially desired in vehicles in which available supplying energy is limited. Commonly,

dampers with variable parameters are utilized in vehicle suspensions due to their short time response [72]. For semiactive dampers, the rate of energy dissipation can be controlled which is an another advantage of semiactive dampers is their inherent stability, since no energy is added to the mechanical system.

1.3.1 Design of magnetorheological damper

Different types of semiactive dampers are available on the market, e.g. SVD, ER dampers, MR dampers. Initially, SVDs were used in vehicle suspension control due to their reliable design [64]. Later on, MR dampers became popular and favoured over ER, since the latter require high control voltage up to 5 kV. On the other hand, MR dampers require significantly lower control voltage up to 25 V and control current up to 2 A [14].

Cylindrical housing filled with MR fluid is the main part of the MR damper (see Figure 1.5). MR fluid is one of the intelligent materials which is a composition of magnetically polarizable particles suspended in non-magnetic carrier fluid, e.g. mineral oil, synthetic oil or glycol [124]. The suspended particles, a few micrometers in size, are made of ferromagnetic material with high saturation magnetization, commonly pure iron is used. Additionally, the polarizable particles are intentionally covered by polymers or silica in order to prevent coagulation occurring in the MR fluid. The fluid can be applied in different operational modes, e.g. flow mode, shear mode and squeeze mode [124], while flow mode is used for linear MR dampers.

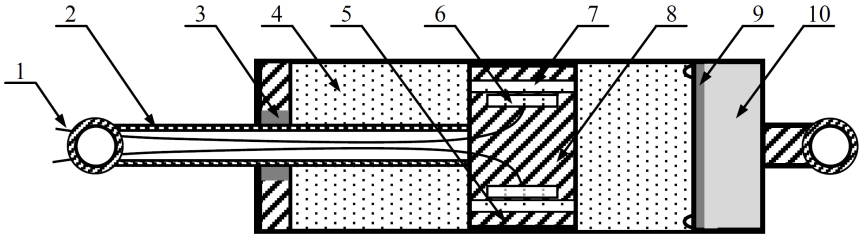

Figure 1.5: Construction of MR suspension damper presented in [81]: 1 - coil wires, 2 - piston rod, 3 - bearing and seal, 4 - MR fluid, 5 - ring, 6 - coil, 7 - orifice, 8 - piston, 9 - diaphragm, 10 - gas accumulator

MR fluid is flowing through gaps built in the MR damper piston while the piston is moving. In the vicinity of the gaps, coils are located and supplied with control current by wirings. When subjected to magnetic field induced by piston coils, particles of MR fluid are polarized and create chain-like structure along the magnetic field lines and

perpendicularly to the direction of fluid flow. Chains of polarizable particles suppress the flow of MR fluid through piston gaps. Consequently, changes of damping parameters of MR damper in the macroscopic scale are observed [137].

Measurement results performed for MR damper using MTS experiment set-up confirmed the expectations about MR damper response for different control currents (see Figure 1.6). It was shown that the greater control current, the greater the average damping of MR damper and consequently, the greater generated force. All plotted force-velocity characteristics cover only two quadrants of the coordinate system. Thus, measured force and relative damper velocity are always conforming, which confirms the dissipative nature of MR dampers.

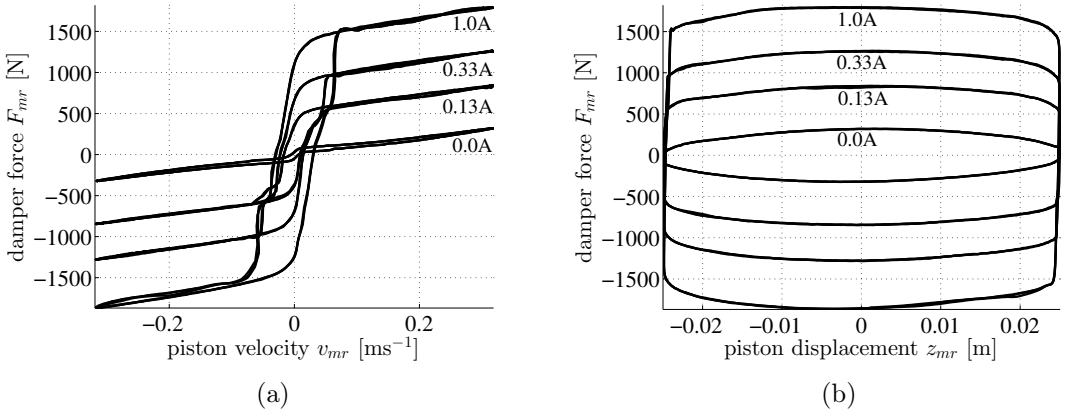

Figure 1.6: Characteristics obtained for MR damper (manufactured by Lord Corporation) controlled with different currents and subjected to sinusoidal kinematic excitation of frequency 2 Hz and amplitude 25 mm: a) force-velocity characteristics, b) force-displacement characteristics

1.3.2 Application of MR damper in vibration control

There is a wide range of applications of linear MR dampers in vibration control starting from large structures, e.g. cable-stayed bridges [21, 51] or seismic protection of buildings [139] and ending with smaller mechanical systems, e.g. typical vehicle suspension systems [29] or seat suspensions [124].

Semiactive dampers are commonly compared with passive and active systems using force range diagrams [126] (see Figure 1.7). Force range diagrams related to viscous dampers indicate possible force which can be generated by the device with respect to its

bound and rebound velocity. The available force generated by real passive, active and semiactive devices is limited due to their physical features.

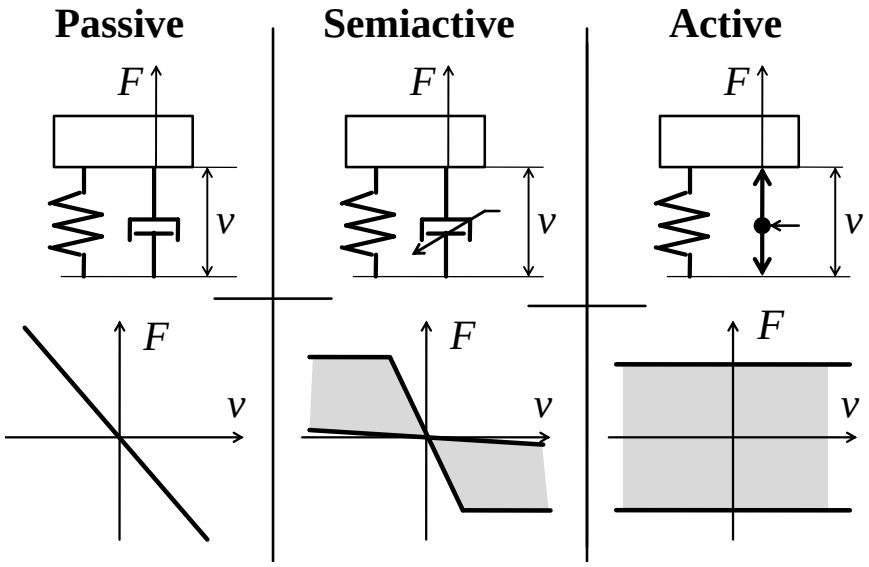

Figure 1.7: Comparison of passive, semiactive and active mechanical systems with respect to their force range characteristics

An active suspension can be assembled by building force generators into the typical suspension system. Force range diagram obtained for an active device, generally, shows independence from their relative velocity. Active devices allow to add extra energy to the mechanical system which significantly improves performance of vibration control. However, high energy-consumption and resultant complicated construction of the suspension system are the main disadvantages of the presented solution.

Invariant passive dampers exhibit only one force-velocity characteristics corresponding to their damping parameters. Semiactive MR damper can be treated as the improved passive damper which offer different shapes of force-velocity characteristics for different levels of the control current. Force range region covered by the family of characteristics is called the dissipative domain of the MR damper [126] (see Figure 1.6). It can be shown that the controllability of MR dampers is limited to cases when vibration energy is dissipated, which corresponds to only two quadrants of force range diagrams. Thus, typical control schemes cannot be used in MR damper-based systems.

MR dampers give a possibility of adaptive changes in the vehicle suspension damping. Hence, the suspension can be tuned and prepared for the instantaneous road conditions. In the case of a vehicle traversing a smooth road, the vehicle speed is increased and greater effort of the controller should be put on a driving safety. For rough road

both, the ride comfort and driving safety quality indices need to be taken into account. Both the research and commercial applications of the MR dampers in vehicle suspension were presented in the literature and are available on the market. The semiactive Skyhook algorithm, which was introduced in [64], is commonly used for vehicle vibration control.

Nowadays, one of the main commercial semiactive suspension system based on the MR dampers is being developed by BWI Company [149]. The system was introduced by Delphi Company [150] as MagneRide and applied in Cadillac Seville model. Later on, MagneRide was installed in e.g. Audi R8, Chevrolet Camaro ZL-1, Range Rover Evoque (see Figure 1.8). Lord Corporation company [154], which is a designer of devices based on intelligent materials, especially MR dampers and MR brakes, offers another suspension control system for seats and cabs.

Due to significantly nonlinear behaviour of the MR damper, research in the field of vehicle vibration control by means of MR dampers is still performed by numerous institutes over the world, e.g. Virginia Tech Institute [2, 135], State Key Laboratory of Mechanic Transmission [29], AGH University of Science and Technology [123], Silesian University of Technology [79].

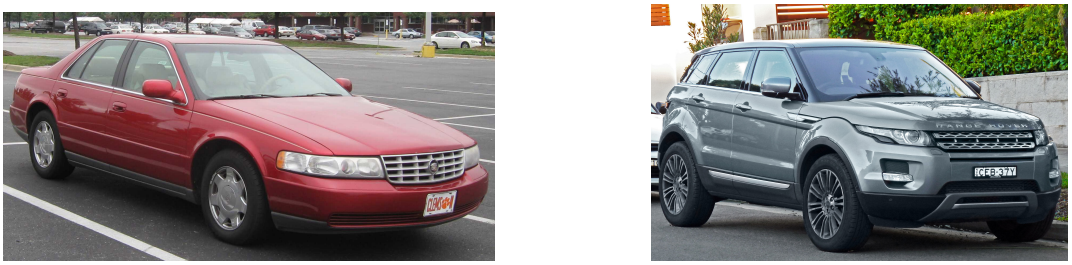

(a) (b)

Figure 1.8: Road vehicles equipped with commercial Magneride semiactive suspension: a) Cadillac Seville [152], b) Range Rover Evoque [153]

Research presented in the current dissertation is related to a semiactive vibration control system installed in an experimental off-road vehicle [79] (see Figure 1.9). Original shock absorbers of the vehicle were replaced by MR dampers of type RD-8040-1 and RD-8041-1 manufactured by Lord Corporation (see Appendix A). The vehicle is of real size and commercially available; it is 2 metres long, 1 metre wide and it weights 340 kilograms.

Measurement part of the system includes numerous sensors, e.g. accelerometers, gyroscopes and vehicle speed sensors located in the vehicle body as well as installed near vehicle wheels. The control part of the system includes peripheral units responsible

Figure 1.9: An off-road vehicle equipped with suspension MR dampers and semiactive suspension control system

for acquisition of measurements and generation of control signals which are transformed to values of current supplying MR dampers. Detailed description of the experimental vehicle is given in Appendix B.

1.4 Thesis of the dissertation

The objective of the dissertation is to develop semiactive vibration control system based on MR dampers installed in an experimental off-road vehicle. The task was assembling the system as well as development, implementation and validation of vibration control algorithms dedicated to MR dampers.

The main thesis of the dissertation is formulated as follows:

Selected algorithms used in control of a vehicle suspension with magnetorheological dampers and utilization of information related to the road profile allow for improvement of the ride comfort, road holding and mitigation of the averaged suspension deflection.

The following particular goals are formulated:

- Creating the MR damper model and its inverse equivalent as well as their application in both simulation and experimental research.
- Development, validation and selection of non-adaptive and adaptive algorithms for MR damper control including utilization of preview information about the road profile.

- Implementation and validation of selected vibration control algorithms based on the semiactive suspension control system installed in the experimental vehicle.

1.5 Summary

Semiactive vehicle suspension systems were developed over years by commercial and scientific institutes. Controllable suspension elements allow to adapt to the instantaneous road conditions and varying control goals. Herein, semiactive devices represented by MR dampers are favoured over active ones for their low energy-consumption and inherent stability. Behaviour of MR dampers is significantly nonlinear and their operation is limited to energy dissipation only. Thus, application of MR dampers is challenging and requires the resultant control algorithms to be complex. Well-known developments in the field of modelling and semiactive control were referred within the chapter and related to the literature. Combination of MR dampers application, analysis of vehicle vibrations in different road conditions and advanced control algorithms makes a lot of future developments possible in the field of semiactive vehicle vibration control.

Chapter 2

Vibrations in road vehicles

Construction of a road vehicle is adapted to its general application, which is mainly determined by road conditions and types of transported objects. Since every real road vehicle exhibits significant nonlinearities, vehicle response requires nonlinear analysis. Main nonlinear behaviour of semiactive suspension is introduced by MR dampers. Due to the complexity of semiactive suspension systems, different classes of road irregularities need to be modelled and applied separately in order to properly identify the model of vehicle vibrations, strictly - its certain parameters, and to validate vibration control algorithms for different road conditions.

Two main questions arise for moving road vehicles: if the destination will be reached and how this task will be accomplished. The former question is strictly related to the analysis of driving safety, the latter one is related to ride comfort which should be analysed both generally and with respect to passengers located in the vehicle. Hence, main goal of a vibration control algorithm is to improve ride comfort while not deteriorating driving safety significantly.

2.1 Road-induced excitation of vehicle vibrations

Generally, roads are classified with respect to their irregularities using IRI (International Roughness Index), which includes a measured road profile and response of the reference vehicle averaged over time [127]. Among all devices used for evaluation of road profiles, low-speed and high-speed road profiling systems can be distinguished. The

former ones are called profilographs [127], the latter ones are commonly equipped with inertial sensors and distance sensors such as ultrasonic sensors [16] or laser scanners [97, 158]. Nowadays, commercial profiling systems are widely developed and offered in the market, e.g. Dynatest [151].

Vehicle response to single-road-bump excitation and continuous road irregularities are commonly analysed when dealing with vehicle vibration control. Bump excitation induces vehicle vibrations in wide frequency band in the form of free vibrations. In the case of continuous excitation, the vehicle response is described as forced vibrations of frequency band determined by road profile. The latter type is further divided into a general case, i.e. wideband stochastic excitation and a special case, i.e. deterministic multiple-bump or sinusoidal road profiles [48]. Modelling of road profile is relevant when optimizing suspension control algorithm for certain road conditions. For continuous excitation, the characteristic features of the road-induced excitation can be identified during ride and such additional information about the road can be used for prediction in the adaptive control algorithm.

The current chapter introduces different types of continuous stochastic and deterministic excitation as well as it defines single-road-bump excitation. Since deterministic sinusoidal excitation allows for detailed analysis of vehicle vibrations performed in frequency domain, it is used in further chapters together with single-road-bump excitation for the purpose of validation of vibration control.

2.1.1 Stochastic wideband excitation

Since the first profilographs were introduced, measurements of vertical displacement were taken for different classes of roads. Road irregularities are treated in such case as continuous road-induced stochastic excitation. Measurement results were summarized and general classification of roads was reported in ISO 8608:1995(E) standard [58] in the form of displacement PSD characteristics defined with respect to spatial frequency p and further denoted as Φ_z. The examined roads were described within the range of classes from A to F ordered with descending road quality. Range of roughness degree, which is defined using limiting values of displacement PSD $\Phi_z(p_0)$ for a reference road spatial frequency denoted as $p_0 = 0.1$ [cycle m^{-1}], is a characteristic parameter of a certain road class. For the purpose of further studies, centres of roughness degree ranges for

classes A - F were used for evaluation of a corresponding road profile in spatial domain (see Figure 2.1). The characteristics indicate that amplitude of a component of road-induced excitation is inversely proportional to its spatial frequency, which is specific for continuous stochastic road profile. Spatial displacement PSD $\Phi_z(p)$ characteristics presented in [58] were transformed into temporal PSD characteristics denoted as $\Psi_z(f)$ and approximated by the following temporal PSD function:

$$\Psi_z(f) = \frac{4\gamma_r \sigma_r^2 \alpha_r v_p}{4\pi^2 f^2 + \gamma_r^2 \alpha_r^2 v_p^2}, \tag{2.1}$$

where f denotes temporal excitation frequency, which is related to spatial excitation frequency according to the following formula:

$$f = v_p p. \tag{2.2}$$

Symbol σ_r^2 denotes variance of road roughness, v_p denotes vehicle speed specified in metres per second, α_r depends on the type of road surface and γ_r was introduced in order to influence the cutoff frequency of the transfer function (2.1). Displacement PSD (2.1) is a modification of the relation presented in [47] and applied for validation of vehicle vibration control in [35, 48, 142]. The approximation (2.1) was validated by comparing it in both spatial and temporal domains with characteristics presented in ISO 8608 for different road classes (see Figure 2.1).

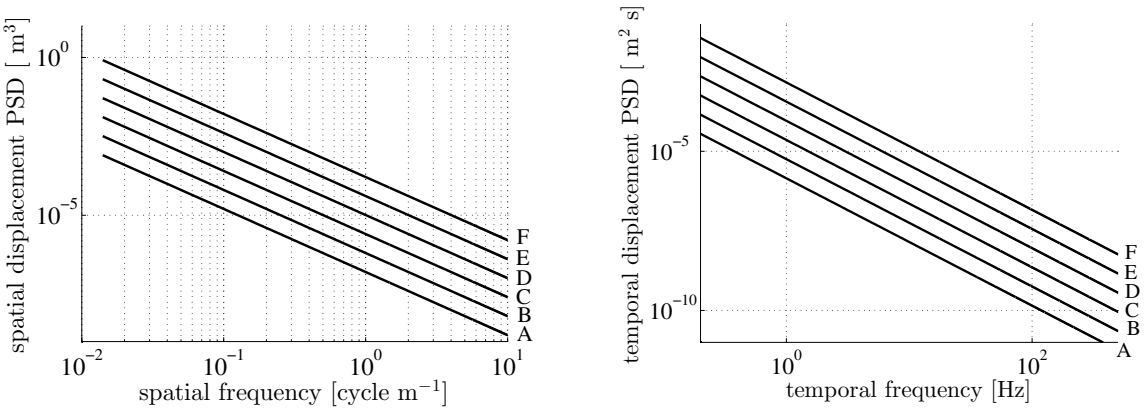

Figure 2.1: Power spectral densities of continuous stochastic road-induced excitation evaluated based on ISO 8608 for different road classes A-F: a) spatial domain, b) temporal domain for vehicle speed of 20 ms^{-1}

Different methods can be used for generation of road-induced excitation of certain

road class, e.g. inverse FFT can be applied [62] or a linear filter can be excited with white noise of certain variance [47].

2.1.2 Continuous sinusoidal excitation

Roads with repeatable structure, e.g. a road made of cobblestones represent a special deterministic case of narrowband excitation which can be modelled as multiple-road-bump or sinusoidal excitation. It is usually expressed in the form of displacement excitation denoted as $\widetilde{z}_{r,f}$. It can consist of a single component of one dominant frequency denoted as f or a group of N harmonic Fourier components with constant amplitudes $A_{f,j}$ and phase angles $\phi_{f,j}$ where j denotes a number of a consecutive component. Such excitation is simulated according to the following expression:

$$\widetilde{z}_{r,f}(t) = \sum_{j=0}^{N-1} A_{f,j} cos(2\pi j f t + \phi_{f,j}). \tag{2.3}$$

The presented deterministic excitation defined in the form of sinusoidal excitation using only parameter $A_{f,0}$ is mainly used in further simulation-based validation. It is mostly used for evaluation of transmissibility characteristics for proposed semiactive vibration control schemes. Aim of the author was to retain similar conditions of MR damper operation for all tested dominant frequencies f. It was reached by retaining the constant variance $\sigma_{\widetilde{v}_{r,f}}$ of road excitation velocity denoted as $\widetilde{v}_{r,f}$. Consequently, the variance of excitation displacement denoted as $\sigma_{\widetilde{z}_{r,f}}$ was obtained based on Ψ_z for a certain reference frequency f_{vs} and bandwidth B_{vs}. The $\sigma_{\widetilde{z}_{r,f}}$ is inversely proportional to the dominant frequency f:

$$\sigma_{\widetilde{z}_{r,f}} = \frac{f}{f_{vs}} \int_{f_{vs}-1/2 B_{vs}}^{f_{vs}+1/2 B_{vs}} \Psi_z(\nu) d\nu, \tag{2.4}$$

where Ψ_z depends on the corresponding road class and vehicle speed. In order to cover resonance frequencies of typical vehicle suspension systems (see e.g. Table 1.1), values of the reference parameters were assumed as follows: $f_{vs} = 1.5$ Hz and $B_{vs} = 1.5$ Hz. Simulations of applied sinusoidal road excitation are presented in Figure 2.2.

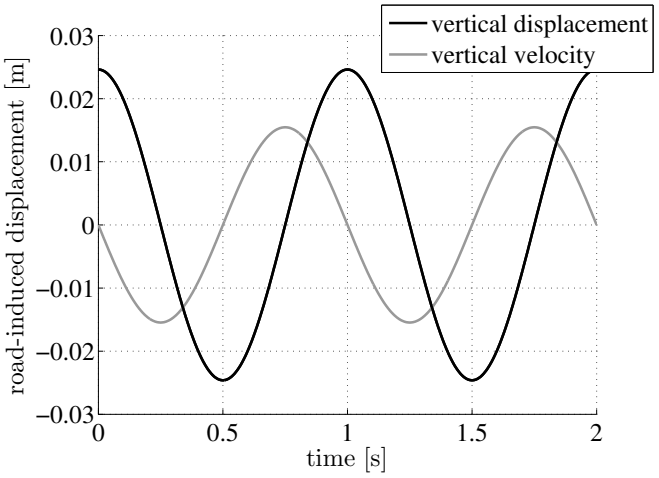

Figure 2.2: Example of continuous sinusoidal road-induced excitation simulated for frequency of 1 Hz, road class E and vehicle speed of 15 ms^{-1}.

2.1.3 Single-road-bump excitation

Single road bumps and holes are road irregularities which are mostly noticeable by the driver during real road experiments. Single road bumps cannot be predicted without additional road profile scanning aimed into the road in front of the vehicle. Thus, synthesis of efficient control algorithms which are dedicated to such excitation is challenging. For the purpose of further analysis, the single-road-bump excitation denoted as $\widehat{z}_r$ is defined assuming that both dimensions of the road obstacle and vehicle wheel are similar to those used in actual road experiments (see e.g. Chapter 7). The road obstacle is of square cross-section shape where its height is equal to $H_b = 0.085$ m, while diameter of the vehicle wheel is denoted as $D_t = 0.6$ m (the radius of vehicle wheel is denoted as R_t). The road-bump excitation is defined in the form of switching function dependent on a spatial variable l as follows:

$$\widehat{z}_r(l) = \begin{cases} \sqrt{R_t^2 - (l - L_b)^2} - R_t + H_b & \text{for} \quad 0 \leq l < L_b \\ H_b & \text{for} \quad L_b \leq l < L_b + H_b \\ \sqrt{R_t^2 - (l - L_b - H_b)^2} - R_t + H_b & \text{for} \quad L_b + H_b \leq l < 2L_b + H_b \\ 0 & \text{for} \quad 2L_b + H_b \leq l \end{cases}, \tag{2.5}$$

where

$$L_b = \sqrt{H_b^2 + D_t H_b}. \tag{2.6}$$

Symbol L_b denotes the distance between the vehicle wheel and the approaching obstacle. Simulation results of single-road-bump excitation for vehicle speed of 3 ms^{-1} performed

are presented in Figure 2.3. Road-induced displacement and velocity are assured to be constrained in order to reflect to the real road-induced excitation and keep numerical solvers of differential equations well conditioned for simulation-based research.

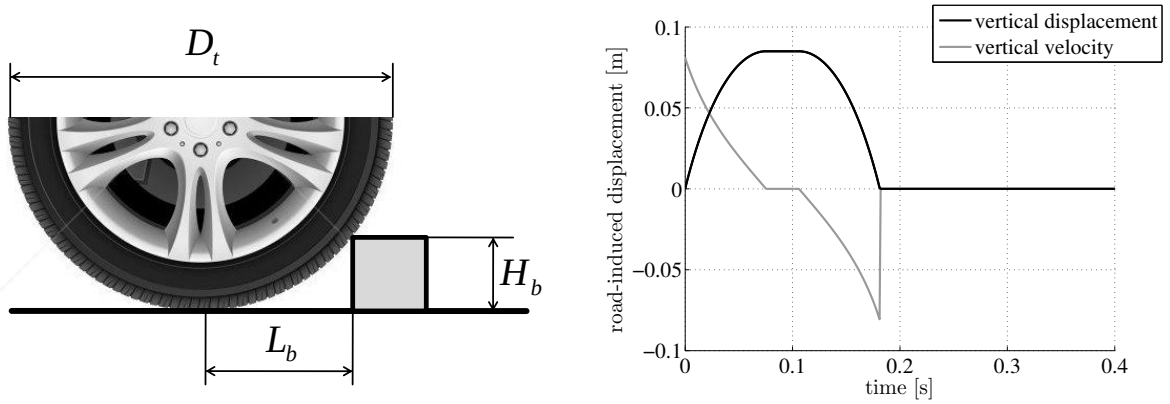

(a) (b)

Figure 2.3: Single-road-bump excitation: a) spatial model, b) simulation performed for vehicle speed of 3 ms^{-1}.

2.2 Analysis of human body and vehicle vibrations

Resonance frequencies of human body and road vehicles have dominant influence on their response to road irregularities. Analysis of vehicles and passengers vibrations needs to be started with their modal analysis (see e.g. Chapter 1). Further analysis of vehicle vibrations can be carried out with respect to both ride comfort and driving safety, where the former is generally related to vibrations of passengers and the latter describes vibrations of the vehicle.

Different goals of vehicle vibration control imply application of different quality indices. Vehicle vibrations can be analysed in all or a certain direction which commonly is the vertical one. Consecutive derivatives of kinematic quantities from displacement to acceleration and jerk, describing motion of passengers and certain elements of a vehicle, are analysed in the literature. Depending on classes of road-induced excitations, free or forced vibrations of the vehicle are induced, which requires application of different quality indices expressed in time and frequency domains. Goal of the vibration control system is inversely proportional to the defined performance indices since the latter are related to the level of vehicle vibrations which are to be mitigated.

2.2.1 Analysis of general vibrations in time and frequency domain

Vibrations of a vehicle are commonly measured in selected directions by inertial sensors, e.g. accelerometers or gyroscopes. Later on, sampled measurements are used for vibration control and assessment of its quality. The analysis of vehicle vibrations is focused on frequency band up to 30 Hz, since components of higher frequency are damped by the mechanical elements of the vehicle [126].

Generally, vibration level is examined regardless of features of objects transported in the moving vehicle. Different quality indices are applied in order to compare results obtained for continuous road unevenness or single road bumps. Absolute scalar quality indices, e.g. RMS value, are recommended for simplification. Level of vibrations of a vehicle can be initially analysed based on RMS value which is related to the power of vibrations signal [17]:

$$I_x = \sqrt{\frac{1}{N}\sum_{n=1}^{N}\{W(z^{-1})\cdot x(n)\}^2}, \tag{2.7}$$

where x denotes a certain measurement or estimated signal related to a selected part of a vehicle or passenger. Different physical quantities can be used, from displacement applied for analysis of suspension travel or tyre deflection to jerk, which well indicates influence and harmfulness of vibrations on human body [52]. An optional transfer function W corresponds to weights set on vibrations signal in frequency domain, which can be related to e.g. ride comfort or driving safety issues. Symbol N denotes number of analysed samples. For the sinusoidal excitation of dominant frequency f or single-road-bump excitation, the quality index is denoted as $\widetilde{I}_x(f)$ or $\widehat{I}_x$, respectively.

Analysis in frequency domain expressed by transmissibility is recommended when analysing the influence of control algorithm on all vibrations modes of a vehicle. Transmissibility is evaluated for a signal path from input to output, which are denoted as u and y, respectively. Different definitions of transmissibility are used depending on the type of applied road-induced excitation. Generally, the spectrums $Y(f)$ and $U(f)$ are computed for the corresponding input and output signals by means of discrete Fourier transform and included in the following definition:

$$T_{u,y}(f) = \frac{Y(f)}{U(f)}. \tag{2.8}$$

Presented form of transmissibility (2.8) requires wideband stochastic road-induced excitation for correct estimation within the desired frequency range, which is a significant limitation of such estimation method. Moreover, frequency analysis is performed for a controlled nonlinear suspension system, which requires atypical approach due to its multi-harmonic response. Thus, definition (2.8) is only used for final validation of vibration control. For research and initial validation, the following is used:

$$\widetilde{T}_{u,y}(f) = \frac{\widetilde{I}_y(f)}{\widetilde{I}_u(f)}, \tag{2.9}$$

where $\widetilde{I}_y$ and $\widetilde{I}_u$ denote values of quality indices estimated for input and output signals for a suspension system subjected to sinusoidal road-induced excitation. Both $\widetilde{I}_y$ and $\widetilde{I}_u$ are defined according to a special case of quality index I_x (2.7) which is dependent on dominant frequency of excitation. Amplitude of road-induced excitation $u(f)$ is dependent on its dominant frequency according to the temporal displacement PSD (2.1).

Single road bump $\widehat{z}_r$ represents another group of road-induced excitations of finite duration and wideband frequency profile. Response of the vehicle suspension to bump excitation denoted as $\widehat{y}$ consists of dominant vibrations modes. For analysis of the vehicle body vibrations, the heave, pitch and roll modes are dominant. Commonly, analysis of bump response is limited to estimation of features which are typical for analysis of general damped free vibrations. Mainly, the RMS value denoted as $\widehat{I}_y$ can be estimated according to Equation (2.7) based on response signal $\widehat{y}$ or the maximum amplitude of vibrations is analysed as follows [17]:

$$\widehat{A}_y = \max_n \{\widehat{y}(n)\}. \tag{2.10}$$

2.2.2 Comfort-related performance indices

Early studies related to ride comfort showed that vibrations in different frequency bands have different influence of human body organs [27]. As a result of further studies, acceleration was proposed for assessment of ride comfort [132]. Moreover, it was stated that jerk can be used as an additional measure of passenger discomfort [54]. List of human body resonance frequencies [17] shows that commonly the frequency band from 3 Hz to 25 Hz needs to be taken into account. Moreover, frequencies lower than 1 Hz induce motion sickness [95], [87]. Furthermore, comprehensive analysis of motion sickness was

performed with respect to pitch and roll oscillation [63]. Studies on influence of vibrations on human body were summarized and reported as the standard ISO 2631 [57]. Estimation of power absorbed by the human body in the form of vibrations based on acceleration weighted in frequency domain was proposed in [88]. Comprehensive review of available performance indices related to ride comfort felt by human body was also presented in [40]. However, analysis of vibrations can be also related to specialized vehicles, e.g. off-road or military vehicles [109].

In conclusion, proposed ride comfort and motion sickness quality indices are commonly related to the analysis of vibrations power estimated based on vertical acceleration measurements, which was recently confirmed in [73, 126]. Additionally, weighting function defined in frequency domain W can be applied as proposed in Equation (2.7). It can be related to human body only [104] or it can be extended to more general case of objects which exhibit certain resonance frequencies. Generally, analysis of ride comfort is performed within the frequency range 0 - 25 Hz.

Several types of ride comfort criteria related to the type of road-induced excitation are presented based on definitions introduced in [126]. All such quality indices are evaluated in the form of integral estimated within the selected frequency range based on transmissibility spectrums defined by Equations (2.8, 2.9). Generalized ride comfort criterion is defined assuming the vehicle suspension is subjected to the continuous sinusoidal road-induced excitation $\widetilde{z}_{r,f}$:

$$\widetilde{J}_{RC} = \sqrt{\int_{0Hz}^{25Hz} [\widetilde{T}_{a_r,a_{s,j}}(f)]^2 df}, \tag{2.11}$$

where a_r denotes vertical acceleration of the road-induced excitation and $a_{s,j}$ denotes vertical acceleration of the selected part of vehicle body.

Motion sickness induced by frequencies lower than 1 Hz belongs to another group of human ride discomfort. Such motion influences the human labyrinth and creates inconsistency between visual and auditory sensations. It was confirmed that pitching and rolling can induce motion sickness as well [63]. Thus, a quality index related to motion sickness was defined within the frequency range up to 1 Hz and can be additionally used

for validation of overall discomfort felt by vehicle passengers:

$$\widetilde{J}_{MS} = \sqrt{\int_{0\,Hz}^{1\,Hz} \{[\widetilde{T}_{a_r,\epsilon_{sp}}(f)]^2 + [\widetilde{T}_{a_r,\epsilon_{sr}}(f)]^2\} df}, \tag{2.12}$$

where ϵ_{sp} and ϵ_{sr} denote angular pitch and roll acceleration of the vehicle body, respectively. The $\widetilde{J}_{MS}$ performance criterion is defined assuming the vehicle suspension is subjected to sinusoidal road-induced excitation.

2.2.3 Driving-safety-related performance indices

Vibration control of the vehicle body part commonly increases deviation of suspension travel. Since design of a real suspension system is limited by the minimum and maximum stroke of its shock-absorbers, the suspension deflection is recommended to operate within the linear zone in order to avoid discontinuities [40]. Thus, the greater ride comfort is desired, the more attention should be paid to the condition of shock-absorbers. General criterion related to averaged suspension deflection within the frequency range from 0 Hz to 30 Hz [126] is defined assuming the vehicle suspension is subjected to the sinusoidal road-induced excitation:

$$\widetilde{J}_{SD} = \sqrt{\int_{0\mathrm{Hz}}^{30\mathrm{Hz}} \{[\widetilde{T}_{z_r,z_{usf}}(f)]^2 + [\widetilde{T}_{z_r,z_{usr}}(f)]^2]\} df}, \tag{2.13}$$

where z_{usf} and z_{usr} denote vertical deflection of the front and rear vehicle suspension, respectively.

Similarly to the suspension deflection, deviation of the vehicle tyre deflection is contradictory to the ride comfort. Road holding quality index assesses the ability of a vehicle to keep contact to the road, especially for higher frequencies [34, 119]. If wheel vibrations occurs close to their resonance, i.e. wheel hop, the amplitude of tyre deflection significantly increases. Consequently, the danger of loss of tyre-to-road adhesion significantly increases. In order to improve driving safety with respect to road holding, the tracking of wheel to the road should be maximized [126], which is expressed by the

following performance index:

$$\widetilde{J}_{RH} = \sqrt{\int_{0\text{Hz}}^{30\text{Hz}} \{[\widetilde{T}_{z_r,z_{ruf}}(f)]^2 + [\widetilde{T}_{z_r,z_{rur}}(f)]^2]\} df}, \tag{2.14}$$

where z_{ruf} and z_{rur} denote vertical deflection of the front and rear vehicle tyre, respectively. The $\widetilde{J}_{RH}$ performance criterion is defined assuming the vehicle suspension is subjected to the sinusoidal road-induced excitation.

2.3 Summary

The way how the road vehicle reacts to road irregularities and how vehicle vibrations need to be analysed strongly depends on the type of road-induced excitation as well as parameters of the vehicle suspension system. Application of road vehicles, e.g. transportation of passengers or other objects definitely influences the analysis of vehicle vibrations. A road vehicle can be subjected to different types of road unevenness, i.e. single road bumps or continuous road irregularities as well as stochastic or deterministic excitation. Since the real vehicle suspension equipped with MR dampers is strongly nonlinear, it has to be analysed and validated for different road conditions. The suspension control system is obligated to detect if the vehicle is traversing rough off road or smooth highway and needs to solve the compromise between ride comfort and driving safety. Both criteria need to be properly assessed and applied by the vibration control algorithm.

Chapter 3

Modelling and application of MR dampers

MR dampers give a possibility of adaptive modification of the suspension characteristics. It can be accomplished at significantly low cost since changing parameters in semiactive devices requires much less energy than generating force in the active ones. Due to the complex structure of MR fluid, behaviour of the MR damper is strongly nonlinear. The force response depends on both kinematic and control current excitations as well as on the temperature of the housing. In order to cope with such phenomena and apply MR dampers in vibration control systems, it is recommended to at least partly describe and map their behaviour. Simulation-based research and validation of control algorithms require reference MR damper model to be used, while partial linearisation of MR damper behaviour using inverse modelling improves quality of vibration control.

3.1 Procedure of MR damper investigation

Procedure of MR damper investigation is divided, according to [134], into the following phases:

- Configuration of experimental setup including selection of excitation signals.
- Conduction of identification experiment and measurements preprocessing.
- Model selection.

- Estimation of model parameters.
- Model validation.

The three initial phases are strictly related to each other. Selection of excitation signals applied during identification experiment is strictly related to the class of model which is to be identified. However, complexity of MR damper model needs to take into account limitations of the experimental setup, i.e. its parameters which influence available types of excitation signals and its sensors, which define the set of available measurement data. Finally, estimation procedure for MR damper model parameters and their validation similarly depend on the model structure which is to be identified.

3.1.1 Acquisition of measurements

Behaviour of MR dampers was investigated using MTS. Identification experiments were performed for linear suspension MR dampers of type RD-8040-1 (55 mm short stroke) and RD-8041-1 (74 mm long stroke) manufactured by Lord Corporation (see Appendix A), which are both installed in the presented experimental vehicle (see Figure 1.9). Both types exhibit maximum allowed generated force equal to 8896 N [25]. Since measurement results obtained for RD-8040-1 and RD-8041-1 were similar, the further analysis was focused on behaviour of the latter one.

During every experiment, the damper piston was subjected to kinematic excitation defined as axial sinusoidal displacement of certain amplitude and frequency (see Figure 3.1). In order to generate a PWM control current signal for the damper, the semiactive suspension controller was used which is actually installed in the experimental vehicle (see Appendix B). Both the MTS and suspension controller were operating simultaneously during each experiment. All experiments were performed for control current generated in the form of multi-step function within the range from 0 to 1.33 A of averaged control current (see Figure 3.1). Levels of consecutive control current steps were increasing, since the relation between control current and force response is strongly nonlinear. Later on, separate analysis of MR damper behaviour for different invariant control currents was performed.

The identification procedure took advantage of the following measurement data. Damper piston displacement and MR damper force response were taken by MTS with

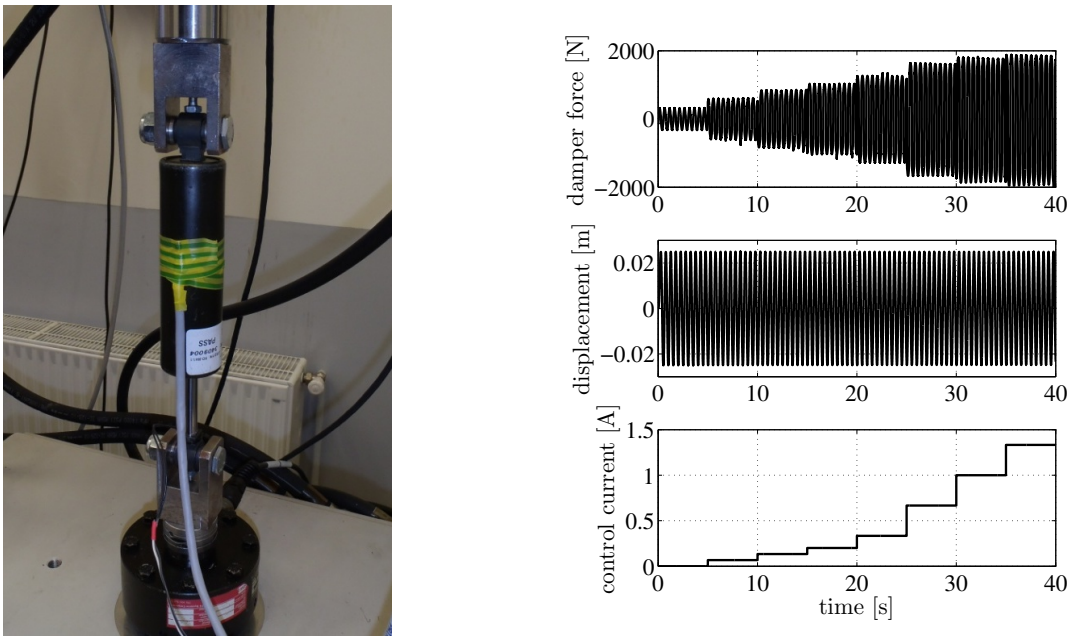

(a) (b)

Figure 3.1: MR damper experimental setup: a) MR damper investigated using MTS, b) exemplary measurements of force response to control current excitation and sinusoidal displacement excitation of amplitude 25 mm and frequency 1.5 Hz

sample rate of 1 kHz. The averaged control current signal was taken by the suspension controller with sample rate equal to 500 Hz. Additionally, a temperature sensor was attached to MR damper for safety issues in order to avoid its overheating. Different MR damper models were proposed in literature which include information about temperature of MR damper housing [32]. However, the temperature measurements were not included in the identified MR damper model. Availability of measurement data determines the class of MR damper model to be identified and type of identification algorithm to be used. In order to identify the most MR damper models, piston velocity and acceleration were estimated based on displacement measurements using central difference method.

Two types of identification experiments were performed. Firstly, the MR damper was investigated for different excitation frequencies and invariant amplitude of piston displacement excitation equal to 25 mm in order to study its dynamics for wide range of experimental conditions. Later on, since resonance frequencies of the vehicle body for common road vehicles vary from 1 to 2 Hz (see Table 1.1), selected MR damper models applied in control schemes were identified based on measurement data obtained for excitation frequency equal to 1.5 Hz. Secondly, behaviour of MR damper was additionally analysed for piston velocity excitation of different frequencies. Since behaviour of MR

damper mainly depends on piston velocity, it was ensured for such experiments that the amplitude of velocity was invariant over consecutive experiments. Such requirement was met by decreasing the amplitude of excitation displacement while increasing excitation frequency.

Exemplary measurement results are presented in Figure 3.1 for damper piston subjected to sinusoidal displacement excitation of amplitude 25 mm and frequency 1.5 Hz. Every experiment was preceded by zeroing of force measurements. Force offset value can be influenced mainly by the weight of MR damper as well as reaction of the built-in gas accumulator [124]. Thus, within further identification procedures only the dynamic features of MR dampers were studied.

3.1.2 General form of MR damper model

MR damper model is described as nonlinear two-input dynamic system, in which control current and kinematic excitation of damper piston correspond to the inputs, while force generated by MR damper corresponds to the output [124]. Thus, two input-output signal paths can be distinguished for the analysis of MR damper behaviour. Both signal paths exhibit dynamics and significant nonlinearity.

In order to analyse damper behaviour, two types of characteristics are plotted. Commonly, each characteristics is measured assuring one of MR damper excitations is invariant. First group consists of characteristics related to damper piston motion, i.e. piston displacement against force or piston velocity against force characteristics estimated for different invariant values of control current. Due to MR damper behaviour, which is related to viscous damping, the force-velocity characteristics are commonly analysed. Second type of characteristics, which are related to control current, are generated assuming invariant piston velocity. Experiments performed for simultaneously varying both control current and kinematic excitations require complex experimental setup and are not considered in the further analysis.

The MR damper model can be decomposed into a nonlinear static shape function and dynamic components which are included in both input and output signal paths (see Figure 3.2). Hysteretic behaviour dependent on the piston velocity and indicated in force-velocity characteristics is an example of dynamics of kinematic signal path denoted

as H_v. Dynamics of the control signal path denoted as H_i is influenced by parameters of the supplying electrical circuit [124]. Output dynamics of MR damper denoted as $H_{F_{mr}}$ defined from F_{mr} to F^*_{mr} is assumed according to experimental results of time response estimations presented in [72]. Moreover, dynamics of both signal paths are strictly related, i.e. force response to kinematic excitation is related to the control current [81], while dynamics of the control signal path depends on the velocity of damper piston [72].

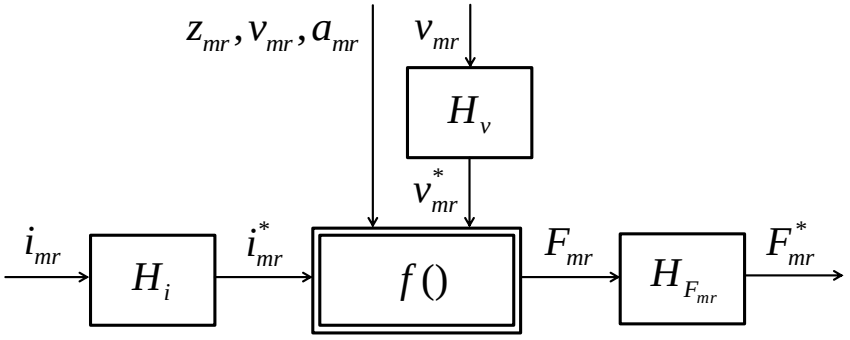

Figure 3.2: General MR damper model including dynamics of kinematic and control current excitation inputs as well as dynamics of force response output

Current excitation is controllable, while kinematic excitation is treated as a non-controllable input, i.e. disturbance. Thus, for the purpose of vibration control applications, the MR damper model can be presented in the form of single dynamic signal path related to control current. Such control signal path is modulated by piston motion, which indicates the maximum possible rate of vibration energy dissipation [77].

3.1.3 Estimation and validation of model parameters

Presented studies were mainly focused on experimental identification performed for the velocity to force signal path including the input dynamics H_v related to the kinematic excitation. Parameters of the input dynamics of the control signal path H_i as well as parameters of the output dynamics $H_{F_{mr}}$ were established based on the results presented in the literature. The displacement, velocity and acceleration measurements of the sinusoidal kinematic excitation were treated as inputs of the identified model. Identification of the selected MR damper model was performed in two stages, i.e. separate identification performed for different control current values as well as final identification of the model which include additional dependencies on current evaluated in the first stage.

Within the first stage measurement data were separated into several data sets dedicated to different excitation frequencies and different values of control current. Consequently, the identification procedure was performed for the each group separately. Next, relationships between estimated parameter, control current and excitation frequency were analysed, approximated and used for synthesis of the final model. In the end, within the second stage, the final MR damper model was identified simultaneously for all current values and for the selected excitation frequency. Identification algorithms applied for both stages stand for optimization carried out according to the following mean square expression:

$$\hat{\Theta}_{mr} = \arg\min_{\Theta_{mr}} \frac{1}{N} \sum_{n=1}^{N} \left\{ F_{mr}(j) - F_{mr,model}(n, z_{mr}, v_{mr}, a_{mr}, i_{mr}, \Theta_{mr}) \right\}^2, \tag{3.1}$$

where $F_{mr,model}$ denotes response of MR damper model which is defined by estimated parameters Θ, while F_{mr} denotes measurements of force generated by the actual MR damper. Measurements of kinematic excitation, i.e. displacement, velocity and acceleration are denoted as z_{mr}, v_{mr}, a_{mr}, respectively, while control current is denoted as i_{mr}. Different optimization algorithms were applied for solution of expression (3.1). Quasi-static and linear models, e.g. Bingham model [120] can be identified using classical gradient-based or least-mean-square optimization algorithms. In the case of models which consist of nonlinear differential equations, e.g. Bouc-Wen, Spencer [137], a multimodal solution space needs to be analysed, which requires nonlinear stochastic optimization algorithms, e.g. evolutionary algorithms [12].

Different validation approaches proposed in [124] are based on comparison of force diagrams in the time domain as well as displacement-force and force-velocity characteristics [137]. In order to select the most appropriate MR damper models, results of the first and second identification stage are validated using the following quality index:

$$J_{mr} = \sqrt{\frac{\sum_{n=1}^{N} \{F_{mr}(n) - F_{mr,model}(n, z_{mr}, v_{mr}, a_{mr}, i_{mr}, \Theta_{mr})\}^2}{\sum_{n=1}^{N} \{F_{mr}(n)\}^2}}. \tag{3.2}$$

The quality index (3.2) indicates fitness of the model response to force measurements. Moreover, in further studies force-velocity characteristics are compared and discussed in order to assess the quality of hysteretic behaviour modelling.

3.2 Analysis of velocity to force signal path

Analysis of the velocity-to-force signal path reveals strongly nonlinear behaviour of the MR damper including regions of force saturation and hysteresis loops. Moreover, the shape of such force-velocity characteristics significantly depends on the frequency and displacement amplitude of piston excitation signal (see Figure 1.6, Chapter 1). Numerous models were proposed in the literature, which can be divided into three classes, i.e. phenomenological models, behavioural models and input-output models.

Phenomenological MR damper models take advantage of two common physical rules, i.e. Navier-Stokes equations, which describe dynamics of MR fluid flow, and Maxwell's equations, which describe electromagnetic field induced by electromagnets [68]. What is more, MR fluid subjected to the magnetic field changes its properties and needs to be assumed as non-Newtonian. Consequently, structure of MR damper is described using nonlinear partial differential equations which are mutually dependent on each other since MR fluid and magnetic field interact. Such equations can be solved only numerically. Thus, high effort needs to be expended to apply phenomenological models in simulation and control. Phenomenological models exhibit huge number of parameters, which makes them sensitive to inaccuracy of estimation procedure. Moreover, such models tend to be over-parametrized and not consistent with the actual MR damper. Commonly, they are defined on the basis of available MR damper design data [33, 147], which are hardly accessible. The complexity of phenomenological models makes them inapplicable in the real-time vibration control application.

In order to apply MR damper models, a compromise needs to be found between accuracy of model description and applicability. Some authors present an approach of MR damper description which is not made with respect to MR damper physical structure but with respect to dominant phenomena, resulting in behavioural models. Other applications require the MR damper model to be further simplified to the modelling

of only input-output relations regardless of the occurring phenomena, which results in input-output models.

3.2.1 Velocity to force characteristics

Dynamics of the velocity-to-force signal path is mainly indicated in the form of hysteresis loops shown in the force-velocity characteristics. Numerous models of hysteretic behaviour, especially for MR dampers or similar devices, were proposed in the literature. Preisach hysteresis model [37, 112] describes dynamics of various smart materials and actuators such as SMAs (smart memory alloys), piezoceramic [55] as well as MR [128] and ER [45] fluids and dampers. It merges numerous transition functions of relay elements, which in result gives smooth shapes of hysteresis loops. Thus, a large number of model parameters is required, which is its main disadvantage. Bouc-Wen hysteresis component is an example of more compact hysteresis model, which includes single nonlinear differential equation [137]. Hysteretic behaviour can be mapped using switching MR damper model for positive and negative part of the hysteresis loop. Switching is triggered using relative piston displacement or acceleration and can be applied for all non-hysteretic MR damper models [24, 29, 143, 161].

All models presented above can be called the input-output models of hysteretic behaviour. Furthermore, acceleration-based models are quasi-static and map hysteresis loops only for sinusoidal kinematic excitation. Apart from the input-output modelling approach, the behavioural approach was proposed in the literature. According to [3], hysteretic behaviour can be modelled using input linear dynamics H_v (see Figure 3.2). Moreover, in the case of such models, the hysteresis component is excluded from the static nonlinear shape function, which simplifies the model. Behavioural hysteresis modelling is also confirmed in further analysis [124, 136].

Parameters of dynamic model H_v, strictly its phase shift denoted as φ_{H_v}, were identified separately for different values of control current and excitation frequencies f_{mr} according to the method proposed in [81]. Amplitude of the piston excitation velocity was ensured to be invariant for all experimental cases. Identification procedure of the phase shift parameter is based on minimization of estimated area encircled by the hysteresis

loops, according to the following expression:

$$\hat{\varphi}_{H_v}(f_{mr}, i_{mr}) = \{\arg\min_{\varphi_{H_v}} \sum_{v_k} [F_{mr}(v^*_{mr,a+}) - F_{mr}(v^*_{mr,a-})]^2 \; ; \; v^*_{mr,a+}, v^*_{mr,a-} = v_k\}\Big|_{f_{mr}, i_{mr}}, \tag{3.3}$$

where v_k corresponds to consecutive point of the force-velocity characteristics. Symbols $v^*_{mr,a+}$ and $v^*_{mr,a-}$ denote piston velocities v_{mr} which are delayed by phase shift of φ_{H_v}. They are related to the positive $a+$ and negative $a-$ piston acceleration, respectively. Symbols $F_{mr}(v^*_{mr,a+})$ and $F_{mr}(v^*_{mr,a-})$ denote force measurements which were synchronized with $v^*_{mr,a+}$ and $v_{mr,a-}$, respectively.

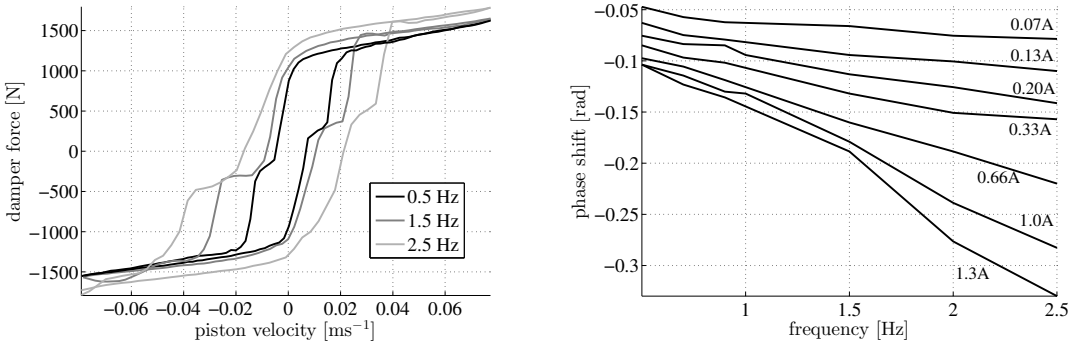

(a) (b)

Figure 3.3: Modelling of hysteretic behaviour as H_v input dynamics of velocity to force signal path for different excitation frequencies: a) force-velocity characteristics for control current of 1.33 A, b) phase shift characteristics of desired H_v dynamics

Results of identification (see Figure 3.3) show that the phase shift is inversely proportional to the excitation frequency. Moreover, phase shift decreases with increasing control current. Thus, it is recommended, within the future studies of the vibration control, to apply a frequency-dependent MR damper model. Such model needs to take into consideration dependencies occurring between shapes of hysteresis loop and excitation frequency.

3.2.2 Behavioural versus input-output models

In contrary to phenomenological models, behavioural models describe MR damper in macroscopic scale instead of analysing certain phenomena in microscopic scale. Three main behavioural components can be used, i.e.: perfect elastic body (Hooke's body), perfect viscous body (Newtonian body) and perfect plastic body (Saint-Venant body).

The Bingham model [120] includes two of the components (see Figure 3.4), i.e. Coulomb friction and viscous damping, which can be corresponded to the perfect plastic and perfect viscous body models, respectively. In order to map hysteretic behaviour using Bingham model, an additional expression dependent on piston acceleration needs to be used, resulting in the following form of Bingham model:

$$F_{mr,bh} = -f_{bh} \cdot \text{sign}(v_{mr} - \gamma_{bh} \cdot a_{mr}) - c_{bh} \cdot v_{mr} - \delta_{bh}, \tag{3.4}$$

where f_{bh} denotes a Coulomb friction parameter, c_{bh} denotes viscous damping parameter, γ_{bh} influences hysteretic behaviour of the model and δ_{bh} denotes the force offset component.

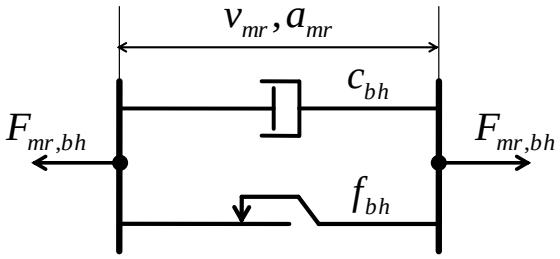

Figure 3.4: Mechanical representation of Bingham MR damper model

Bingham model can be extended to Bingham body model [121] by taking into account an additional component of perfect elastic behaviour, represented in the mechanical diagram as a spring connected in series. Further extension, i.e. Gamota-Filisko model was presented in [121, 137] as three components connected in series, i.e. Bingham model, Kelvin-Voight body and Hooke body models. The Kelvin-Voight body model describes a solid body accompanied with relationship between maximum damper length and applied force [19]. Moreover, pre-yield and post-yield behaviour phenomena were taken into account in behavioural MR damper models in [89, 148].

Some phenomena which are observable in MR damper behaviour, such as frequency dependence or additional backlash of couplings inside the damper, are still not fully explained. However, they should be mapped, which can be solved by neglecting physical explanation and using input-output models. Such approach allows to more efficiently fit the model response to measurement data for certain experimental conditions. Application of polynomials as an example of input-output models allows to simplify the model structure as well as the identification process [24, 29]. The model of MR damper

including hysteretic behaviour which is based on polynomials is defined by the following expression:

$$F_{mr,pn} = \begin{cases} -\sum_{j=0}^{N} b_{pn,a+,j} \cdot v_{mr}^{j} & \text{for } a_{mr} \geq 0 \\ -\sum_{j=0}^{N} b_{pn,a-,j} \cdot v_{mr}^{j} & \text{for } a_{mr} < 0 \end{cases}, \tag{3.5}$$

where $b_{pn,a+,j}$ and $b_{pn,a-,j}$ are parameters of the polynomial models related to the positive and negative piston acceleration, respectively. Lack of mechanical representation of input-output models is their characteristic feature.

Another method of input-output modelling is to construct a biviscous model [42, 148]. Such models involve switching between lower and higher viscosity parameters dedicated to pre-yield and post-yield behaviour, respectively. Other modelling methods are based on neural networks [8, 31, 108] as well as on trigonometric [68, 106] and hyperbolic [121, 124, 136] functions, which serve as shape functions included in the MR damper model.

In conclusion, behavioural models can describe MR damper in wide range of experimental conditions. However, they are limited to the known phenomena, which cannot fully describe the damper behaviour. An input-output model can become a complete MR damper model but it tends to be over-parametrized and valid only for specific experimental conditions. Thus, usually mixed models are used, e.g. Bouc-Wen and Spencer-Dyke models as well as the model based on *tanh* function. Such models include classical stiffness and viscous damping behavioural components, while some phenomena are mapped using input-output modelling approaches, e.g. using hyperbolic functions or Bouc-Wen hysteretic component.

3.2.3 Bouc-Wen and Spencer-Dyke models

The Bouc-Wen model was formulated based on studies introduced in [11] and [146]. It includes the Bouc-Wen component, i.e. an input-output model which can be used for mapping of the velocity to force hysteretic behaviour of MR damper. Additionally, behavioural components are included in the model describing stiffness (partly related to the damper accumulator) and viscous damping parameters denoted as k_{bw} and c_{bw}, respectively. The hysteretic displacement of the Bouc-Wen component denoted as p_{bw} is

evaluated using first-order nonlinear differential equation:

$$\dot{p}_{bw} = -\gamma_{bw} \cdot |v_{bw}| \cdot p_{bw} \cdot |p_{bw}|^{n_{bw}-1} - \beta_{bw} \cdot v_{bw} \cdot |p_{bw}|^{n_{bw}} + A_{bw} \cdot v_{bw}, \tag{3.6}$$

where v_{bw} denotes relative velocity of the Bouc-Wen model. Parameters γ_{bw}, β_{bw} and A_{bw} define shape and size of hysteresis loops observable in force-velocity characteristics. Resultant force generated by Bouc-Wen model is defined as follows:

$$F_{mr,bw} = -\alpha_{bw} p_{bw} - c_{bw} v_{bw} - k_{bw} z_{bw} - \delta_{bw}. \tag{3.7}$$

The Bouc-Wen model was improved in [137] and proposed as enhanced Bouc-Wen or Spencer-Dyke model. Apart from k_{bw} and c_{bw} parameters, additionally stiffness k_{sc} and viscous damping parameters c_{sc} were included. Mechanical representation of Spencer-Dyke model is shown in Figure 3.5. Behavioural part of the model is defined by two interchangeable equations:

$$\begin{aligned} F_{mr,sc} &= -\alpha_{bw} p_{bw} - c_{bw} v_{bw} - k_{bw} z_{bw} - k_{sc} z_{mr} - \delta_{sc}, \\ F_{mr,sc} &= -c_{sc}(v_{mr} - v_{bw}) - k_{sc} z_{mr} - \delta_{sc}, \end{aligned} \tag{3.8}$$

where p_{bw} is hysteretic displacement simulated according to the Equation (3.6). Relative velocity of the internal Bouc-Wen model within the Spencer-Dyke model is defined by the following expression:

$$v_{bw} = \frac{1}{c_{bw} + c_{sc}} [c_{sc} v_{mr} - \alpha_{bw} p_{bw} - k_{bw} z_{bw}]. \tag{3.9}$$

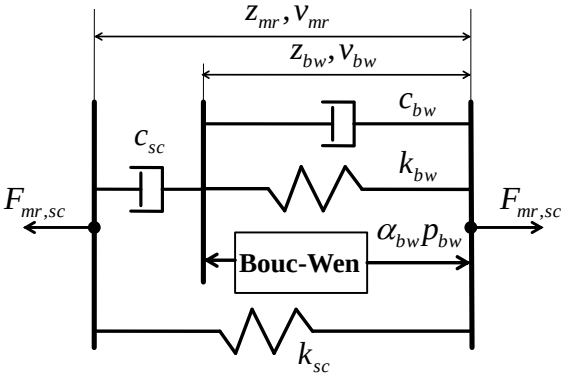

Figure 3.5: Mechanical representation of Spencer-Dyke model

Bouc-Wen and Spencer-Dyke models were identified based on measurement data obtained for excitation frequency equal to 1.5 Hz and different values of control current varying from 0 to 1.33 A. Parameters of the models were estimated by minimizing the cost function according to Expression (3.1). Quality of fitness for both models was compared using the quality index (3.2) and listed in Table 3.1 where lower values correspond to better fitness. Results obtained for all values of control current confirmed the superiority of Spencer-Dyke model over Bouc-Wen model. Significant deterioration of fitness quality for both models can be shown for control current equal to zero.

Table 3.1: Values of fitness quality index J_{mr} evaluated for Bouc-Wen and Spencer-Dyke models in the case of excitation displacement amplitude of 25 mm, excitation frequency of 1.5 Hz and control current varying from 0 to 1.33 A

i_{mr} [mA]	0	67	133	200	333	667	1000	1333	AVG
Bouc-Wen model									
$J_{mr} \cdot 10^{-3}$	117	52	49	50	53	53	58	56	61
Spencer-Dyke model									
$J_{mr} \cdot 10^{-3}$	115	36	27	26	27	35	56	52	47

The force-velocity characteristics plotted for force measurements and responses of both models confirm results of validation performed based on quality indices (see Figure 3.6). Both Bouc-Wen and Spencer-Dyke models accurately map the shape of force-velocity characteristics, particularly, hysteretic loops and force saturation phenomena, with the predominance of the latter model.

3.2.4 Tanh-function-based model

Commonly, inverse MR damper models are applied in semiactive vibration control. Bouc-Wen or Spencer-Dyke models can be inverted only numerically [77], which leads to processor-intensive calculations not recommended in real-time applications. The characteristic shape of the MR damper force-velocity characteristics can also be mapped using trigonometric hyperbolic tangent function [62, 69, 124, 136] or cyclometric inverse tangent function [68, 106]. Such functions serve as a backbone of model which maps behaviour occurring close to zero velocity and for force saturation regions. Furthermore,

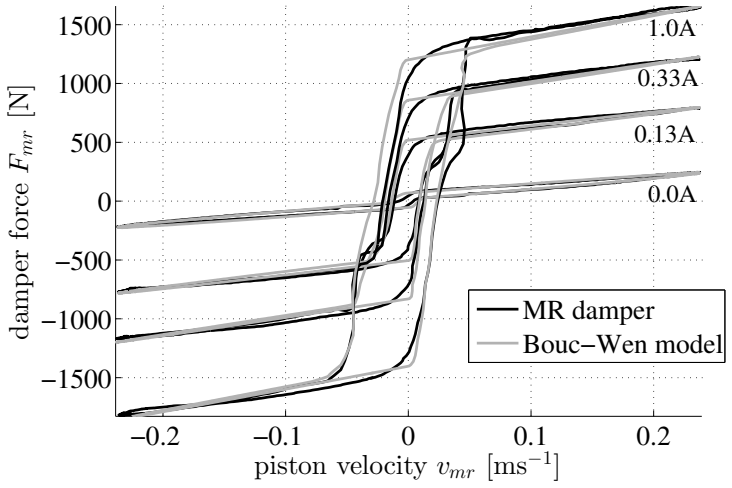

(a)

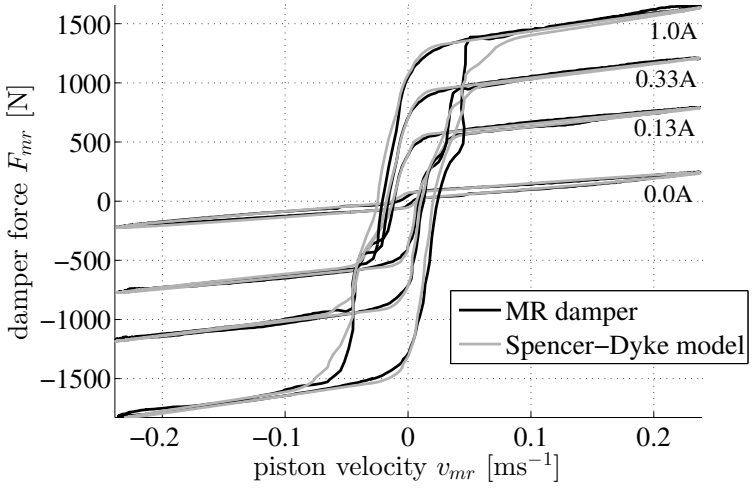

(b)

Figure 3.6: Quality of modelling of MR damper behaviour performed based on measurements obtained for excitation displacement amplitude of 25 mm, excitation frequency of 1.5 Hz and separately for all values of control current varying from 0 to 1 A: a) Bouc-Wen model, b) Spencer-Dyke model

application of Tanh model as an inverse model in the control algorithm while Spencer-Dyke model is included in the vehicle suspension model resembles the real case, for which the model of MR damper is not known exactly.

Contrary to Bouc-Wen or Spencer-Dyke models, the Tanh model is a quasi-static model. It includes both behavioural and input-output tanh-based components, which is illustrated in the form of mechanical representation (see Figure 3.7). It can additionally include piston displacement or acceleration signal, which maps hysteretic behaviour.

Acceleration measurements are commonly burdened with measurement noise which significantly influences behaviour of tanh-based model. However, in the case of identification experiments where the MR damper piston is excited by sinusoidal kinematic excitation, both piston displacement [26, 43, 125] and acceleration signals can be applied to modelling hysteretic behaviour. The given form of Tanh model is defined by the following expression:

$$F_{mr,th} = -\alpha_{th}\tanh(\beta_{th}v_{mr} - \gamma_{th}a_{mr}) - c_{th}v_{mr} - k_{th}z_{mr} - \delta_{th}, \tag{3.10}$$

where α_{th}, β_{th}, γ_{th}, c_{th} and k_{th} denote parameters of the model, while δ_{th} denotes a force offset component.

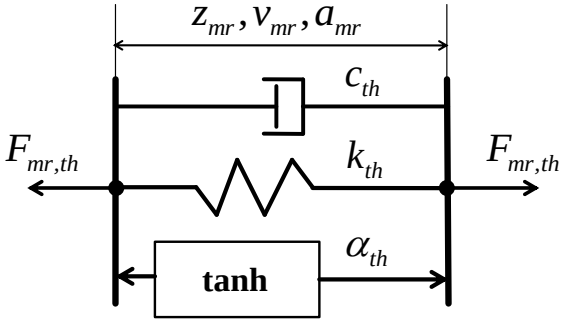

Figure 3.7: Mechanical representation of tanh-function-based model

Similarly to previously given models, the Tanh model was identified based on measurement data obtained for excitation frequency equal to 1.5 Hz and different values of control current varying from 0 to 1.33 A. Values of fitness quality index evaluated for the Tanh model are listed in Table 3.2.

Table 3.2: Values of fitness quality index J_{mr} evaluated for Tanh model in the case of excitation displacement amplitude of 25 mm, excitation frequency of 1.5 Hz and control current varying from 0 to 1.33 A

i_{mr} [mA]	0	67	133	200	333	667	1000	1333	AVG
$J_{mr} \cdot 10^{-3}$	113	33	26	26	31	35	34	34	42

Similarly to Bouc-Wen and Spencer-Dyke models, significantly higher value of quality index for zero control current indicates that MR damper exhibits different behaviour for off state. Results of identification are additionally shown in the form of force-velocity characteristics plotted for force measurements and responses of Tanh model (see Figure

3.8). Besides, comparison of all analysed models is presented based on fitness quality indices, which shows that the Tanh model exhibits best mapping of MR damper behaviour. The average value of quality index listed in Table 3.2 confirms such observation.

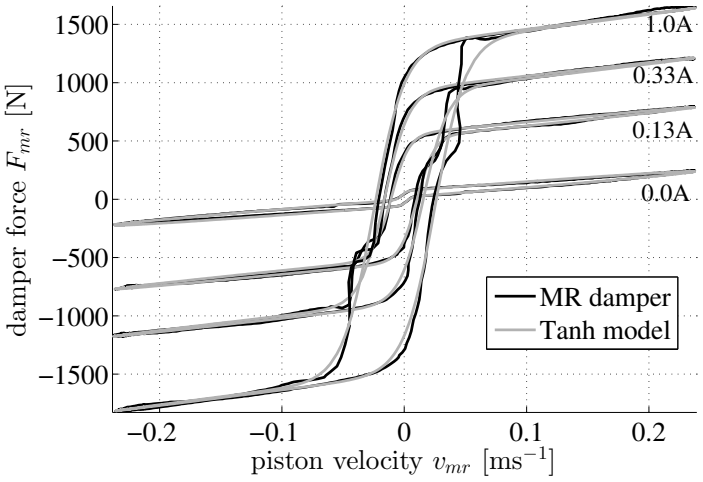

(a)

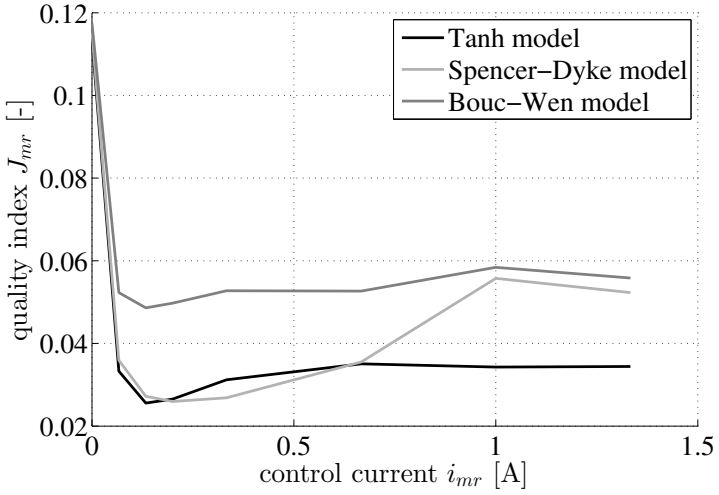

(b)

Figure 3.8: Quality of modelling of MR damper behaviour performed based on measurements obtained for excitation displacement amplitude of 25 mm, excitation frequency of 1.5 Hz and control current varying from 0 to 1 A: a) force-velocity characteristics for Tanh model, b) comparison of Bouc-Wen, Spencer-Dyke and Tanh models

3.3 Synthesis and application of MR damper model

Application of MR damper in control systems requires identification of at least coarse model of the signal path from control current to MR damper force response. Such signal path is deteriorated by both static nonlinearities as well as dynamics of the

electrical supply circuit and MR fluid reaction to changes of magnetic field. Both types of dynamics are marked in the general MR damper (see Figure 3.2) as H_i and $H_{F_{mr}}$, respectively, while static nonlinearities are marked as the arbitrary nonlinear function.

Commonly, approximation of static relationships from control current to parameters of velocity to force models is used. In the case of inverse model evaluation, the approximation approach requires the resultant MR damper model to be invertible with respect to control current. Certain values of control current have different influence on MR damper behaviour, e.g. its force saturation level, shape of hysteresis loops. Apart from saturation which is revealed in the force-velocity characteristics, the saturation in the control current to force signal path can be noticed. Thus, nonlinear functions are used for approximation, e.g. polynomials [29] or square root functions [108].

3.3.1 Dynamics of control current to force signal path

Dynamics of the input electrical circuit supplying coils located in MR damper piston is mainly influenced by its resistance and inductance parameters. Generally, the RL oscillating input circuit is modelled as a SISO dynamical system with input related to control voltage and output related to control current. Numerous studies presented in literature proposed modelling approach of the input circuit [123, 159]. In the case of the analysed MR damper of type RD-1005-3 (i.e. predecessor of RD-8041-1), parameters of its resistance and inductance were adopted by other authors at values of 5 Ω and 100 mH which results in time constant of 20 ms. Other comprehensive studies on MR damper dynamics were reported in [72], where response time of the input circuit of suspension MR damper varies from 1 ms up to 12 ms and depends on the control current.

Despite the fact that MR dampers are directly controlled by PWM voltage, commonly, the averaged value of the resultant control current is stabilized using dedicated voltage to current converters, e.g. Wonderbox produced by Lord Corporation [154]. Such controllers significantly improve the voltage to current time response. Moreover, for the purpose of given studies, the MR damper behaviour is identified with respect to control current, which is directly related to magnetic field induced within the damper piston. Thus, dynamics of the MR damper input circuit denoted as H_i is neglected in the further analysis, i.e.:

$$H_i = 1. \tag{3.11}$$

Further simulation research takes into account the output dynamics of the control current to force signal path. Response of the MR fluid itself influences the finite time of MR damper reaction to changes of control current, which is observable in macroscopic scale. Results of force response estimation were presented in [72, 123], where MR damper was subjected to a triangular kinematic displacement excitation. Such excitation ensures the velocity to be invariant during the test. Meanwhile, the step excitation of the control current was generated and the force response time was estimated. It was shown in [72] that the response time depends on both control current as well as kinematic excitation of damper piston. However, based on reported results, the response time can be assumed with high accuracy as invariant and equal to 20 ms, since it increases only for piston velocities close to zero. Thus, for the purpose of further studies, the output dynamics of MR damper model denoted as $H_{F_{mr}}$ was modelled by a first-order inertia filter with response time equal to 20 ms, as follows:

$$H_{F_{mr}}(s) = \frac{1}{1 + s \cdot 0.0067}. \tag{3.12}$$

3.3.2 Relationship between model parameters and current

Relationship between current and parameters of Spencer-Dyke or Tanh models is strongly nonlinear. Thus, many approximation methods were proposed in the literature, e.g. polynomials [29] or neural networks [108]. Other authors showed in [160] that in the case of Spencer-Dyke model, three parameters, i.e. α_{bw}, c_{bw} and c_{sc} should be related to control current using polynomials of the third order. Thus, in the further analysis these parameters of Spencer-Dyke model defined by Equations (3.8-3.9) were assumed to be dependent on current as follows:

$$\theta_{sc} = \sum_{j=0}^{3} (\theta_{sc,j} \cdot i_{mr}^{j}) \quad \text{for} \quad \theta_{sc} \in \{\alpha_{bw}, c_{bw}, c_{sc}\}. \tag{3.13}$$

Other parameters are assumed as invariant. The identification procedure was performed for extended set of parameters, while a quality index was minimized which was evaluated according to Equation (3.2) based on force responses obtained for all control current values. Estimated parameters are listed in Table 3.3. It can be noticed that due to the additional requirements related to dependence on control current, the quality of model fitness to force measurements was deteriorated compared to results obtained for separate

identification (see Table 3.1). However, functionality of such extended current-dependent model allows for its application as a reference model within studies of semiactive vibration control.

Table 3.3: Parameters of Spencer-Dyke model

Estimated parameters		
$n_{bw} = 2$	$A_{bw} = 45.8275$ [-]	$\beta_{bw} = 379780$ [m^{-1}]
$\gamma_{bw} = 49867$ [m^{-1}]	$k_{bw} = 997.04$ [Nm^{-1}]	
[$\alpha_{bw,0}$, $\alpha_{bw,1}$, $\alpha_{bw,2}$, $\alpha_{bw,3}$] = [0.1533 , 3.4150 , -3.4799 , 1.2127] $\cdot 10^5$ [Nm^{-1}]		
[$c_{bw,0}$, $c_{bw,1}$, $c_{bw,2}$, $c_{bw,3}$] = [0.9779 , -0.4317 , 2.7046 , -1.4410] $\cdot 10^3$ [Nsm^{-1}]		
$\delta_{sc} =$ -8.2892 [N]	$k_{sc} = 0$ [Nm^{-1}]	
[$c_{sc,0}$, $c_{sc,1}$, $c_{sc,2}$, $c_{sc,3}$] = [0.0128 , 1.1688 , -0.7145 , 0.1960] $\cdot 10^5$ [Nsm^{-1}]		
Fitness quality index	$J_{mr} = 86 \cdot 10^{-3}$	

Most algorithms applied for MR damper control require an inverse MR damper model in order to make the MR damper generate force which is as close as possible to the force desired by the algorithm. On the one hand, the inverse model should fit well to measurement data. On the other hand, possibility of analytical inversion of MR damper model is recommended in order to avoid numerical inversion due to computation limitations of real-time application. Thus, a square root function was proposed for Tanh MR damper model in [69] to approximate its dependence on control current. For the purpose of the dissertation, two parameters of Tanh model defined by Equation (3.7) were related to control current as follows:

$$\theta_{th} = \theta_{th,0} + \theta_{th,1} \cdot \sqrt{i_{mr}} \quad \text{for} \quad \theta_{th} \in \{\alpha_{th}, c_{th}\} \tag{3.14}$$

while other parameters were assumed as invariant. Similarly to extended Spencer-Dyke model, the identification procedure was repeated for extended set of Tanh model parameters. Estimated parameters and corresponding value of fitness quality index are listed in Table 3.4.

Force responses obtained for extended Spencer-Dyke and Tanh models are compared with force measurements and presented in Figure 3.9. It can be noticed that despite the additional control-related requirements set on both models, they still fit to measurement data with high accuracy, which allows for their application in further studies.

Table 3.4: Parameters of Tanh model

Estimated parameters	
[$\alpha_{th,0}$, $\alpha_{th,1}$] = [0.0624 , 1.3398] $\cdot 10^3$ [N]	
β_{th} = 39.955 [sm^{-1}]	γ_{th} = 0.4127 [s^{2}m^{-1}]
k_{th} = 170.0436 [Nm^{-1}]	δ_{th} = -0.8072 [N]
[$c_{th,0}$, $c_{th,1}$] = [802.8 , 488.53] [Nsm^{-1}]	
Fitness quality index	$J_{mr} = 127 \cdot 10^{-3}$

3.3.3 Inverse modelling: evaluation and validation

In the case of semiactive vibration control, partial compensation of the strongly nonlinear behaviour of MR damper is recommended. Linearisation of nonlinear relationship between control current and damper force significantly simplifies the applied control scheme. Two approaches, which are based on feedback and feedforward control, can be distinguished. The former one is based on feedback control algorithm which adjusts the actual MR damper force. Such algorithm takes advantage of measured MR damper force, which is its limitation, since additional force sensors need to be installed in the vehicle suspension. The latter approach is based on inverse modelling of MR damper, a well-known idea in vehicle vibration control.

The inverse MR damper model can be evaluated analytically by inversion of the static nonlinear part of MR damper model (see Figure 3.2). Numerous structures of inverse MR damper models were proposed in the literature [69, 84, 107]. For the further analysis, the inverse Tanh model is used which was obtained based on Tanh model defined by Equations (3.14) and (3.10). Such inverse model was evaluated as follows:

$$i_{mr,th} = \left[\frac{-F_{alg} - \alpha_{th,0}\tanh(\beta_{th} v_{mr} - \gamma_{th} a_{mr}) - c_{th,0} v_{mr} - k_{th} z_{mr}}{\alpha_{th,1}\tanh(\beta_{th} v_{mr} - \gamma_{th} a_{mr}) + c_{th,1} v_{mr}} \right]^2, \tag{3.15}$$

where all parameters are listed in Table 3.4. The inverse model gives a value of current denoted as $i_{mr,th}$, which should be used for control of MR damper in order to make the damper generate force denoted as F_{alg}, which is desired by the control algorithm. However, the current $i_{mr,th}$ needs to be limited to positive values, which is a characteristics feature and limitation of semiactive systems.

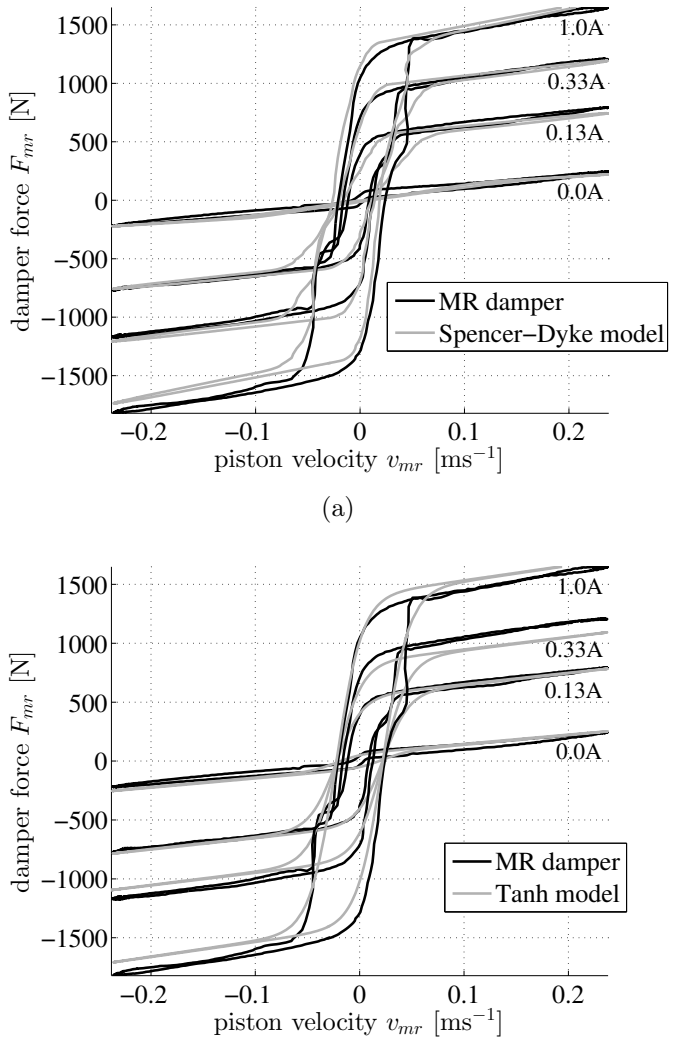

Figure 3.9: Quality of modelling of MR damper behaviour performed based on measurements obtained for excitation displacement amplitude of 25 mm, excitation frequency of 1.5 Hz and simultaneously for all values of control current varying from 0 to 1 A: a) Spencer-Dyke model, b) Tanh model

Validation of the inverse model is performed using reference Spencer-Dyke and inverse Tanh model connected in series (see Figure 3.10). Such connection creates the main component of the simulation environment for vehicle vibrations. Since MR damper cannot generate force which is outside its dissipative domain, i.e. is indivertible, the desired force denoted as F_{alg} is also simulated using the reference model. Such validation approach ensures that inaccuracy of generating F_{mr} based on F_{alg} is caused only by inaccuracy of the inverse model and not by force constraints related to the dissipative domain. Thus, in the case of ideal inverse model, the force generated by the final reference model F_{mr} should be the same as the desired force F_{alg}.

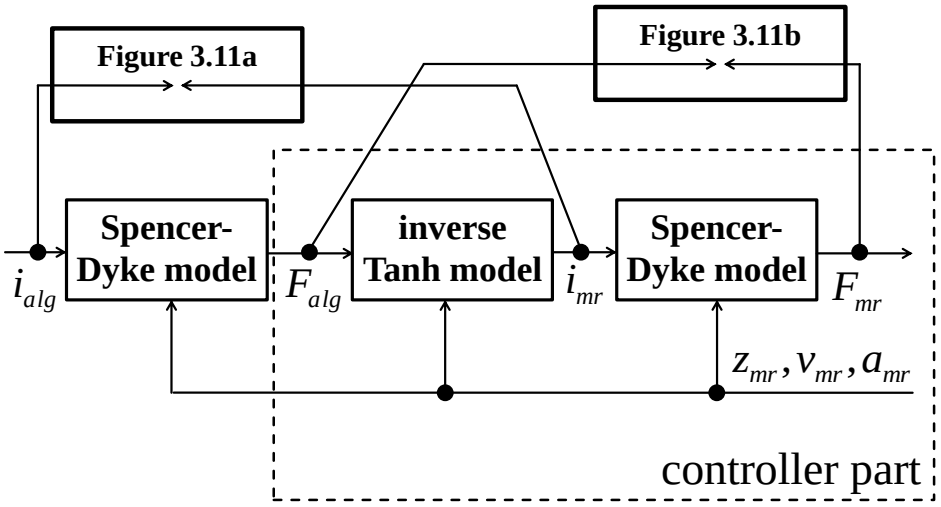

Figure 3.10: Validation procedure for Tanh inverse MR damper model and Spencer-Dyke reference model

The validation is done using control current excitation signal denoted as i_{alg} rising from 0 A to 1.33 A. Both reference and inverse models are subjected to the same kinematic sinusoidal excitation of frequency equal to 1.5 Hz defined by z_{mr}, v_{mr} and a_{mr}. The validation procedure can be based on comparison of desired i_{mr} and reference i_{alg} currents or comparison of actual F_{mr} and desired F_{alg} forces. Initially, validation procedure was tested using Tanh model as a reference model. Finally, both Spencer-Dyke and inverse Tanh models were tested, which is shown in Figure 3.11 in the form of time diagrams obtained for the control current and force signals. In order to improve clarity of figures the diagram of desired control current was smoothed using Savitzky-Golay filter with polynomial order equal to 1 and window size equal to 301. Since reference and inverse models exhibit different structures, an inconsistency between time diagrams can be seen. The force generated by the final Spencer-Dyke model is underestimated for lower and overestimated for higher control current values.

Besides, it was noticed that slight numerical errors included in the damper piston acceleration signal significantly influence the control current i_{mr} given by the inverse model. Such errors were common not in the case of identification experiments but for the simulation and experiments of the vehicle suspension. Thus, the γ_{th} parameter describing hysteretic behaviour was decided to be set to zero for the purpose of further validation of control schemes.

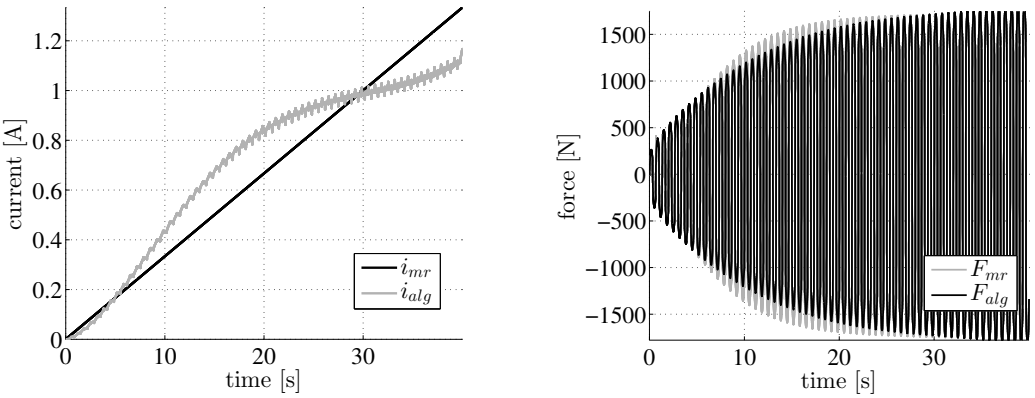

(a) (b)

Figure 3.11: Validation of tanh-based inverse model versus Spencer-Dyke reference model for excitation displacement amplitude of 25 mm, excitation frequency of 1.5 Hz and control current varying from 0 to 1.33 A: a) desired i_{mr} and reference i_{alg} currents, b) actual F_{mr} and desired F_{alg} forces

After the modification was proposed, two approaches to the Tanh model identification was distinguished. For the first one, an initial identification of Tanh model including hysteresis is performed and consequently the γ_{th} is neglected. For the second approach, a direct identification of the Tanh model without hysteresis is performed. The model without hysteresis unfavourably tends to describe the hysteretic behaviour using stiffness parameter, while it gives only slight improvement in identification results. Thus, the first two-step method was applied for the inverse model evaluation.

3.4 Summary

Specific features of MR dampers such as inherent stability and low energy consumption make them widely applied in the vibration control systems. The possibility of adjusting damping parameters of a vibrating mechanical system allows to adapt the system to instantaneous ambient conditions. However, application of MR dampers requires analysis of their nonlinear behaviour. Both nonlinear signal paths, defined for the control current and kinematic excitations to force response, are recommended to be modelled. Thus, analysis and comparison of selected models including Spencer-Dyke model were carried out, as well as Tanh inverse model was evaluated and validated for further application in vibration control algorithms.

Chapter 4

Dynamics of vehicle suspension system with MR dampers

Modelling of vehicle vibrations is recommended for different types of systems installed in road vehicles, e.g. related to suspension diagnosis or control. On-line identification of a vehicle model can be used for tracking vehicle parameters and detecting suspension damage. Furthermore, the identified model of vehicle vibrations can be used for preliminary synthesis and tuning of the control algorithm as well as its final validation.

It is recommended to at least coarsely analyse the dynamics of the object in order to make the structure of the algorithm more appropriate for the desired application. The more information about vehicle vibrations are available, the better performance of the algorithm can be obtained. The identification procedures can also be included in the control algorithm in order to make it adjustable to varying vehicle parameters and road conditions.

All control algorithms need to be validated before they can be applied, since no ideal control optimization method can be found. Generally, several stages of algorithm validation can be distinguished. The earlier the validation process starts, the shorter its length is. Herein, two validation methods can be distinguished, i.e. simulation-based studies and hardware-in-the-loop approach, both of which require a model of vehicle vibrations. All arguments presented above confirm that modelling and analysis of vehicle vibrations is inevitable for synthesis and validation of vehicle vibration control.

4.1 Modelling of road-induced vehicle vibrations

Model of vehicle vibrations can be assumed as MIMO dynamic system (see Figure 4.1). It takes into account two groups of excitation signals. The first group includes road-induced excitations of vehicle wheels in the form of vertical displacement, velocity and acceleration, denoted $\boldsymbol{z_r}$, $\boldsymbol{v_r}$, $\boldsymbol{a_r}$, respectively. The second group includes control currents of MR dampers installed in the vehicle, denoted as $\boldsymbol{i_{mr}}$. The latter signals are generated by the vehicle vibration control system, while the former ones are treated as disturbances of the system, i.e. they are measurable but cannot be influenced by the control algorithm. All measurable quantities describing the motion of the vehicle are grouped and assumed as the output of the system denoted as $\boldsymbol{y}$.

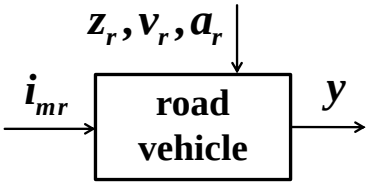

Figure 4.1: General road vehicle model including MR dampers

Generally, a behavioural approach to modelling of vehicle vibrations is applied which reflects the actual construction of the road vehicle. Further analysis will be limited to low frequencies since vehicle vibrations related to ride comfort or driving safety are analysed within frequency bandwidth up to 25 Hz or 30 Hz, respectively (see Table 1.1). Commonly, multi-body vehicle models are used [101], [56], where the vehicle construction is divided into a finite number of rigid elements connected with stiffness and viscous damping elements, which is described by the following general form of matrix differential equation:

$$\boldsymbol{M\ddot{q} + C\dot{q} + Kq = u}, \tag{4.1}$$

where $\boldsymbol{M}$, $\boldsymbol{C}$ and $\boldsymbol{K}$ denote mass, damping and stiffness matrices, respectively. Symbol $\boldsymbol{q}$ denotes a vector of generalised coordinates and $\boldsymbol{u}$ denotes a vector of applied forces. Generally, models of vehicles equipped with automotive MR dampers are decomposed into a linear model of vehicle vibrations and separate MR dampers models. Then, vector $\boldsymbol{u}$ includes both the kinematic excitation signals and forces generated by MR dampers.

The more degrees of freedom are included in the vehicle model, the more accurate model can be obtained. However, higher number of parameters requires longer and

more complex identification procedures. Thus, in the case of vehicle suspension analysis, such models can be limited to the most relevant components, e.g. wheels or vehicle body which makes them applicable and less computation-intensive. Models of vehicle vibrations proposed in literature are usually divided with respect to the number of DOFs. Dynamics of various vehicle components can be taken into account, e.g. vehicle engine and its suspension in heavy vehicles [162], passengers seats [39] or passengers themselves [15]. The classical full-car model which exhibits 7 DOFs takes into account heave, pitch and roll motion of the vehicle body as well as vertical motion of each wheel [29].

4.1.1 Half-car model with 4 DOFs

The full-car model can be simplified in justified cases to longitudinal half-car model which exhibits 4 DOFs, e.g. for the symmetrical road-induced excitation or if the symmetry of the vehicle construction is indicated (see Figure C.1). The half-car models can also be directly applied for description of dynamics of bicycle vehicles. Vibration modes of the presented half-car model are related to heave and pitch vehicle body dynamics and vertical motion of wheels. Influence of a human body on the response of the vehicle is neglected in the further analysis.

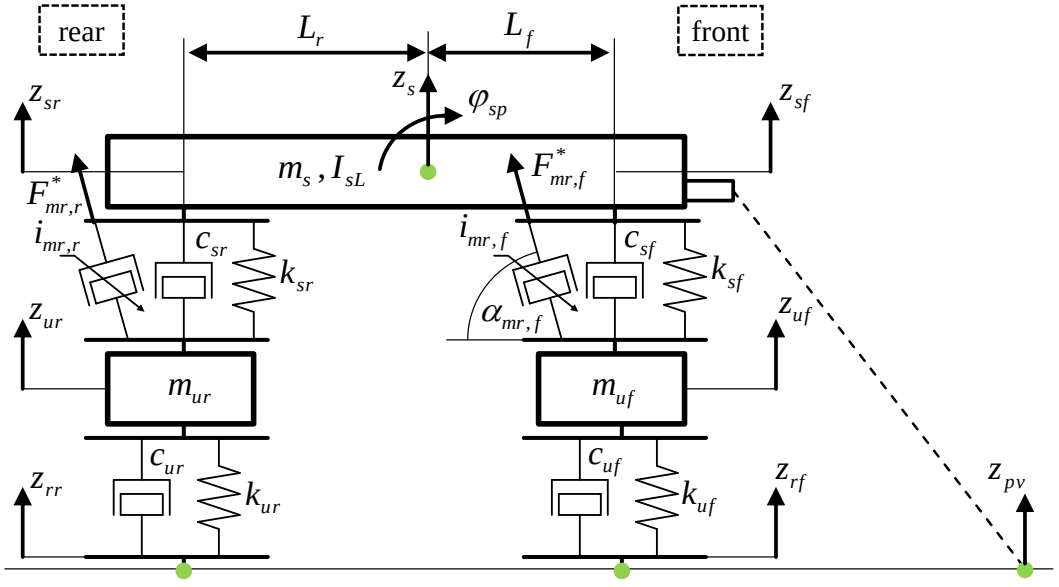

Figure 4.2: Half-car model of vehicle vibration model with 4 DOFs including suspension MR dampers

The vehicle body is modelled as a 2-dimensional beam of length denoted as L. Subscripts f and r denote the front and rear parts of the vehicle, respectively. The

vehicle body beam exhibits the following features: the center of gravity whose distances from the ends are L_f and L_r, the mass of the vehicle body m_s and the moment of inertia about the pitch axis denoted as I_{sL}. The sprung and unsprung parts of the vehicle are denoted using subscripts s and u, respectively.

Additional masses moving only vertically, denoted as m_{uf}, m_{ur}, are included in the model. They are related to the vehicle front and rear wheel. Vehicle body mass and wheel masses are connected by linear springs k_{sf}, k_{sr} and viscous dampers c_{sf}, c_{sr}, which stands for the front and rear parts of the vehicle suspension system, respectively. Road-induced kinematic excitation influences the half-car model via springs k_{uf}, k_{ur} and dampers c_{uf}, c_{ur}, which are related to parameters of tyres and are connected to the front and rear wheel masses. Since it was assumed that pitch angle varies in small range, the trigonometric relationships of half-car model description were neglected.

Additionally, for the purpose of further vibration control analysis it is assumed that the vehicle is equipped with a road profile measurement system, which is aimed at the front of the vehicle and gives information about road-induced excitation in advance. This excitation is available in the form of vertical displacement, velocity and acceleration of the road profile, denoted as z_{pv}, v_{pv} and a_{pv}, respectively. Such measurement data can be used by the so-called preview control in order to improve vibration control.

Differential equations describing half-car model with 4 DOFs were obtained using Euler-Lagrange equations including Rayleigh dissipation function (see Appendix C), resulting in the following:

$$\begin{aligned} m_s\ddot{z}_s =& -k_{sf}(z_{sf}-z_{uf})-c_{sf}(\dot{z}_{sf}-\dot{z}_{uf})+F^*_{mr,f}\sin(\alpha_{mr,f}) \\ & -k_{sr}(z_{sr}-z_{ur})-c_{sr}(\dot{z}_{sr}-\dot{z}_{ur})+F^*_{mr,r}\sin(\alpha_{mr,r}), \end{aligned} \tag{4.2}$$

$$\begin{aligned} I_{sL}\ddot{\varphi}_{sp} =& L_f\left[k_{sf}(z_{sf}-z_{uf})+c_{sf}(\dot{z}_{sf}-\dot{z}_{uf})-F^*_{mr,f}\sin(\alpha_{mr,f})\right] \\ & -L_r\left[k_{sr}(z_{sr}-z_{ur})+c_{sr}(\dot{z}_{sr}-\dot{z}_{ur})-F^*_{mr,r}\sin(\alpha_{mr,r})\right], \end{aligned} \tag{4.3}$$

$$\begin{aligned} m_{uf}\ddot{z}_{uf} =& -k_{uf}(z_{uf}-z_{rf})-c_{uf}(\dot{z}_{uf}-\dot{z}_{rf})-F^*_{mr,f}\sin(\alpha_{mr,f}) \\ & +k_{sf}(z_{sf}-z_{uf})+c_{sf}(\dot{z}_{sf}-\dot{z}_{uf}), \end{aligned} \tag{4.4}$$

$$\begin{aligned} m_{ur}\ddot{z}_{ur} =& -k_{ur}(z_{ur}-z_{rr})-c_{ur}(\dot{z}_{ur}-\dot{z}_{rr})-F^*_{mr,r}\sin(\alpha_{mr,r}) \\ & +k_{sr}(z_{sr}-z_{ur})+c_{sr}(\dot{z}_{sr}-\dot{z}_{ur}), \end{aligned} \tag{4.5}$$

where vehicle body heave displacement and pitch angle are denoted as z_s and φ_{sp}, respectively. Additional inclination of MR dampers is included in the half-car model by introducing angles $\alpha_{mr,f}$ and $\alpha_{mr,r}$. Symbols z_{uf} and z_{ur} denote vertical displacement of wheels. Vertical displacements of the vehicle body z_{sf} and z_{sr} are defined as:

$$z_{sf} = z_s - L_f\varphi_s, \quad z_{sr} = z_s + L_r\varphi_s. \tag{4.6}$$

Parameters of the half-car model were obtained by rescaling these presented in [29] for a full-car model by the factor 0.47 (see [75], Table 4.1), which is evaluated based on comparison of mass of the reference full-car model and mass of the experimental off-road vehicle (see Figure 1.9 in Chapter 1). Parameters of tyre damping were obtained assuming that damping ratio of majority of road vehicle tyres varies close to 0.05 [70]. Modal analysis of the half-car model excluding models of MR dampers was performed, showing 4 resonance frequencies equal to 1.90, 2.13, 7.06 and 13.79 Hz and corresponding damping ratios equal to 0.19, 0.48, 0.46 and 0.28, respectively. First two vibration modes are related to vehicle body, while the latter two correspond to vertical vibrations of wheels.

Table 4.1: Parameters of 4-DOFs half-car model for vehicle pitch dynamics

Vehicle body and suspension system			
$m_s = 348$ kg	$I_{sL} = 359.0$ kgm^2		
$L = 2.348$ m	$L_f = 1.116$ m	$L_r = 1.232$ m	
$k_{sf} = 28.0$ kNm^{-1}	$k_{sr} = 30.4$ kNm^{-1}		
$c_{sf} = 971$ Nsm^{-1}	$c_{sr} = 2464$ Nsm^{-1}		
$\alpha_{mr,f/mr,r} = 63$ °			
Vehicle wheels and tyres			
$m_{uf} = 23.7$ kg	$m_{ur} = 64.3$ kg		
$k_{uf/ur} = 169$ kNm^{-1}	$c_{uf} = 200$ Nsm^{-1}	$c_{ur} = 330$ Nsm^{-1}	
Damped natural frequencies f_n and damping ratios ξ			
front wheel	rear wheel	body heave	body pitch
13.79 Hz	7.06 Hz	1.90 Hz	2.13 Hz
0.28	0.46	0.19	0.48

4.1.2 Different types of road-induced excitation

The level of vehicle vibrations depends not only on the transmissibility of vehicle suspension, but also on the type of road-induced excitation. In the case of the half-car model, heave and pitch vehicle body vibrations are influenced by the relationship of excitation signals of the front and rear vehicle parts. Two particular cases of synchronous and inverted front and rear road-induced excitation can be distinguished for a selected sinusoidal component of an arbitrary spatial displacement PSD function Φ_z (see Equation (2.2) in Chapter 2). In the case of synchronous excitation, the heave vibration mode is mostly excited, while the inverted excitation influences mostly the pitch vibration mode. Those two types of excitation are mainly considered within further simulation-based analysis. They are hardly found in reality but they are very useful for the validation of control algorithms, since they cover a wide range of realistic types of road excitation.

Road-induced excitation of the half-car model can be decomposed into the heave- and pitch-related components, denoted as h_{z_r} and $h_{\varphi_{rp}}$, respectively, according to the following formulas [75]:

$$h_{z_r}(f) = \frac{|Z_r(f)|}{|Z_{rf}(f)|} = \frac{1}{L_{fr}}\sqrt{L_f^2 + L_r^2 + 2L_f L_r \cos(2\pi f t_{d,fr})} \tag{4.7}$$

and

$$h_{\varphi_{rp}}(f) = \frac{|\Phi_{rp}(f)|}{|Z_{rf}(f)|} = \frac{2}{L_f + L_r}\left|\sin\left(2\pi f \frac{t_{d,fr}}{2}\right)\right|, \tag{4.8}$$

where $Z_r(f)$ and $\Phi_{rp}(f)$ meet the following equations:

$$Z_{rf}(f) = Z_r(f) - L_f\Phi_{rp}(f), \;\; Z_{rr}(f) = Z_r(f) + L_r\Phi_{rp}(f). \tag{4.9}$$

The components, described by Equations (4.7) and (4.8), indicate the contribution of heave and pitch to the overall road-induced excitation of the half-car model. Symbol $t_{d,fr}$ denotes time delay between excitation signals of the front and rear vehicle parts and is defined as follows:

$$t_{d,fr} = \frac{L}{v_p}, \tag{4.10}$$

where v_p is assumed as constant and denotes progressive velocity of the vehicle.

In the case of deterministic excitation (i.e. sinusoidal), the vibration control schemes are initially synthesized and validated for both synchronous and inverted cases. Quality

of heave vibration control is tested for the first case, while pitch vibration control is analysed for the second case. Finally, the algorithms are validated for typical road-induced excitation where the relationship between the front and rear excitations depends on both the temporal excitation frequency and the vehicle speed, which is indicated by h_{z_r} and $h_{\varphi_{rp}}$ (see Figure 4.3). The characteristics of heave-related component indicates that the heave component is always greater than zero, which is caused by asymmetry exhibited by the analysed half-car model.

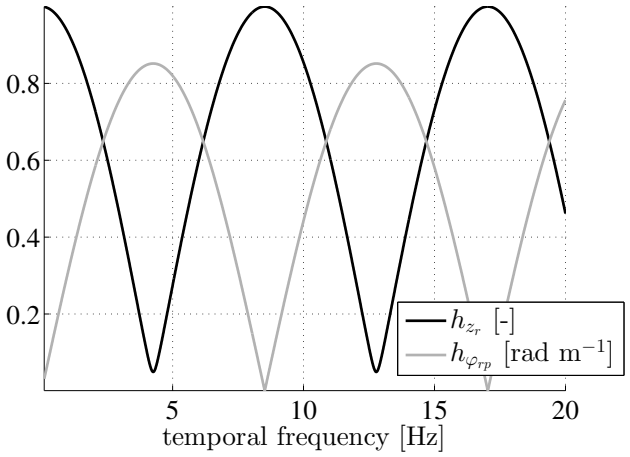

Figure 4.3: Heave- h_{z_r} and pitch-related $h_{\varphi_{rp}}$ components of sinusoidal road-induced excitation for vehicle speed of 20 ms^{-1}

4.1.3 Decoupling of vehicle vibrations

Vibration control performed separately for each DOF within one multi-DOF system is applied in many cases in order to simplify the control system. Generally, each separate algorithm is adjusted using the appropriate quarter-car model obtained by vibration decoupling performed for the analysed system. In the case of the 4-DOF half-car model, two quarter-car models can be obtained, which exhibit 2 DOFs each (see Figure 4.4). Due to their low complexity, they can be additionally applied in theoretical analysis of the suspension dynamics and are used for preliminary analysis of various vibration control algorithms. Moreover, quarter-car models are suitable to describe vertical dynamics of other vehicle parts, such as engine suspension or passenger seats.

Vibrations decoupling performed for half-car model is based on decomposition of the vehicle body mass into the equivalent configuration of the three masses. The two masses denoted as m^*_{sf}, m^*_{sr}, respectively, are related to the front and rear vehicle body,

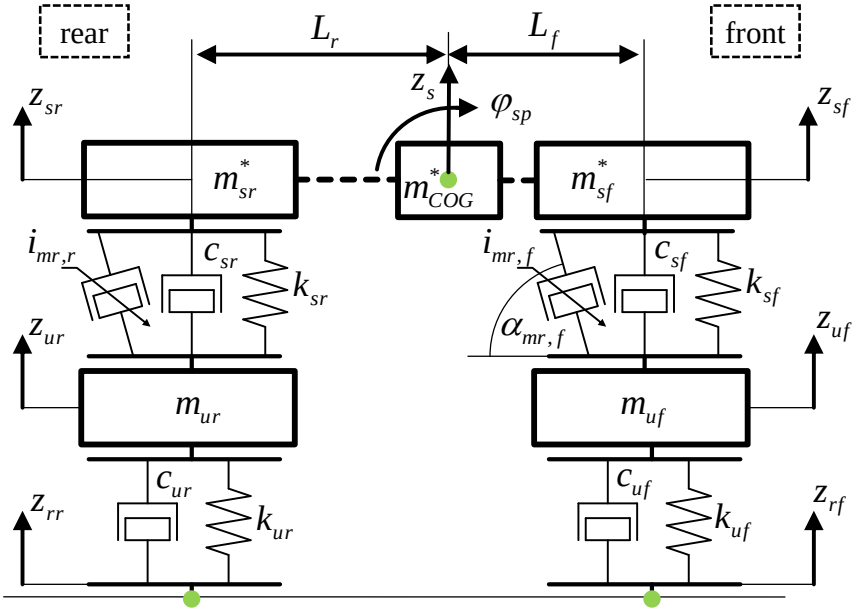

Figure 4.4: Half-car model of vehicle vibrations decoupled into quarter-car models with 2 DOFs including suspension MR dampers

while the last supplementary mass, a so-called coupling mass denoted as m^*_{COG}, either positive or negative, is located in the vehicle body centre of gravity. The coupling mass indicates the level of mutual influence of the vibrations of front and rear vehicle parts. Thus, commercial road vehicles are designed in a way which minimizes the absolute value of the coupling mass [99]. The decoupling process must retain three properties of the vehicle body mass, i.e. location of center of gravity, vehicle body resultant mass and moment of inertia. Thus, the decoupled configuration of vehicle body masses is evaluated due to the following requirements:

$$m^*_{sf} L_f = m^*_{sr} L_r, \tag{4.11}$$

$$m_s = m^*_{sf} + m^*_{sr} + m^*_{COG}, \tag{4.12}$$

$$I_{sL} = m^*_{sf} L_f^2 + m^*_{sr} L_r^2. \tag{4.13}$$

The presented 2-DOF quarter-car model includes two masses and a group of springs and dampers which are related to stiffness and damping of vehicle suspension and tyres. The quarter-car model is defined using two differential equations, where motion of the vehicle body is expressed as follows:

$$m^*_s \ddot{z}_s = k^*_s (z_s - z_u) + c^*_s (\dot{z}_s - \dot{z}_u) + F^*_{mr} \sin(\alpha_{mr}), \tag{4.14}$$

while dynamics of vehicle wheel can be defined according to differential equations shown in (4.4-4.5). Symbols m_s^*, k_s^* and c_s^* denote mass, suspension stiffness and damping of the decoupled quarter of the vehicle and are equivalent to suspension parameters of the half-car model. Parameters of the decoupled front and rear quarter-car models were evaluated using Equations (4.11-4.13) and are listed in Table 4.2. Results of modal analysis excluding models of MR dampers reveal that resonance frequencies of both quarter-car models are close to the corresponding frequencies of the half-car model, where the wheel-related frequencies are close to 7 and 14 Hz and the vehicle-body-related frequencies vary close to 2 Hz. Moreover, decoupling results indicate significant value of the coupling mass, which justifies application of multi-dimensional control algorithms (see details in Chapters 5, 6 and 7).

Table 4.2: Parameters of decoupled 4-DOF half-car model for vehicle pitch dynamics

Front quarter-car model		**Rear quarter-car model**	
$m^*_{COG} = 87$ kg			
$m^*_{sf} = 137$ kg		$m^*_{sr} = 124$ kg	
$k_{uf} = 169$ kNm^{-1}	$c_{uf} = 200$ Nsm^{-1}	$k_{ur} = 169$ kNm^{-1}	$c_{ur} = 330$ Nsm^{-1}
$k_{sf} = 28.0$ kNm^{-1}	$c_{sf} = 971$ Nsm^{-1}	$k_{sr} = 30.4$ kNm^{-1}	$c_{sr} = 2464$ Nsm^{-1}
Damped natural frequencies f_n and damping ratios ξ			
front wheel	front vehicle body	rear wheel	rear vehicle body
13.76 Hz	2.09 Hz	6.85 Hz	2.23 Hz
0.28	0.20	0.47	0.52

4.2 Analysis of vehicle vibrations

Spencer-Dyke model of MR damper dynamics introduces significant nonlinearity into the half-car vehicle model, which limits the analysis to the simulation-based or experimental approaches. Thus, the analytical approach can be applied only for validation of the simulation environment after excluding MR dampers models. Furthermore, in the first stage of research, the simulation approach is favoured over experimental one, since different scenarios can be validated which are impossible to be tested in reality in a repeatable manner.

Studies presented in the current chapter are commonly performed in frequency domain and based on frequency-related quality indices for quasi-passive suspension, i.e.

controlled with invariant MR damper current. Frequency-based analysis can clearly reveal important features of vehicle vibrations, such as resonance frequencies or damping ratios depending on different types of road-induced excitation or applied control currents.

Since presented studies are dedicated to the physical off-road vehicle (see Figure 1.9), operation of the vehicle suspension is analysed within further parts of the dissertation for road classes in range from D to F class. Speed of the moving vehicle is assumed at the standard level of 15 ms^{-1}. Besides, influence of suspension configuration on trade-offs of ride comfort versus road holding and ride comfort versus suspension deflection are studied. The vehicle suspension model is subjected to sinusoidal road excitation $\widetilde{z}_{r,f}$ of compatible and inverted types, which allows to analyse the suspension response for different dominant excitation frequencies f. Meanwhile, the vibration decoupling of half-car model is presented and results for both original and decoupled models are compared.

4.2.1 Description of simulation environment

Simulation environment consists of vehicle vibrations simulator and controller modules. The simulator, whose structure is presented in Figure 4.5, includes linear half-car model of vehicle vibrations described by Equations (4.2-4.6). Additionally, two nonlinear Spencer-Dyke models of MR damper (analysed in Chapter 3) defined by Equations (3.6-3.9) are considered including polynomial relations between current and parameters (see Equation 3.13). The input-current-related dynamics of MR damper model is neglected (see Equation 3.11), while the output dynamics is modelled by Equation (3.12).

Both the vehicle simulator and the controller operate in different time domains, which reflects the situation of the real experiments when only a finite sampling frequency can be reached. The vehicle simulator operates in so-called quasi-continuous time domain, since the related linear and nonlinear differential equations describing the overall vibrations of vehicle are solved numerically using Runge-Kutta method with varying integration step.

All measurement signals are sampled with a longer sampling period denoted as $T_s = 2$ ms. Thus, the control scheme is evaluated in discrete-time domain, while control current signals are fed back to the simulator module after reconstruction using

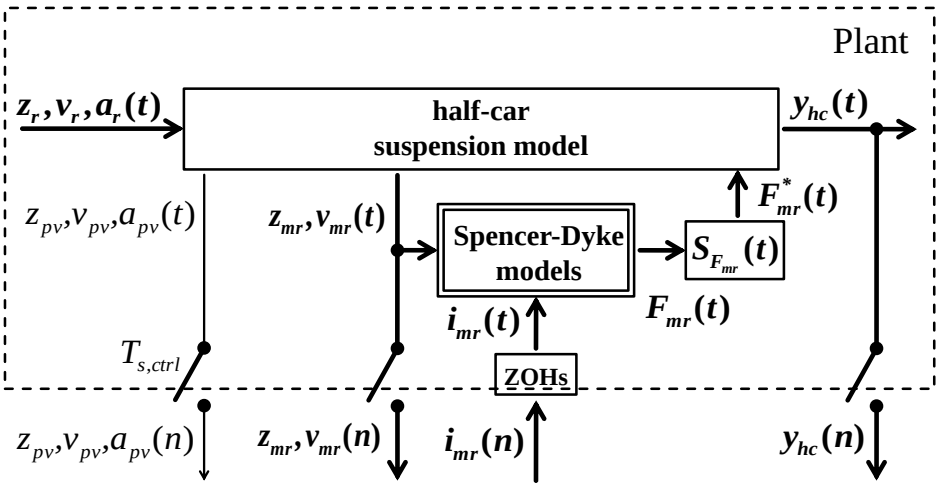

Figure 4.5: Block diagram of the vehicle vibrations simulation environment

zero-order hold. Herein, a vector of general vehicle response signals $\boldsymbol{y_{hc}}$ is available for the controller, while additional measurements of relative MR damper motion $\boldsymbol{z_{mr}}$, $\boldsymbol{v_{mr}}$, $\boldsymbol{a_{mr}}$ and road profile z_{pv}, v_{pv}, a_{pv} are distinguished separately.

4.2.2 Validation of simulation environment

After excluding Spencer-Dyke model, the linear part of the simulation environment was validated by comparing model responses obtained analytically with those of two cases evaluated numerically. Response of the linear part is influenced by the sinusoidal road-induced disturbance $\widetilde{z}_r$ and forces F^*_{mr} generated by additional dampers. In order to validate both disturbance-related and control-related signal paths the parameters of suspension viscous damping parameters c_{sf} and c_{sr} were doubled, comparing to those listed in Table 4.1. In the first numerical case, viscous damping parameters were modified without using any additional damper. In the second case, additional linear dampers were introduced in the model in place of MR dampers.

Results obtained for analytical case were compared with those obtained for numerical approach assuming similar viscous damping parameters. Transmissibility characteristics obtained for acceleration of front and rear wheels as well as heave and pitch vehicle body vibrations within frequency range of 20 Hz were used for validation (see comparisons in Figure 4.6). Since the consistency between characteristics is shown, it is stated that the simulation environment was implemented properly and may be utilized for further research.

Transmissibility characteristics for both numerical cases were plotted according to the definition of ride-comfort-related acceleration transmissibility defined in Equation (2.9). In the case of analytical approach, the transmissibility characteristics were evaluated after reformulating differential Equations (4.2-4.6) of the linear half-car model into the general matrix form representation of the mechanical system presented in Equation (4.1). Moreover, such matrix form is converted into the matrix form of state $\boldsymbol{x_{hc}}$ and output $\boldsymbol{y_{hc}}$ differential equations as follows:

$$\begin{gathered}\dot{\boldsymbol{x}}_{\boldsymbol{hc}} = \boldsymbol{A_{hc}} \cdot \boldsymbol{x_{hc}} + \boldsymbol{B_{hc}} \cdot \boldsymbol{u_{hc}} \\ \Updownarrow \\ \begin{bmatrix} \dot{\boldsymbol{q}}_{\boldsymbol{hc}} \\ \ddot{\boldsymbol{q}}_{\boldsymbol{hc}} \end{bmatrix} = \begin{bmatrix} \boldsymbol{0} & \boldsymbol{1} \\ -\boldsymbol{M}^{-1}\boldsymbol{K} & -\boldsymbol{M}^{-1}\boldsymbol{C} \end{bmatrix} \cdot \begin{bmatrix} \boldsymbol{q_{hc}} \\ \dot{\boldsymbol{q}}_{\boldsymbol{hc}} \end{bmatrix} + \begin{bmatrix} \boldsymbol{0} \\ \boldsymbol{M}^{-1} \end{bmatrix} \cdot \boldsymbol{u_{hc}},\end{gathered} \tag{4.15}$$

$$\boldsymbol{y_{hc}} = \boldsymbol{C_{hc}} \cdot \boldsymbol{x_{hc}} + \boldsymbol{D_{hc}} \cdot \boldsymbol{u_{hc}}, \tag{4.16}$$

where matrices $\boldsymbol{A_{hc}}$, $\boldsymbol{B_{hc}}$, $\boldsymbol{C_{hc}}$ and $\boldsymbol{D_{hc}}$ are used for analytical evaluation of the transmissibility characteristics. Extended description of characteristics evaluation process as well as consecutive steps of half-car model reformulation are presented in Appendix C.

Selected types of transmissibility dedicated to sinusoidal excitation are applied within the further analysis. In the case of safety issues, the suspension deflection and road holding quality indices are evaluated based on $\widetilde{T}_{z_r,z_{us,j}}$ and $\widetilde{T}_{z_r,z_{ru,j}}$ transmissibilities, respectively. Symbol j denotes front or rear vehicle part. Moreover, description of wheel acceleration is used in the preliminary studies performed based on $\widetilde{T}_{a_r,a_{u,j}}$. Vibrations of the vehicle body part can be analysed using $\widetilde{T}_{a_r,a_{s,j}}$, $\widetilde{T}_{a_r,a_s}$ or $\widetilde{T}_{a_r,\epsilon_{sp}}$ for the front or the rear vehicle body parts as well as heave and pitch vehicle body vibration modes, respectively. Conclusions drawn in Chapter 2 suggest analysis of vibrations power with respect to human body and comfort issues based on vertical acceleration measurements. Thus, an averaged effective value of vehicle body acceleration was derived based on vertical acceleration signals in the front and rear vehicle body as follows:

$$a_{s,avg} = \sqrt{\frac{1}{L}\int_0^L a_{s,l}^2 dl}, \tag{4.17}$$

which stands for an averaged integral of squared acceleration taken for all points of vehicle body part, where acceleration of certain vehicle body point is denoted as $a_{s,l}$.

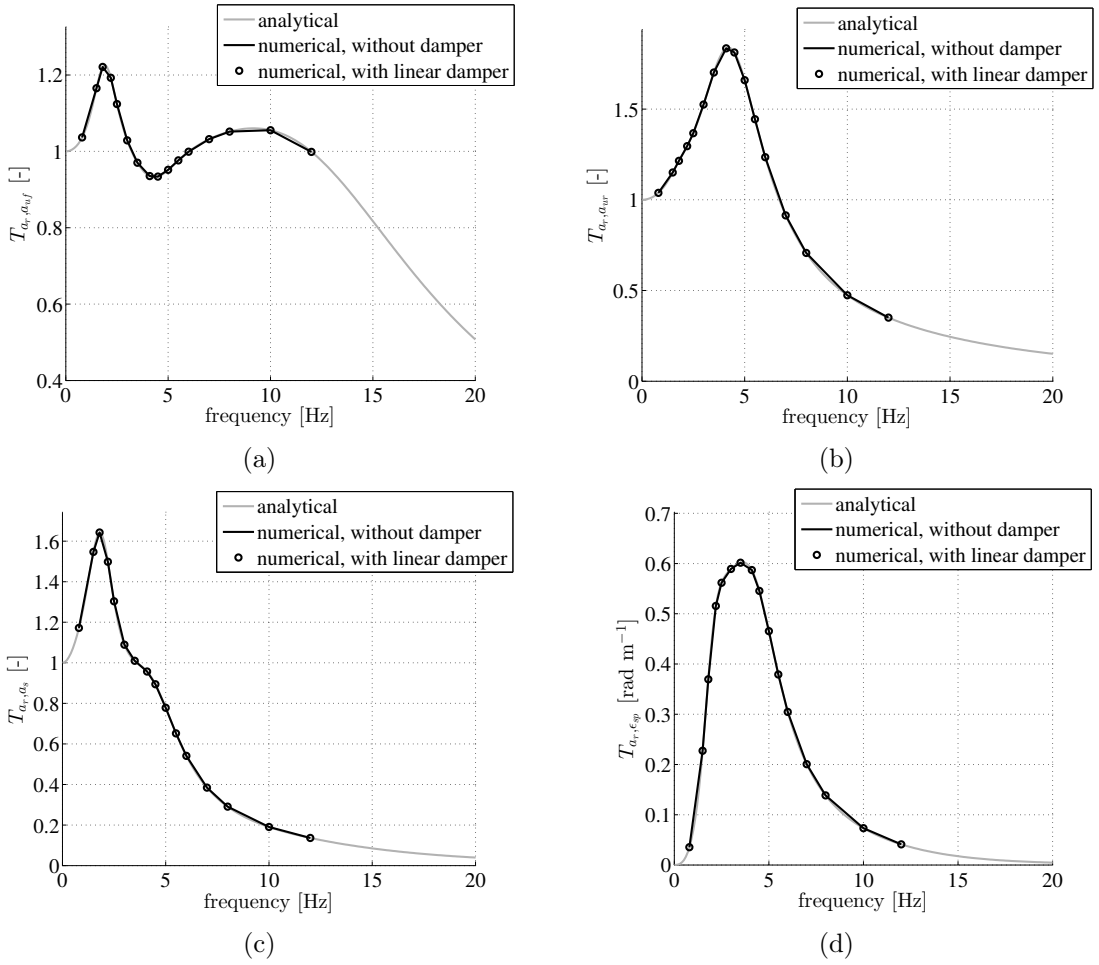

Figure 4.6: Validation of linear part of the simulation environment for doubled suspension viscous damping parameters using acceleration transmissibility characteristics obtained for: a) front wheel, b) rear wheel, c) vehicle body heave and d) pitch vibrations

Such quality signal is mainly used in further analysis related to ride comfort in the form of vehicle body acceleration transmissibility denoted as $\widetilde{T}_{a_r,a_{s,avg}}$, evaluated for both the compatible and inverted road excitation.

4.2.3 Analysis of decoupled vehicle vibration model

Decoupling procedure of half-car model vibrations including Spencer-Dyke models, which was reported in Section 4.1.3, was validated numerically. Three cases related to different models of vehicle vibration were analysed, i.e.: the half-car with modified vehicle body mass, decoupled front and rear 2-DOF quarter-car models as well as the nominal half-car model before modification. Vehicle body mass of the modified half-car model was changed by subtracting the coupling mass m^*_{COG} value from the nominal vehicle body mass in order to make the ideal vibrations decoupling possible.

Validation of the decoupling process was performed for sinusoidal road-induced excitation of road class F. Responses of the front and rear vehicle body parts were compared using comfort-related acceleration transmissibility characteristics evaluated according to expression (2.9) within frequency range of 25 Hz (see Figure 4.7). Consistency between results obtained for the modified half-car model and those obtained for the separate decoupled quarter-car models indicates correctness of the vibration decoupling. Besides, in order to study influence of the decoupling-related modification on model features, the characteristics evaluated for the nominal half-car model is shown. It is indicated within results of the modal analysis shown in Tables 4.1 and 4.2 and by comparing the nominal and modified half-car models that due to the decreased vehicle body mass, both heave and pitch resonance frequencies increased. Such observation was confirmed by the increased values of resonance frequencies of the front and rear vehicle body vibrations, which is shown in the given frequency characteristics.

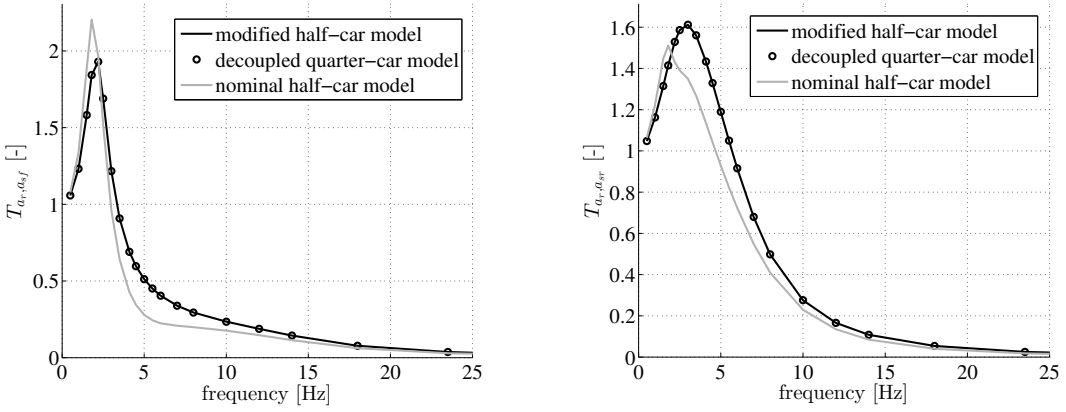

Figure 4.7: Validation of vibrations decoupling procedure for modified and nominal 4-DOF half-car models as well as decoupled 2-DOF quarter-car models in the case of road class F, using acceleration transmissibility characteristics evaluated for: a) front vehicle sprung mass, b) rear vehicle sprung mass

4.2.4 Characteristic features of nonlinear vehicle suspension

Nonlinearity of the applied Spencer-Dyke MR damper models requires the analysis of vehicle vibrations to be related not only to different control current value, but also to different types of road-induced excitations and their amplitudes. Further analysis is focused on nonlinearity introduced by MR dampers. Road vehicles are additionally susceptible to significant discontinuities caused by limitation of suspension deflection and

wheels loss of traction phenomena. However, such phenomena are not taken into account in the presented analysis.

Both the control currents and amplitudes of the road-induced excitation influence the resultant linearized damping caused by automotive MR dampers. A series of vehicle body acceleration transmissibility characteristics is shown in Figure 4.8 for compatible and inverted front and rear road excitation. The results were evaluated for control current values of the front and rear MR damper varying from 0 to 0.4 A and road classes D, E and F, respectively. Despite the fact that the MR damper was examined for control current values up to 1.3 A (see Chapter 3), the current value of 0.4 A already gives a significant increase in suspension damping parameters. Thus, evaluation of the transmissibility characteristics for greater currents is omitted.

Invariant points of the transmissibility characteristics are inherent features of certain vehicle suspension model. For the half-car model, the invariant points were revealed for 2.4 Hz and 2.9 Hz for compatible and inverted types, respectively. Furthermore, such invariant points exhibit similar values of transmissibility characteristics for all analysed road classes which can facilitate associating the different experimental cases performed within future research.

The results obtained for all considered road classes also show that the greater control current value, the stiffer the vehicle body is fixed with wheels and more features of the reduced-order 2-DOF half-car are exhibited by the 4-DOF half-car model. Such reduced-order model has heave resonance frequency equal to 4.2 Hz, which is noticeable in the given characteristics and was confirmed based on modal analysis performed for linear half-car model with significantly increased suspension damping parameters.

Response of the vehicle suspension with MR dampers is significantly related to the type of road-induced excitation. Due to saturation regions in force-velocity characteristics of MR damper, its resultant linearized damping decreases with respect to the amplitude of piston excitation. Comparison of acceleration transmissibility characteristics evaluated for values of control current equal to 0, 0.05 and 0.2 A are shown in Figure 4.9. It is shown that the greater the amplitude of road-induced excitation (worse road class), the greater value of current needs to be generated in order to reach similar resultant suspension damping parameters.

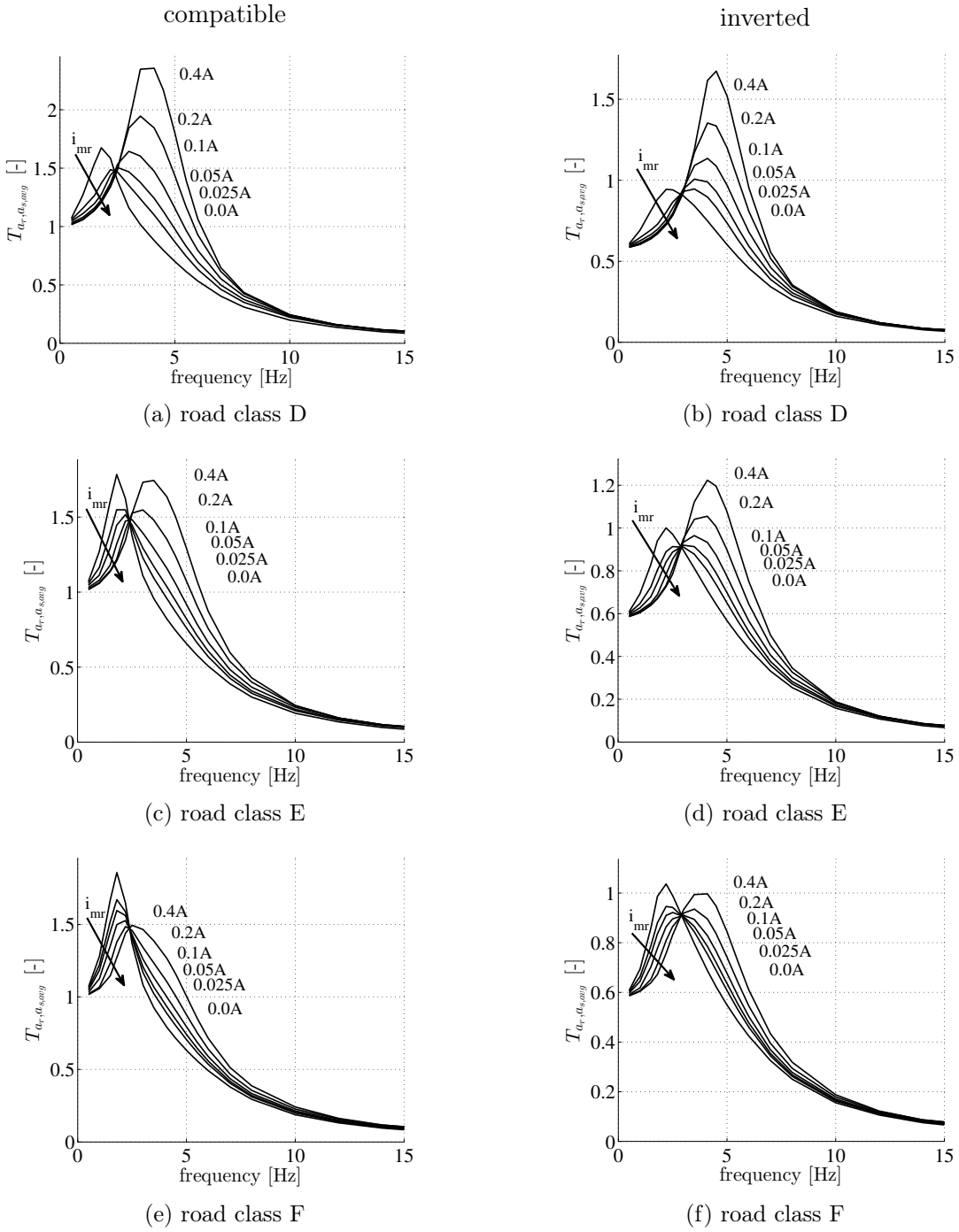

(a) road class D (b) road class D

(c) road class E (d) road class E

(e) road class F (f) road class F

Figure 4.8: Comparison of body acceleration transmissibility characteristics evaluated for different values of control current and two types of road-induced excitation, i.e. compatible and inverted sinusoidal excitation: a-b) road class D, c-d) road class E, e-f) road class F

4.2.5 Ride comfort versus suspension deflection and road holding

Ride comfort, road holding and suspension deflection indices are strictly related to each other and are recommended to be analysed simultaneously. Since they are related

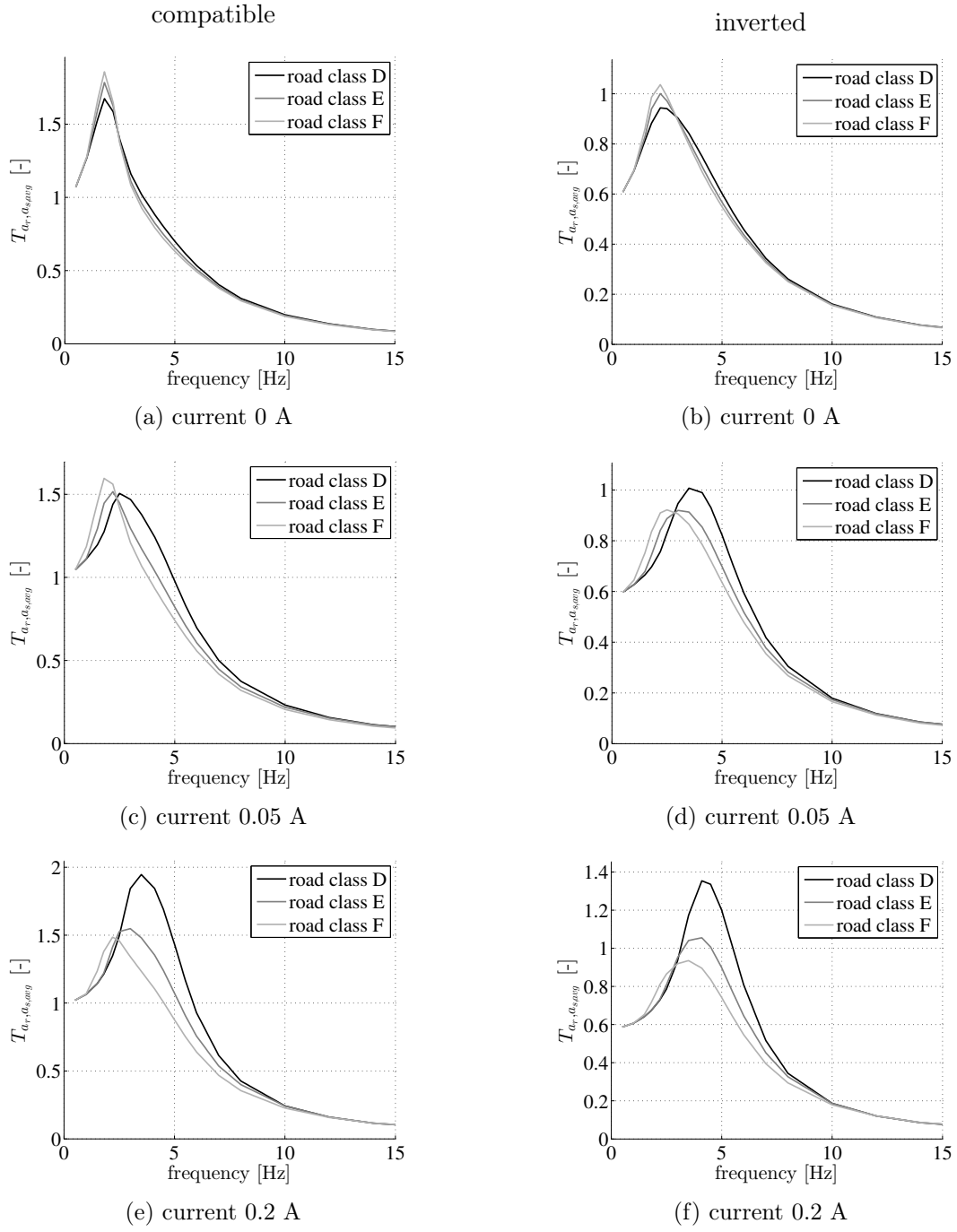

(a) current 0 A (b) current 0 A

(c) current 0.05 A (d) current 0.05 A

(e) current 0.2 A (f) current 0.2 A

Figure 4.9: Comparison of body acceleration transmissibility characteristics evaluated for compatible and inverted excitation, as well as different road classes and control currents equal to: a-b) 0 A, c-d) 0.05 A, e-f) 0.2 A

to the level of vehicle vibrations which are to be mitigated, goal of the vibration control system is to minimize their values as much as possible.

In the case of passive suspension system, improving ride comfort always deteriorates the latter indices. During the design process of road vehicle, parameters of its suspension system are adjusted in order to obtain certain goals, resulting in comfort- or

safety-targeted vehicle suspension corresponding to damping ratios equal to 0.3 or 0.7, respectively (see Chapter 1).

The below-presented diagrams of road holding and suspension deflection versus ride comfort indices were obtained using definitions of indices $\widetilde{J}_{RH}$, $\widetilde{J}_{SD}$, $\widetilde{J}_{RC}$ for sinusoidal excitation introduced in Equations (2.11), (2.13), (2.14). The analysed indices were normalised according to the following formula:

$$NJ_{RC} = \sqrt{\frac{1}{2}\left(\frac{\widetilde{J}^2_{RC,comp}}{\widetilde{J}^2_{RC,0,comp}} + \frac{\widetilde{J}^2_{RC,inv}}{\widetilde{J}^2_{RC,0,inv}}\right)}, \tag{4.18}$$

where $\widetilde{J}_{RC,0,comp}$ and $\widetilde{J}_{RC,0,inv}$ denote reference ride comfort indices which in the presented case were obtained based on analytical results given by the linear part of nominal half-car model (see Table 4.1). Subscripts *comp* and *inv* indicate compatible and inverted types of road excitation. Similarly to NJ_{RC}, the normalized indices dedicated to suspension deflection or road holding were defined and denoted as NJ_{SD} or NJ_{RH}, respectively.

Different scenarios were analysed, including the linear half-car model and its nonlinear representation with MR damper models (see Figure 4.10). Initially, diagrams for linear half-car model were analytically evaluated, assuming that damping parameters of the front and rear suspension c_s were changing from 40% to 600% of their nominal values. Additionally, suspension damping parameters were modified for consecutive experiments in such a way that damping ratios related to sprung masses obtained for the resultant decoupled quarter-car models (see Table 4.2) were equal to 0.3 or 0.7 which are related to a comfortable road vehicle or a racing car [56].

Further analysis is performed for nonlinear vehicle suspension including MR damper models, for road classes D, E and F. Such diagrams are evaluated for values of control current varying from 0 to 0.4 A, whereas control currents were the same for the front and rear suspension parts. It can be noticed that different types of road-induced excitation result in different shapes of shown diagrams. Since curves obtained for the nonlinear cases do not overlap the one obtained for linear suspension, detailed analysis of nonlinear suspension is especially recommended. Besides, the effect of MR damper nonlinearity is shown where for lower amplitude of road excitation the results can be obtained which indicate higher equivalent suspension damping parameters.

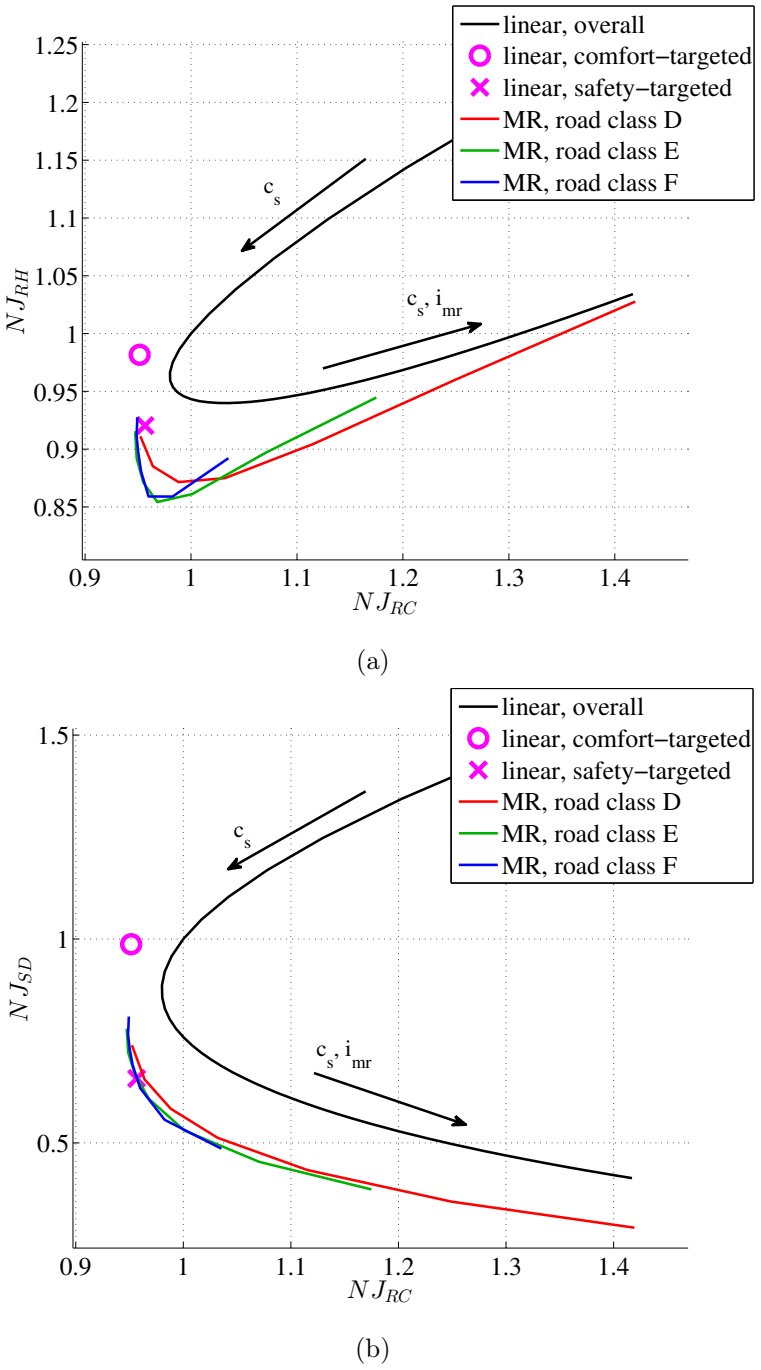

Figure 4.10: Comparison of performance of linear vehicle suspension including comfort- and safety-targeted configurations as well as of MR-damper-equipped vehicle suspension subjected to road-induced excitation of different road classes: a) road holding and b) suspension deflection indices versus ride comfort index

4.3 Summary

Modelling of vehicle vibrations plays a crucial role in vehicle vibration control. The more parameters are included in such model, the more difficulties are involved in model

analysis and application. Thus, the model of vehicle vibrations was simplified and described using 4-DOF half-car and decoupled 2-DOF quarter-car models. Two approaches to the analysis of vehicle vibrations were applied, i.e.: comfort-related acceleration transmissibility characteristics as well as diagrams of road holding and suspension deflection indices versus ride comfort index. Both approaches confirm the complexity of nonlinear vehicle suspension equipped with MR dampers and its responses varying for different types of road-induced excitation. Results and conclusions drawn in the presented chapter were used for comparison and analysis in further Chapters related to semiactive vehicle vibration control.

Chapter 5

Semiactive control of vehicle vibrations

Vehicle suspension systems with MR dampers are controlled by adjusting their damping parameters. Thus, they belong to the group of bilinear dynamic systems [105]. Bilinear systems represent a specific case of nonlinear systems which are uncontrollable in zero state. Such feature can be clearly shown in the case of unmoving vehicle suspension, when the state of the installed MR dampers cannot be influenced.

The complexity of semiactive suspension controller is additionally increased because of the significant nonlinearity of MR damper behaviour. Generally, control schemes related to MR dampers are decomposed into separate inverse models of the MR dampers and main vehicle suspension control (see Figure 5.1). The main control algorithm gives a desired forces $\boldsymbol{F_{alg}}$ which are to be generated by the MR dampers for the front and the rear vehicle parts. The inverse models take advantage of signals describing relative motion of damper pistons, i.e. $\boldsymbol{z_{mr}}$, $\boldsymbol{v_{mr}}$ and $\boldsymbol{a_{mr}}$. Such models are used for partial linearization of MR damper characteristics and give values of control currents $\boldsymbol{i_{mr}}$.

Vehicle suspension control can be divided into adaptive and non-adaptive or feedback and feedforward control approaches. The feedback control is applied using signals of the vehicle response $\boldsymbol{y_{hf}}$ while the feedforward control can be added using signals z_{pv}, v_{pv}, a_{pv} which describe the road profile in front of the vehicle. Moreover, suspension control algorithms can be grouped with respect to their scalability to different road vehicle constructions. The current chapter is related to the well-known classical semiactive

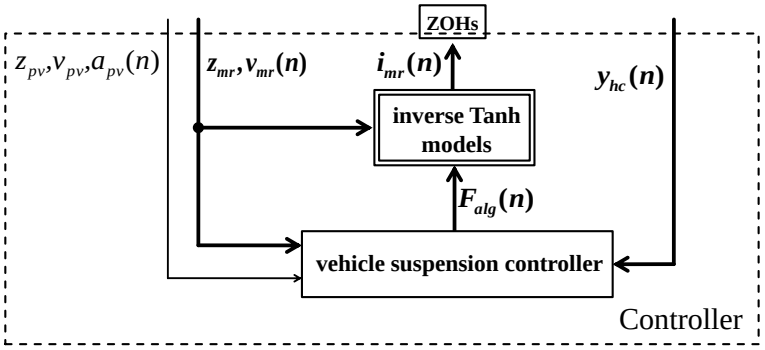

Figure 5.1: Block diagram of the simulation environment for a vehicle suspension controller

control algorithms which are non-adaptive and belongs to the group of feedback control schemes, as well as are dedicated to automotive MR dampers.

5.1 Topology of suspension control

Vehicle suspension control system can be organised in a hierarchical topology including layers related to optimization, vibration control and MR damper force control (see Figure 5.2). The optimization layer is responsible for solving a trade-off between contradictory goals, i.e. ride comfort and driving safety. The solution can be obtained based on instantaneous road conditions using online analysis and classification of road situations in relation to corresponding responses of the vehicle. Algorithms for prediction of a vehicle rollover, loss of traction or detection of suspension bottoming out and its failure can be applied herein.

Since the vehicle suspension, which is controlled, is strongly nonlinear, for some cases it is recommended to solve the ride comfort versus driving safety trade-off in real time during vehicle ride. Algorithms of the optimization control layer are commonly implemented in the supervisory control unit and can take advantage of different sophisticated artificial intelligence methods, e.g. neural networks or evolutionary optimization algorithms which operate with longer time periods in comparison to algorithms within lower control layers. Consequently, results of higher level analysis are passed in the form of desired control gains to the lower vibration control layer.

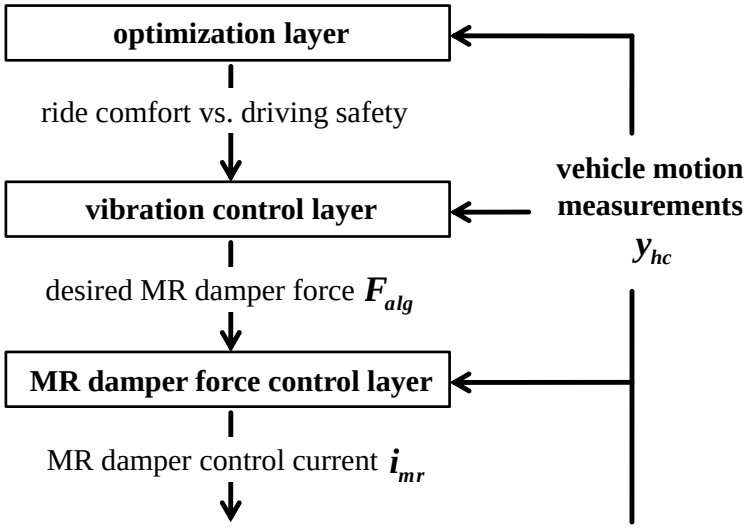

Figure 5.2: Topology of the semiactive control system for vehicle suspension

5.1.1 State-of-the-art in vehicle vibration control

The vibration control layer is responsible for transforming solutions of ride comfort versus driving safety trade-offs to appropriate desired forces which are to be generated by the actuators, i.e. MR dampers. Several criteria of grouping of vibration control algorithms can be distinguished. Control algorithms can be differed based on type of their structure or the quality index which is to be minimized. Furthermore, adaptive control schemes form a separate group apart from the non-adaptive control approaches. This chapter is focused on non-adaptive control, while adaptive algorithms are proposed in Chapter 6.

General structure of semiactive control can be introduced as a composition of feedback and feedforward components, as it was presented in Figure 5.1. The mixed feedforward-feedback control structure for the mitigation of vehicle vibrations is distinguished in the literature as the preview control. In the case of feedforward control, the finite response time of the semiactive devices can be compensated using additional reference signal obtained as road profile measured in front of a vehicle. Such reference signal can be collected by an additional road scanning devices, such as laser scanner or ultrasound sensor. Studies on preview control were started based on a simplified quarter-car model assuming that active suspension elements are applied [48]. Furthermore, the analysis was extended to semiactive suspension dampers [49] and a half-car

model [50]. Within the further research different vehicle models and different types of vehicle suspension presented in the literature [46, 94, 114] were analysed.

All algorithms presented above are synthesized in order to minimize a quadratic quality function in the infinite-time or finite-time horizon. Contrary to that, some authors proposed synthesis of control schemes based on a quality index defined using an infinity norm, which results in a robust control formulated for both active and quarter-car [117] or semiactive and half-car [111] models. Since mitigation of vibrations of selected vehicle parts can be assumed as critical as well as semiactivity itself introduces additional constraints set on control forces, the robust control approach is recommended in some cases.

Feedforward control applied in vehicles requires additional measuring devices. Thus, common vehicle suspension control systems are limited to feedback control, which simplifies the structure of the control system and implementation of the control algorithm as well as reduces cost of future commercial applications. Generally, classical LQ control is applied and adjusted to semiactive devices resulting in clipped-LQ control. Optimal LQ control was initially proposed for active vehicle suspensions [52, 53, 82], while further studies were aimed at its application for automotive MR dampers [75, 76, 130]. Similarly to LQ control, the feedback robust control, i.e. H_∞ is applied for vehicle vibration control and presented in [23, 30, 44, 133].

LQ control applied to vehicle suspension can commonly be optimized for certain vehicle body vibration modes, i.e. pitch or heave as well as for wheels vibrations, resulting in specific Skyhook or Groundhook control algorithms. For such algorithms, the vector of feedback variables is limited to vertical velocities of the vehicle body or wheels comparing to LQ control which takes advantage of a full vector of state variables. The Skyhook algorithm was introduced in [64] based on a quarter-car model. Further applications of Skyhook algorithm were presented in the following papers related to the quarter-car [22, 42, 79, 93, 108, 122], half-car [77] and full-car [56] model.

Some types of vehicles, e.g. heavy vehicles are particularly exposed to loss of traction while performing road manoeuvres, which is induced by significant mass of their vehicle bodies. They require paying more attention to vibrations of wheels in order to improve driving safety. Thus, LQ control was optimized for wheel vibrations resulting in Groundhook control [56, 126]. Skyhook and Groundhook control approaches were extended to

Hybrid approach, where influence of both algorithms is weighted depending on instantaneous road conditions. Both algorithms can also be applied in the so-called On-Off MR damper control approach, where damping coefficients are not adjusted smoothly using inverse MR damper model, but switched between two control current values [1, 92, 104]. However, the control based on the inverse model is commonly applied.

Numerous nonlinear control approaches were proposed in the literature. Initially, the linear feedback applied in Skyhook control was replaced by a nonlinear one in [85], while H_∞ was extended to LPV (linear parameter-varying) controller [110]. Other authors proposed application of fuzzy controllers [84, 91, 101] and neural networks [41, 75, 76, 113] in both active and semiactive vehicle control. Genetic algorithms are widely used for offline optimization of vibration control algorithms, apart from being applied within the already mentioned online optimization layer [20, 29, 101]. However, long time response and difficulties in implementation and real-time execution make it difficult to use such algorithms in wider applications related to road vehicles, especially commercial.

5.1.2 MR damper force control layer

The MR damper force control layer is used for generation of the appropriate control current signal which gives the control force generated by the MR damper close to that desired by the vibration control layer. The main disadvantage of vehicular applications, including the analysed experimental vehicle, is a common lack of force sensors and difficulties related to their assembly. Such limitation requires application of feedforward control of MR damper force based on the MR damper inverse model which partially linearises the relationships defined from damper piston motion to force and from control current to force. Semiactive behaviour, inaccuracy of the inverse model and changes in MR damper parameters during its exploitation are the main sources of errors in predicting the appropriate value of control current.

Ideal inversion of the MR damper model would occur if an actual MR damper was fully compatible with its model. Such case shows the maximum range of possible forces generated by the MR damper for its instantaneous state. It is a hypothetical case, since MR damper behaviour is strongly nonlinear and no ideal inverse model can be obtained. Furthermore, constraints set on control current, i.e. the lower and upper bounds limiting

current to realistic, only positive values introduce semiactivity into the system and cannot be overpassed. Such constraints can be presented in the form of a dissipative domain of the MR damper - it cannot be improved even if the inverse model is ideal (see Figure 5.3). Desired force value F_{alg} which is outside the dissipative domain should be automatically transformed to this realistic one (denoted as F_{mr}) which is inside it. The MR damper dissipative domain is obtained by evaluating force-velocity characteristics for all possible control currents which range from 0 to 1.3 A. Such characteristics is obtained for the reference Spencer-Dyke model and for compensated force-velocity hysteretic behaviour (see Chapter 3 and Appendix A).

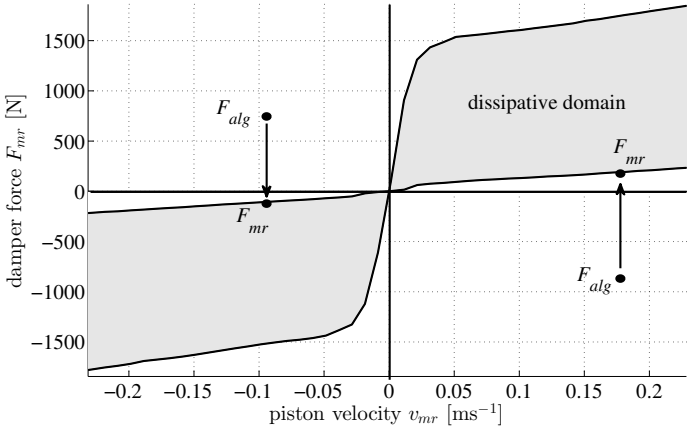

Figure 5.3: Dissipative domain of automotive MR damper obtained using the reference Spencer-Dyke model

The half-car model of a vehicle with MR dampers can be decomposed into primary and secondary signal paths [67]. The primary signal path corresponds to dynamics defined from the road-induced excitation, treated as a system disturbance, to selected vibration modes of the vehicle body which are minimized by the control algorithm. The linear part of half-car secondary signal path is the dynamics defined from MR damper force F_{mr} to vehicle body motion y_{hc} and described by the transmissibility $T_{F_{mr},y_{hc}}$. Full secondary path consists of the inverse Tanh model included in the controller, the reference Spencer-Dyke model included in the vehicle model and the transmissibility $T_{F_{mr},y_{hc}}$ (see Figure 5.4). For ideal inverse modelling, the inverse and the reference models can be simplified to one force saturation block which corresponds to the MR damper dissipative domain.

Analysis of the linear part of secondary signal path was performed for vehicle body

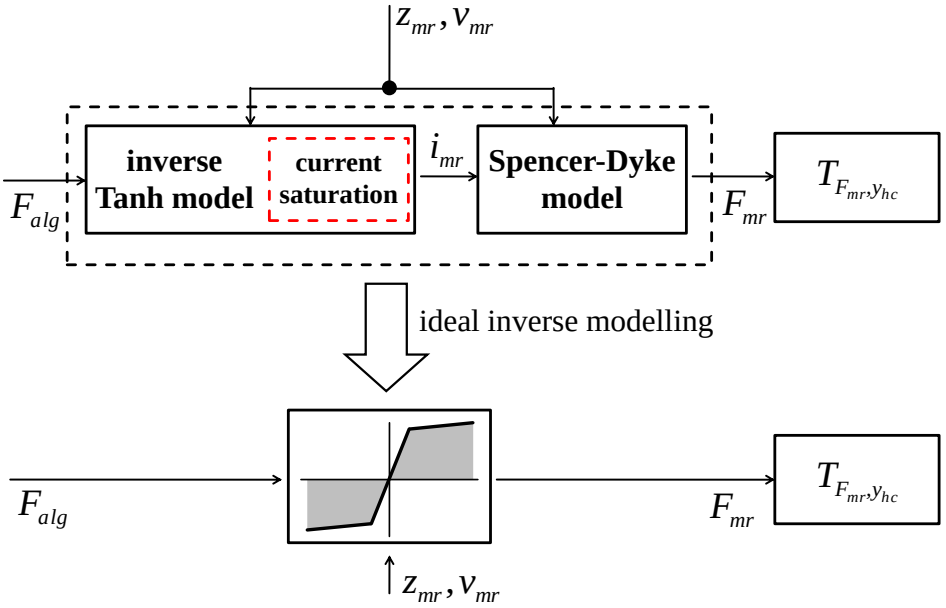

Figure 5.4: Secondary signal path for vehicle suspension with MR damper and its simplification for ideal inverse modelling

heave a_s and pitch ϵ_{sp} signals since they clearly define motion of the vehicle body. The influence of forces generated by both front $F_{mr,f}$ and rear $F_{mr,r}$ MR dampers was shown in the form of characteristics evaluated for transmissibilities denoted as $T_{F_{mr,f},a_s}$, $T_{F_{mr,r},a_s}$, $T_{F_{mr,f},\epsilon_{sp}}$ and $T_{F_{mr,r},\epsilon_{sp}}$ defined from selected MR damper forces to selected vehicle responses (see Figure 5.5). Such characteristics indicate that the vehicle responses can be influenced by the control forces F_{alg} for the whole frequency band from 0 to 25 Hz, while vibration control for heave and pitch resonance at 1.90 Hz and 2.13 Hz, respectively, are particularly preferred. However, it is also shown, that heave and pitch related control is significantly deteriorated for front and rear wheel resonance at frequencies equal to 13.79 Hz and 7.06 Hz, respectively.

5.2 Synthesis of classical control schemes

The following analysis of classical control schemes which are presented in the current chapter and in Chapter 6 is mainly focused on Skyhook control related to the quarter-car and the half-car models. These algorithms are commonly presented in the literature as a reference in semiactive control of vehicle suspension due to their low complexity and reliability. The LQ control is not recommended to be included in the final comparison of semiactive control since it requires all state variables whereas not all of them are

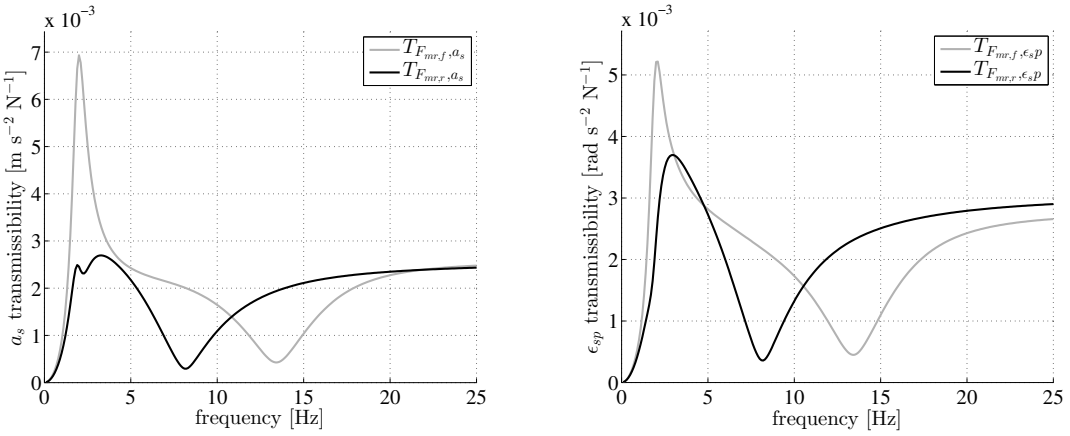

Figure 5.5: Transmissibility characteristics of linear part of the half-car model secondary path for forces generated by the front and the rear MR dampers: a) heave acceleration, b) pitch acceleration

measurable. The immeasurable signals can be additionally estimated which makes the algorithm more complex and sensitive to measurement noise. They can be also assumed as available within simulation-based research which favours the LQ control over simplified Skyhook control schemes. It was shown that Skyhook control scheme has its origin in LQ problem [64]. Thus, the analysis of the full-state LQ control scheme is followed by description of Skyhook algorithm and presented as an introduction to the classical semiactive control scheme.

Validation of the presented algorithms is accompanied by application of the inverse Tanh model, which was evaluated in Chapter 3. It was indicated that numerical errors included in the simulated signals of damper piston acceleration a_{mr} significantly deteriorate the control current i_{mr} obtained from the inverse model. Thus, in the further studies the acceleration a_{mr} was neglected within the inverse model by setting its hysteresis-related parameter γ_{th} to zero.

5.2.1 LQ control related to MR dampers

In LQ control all excitation signals of a vehicle which cannot be influenced by the controller need to be assumed as disturbances. Thus, state and output matrices defined by Equations (4.15-4.16) are reformulated by separating road-induced excitations and

control forces as follows:

$$\dot{\boldsymbol{x}}_{\boldsymbol{hc}} = \boldsymbol{A}_{\boldsymbol{hc}} \cdot \boldsymbol{x}_{\boldsymbol{hc}} + \boldsymbol{B}_{\boldsymbol{hc,F}} \cdot \boldsymbol{F}_{\boldsymbol{alg}} + \boldsymbol{B}_{\boldsymbol{hc,r}} \cdot \boldsymbol{u}_{\boldsymbol{r}}, \tag{5.1}$$

$$\boldsymbol{y}_{\boldsymbol{hc}} = \boldsymbol{C}_{\boldsymbol{hc}} \cdot \boldsymbol{x}_{\boldsymbol{hc}} + \boldsymbol{D}_{\boldsymbol{hc,F}} \cdot \boldsymbol{F}_{\boldsymbol{alg}} + \boldsymbol{D}_{\boldsymbol{hc,r}} \cdot \boldsymbol{u}_{\boldsymbol{r}}, \tag{5.2}$$

where matrices $\boldsymbol{B}_{\boldsymbol{hc,F}}$, $\boldsymbol{D}_{\boldsymbol{hc,F}}$ and $\boldsymbol{B}_{\boldsymbol{hc,r}}$, $\boldsymbol{D}_{\boldsymbol{hc,r}}$ are related to control forces and road-induced disturbances, respectively. Thus, previously defined general excitation of the system $\boldsymbol{u}_{\boldsymbol{hc}}$ used in Equations (4.15-4.16) was decomposed into a vector of control forces generated by front and rear automotive MR dampers $\boldsymbol{F}_{\boldsymbol{alg}} = [F_{alg,f}, F_{alg,r}]^T$ and a vector of derivatives of road-induced excitation signals of the front and rear vehicle parts $\boldsymbol{u}_{\boldsymbol{r}} = [z_{rf}, v_{rf}, a_{rf}, z_{rr}, v_{rr}, a_{rr}]^T$.

The time-infinite quadratic cost function which is to be minimized by LQ control is defined as a weighted sum of squared state variables of the half-car model $\boldsymbol{x}_{\boldsymbol{hc}}$ and control forces $\boldsymbol{F}_{\boldsymbol{alg}}$ as follows:

$$J_{LQ} = \int_0^\infty [\boldsymbol{x}_{\boldsymbol{hc}}(\tau)^T \boldsymbol{Q}_{\boldsymbol{x}} \boldsymbol{x}_{\boldsymbol{hc}}(\tau) + \boldsymbol{F}_{\boldsymbol{alg}}(\tau)^T \boldsymbol{Q}_{\boldsymbol{F}} \boldsymbol{F}_{\boldsymbol{alg}}(\tau)] d\tau. \tag{5.3}$$

Synthesis of the algorithm is initialized by indirect definition of diagonal weighting matrices $\boldsymbol{Q}_{\boldsymbol{x}}$ and $\boldsymbol{Q}_{\boldsymbol{F}}$ according to the Bryson's rule (5.4), see e.g. [13]:

$$\boldsymbol{Q}_{\boldsymbol{x}} = {\boldsymbol{S}_{\boldsymbol{x}}}^{-2}, \quad \boldsymbol{Q}_{\boldsymbol{F}} = {\boldsymbol{S}_{\boldsymbol{F}}}^{-2}, \tag{5.4}$$

where $\boldsymbol{S}_{\boldsymbol{x}}$ and $\boldsymbol{S}_{\boldsymbol{F}}$ denote diagonal matrices which include constraints set on consecutive state variables and control forces. For control approach dedicated to ride comfort improvement only the constraints set on vehicle body heave velocity, pitch velocity and control forces denoted as s_{v_s}, s_{ω_s} and $\boldsymbol{s}_{\boldsymbol{F_{mr}}}$, respectively, are significant. Constraints set on other state variables are neglected and equals infinity. Constraints set on MR damper forces $\boldsymbol{s}_{\boldsymbol{F_{mr}}}$ were assumed based on maximum available force (see dissipative domain in Figure 5.3) and equal to 2000 N. The time-infinite LQ problem was evaluated by obtaining solution $\boldsymbol{P}$ of the continuous time ARE (Algebraic Riccati Equation) which is defined as follows:

$${\boldsymbol{A}_{\boldsymbol{hc}}}^T \boldsymbol{P} + \boldsymbol{P} \boldsymbol{A}_{\boldsymbol{hc}} - \boldsymbol{P} \boldsymbol{B}_{\boldsymbol{hc,F}} {\boldsymbol{Q}_{\boldsymbol{F}}}^{-1} {\boldsymbol{B}_{\boldsymbol{hc,F}}}^T \boldsymbol{P} + \boldsymbol{Q}_{\boldsymbol{x}} = 0. \tag{5.5}$$

Matrix of control gains denoted as $\boldsymbol{G_{LQ}}$ is obtained using ARE solution $\boldsymbol{P}$ matrix as follows:

$$\boldsymbol{G_{LQ}} = \boldsymbol{Q_F}^{-1}\boldsymbol{B_{hc,F}}^{T}\boldsymbol{P}. \tag{5.6}$$

Block diagram of the vibration control layer based on LQ algorithm is presented in Figure 5.6. Generally, only limited number of state variables are measurable in real objects. However, all state variables are assumed to be available which makes it a reference for further algorithms with limited state variables. Force values of the front and rear MR dampers are evaluated by multiplying a vector of state variables by the matrix of control gains (see Equation 5.6) according to the following:

$$\boldsymbol{F_{alg}} = -\boldsymbol{G_{LQ}} \cdot \boldsymbol{x_{hc}}. \tag{5.7}$$

Consequently, the inverse MR damper model is used to evaluate appropriate control current $\boldsymbol{i_{mr}}$ for both MR dampers. Evaluated currents should give the generated forces $\boldsymbol{F_{mr}}$ as close to the desired ones $\boldsymbol{F_{alg}}$ as possible. Constraints set on control currents mainly limiting them to positive values are critical and characteristic for semiactve systems which significantly deteriorates the quality of the classical LQ control.

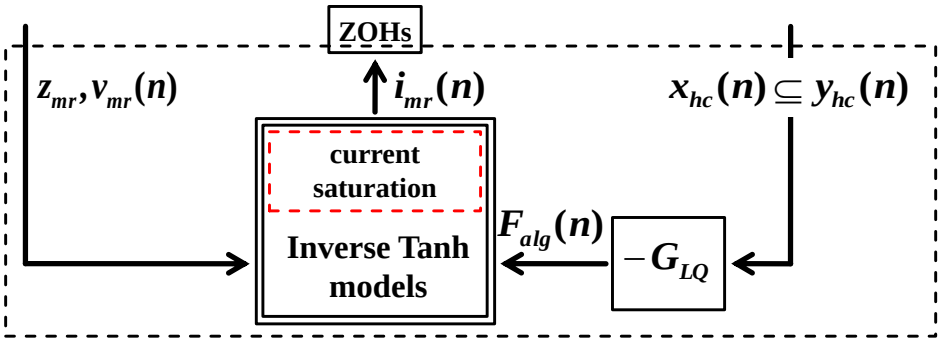

Figure 5.6: Block diagram of the vibration control layer for LQ control of automotive MR dampers

5.2.2 Coupled and separate Skyhook control of vehicle body vibrations

The analysis presented in the dissertation is mainly focused on improving ride comfort. Thus, the optimization of vibration control layer is to be performed for only heave and pitch vehicle body velocities denoted as v_s and ω_{sp}. Besides, the solution is applicable since such signals can be easily estimated or measured in a vehicle using accelerometers

and gyroscopes. Similarly to the LQ control, matrix of control gains is evaluated for previously selected constraints $\boldsymbol{S_x}$ and $\boldsymbol{S_F}$ and limited to heave and pitch velocity dependent gains resulting in $\boldsymbol{G_{SH2}}$ matrix. It includes four parameters related to heave and pitch velocities which are applied for evaluation of control forces as follows:

$$\boldsymbol{F_{alg}} = -\boldsymbol{G_{SH2}} \cdot \begin{bmatrix} v_s \\ \omega_{sp} \end{bmatrix} \quad \text{, where} \quad \boldsymbol{G_{SH2}} = \begin{bmatrix} g_{v_s,f} & g_{\omega_{sp},f} \\ g_{v_s,r} & g_{\omega_{sp},r} \end{bmatrix} \subset \boldsymbol{G_{LQ}}. \tag{5.8}$$

Some control systems due to their computational limitations require further simplification of control schemes resulting in the separate Skyhook control of the each quarter of a vehicle suspension. Herein, the Skyhook algorithm dedicated to quarter-car model minimizes vibrations of the front and rear vehicle body parts. It can be synthesized based on LQ control defined for a quarter-car model and simplified similarly to the half-car related Skyhook control. According to the separate Skyhook control, the control forces are evaluated using vertical velocity of the front or rear vehicle body parts as follows:

$$\boldsymbol{F_{alg}} = -\boldsymbol{g_{SH1}} \circ \begin{bmatrix} v_{sf} \\ v_{sr} \end{bmatrix} \quad \text{, where} \quad \boldsymbol{g_{SH1}} = \begin{bmatrix} g_{v_{sf},f} \\ g_{v_{sr},r} \end{bmatrix}. \tag{5.9}$$

Operation marked as "$\circ$" is a Hadamard product, corresponding to the element-wise product of vectors.

5.3 Optimization and validation of vibration control

Nonlinear behaviour of MR dampers requires the analysed algorithms to be validated for different control goals and road conditions. Two types of road-induced excitations were taken into account, i.e. continuous sinusoidal and single road bumps. For sinusoidal excitation different road classes were analysed while the suspension was subjected to compatible and inverted front and rear excitation signals. Shape of the road bumps was assumed to be consistent with that applied during real road experiments (see Chapter 7). Results obtained for the following algorithms are compared using several quality indices. Normalized ride comfort, road holding and suspension deflection indices for continuous sinusoidal excitation were evaluated according to Equation (4.18). Standard deviation for single-road-bump excitation was evaluated according to Equations

(4.17) and (4.18), while maximum value was evaluated based on Equation (2.10). The vehicle speed was assumed at the standard level of 15 ms^{-1} for continuous excitation and approximately 2.8 ms^{-1} for single-road-bump excitation.

5.3.1 Optimization of LQ and Skyhook control of a half-car model

Optimization of LQ control and Skyhook control synthesized for a half-car model (denoted as SH2) was performed assuming both constraints s_{v_s}, s_{ω_s} related to body heave and pitch velocities varies from 0.1 to 0.6. Validation of LQ control was performed in order to study the influence of additional state variables on control quality. Preliminary studies of presented algorithms were carried out in a wider range of the constraints. However, it was stated the solution space of the control optimization problem is unimodal and consequently the range of analysis was limited.

Optimization spaces for LQ and SH2 were evaluated for road classes of D, E and F of the sinusoidal excitation and presented in Figures 5.7 and 5.8, respectively. The minimum values indicated for ascending road classes are equal to 0.91, 0.89 and 0.87 in average for LQ and SH2 control schemes. It can be noticed that for higher road classes and amplitudes of road-induced excitation the quality of vibration control was improved. It is related to nonlinearity of MR damper model which is described more accurately for higher damper piston amplitudes by the inverse model included in control algorithm.

For LQ control the minimum values were found for heave and pitch velocity constraints equal to 0.3 and 0.3, respectively, for all road classes. Results show that changing road class of the excitation presents negligible influence on optimized parameters of the LQ control of MR dampers.

Optimization of SH2 control results in optimized heave and pitch velocity constraints equal to 0.3 and 0.3, respectively, for road class D as well as 0.4 and 0.4 for road classes E and F. Similarly to results obtained for LQ control, the optimized SH2 parameters are hardly changing for different road classes.

Moreover, the diagrams show that over-parametrized LQ control for narrower s_{v_s} and s_{ω_s} constraints introduces higher deterioration of quality of vibration control in comparison to under-parametrised control for wider constraints. The On-Off Skyhook control exhibits similar disadvantage as a representation of a boundary case of analysed

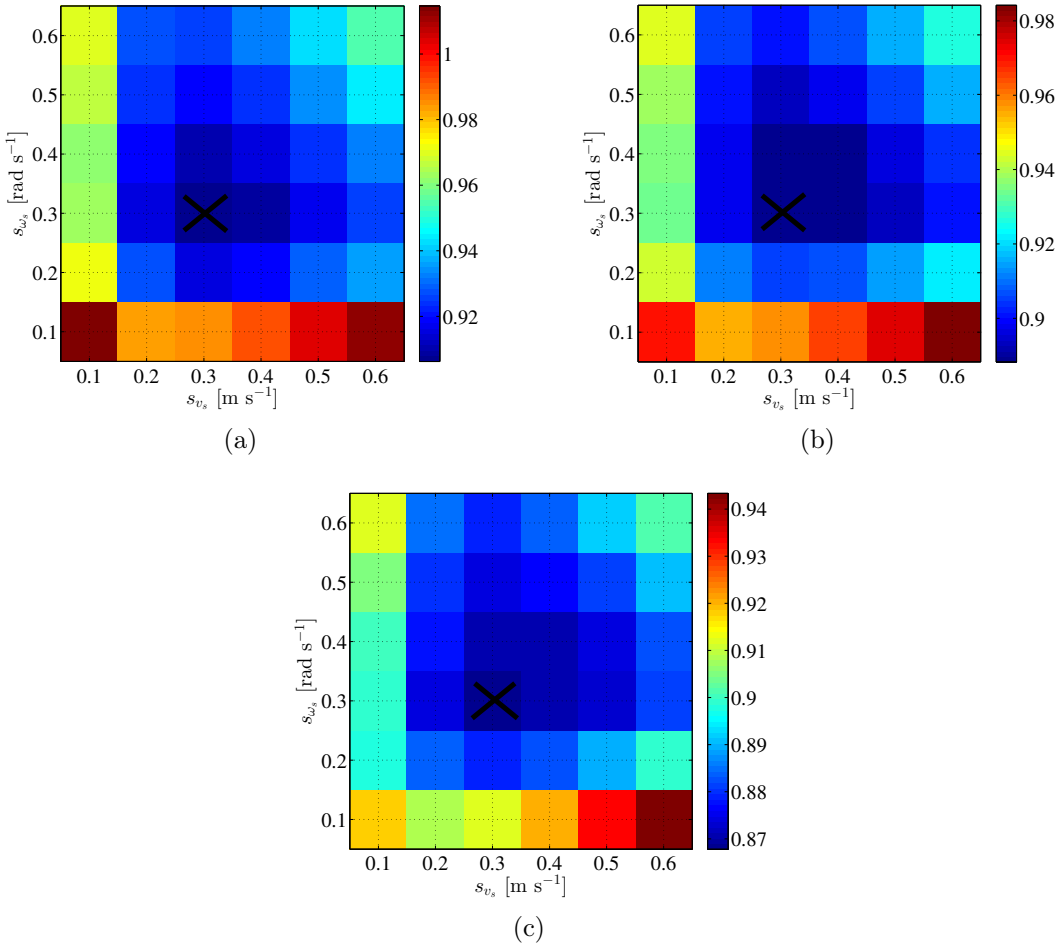

Figure 5.7: Optimization solution spaces evaluted for LQ control scheme and different road classes: a) road class D, b) road class E, c) road class F

"continuous" Skyhook control with narrow constraints. Since presented values of NJ_{RC} are normalized, it can be stated that 10 percent improvement was reached by both LQ and SH2 algorithms in comparison to passive suspension with uncontrolled MR dampers.

5.3.2 Optimization of quarter-car model related Skyhook control

The Skyhook control synthesized for a quarter-car model (denoted as SH1) represents an approach based on separate control of each vehicle suspension part. Such algorithm is favoured for its simplicity which is recommended especially in commercial application of MR dampers. However, it does not take into account vibration control of half-car model modes, e.g. pitch motion. The optimization space dedicated to SH1 is presented in Figure 5.9.

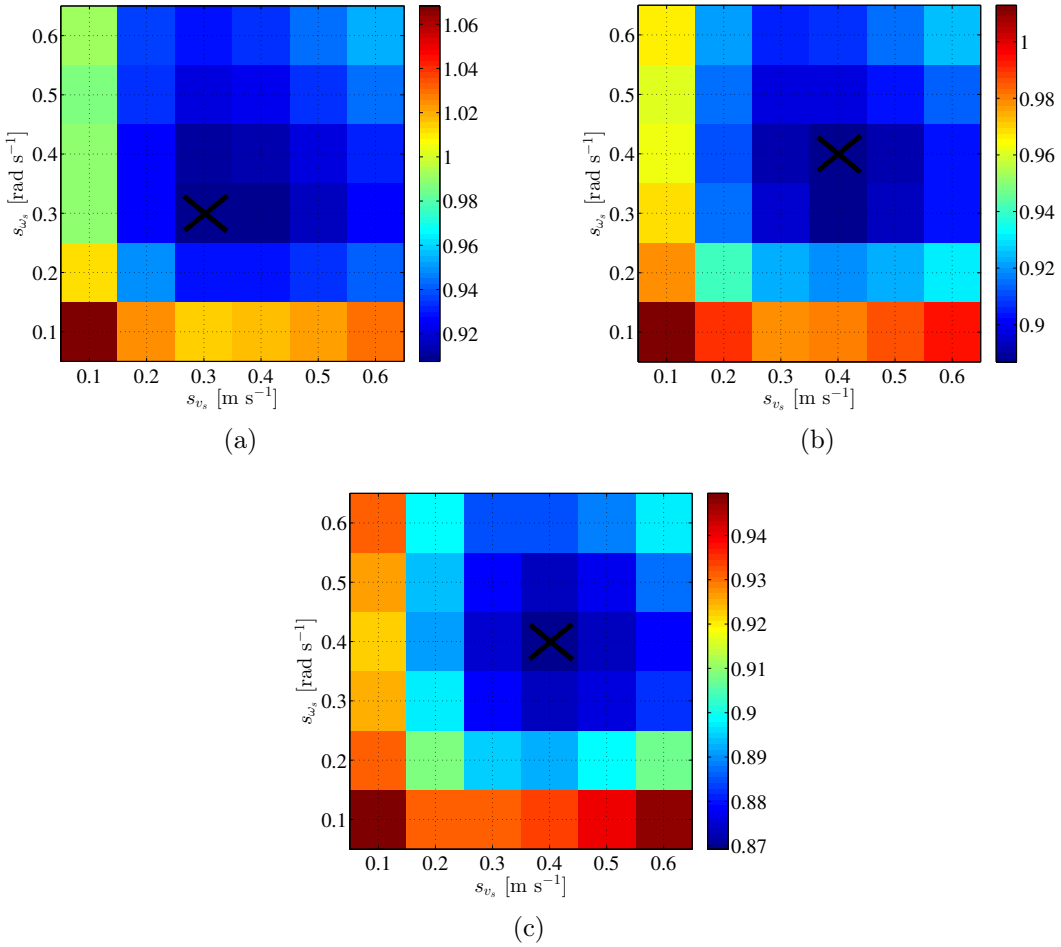

Figure 5.8: Optimization solution spaces evaluated for SH2 control scheme and different road classes: a) road class D, b) road class E, c) road class F

It was evaluated for parameters of Skyhook control (denoted as $\boldsymbol{g_{SH1}}$) of the front and rear vehicle suspension varying in range from 500 to 6000 Nsm^{-1} (see Figure 5.9). The following minimum values was obtained for road classes D, E and F, respectively: 0.91, 0.89 and 0.87 which are similar to those represented by both LQ and SH2 control schemes. For all three road classes the optimized values of Skyhook parameters $g_{v_{sf},f}$ and $g_{v_{sr},r}$ are equal to 2000 and 3400 Nsm^{-1}, respectively. Contrary to LQ and SH2, disadvantage of over-parametrization is not clearly visible since parameters of SH1 were optimized in a narrower range.

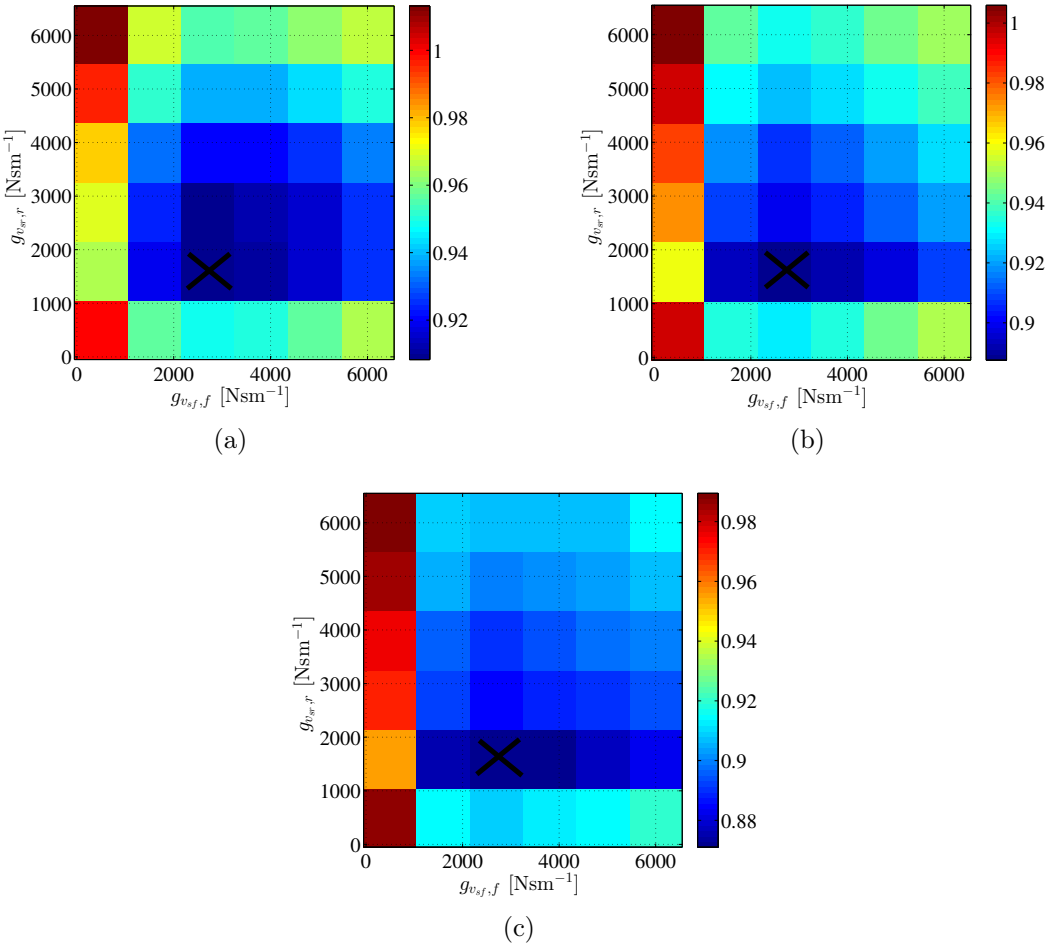

Figure 5.9: Optimization solution spaces evaluated for SH1 control scheme and different road classes: a) road class D, b) road class E, c) road class F

5.3.3 Analysis of LQ and Skyhook control schemes in frequency domain

Optimized configurations of LQ, SH2 and SH1 control were analysed in frequency domain based on vehicle body acceleration transmissibility denoted as $\widetilde{T}_{a_r,a_{s,avg}}$ evaluated for continuous sinusoidal road-induced excitation for compatible and inverted synchronization (see Figures 5.10, 5.11, 5.12). Results obtained for semiactive control were compared with those obtained for passive suspension with uncontrolled MR dampers.

It can be stated that all three semiactive control schemes improve the vibration control at similar level for both compatible and inverted road excitations. Thus, the SH1 control scheme is recommended to be applied for the analysed half-car model since it is the least complex and easily applicable. Furthermore, the control quality is retained for all analysed road classes from D to F. Differences visible between results of passive and

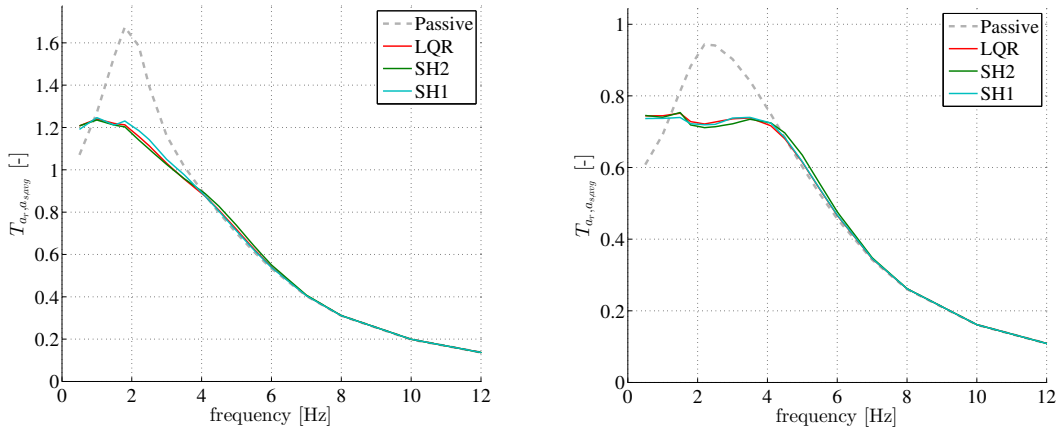

Figure 5.10: Comparison of body acceleration transmissibility characteristics evaluated for different semiactive control strategies and road excitation of D class: a) compatible excitation, b) inverted excitation

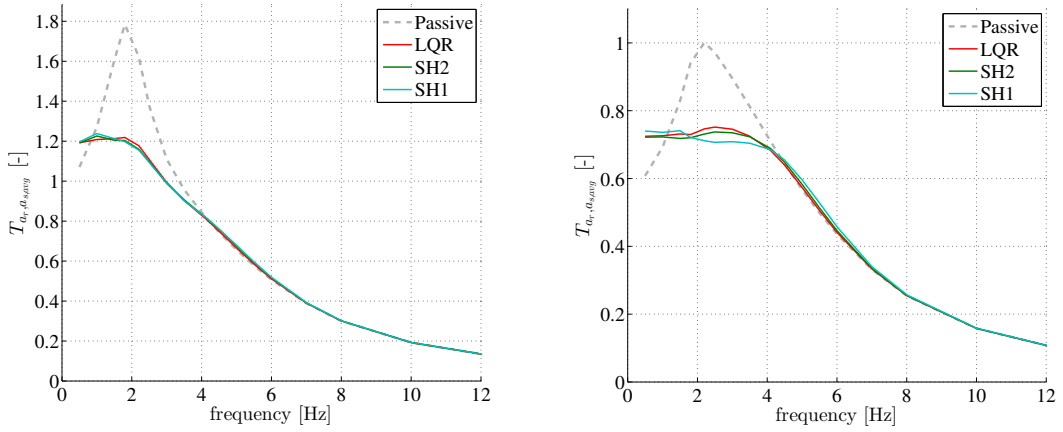

Figure 5.11: Comparison of body acceleration transmissibility characteristics evaluated for different semiactive control strategies and road excitation of E class: a) compatible excitation, b) inverted excitation

semiactive control represent 10 percent improvement indicated by NJ_{RC} quality index. Such improvement is focused on frequency range from 1 to 4 Hz and is critical since many of human body resonance frequencies are covered by such frequency range (see Table 1.1).

5.3.4 Ride comfort, road holding and suspension deflection diagrams

More detailed analysis of semiactive vibration control in road vehicles requires taking into account not only the ride comfort issue but also influence of the control on both

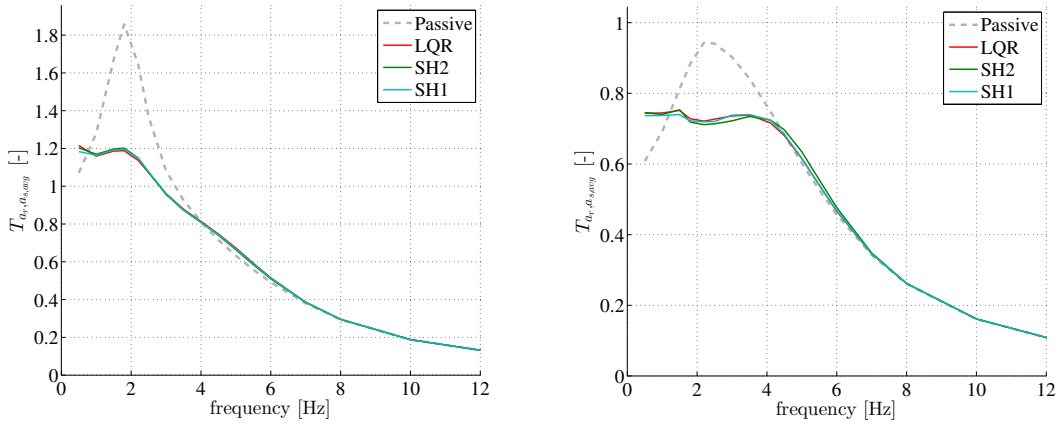

(a) (b)

Figure 5.12: Comparison of body acceleration transmissibility characteristics evaluated for different semiactive control strategies and road excitation of F class: a) compatible excitation, b) inverted excitation

road holding and suspension deflection issues. Similarly to the analysis performed for passive suspension system, the following is carried out based on ride comfort versus road holding or suspension deflection diagrams. The aim of the vehicle vibration control presented in the dissertation is to minimise the ride comfort quality index but taking into account other ride safety related indices.

The ride comfort versus road holding diagrams (see Figure 5.13) were evaluated for road classes D, E and F. Results obtained for passive suspension and constant values of control current varying from 0 to 0.4 A are marked by a solid line while results obtained for semiactive control are marked in the left bottom side of the diagrams. Since the normalization of quality indices was performed with respect to results obtained for uncontrolled MR dampers the line dedicated to passive suspension starts from (1,1) point. Increasing control current leads to deterioration of both ride comfort and road holding. It can be stated that the semiactive control significantly improves ride comfort. However, the improvement is reached with the cost of slight deterioration in road holding quality which is equal approximately to 5 percent for all analysed road classes.

Presented ride comfort versus suspension deflection diagrams (see Figure 5.14) were evaluated for road classes D, E and F . Similarly to previous diagrams, results for passive suspension are visible in diagrams as solid line starting from reference (1,1) point. Results obtained for LQ, SH2 and SH1 control schemes are marked in the left up part of diagrams. They show that for greater value of control current the suspension system stiffens which

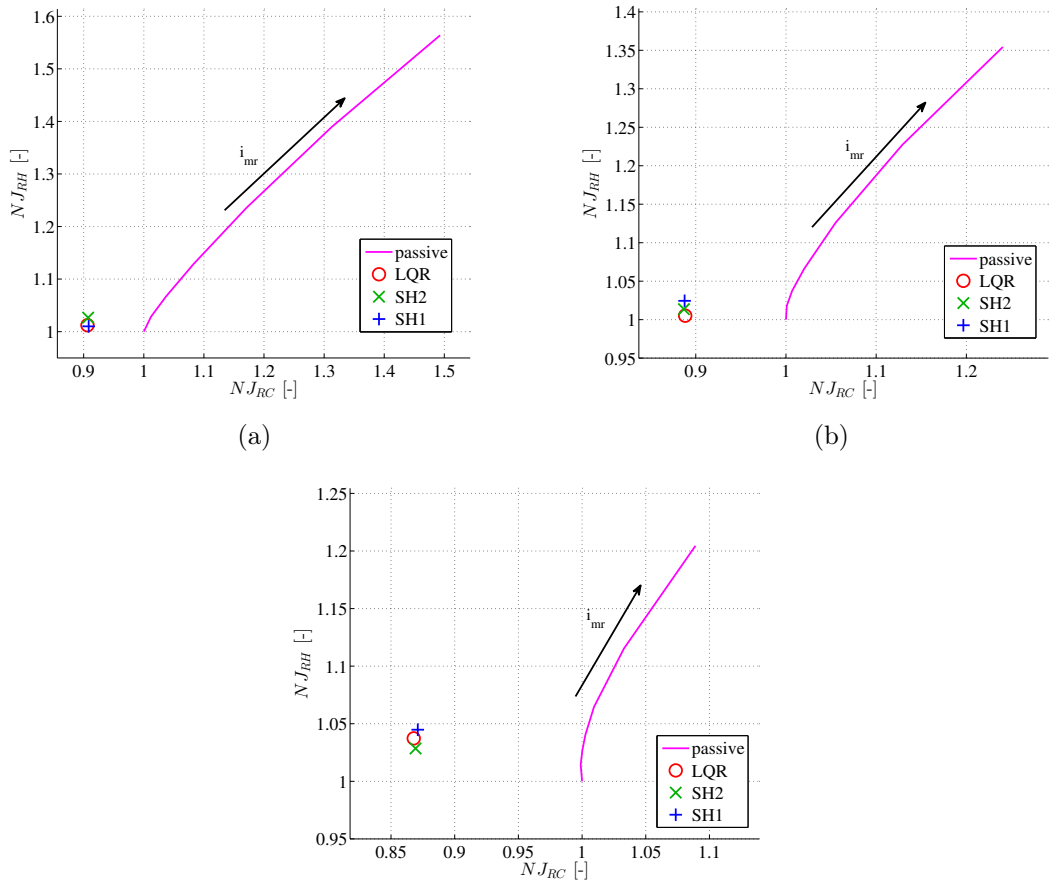

Figure 5.13: Ride comfort versus road holding diagrams obtained for semiactive control and passive MR damper equipped vehicle suspension subjected to road-induced excitation of different road classes: a) road class D, b) road class E, c) road class F

leads to the decrease of suspension deflection index. Besides, semiactive control causes improvement not only in ride comfort but also in the suspension deflection by 5 percent comparing to uncontrolled suspension MR dampers.

5.3.5 Analysis of semiactive control for single-road-bump excitation

Single-road-bump excitation represent one of main causes of passenger inconvenience during vehicle ride. Both passive and semiactive control were validated for such excitation defined according to the description presented in Chapter 2. Similarly to the previous analysis related to continuous excitation, the following was performed using an averaged vehicle body acceleration by evaluation of its standard deviation and maximum

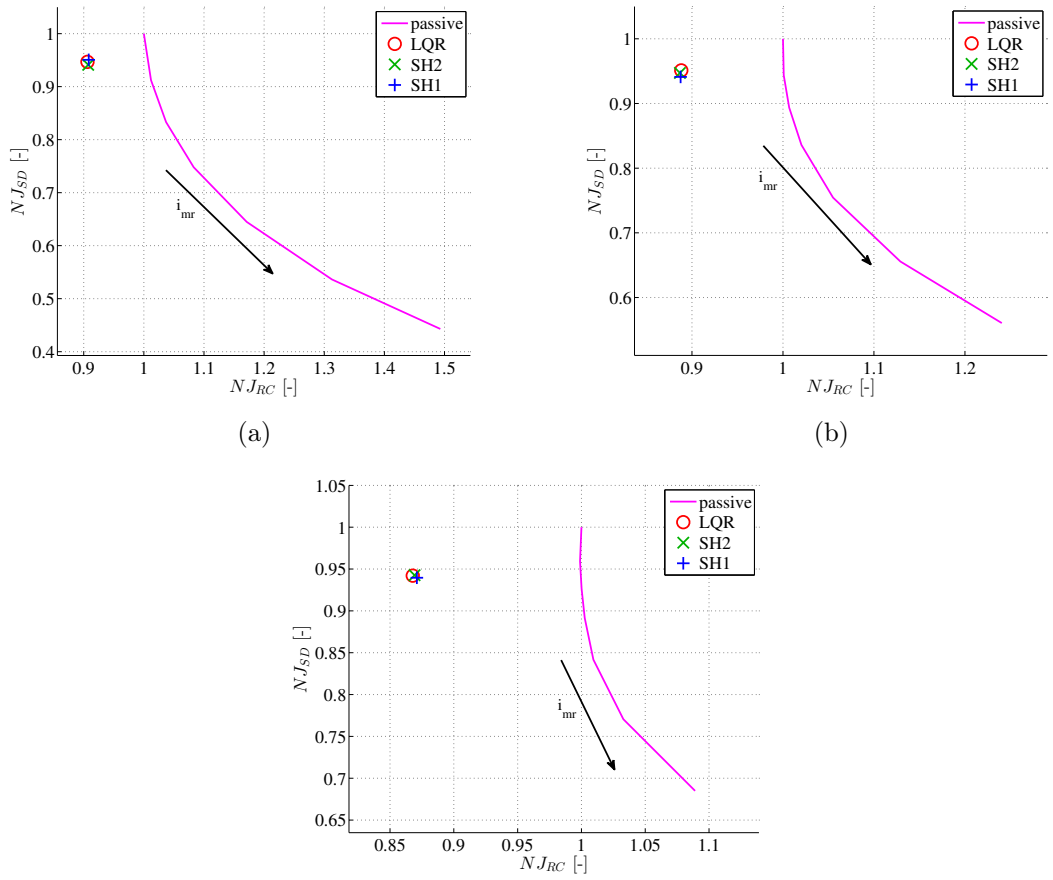

Figure 5.14: Ride comfort versus suspension deflection diagrams obtained for semiactive control and passive MR damper equipped vehicle suspension subjected to road-induced excitation of different road classes: a) road class D, b) road class E, c) road class F

values which are denoted as $\hat{I}_{a_{s,avg}}$, $\hat{A}_{a_s}$, respectively. The "hat" symbol stands for experiments performed for single-road-bump excitation. For the purpose of further analysis both quality indices are normalized resulting in $NI_{a_{s,avg}}$ and NA_{a_s} , respectively.

Analysed optimization spaces evaluated for LQ, SH2 and SH1 algorithms are presented in Figures 5.15, 5.16 and 5.17, respectively. The presented spaces were generated using the $NI_{a_{s,avg}}$ quality index. Optimized values of heave and pitch velocity constraints differ more significantly from each other in comparison to those obtained for continuous sinusoidal excitation. For LQ control it is suggested to define the s_{v_s} and s_{ω_s} equal to 0.3 and 0.8, respectively. Contrary to LQ control, the optimized parameters are equal to 0.4 and 0.6 for SH2 algorithm. Finally, for SH1 optimized control parameters dedicated to the front and rear vehicle suspension parts are equal to 2400 and 1300 Nsm^{-1}, respectively.

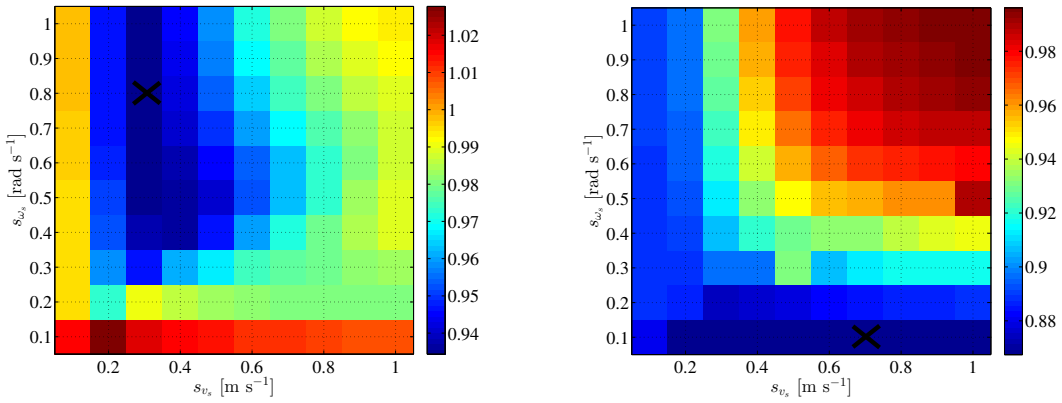

(a) (b)

Figure 5.15: Optimization solution spaces evaluated for LQR control scheme using different indices evaluated based on vehicle body acceleration: a) standard deviation of averaged acceleration, b) acceleration maximum value

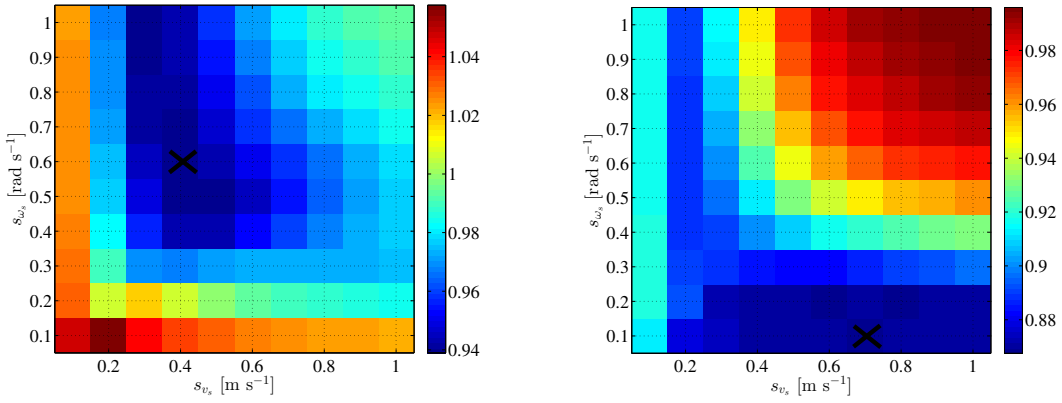

(a) (b)

Figure 5.16: Optimization solution spaces evaluated for Skyhook control scheme dedicated to half-car model using different indices evaluated based on averaged body acceleration: a) standard deviation, b) maximum value

In the case of LQ and SH2 control schemes both minimum values of $NI_{a_{s,avg}}$ were indicated at the level of 0.93 and 0.94, respectively. The level of $NI_{a_{s,avg}}$ is similar and equal to 0.94 for SH1 algorithm. Thus, presented results indicate close performance of three presented semiactive algorithms for bump excitation. Validation was also performed assuming that the NA_{a_s} quality index is used. Such approach gives significantly different parameters i.e. (0.7, 0.1), (0.7, 0.1) and (7000, 2800) for LQ, SH2 and SH1 control schemes, respectively.

Similar analysis was performed for MR dampers controlled using constant values of control current varying from 0 to 0.4 A (see Figure 5.18) which is the same for front and rear MR dampers. It can be stated based on both $NI_{a_{s,avg}}$ and NA_{a_s} quality indices that

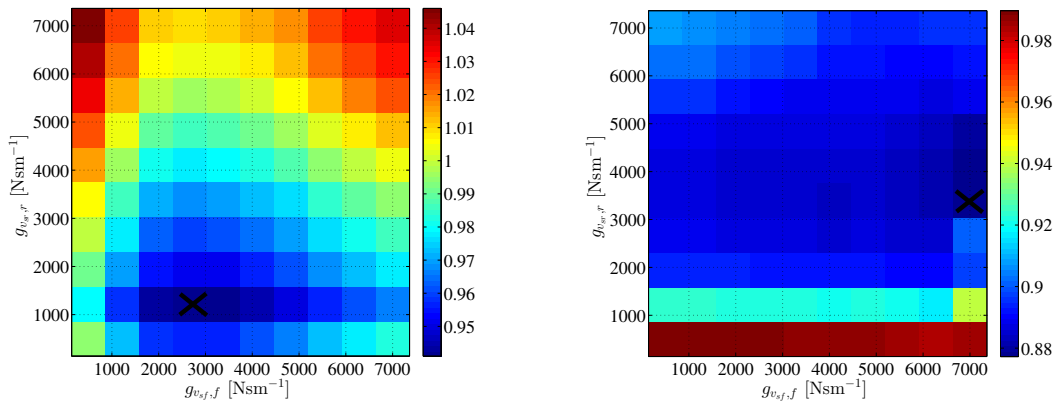

(a) (b)

Figure 5.17: Optimization solution spaces evaluated for Skyhook control scheme dedicated to quarter-car model using different indices evaluated based on averaged body acceleration: a) standard deviation, b) maximum value

best performance of vibration control is reached for uncontrolled MR damper. Increase of control current leads to the increase of both indices and deterioration of vibration control quality.

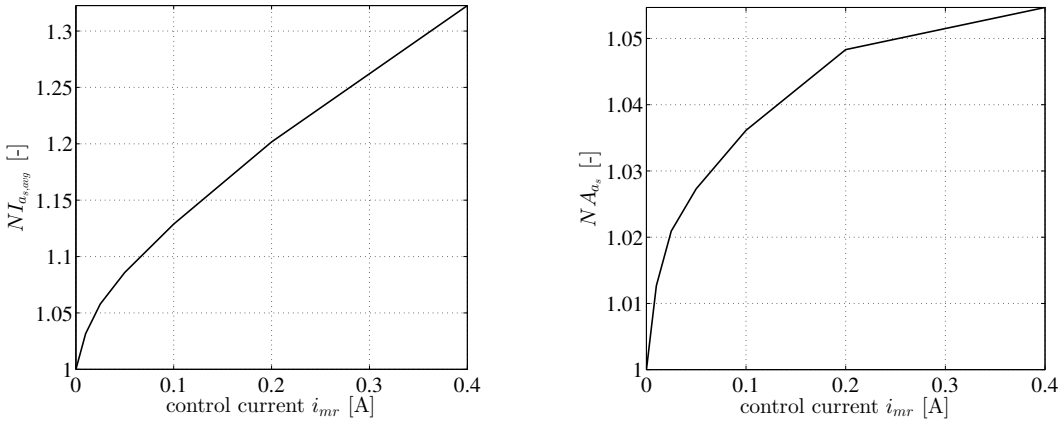

(a) (b)

Figure 5.18: Optimization solution spaces evaluated for passive suspension using different indices evaluated based on averaged body acceleration: a) standard deviation, b) maximum value

All results obtained for passive and semiactive control, which was optimized with respect to $NI_{a_{s,avg}}$, were concluded in time diagram which presents single response of a half-car model (see Figures 5.19 and 5.20). Time diagrams were plotted for both $a_{s,avg}$ and a_s quality indices. It can be noticed that vibration control for passive suspension is significantly worse comparing to semiactive control. As a confirmation of previous analysis it can be stated that performance of three semiactive control schemes is similar.

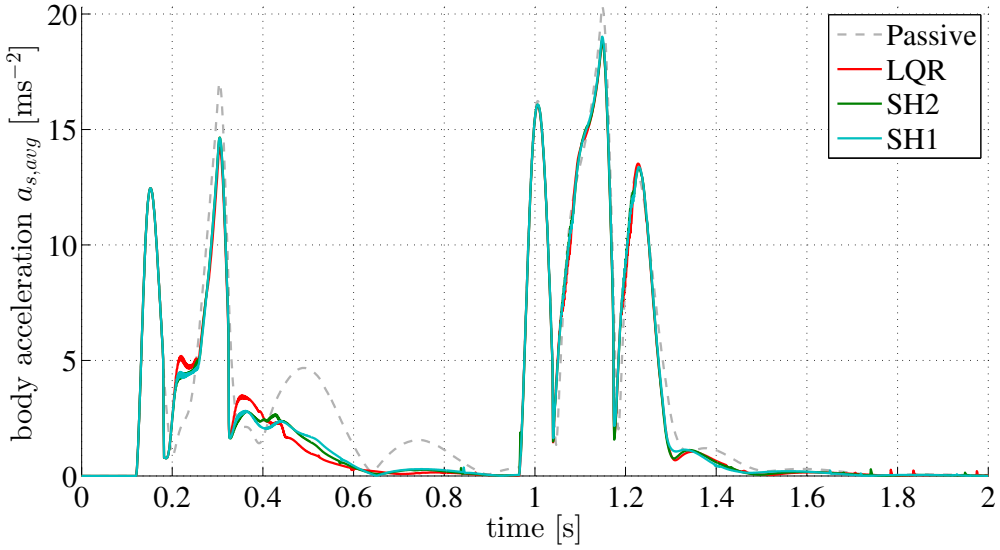

Figure 5.19: Comparison of vehicle body acceleration response to single-road-bump excitation in time domain for passive and semiactive control

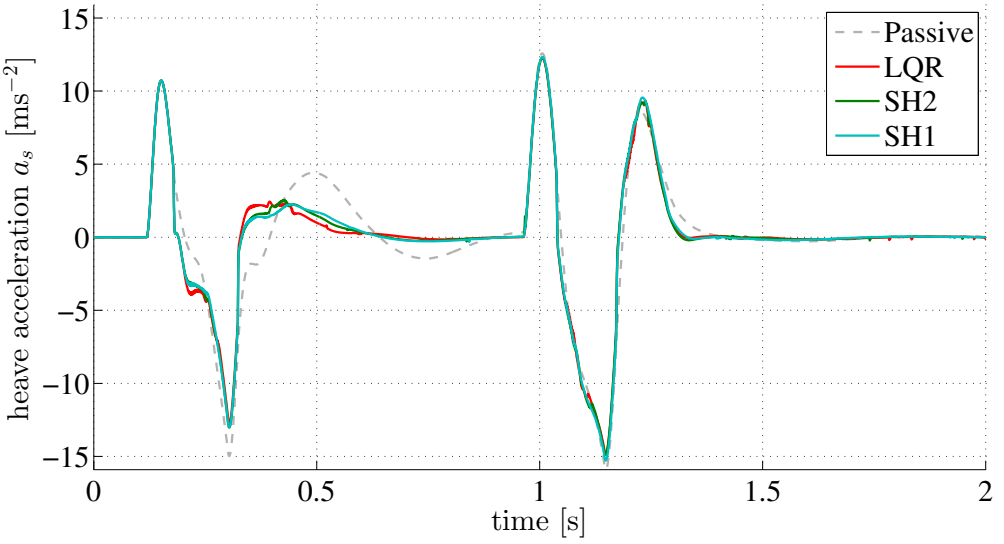

Figure 5.20: Comparison of vehicle body heave acceleration response to single-road-bump excitation in time domain for passive and semiactive control

5.4 Summary

Appropriate synthesis of semiactive control dedicated to automototive MR dampers has decisive influence on further quality of vibration control. Dissipative domain of MR damper significantly increases difficulties in optimization and application of classical control schemes. Three algorithms were validated, i.e. LQ control and Skyhook synthesized for half-car or quarter-car models. All algorithms were optimized numerically assuming

the vehicle is subjected to continuous sinusoidal excitation or single-road-bump excitation which can be assumed as common excitation during exploitation of typical road vehicles.

Further analysis of optimized algorithms performed in time and frequency domain as well as based on ride comfort versus road holding and suspension deflection diagrams indicated significant improvement of semiactive algorithms in comparison to passive control. Furthermore, similar performance was shown for all three analysed algorithms. Results obtained in the presented chapter were used for comparison in the following chapter considering adaptive control algorithms.

Chapter 6

Adaptive control of suspension system with MR dampers

All road vehicles exhibit changes in parameters during their exploitation. Varying dynamics of vehicles can be induced by varying weight of vehicle load, wearing out or damage of suspension system elements as well as by varying pressure levels of tyres. In the case of vehicle suspension systems equipped with MR dampers significant non-stationarity is revealed by MR dampers themselves. MR dampers are known to exhibit different behaviour for different types of road-induced excitation and different ambient temperatures. Thus, it is recommended for a suspension control system to include algorithms which are responsible for online observation, analysis and diagnosis of vehicle vibrations. Moreover, it is desired to adaptively adjust control algorithms while the vehicle is moving in different conditions.

6.1 Introduction to adaptive control of MR dampers

An adaptive controller generally consists of two control loops, i.e. the first is related to the normal feedback or feedforward with the process and the other is related to the adjustment loop for control parameters. Thus, according to [6] "an adaptive controller is a controller with adjustable parameters and a mechanism for adjusting the parameters". "Online determination of process parameters is a key element in adaptive control", where

process parameters can be influenced by varying parameters of the controlled object or variable character of disturbances.

Each layer of the vehicle suspension control scheme (see Figure 5.2) can separately include an adaptation mechanism. Parameters of the inverse MR damper model included in the force control layer can be adjusted to the varying conditions of the MR damper operation. The adaptive mechanism can be included in the vibration control layer in which it is responsible for identification of vehicle vibration model and online adjustment of control gains. Finally, the optimization control layer can include algorithms which are dedicated to a long-term analysis of vehicle vibrations and are responsible for diagnosis of the vehicle suspension elements. The goal of the optimization control layer is to improve vehicle lifetime by appropriate adjustment of parameters of the lower vibration control layer.

6.1.1 Classification of adaptive control

Adaptive control algorithms can be characterized with respect to different criteria, i.e. feedforward and feedback are distinguished or direct and indirect control methods can be applied. In the case of direct control, parameters of the control algorithm are directly estimated. Whereas for indirect control, the synthesis of a controller is performed separately, while its parameters are calculated according to the estimated parameters of the process [6].

Generally, adaptive algorithms presented in the literature and dedicated to automotive MR dampers are focused on two goals which are related to the vibration or force control layer. Both mentioned adaptive approaches are responsible for improving vibration control of certain vehicle parts. Such algorithms can be synthesized assuming both feedback or feedforward control structures. In the case of the force control layer, the feedback approach requires force sensors to be installed in the automotive shock-absorbers. The feedforward force control, which is based on the inverse MR damper model, does not need additional sensors. Thus, it is commonly applied in the semiactive vibration control.

Similarly to the force control layer, both the feedback and feedforward control strategies can be applied in the vibration control layer. The feedback control approach commonly take advantage of inertial sensors installed in the vehicle body and underbody parts. Contrary to feedback control, the feedforward vibration control can compensate the finite response of MR dampers. However, it requires the additional sensors scanning the road surface in front of the vehicle in order to track the road-induced excitation in advance. Both direct and indirect control methods reveal their advantages and disadvantages which is referred in the current chapter.

6.1.2 Adaptive devices versus adaptive control

Idea of application of adaptive vibration controllers is well-known in the literature for active elements, see examples given in [61] and [71]. The first paper deals with vibration control of a composite beam. The control is presented as semiactive despite the fact that typically active elements are used such as piezoelectric actuators. Vibration control is performed according to LMS algorithms which represent the direct method of the adaptive control. The second paper presents an application of adaptive algorithms in control of a vehicle suspension using active elements. Adaptability presented in that article is an example of the indirect adaptive control. It is based on two separated blocks which are responsible for identification of the vehicle vibration model and for the suspension control.

Adaptive control of the vehicle suspension presented in the literature is commonly dedicated to active suspension elements. Control of semiactive automotive MR dampers is more complex due to the constrained MR damper dissipative domain and significant nonlinearities in its behaviour. Moreover, adaptive control of MR dampers presented in the literature is very often dedicated to vibration control of structures, strictly, buildings in case of earth-quakes. Herein, two cases of adaptive devices needs to be distinguished, i.e. those which are controlled using adaptive algorithms and those which are adaptive itself, due to the fact that their parameters can be adjusted online, e.g., control of MR dampers in buildings presented in [10] and [9] based on the PID controller. Another example of adaptive impact absorbers, but not adaptive control, can be found in [96].

6.2 Modified FxLMS for automotive MR dampers

A novel adaptive approach was proposed for the vehicle suspension control using MR dampers in [74] which is based on the classical LMS adaptive algorithm. The LMS algorithm is commonly applied in the noise control due to its scalability to the different types of controlled objects. It also allows for simple switching between different control goals and offers feedforward control structure. However, semiactive nature of the MR damper requires additional modification of the LMS algorithm in order to retain the algorithm's stability and performance since it is dedicated to active elements. The idea was improved by applying FxLMS with normalized adaptation step for both quarter-car [77] and half-car [78] models. It is referred in details within further parts of the current chapter.

6.2.1 State-of-the-art in semiactive adaptive control

Adaptive algorithms related to control of MR dampers applied for vehicle suspension are commonly synthesized assuming feedback structure. Algorithms of such type which are presented in the literature can be distinguished with respect to their complexity starting from those which are based on quasi constant MR damper current control and represent indirect adaptive method [135]. Second group represents the adaptive indirect method, as well, and is constituted by algorithms which include classical non-adaptive control schemes, such as Skyhook, sliding mode control or fuzzy control and additional modules responsible for online identification. Last group of adaptive control represents the adaptive direct method including application of LMS or FxLMS algorithms and offers both feedback or feedforward structure.

Applications of adaptive algorithms dedicated to analysis of both the character of disturbances or the dynamics of the controlled object are widely presented in the literature. The adaptive notch filter was proposed in [108] for analysis of road-induced excitation. Its application was presented in [80] where it was applied for tracking of vehicle engine speed based on acceleration measurement. Moreover, excitation frequency tracking was presented in [144] for adaptive adjustment of tuned mass damper applied in vibration control of buildings.

Another approach of indirect adaptive control is related to identification of the controlled object. Application of identification modules in vibration control of buildings is very popular in the literature. Numerous papers present methods of selective [90] or overall identification of structures including masses, stiffness and damping parameters [18, 19, 140]. Applications of indirect control of vehicle suspension are also presented in the literature, however, they are commonly dedicated to the simple quarter-car model [100, 103, 163] which is not sufficient for accurate mapping of road vehicles dynamics.

Contrary to indirect adaptive method, application of direct method is very often based on classical feedback control algorithms whose parameters are tuned via an adaptation mechanism. Similarly to indirect methods, many articles presents the direct adaptive methods for vibration control of buldings including sliding mode controller which adaptively adjusted gains [102] or fuzzy controller whose weights are tuned using neural network [118]. Papers related strictly to vibrating models which are typical for vehicle suspension control are also presented, e.g. [28] which shows adaptation of fuzzy controller dedicated to quarter-car model.

All above presented adaptive algorithms are synthesized assuming feedback structure. Moreover, they are not scalable, their synthesis is complex while control goals cannot be simply switched from one to the another depending on instantaneous road conditions or passengers needs. Additionally, in the case of semiactive devices the control current is limited to only positive values which makes the optimization of the algorithm complex. Such disadvantages confirm the need of developing adaptive control which is based on modified FxLMS algorithm easily applicable for different constructions of vehicle suspension systems and for varying road conditions.

6.2.2 Decomposition of MR damper dissipative domain

Well-known control algorithms, e.g. robust or optimal control (including LQ control presented in Chapter 5), assumes that an ideal actuator is applied which exhibits no limitations or output force dependent on its internal state. It was shown that the shape of the dissipative domain of the MR damper is far from the typical shape of force range covered by active elements (see Figure 1.7). Thus, a modification of an MR damper dissipative domain was proposed in the literature for synthesis and optimization of the semiactive control. A straight-forward method is based on decomposition of a dissipative

domain into a characteristics of a so-called linearised nominal damping parameters evaluated based on the dissipative domain and a modified control force range of a fictitious quasi-active element [126]. Such approach additionally ensures constraints of control force to be symmetrical with respect to the zero force axis. Improvement of the proposed decomposition method was presented in [77, 78] for semiactive adaptive control and is applied in the further analysis.

From the controller's point of view only the Tanh MR damper model identified for piston excitation of 1.5 Hz plotted for the control current range from 0 to 1.33 A, presented in Chapter 3, is available. Thus, it is applied for the mentioned procedure of decomposition. Furthermore, similarly to the assumption which was made in Section 5.2, the damper piston acceleration a_{mr} was neglected within the inverse model by setting its parameter γ_{th} to zero. Characteristics of the proposed nominal damping c_{avg} can be defined as an average of the dissipative domain evaluated with respect to the certain piston velocity according to the following formula:

$$F_{avg}(v_{mr}) = \frac{1}{2}[F^{min}_{mr,th}(v_{mr}) + F^{max}_{mr,th}(v_{mr})], \tag{6.1}$$

where

$$F^{min}_{mr,th}(v_{mr}) = F_{mr,th}(v_{mr}, i^{min}_{mr}) \quad , \quad F^{max}_{mr,th}(v_{mr}) = F_{mr,th}(v_{mr}, i^{max}_{mr}). \tag{6.2}$$

Symbols i^{min}_{mr} and i^{max}_{mr} denote lower and upper limits of the control current equal to 0 and 1.33 A, respectively. Both boundary characteristics $F^{min}_{mr,th}$, $F^{max}_{mr,th}$ of the MR damper dissipative domain and force characteristics F_{avg} of the nominal damping c_{avg} are presented in Figure 6.1.

A control algorithm, which was synthesized based on the decomposed dissipative domain, generates desired force F^{*}_{alg} around a working point defined by the nominal damping coefficient c_{avg}. Thus, it is assumed that an additional fictitious nonlinear passive damper of nominal damping c_{avg} is included in the suspension system. Such additional damping needs to be included in the vehicle suspension model applied in adaptive vibration control in the form of secondary signal path model (see Subsection 6.2.4). The algorithm operates assuming not MR damper but the quasi-active fictitious element is applied. In order to obtain the resultant control force F_{alg}, which is processed

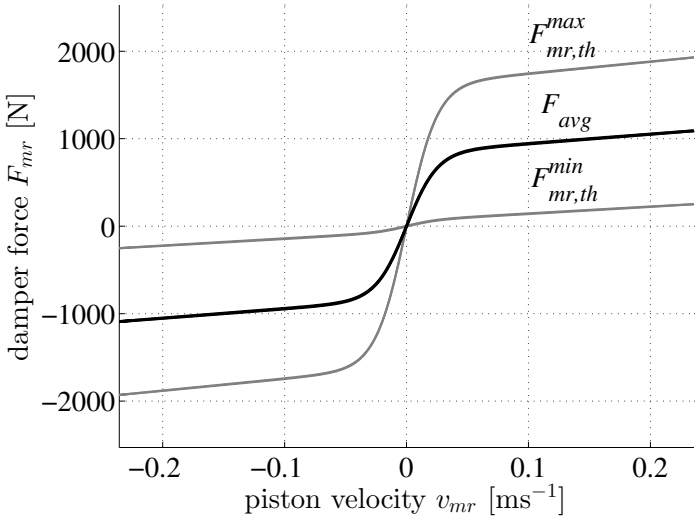

Figure 6.1: Boundary characteristics of MR damper dissipative domain and the nominal damping characteristics F_{avg}

by an inverse MR damper model, the preliminary control force F^*_{alg} is summed with that generated by the nominal c_{avg} (see Figure 6.2).

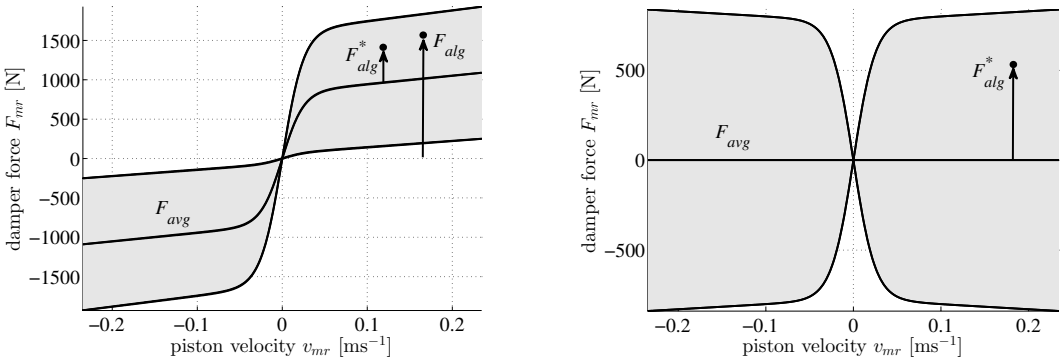

Figure 6.2: Modification of MR damper dissipative domain related to the semiactive control: a) decomposition of dissipative domain, b) control force range of a fictitious quasi-active element

Despite the fact that MR damper dissipative domain was modified resulting in the quasi-active force range (see Figure 6.2b), the main disadvantages of the semiactive damper have been maintained. Firstly, the lower piston velocity - the less controllable such quasi-active element. Secondly, application of the MR damper adds additional feedback loop into the suspension model. Force generated by the MR damper is dependent on and influences the piston velocity, simultaneously, which introduces the additional

self-stabilizing feedback mechanism and limits the maximum available force generated by the damper.

6.2.3 Synthesis of the modified FxLMS control scheme

The classical LMS algorithm represents a group of adaptive feedforward control [83], it origins in gradient descent optimization methods, but significant modifications convert it to a separate group of control algorithms [65]. The LMS algorithm tends to minimize variance of a selected error signal for a disturbed system using a given reference signal. Strictly, the algorithm minimizes cross-correlation between the error and reference signals since the reference signal is correlated with the disturbance of the system.

In the case of simultaneous minimization of multiple error signals, a so-called multi-channel LMS algorithm was proposed in the literature [59, 164]. Furthermore, in order to improve convergence of the LMS algorithm, an extended FxLMS algorithm was introduced which take advantage of the estimated model of the secondary path as well as it includes normalization of the adaptation step, see e.g. [78]. Zero mean value of the control signal is an additional characteristic feature of the LMS algorithm. Thus, for the MR damper control, the FxLMS needs to be modified and suited for the assymetrical shape of MR damper dissipative domain.

The vibration control applied in vehicles takes advantage of an error signal which is defined as a signal describing vibrations of the selected vehicle part or the selected vibration mode which are to be stabilized (see control block diagram in Figure 6.3). Furthermore, it is assumed here that the reference signal related to the road profile is obtained using an additional laser sensors aimed at the front of the vehicle.

The applied adaptation mechanism related to the FxLMS includes two error signals dedicated to the vehicle body heave and pitch velocities denoted as v_s and ω_s, respectively, and is described as follows [83]:

$$\boldsymbol{h_{f/r}}(n+1) = \boldsymbol{h_{f/r}}(n) - \\ - \mu \cdot \left[\alpha_{v_s} v_s(n) \cdot \frac{\boldsymbol{r_{f/r,v_s}}(n)}{\boldsymbol{r_{f/r,v_s}}^T(n) \cdot \boldsymbol{r_{f/r,v_s}}(n) + \zeta} + \alpha_{\omega_s} \omega_s(n) \cdot \frac{\boldsymbol{r_{f/r,\omega_s}}(n)}{\boldsymbol{r_{f/r,\omega_s}}^T(n) \cdot \boldsymbol{r_{f/r,\omega_s}}(n) + \zeta} \right], \tag{6.3}$$

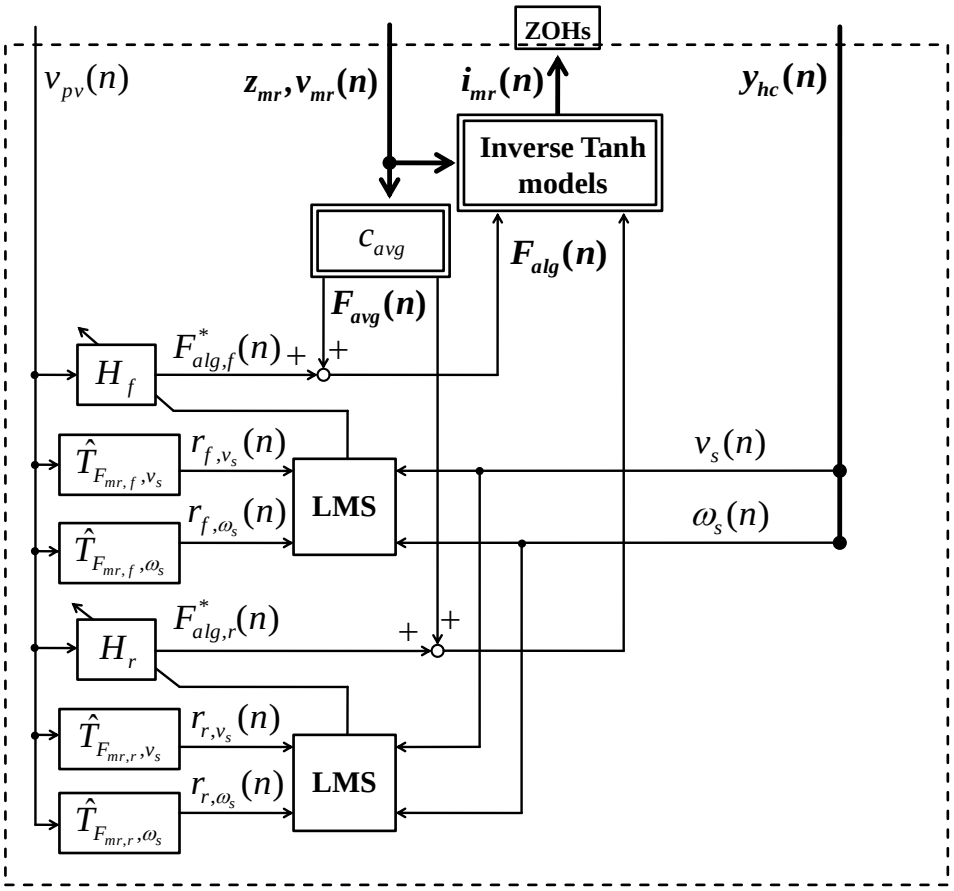

Figure 6.3: Block diagram of the modified FxLMS control related to the MR dampers

where μ denotes the adaptation step of the algorithm, while ζ is used in order to avoid the division by zero in the case of zeroing of the vectors $\boldsymbol{r}$. Symbol $\boldsymbol{h_{f/r}}$ denote vectors of filters parameters H_f and H_r of length denoted as M. Both components of the adaptation formula are weighted using parameters α_{v_s} and α_{ω_s}, where $\alpha_{v_s} + \alpha_{\omega_s} = 1$. The parameter μ is additionally normalized by expression $\boldsymbol{r}^T \cdot \boldsymbol{r}$. Similarly to vector $\boldsymbol{h_f}$ and $\boldsymbol{h_r}$, vectors $\boldsymbol{r_f}$ and $\boldsymbol{r_r}$ consist of M samples of signals r_f and r_r, respectively, which are evaluated as follows, assuming the preview signal of vertical road velocity v_{pv} is used as a reference signal:

$$\begin{aligned} r_{f/r,v_s}(n) &= \hat{T}_{F_{mr,f/r},v_s}(z^{-1}) \cdot v_{pv}(n), \\ r_{f/r,\omega_s}(n) &= \hat{T}_{F_{mr,f/r},\omega_s}(z^{-1}) \cdot v_{pv}(n). \end{aligned} \tag{6.4}$$

Symbols $\hat{T}_{F_{mr,f/r},v_s}$ and $\hat{T}_{F_{mr,f/r},\omega_s}$ denote the estimated models of dynamics of the front and rear secondary signal paths for respective error signals assuming the linearised MR damper nominal damping $\hat{c}_{avg}$ is additionally included in the vehicle suspension model

(see Subsection 6.2.4). The resultant control force is evaluated as follows:

$$F_{alg,f/r} = F^*_{alg,f/r} + F_{avg}, \tag{6.5}$$

where the preliminary control forces $F^*_{alg,f/r}$ are evaluated as a response of FIR filters $H_{f/r}$:

$$F^*_{alg,f/r}(n) = H_{f/r}(z^{-1}) \cdot v_{pv}(n). \tag{6.6}$$

The symmetry of control force domain related to F^*_{alg} ensures the FxLMS algorithm to operate properly since it generate only zero mean value control signals.

Finally, desired forces $F_{alg,f}$ and $F_{alg,r}$ generated by the front and rear MR dampers, respectively, are led into the inputs of the inverse MR damper models resulting in the control currents $i_{mr,f}$ and $i_{mr,r}$, respectively.

6.2.4 Linearised nominal damping of the MR damper

Classical FxLMS algorithm assumes linearity of the controlled objects. It takes advantage of the secondary signal path model which is assumed to be linear as well. It is recommended to apply at least coarse estimation of the secondary path models $\hat{T}_{F_{mr,f/r},v_s}$ and $\hat{T}_{F_{mr,f/r},\omega_s}$ in order to improve the algorithm convergence and stability. However, the complete models of the secondary paths $T_{F_{mr,f/r},v_s}$ and $T_{F_{mr,f/r},\omega_s}$ for the analysed vehicle suspension including MR damper model are nonlinear due to the characteristics of nominal MR damper damping c_{avg}. Such nonlinearity causes different model response for different road classes and different frequencies of road-induced excitation.

For the purpose of FxLMS algorithm a linearised MR damper nominal damping $\hat{c}_{avg}$ was estimated separately for different frequencies of sinusoidal road-induced excitation. Moreover, the estimation was performed for front and rear vehicle suspension parts as well as for compatible and inverted synchronization between the front and rear road excitation. Next, after combining MR damper model responses for different cases averaged linearised damping parameters were obtained for different road classes and vehicle suspension parts. Estimation was performed for all above mentioned averaged experimental conditions according to the following formula:

$$\hat{c}_{avg} = \underset{\Theta_{avg}}{\arg\min}\{J_{F_{avg}}(\Theta_{avg})\}, \tag{6.7}$$

where the relative quality index $J_{F_{avg}}$ being minimized is defined as a root mean squared error estimated between forces of the nominal damping F_{avg} and linear damping model. The $J_{F_{avg}}$ is normalized by multiplying it by the root mean squared force of nominal damping as follows:

$$J_{F_{avg}}(\Theta_{avg}) = \sqrt{\frac{\sum_{n=1}^{N}\{F_{avg}(n) - \Theta_{avg} \cdot v_{mr}(n)\}^2}{\sum_{n=1}^{N}\{F_{avg}(n)\}^2}}. \tag{6.8}$$

Expression $\Theta_{avg} \cdot v_{mr}$ corresponds to the model of the linear viscous damping.

Estimated values of averaged linearised nominal damping of MR damper are as follows for ascending road classes respectively: 7517, 3634, 2031 Nsm^{-1} for the front vehicle suspension and 8786, 4139, 2280 Nsm^{-1} for the rear vehicle suspension. Such results need to be converted to the vertical equivalent damping by including information about MR damper inclination described by $\alpha_{mr,f}$ and $\alpha_{mr,r}$ giving the following: 6698, 3238, 1810 Nsm^{-1} for front vehicle suspension and 7829, 3688, 2032 Nsm^{-1} for rear vehicle suspension. It was indicated that for higher classes of road excitation, i.e. greater amplitudes, the linearised nominal damping decreases. Such dependency results mainly from the nonlinear MR characteristics saturated for greater piston velocity amplitudes for which the linearised damping decreases. Furthermore, it can be noticed that the averaged nominal damping parameter obtained for the front vehicle suspension part is smaller in comparison to the rear vehicle suspension damping parameter for all analysed classes of road excitation.

Consequently, the linearised damping $\hat{c}_{avg}$ was used to derive the linear estimations of the secondary signal path models $\hat{T}_{F_{mr,f/r},v_s}$ and $\hat{T}_{F_{mr,f/r},\omega_s}$ for the different road classes as well as applied in the proposed modification of the FxLMS algorithm.

6.2.5 Stability of the modified FxLMS control scheme

Original FxLMS algorithm assumes no actuator constraints. It increases power and modulates the control signal till compensation of a system disturbance is reached. For constrained actuator despite the continuous increase of control signal energy is not transferred to the system and disturbance cannot be compensated. Thus, an FxLMS

with leakage was proposed in the literature (example of Leaky-FxLMS given in [141]) and commonly applied in noise and vibration control.

Contrary to the active elements, MR dampers exhibit the inherent constraint of the output force. Such constraints ensure that even if the adaptive algorithm is unstable the whole mechanical system is always stable. The problem of the force saturation reveals in any cycle of MR damper vibrations (see Figure 6.2). Consequently, the minimization of the cross-correlation between reference and error signal cannot be reached in the case of semiative elements as for active devices controlled by the LMS algorithm. Experiments performed for modified FxLMS applied for MR damper control indicated that the Leaky-FxLMS needs to be used which results in the following modified adaptation mechanism:

$$\begin{aligned}&\boldsymbol{h_{f/r}}(n+1) = \gamma \boldsymbol{h_{f/r}}(n) - \\ &- \mu \cdot \left[\alpha_{v_s} v_s(n) \cdot \frac{\boldsymbol{r_{f/r,v_s}}(n)}{\boldsymbol{r_{f/r,v_s}}^T(n) \cdot \boldsymbol{r_{f/r,v_s}}(n) + \zeta} + \alpha_{\omega_s} \omega_s(n) \cdot \frac{\boldsymbol{r_{f/r,\omega_s}}(n)}{\boldsymbol{r_{f/r,\omega_s}}^T(n) \cdot \boldsymbol{r_{f/r,\omega_s}}(n) + \zeta} \right],\end{aligned} \tag{6.9}$$

where γ denotes a parameter which controls leakage of the FxLMS and stability of its adaptation process.

Selected results of the modified FxLMS adaptation process are presented in Figure 6.4 and related to the road-induced excitation of the F class. Both control forces and forces generated by MR damper models are dedicated to the front part of the vehicle suspension system. Results obtained for the modified FxLMS including leakage were compared with those generated for the FxLMS algorithm without leakage. It is shown the leakage mechanism stabilize the adaptation process efficiently.

6.3 Optimization and validation of adaptive control

Presented modified FxLMS algorithm is favoured for its adaptability and scalability. Mainly, four elements of FxLMS need to be parametrized, i.e.: adaptation constant, leakage parameters and weights of heave velocity versus pitch velocity denoted as α_{v_s}, α_{ω_s} as well as model of the secondary signal path need to be estimated. However, it was stated that all parameters apart from a pair of α_{v_s}, α_{ω_s} can be derived coarsely and influence the algorithm convergence rate rather than its final performance of vibration

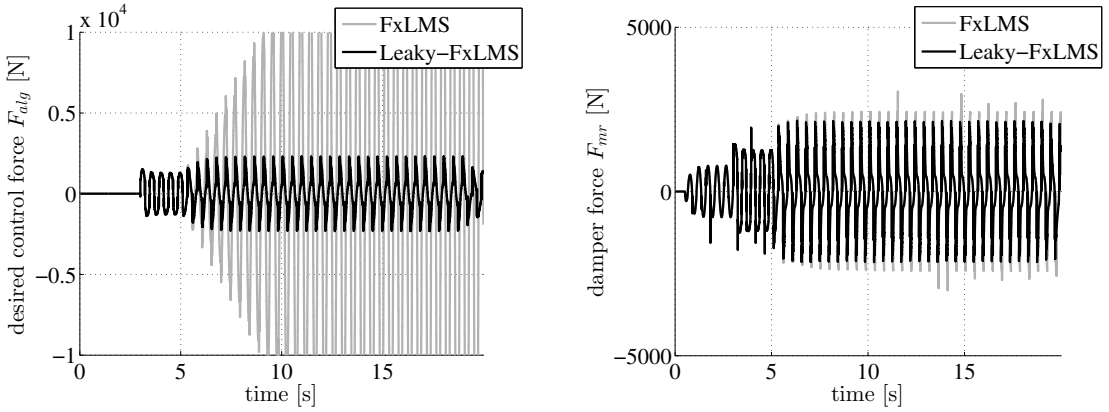

Figure 6.4: Stability of FxLMS adaptation process with/without leakage applied: a) control force desired by an algorithm, b) force generated by MR damper model

control. Initially, the adaptation constant and leakage parameters were optimized. In the case of optimization performed with respect to the secondary signal path models, all combinations of the road classes and models were validated. Similarly, to the classical semiactive control schemes presented in Chapter 5, the analysis is carried out for the half-car vehicle model. Since adaptive algorithms require continuous excitation in order to be properly tuned, the research presented in the dissertation is limited to the simulation-based validation.

6.3.1 Optimization of the modified FxLMS parameters

Quality of vibration control was analysed based on the normalized ride comfort index NJ_{RC}. Initially, the adaptation constant parameter μ was analysed in the range from 0.003 to 0.040, while the leakage parameter γ was validated in the range from 0.990 to 0.9995. Results obtained for defined experimental cases are presented in Figure 6.5. Smaller values of adaptation constant decreases the algorithm's convergence rate, while its larger values deteriorate the vibration control quality. Taking into account both, above mentioned, contradictory criteria, $\mu = 0.007$ was assumed as the optimized value. The greater the value of the leakage parameter the more deteriorated the convergence rate of the FxLMS algorithm is. Thus, $\gamma = 0.997$ was assumed as the optimized value, which simultaneously retains stability of the FxLMS algorithm.

Models of the secondary signal path were validated while the quality of the FxLMS control was tested for the vehicle suspension subjected to the road classes D, E and

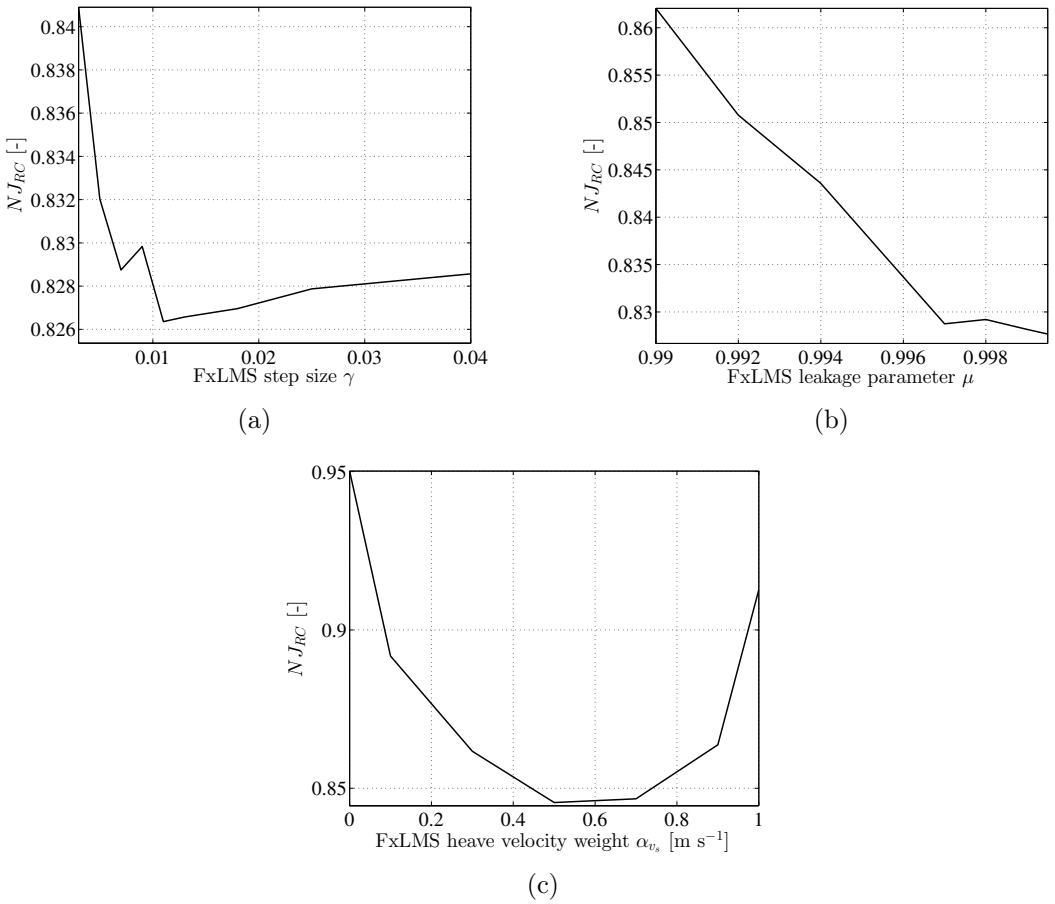

Figure 6.5: Optimization of FxLMS parameters: a) adaptation constant, b) leakage parameter, c) heave and pitch velocity weights

F. Different models of the secondary signal path were used which include previously evaluated values of the averaged linearised nominal damping estimated for different road classes (see Subsection 6.2.4). Results of the control quality evaluated based on the normalized ride comfort index NJ_{RC} were averaged over different classes of the road-induced excitation. Model of the secondary signal path including linearised nominal damping evaluated for the road class E revealed the best performance for FxLMS control of vehicle suspension subjected to road excitation of all three road classes. Thus, such model of the secondary signal path was applied in further simulations.

Besides, partly adjusted FxLMS algorithm was validated for different weights of heave and pitch velocities in range from 0 to 1.0 defined for α_{v_s} weight (see results in Figure 6.5). It was stated that $\alpha_{v_s} = 0.5$ and $\alpha_{\omega_s} = 0.5$ represent optimized combination of parameters.

6.3.2 Adaptive modified FxLMS versus classical Skyhook control

The presented comparison includes classical non-adaptive feedback control schemes analysed in Chapter 5 as well as the proposed modified FxLMS algorithm dedicated to MR damper. Results obtained for all algorithms were presented in the frequency domain for range from 0.5 to 12 Hz and road classes from D to F (see Figures 6.6, 6.7 and 6.8). The FxLMS algorithm take advantage of heave and pitch velocity signals, and of preview signal as well as of signals describing MR damper piston motion. In order to retain the similar number of the available state variables in comparison to the FxLMS algorithm, only SH2 and SH1 were taken into account in the presented comparison. Since the LQ control requires all state variables, results obtained for it were excluded.

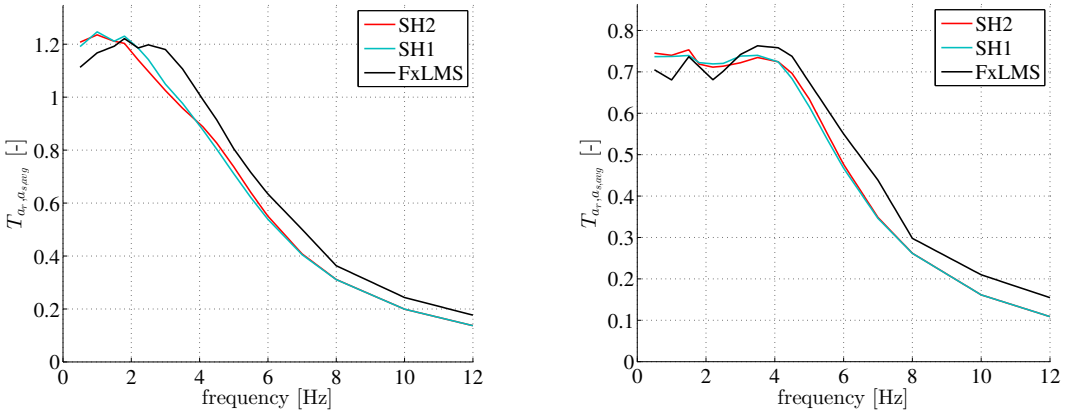

Figure 6.6: Comparison of body acceleration transmissibility characteristics evaluated for different non-adaptive and adaptive semiactive control strategies and road excitation of class D: a) compatible excitation, b) inverted excitation

Based on the presented characteristics it can be stated that the lower road class and lower amplitudes of road-induced excitation the worse results are obtained for adaptive FxLMS algorithm for higher frequencies. Such conclusions suggests application of adaptive control for more rough roads. In the case of the road class F quality of vibration control offered by the FxLMS is slightly better comparing to that obtained for classical non-adaptive control approach. The improvement can be noticed for the whole frequency range and the both compatible and inverted types of the road-induced excitation. Adaptability and no requirement of the fine parameter adjustment for the FxLMS algorithm gives another reason for its application.

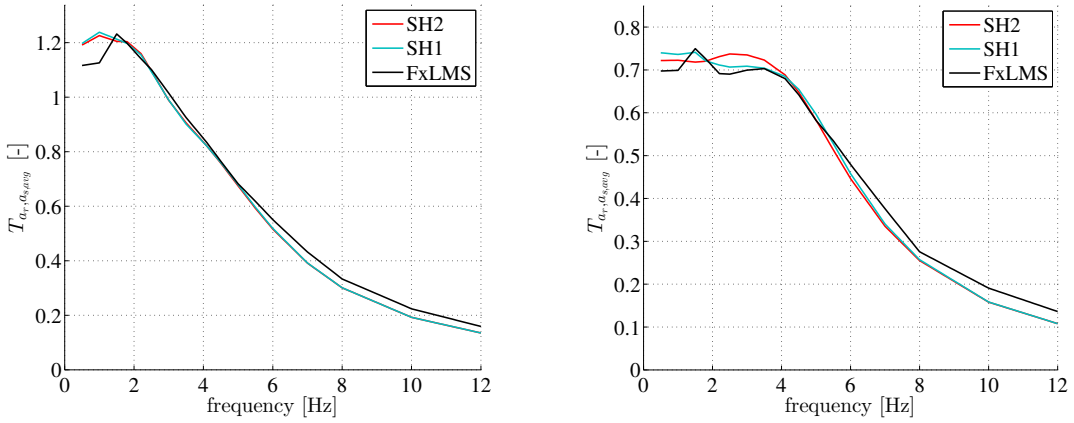

Figure 6.7: Comparison of body acceleration transmissibility characteristics evaluated for different non-adaptive and adaptive semiactive control strategies and road excitation of class E: a) compatible excitation, b) inverted excitation

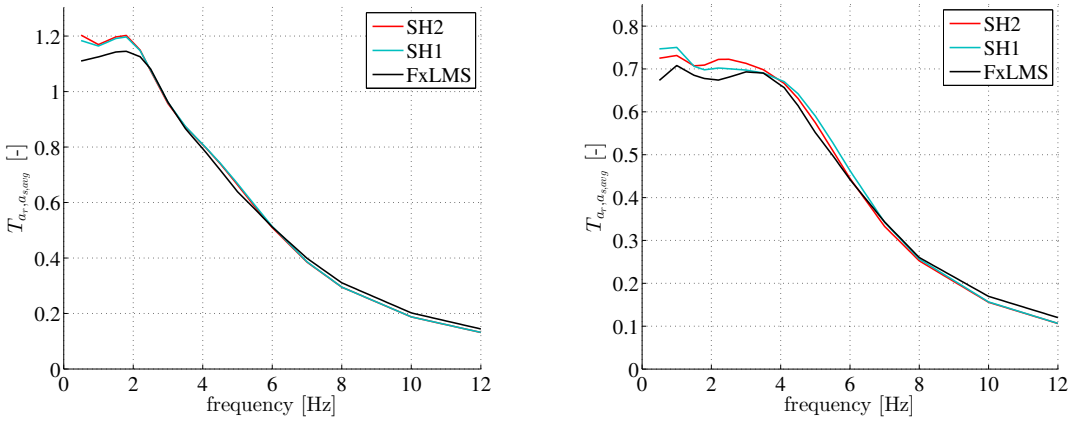

Figure 6.8: Comparison of body acceleration transmissibility characteristics evaluated for different non-adaptive and adaptive semiactive control strategies and road excitation of class F: a) compatible excitation, b) inverted excitation

6.3.3 Analysis of road holding and suspension deflection versus ride comfort

In order to perform detailed analysis, the road holding and suspension deflection indices were evaluated for the Skyhook and FxLMS algorithms under consideration (see Figure 6.9). The presented diagrams show values of the normalized indices evaluated with respect to the reference passive suspension obtained for three road classes. The reference passive case is marked by (1,1) point. Both Skyhook algorithms exhibit improvement of vibration control approximately equal to 10 percent for road classes D and E and 12

percent for F class. For FxLMS the vibration control is improved by 5 percent for road class D, by 10 percent for road class E and by 15 percent for road class F in comparison to passive suspension.

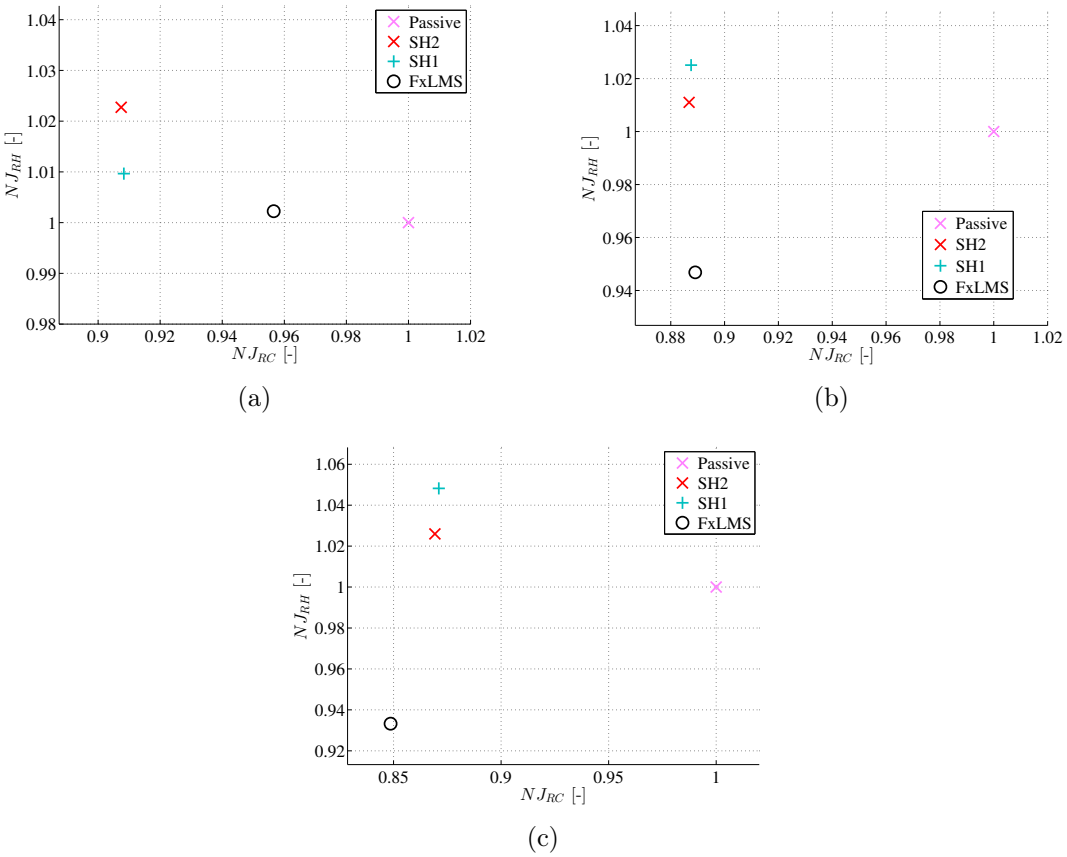

Figure 6.9: Road holding versus ride comfort diagrams obtained for non-adaptive and adaptive semiactive control for vehicle suspension subjected to road-induced excitation of different road classes: a) road class D, b) road class E, c) road class F

Simultaneous improvement in road holding offered by the FxLMS algorithm is its significant advantage; the results are better than obtained for both passive suspension and Skyhook control. In the case of Skyhoook algorithm, improvement in the vibration control was always achieved at the cost of deterioration in road holding, where differences between both control algorithms varied from 2 to 10 percent depending on the road class.

Similar analysis was performed for influence of ride comfort on suspension deflection issue (see Figure 6.10). It can be stated that the FxLMS algorithm significantly improves suspension deflection index, simultaneously, retaining quality of vibration control. Such feature is desired since it can significantly extend the time of vehicle exploitation avoiding failures of the vehicle suspension.

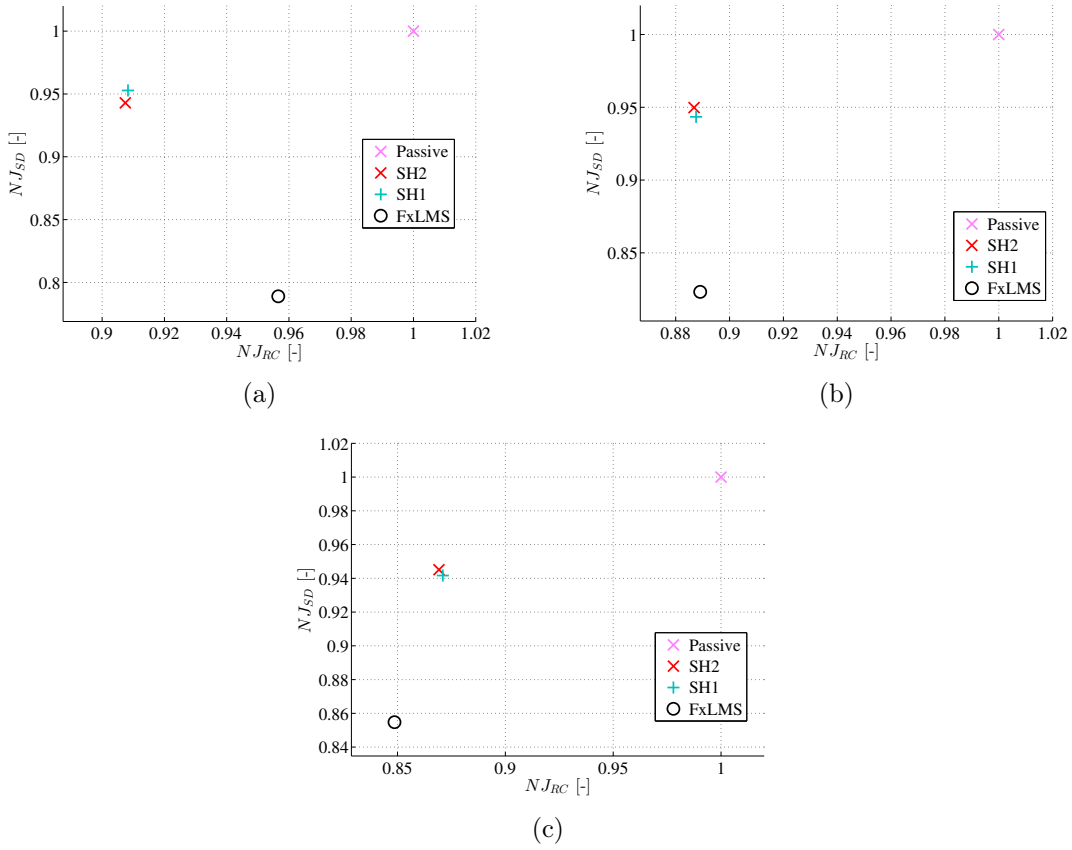

Figure 6.10: Suspension deflection versus ride comfort diagrams obtained for non-adaptive and adaptive semiactive control for road-induced excitation of different classes: a) road class D, b) road class E, c) road class F

6.4 Online identification of the MR damper model

Dynamics of the vehicle with MR dampers is commonly modelled separately using a composition of the simplified vehicle vibration model and a more complex MR damper model. Behaviour of the MR damper is dependent on different ambient conditions and character of the road-induced excitation. Furthermore, since generally the MR damper force control layer is based on the inverse MR damper model, the appropriate estimation of the inverse model has a decisive influence on the vibration control quality. Thus, many papers related to the indirect adaptive control separate identification mechanisms related to the models of the vehicle and the MR damper, and focuses on the latter one.

6.4.1 State-of-the-art in online MR damper model identification

It is important to analyse the MR damper behaviour during vehicle ride together with parameter estimation of the MR damper while the vibration control algorithm is executed. Most papers presented in the literature related to the MR damper modelling refers identification algorithms executed offline and apart from the system and the vibration control scheme, where the adaptive inverse model can be included [72, 81, 122]. Other authors [5] proposed an online identification of the MR damper dynamics by application of the modified LuGre model as an adaptive one. Since the modified LuGre model of dynamic friction is linear in parameters, it significantly simplifies the required estimation mechanism.

Further research on online MR damper identification resulted in execution of the identification procedure concurrently with the control algorithm. Different approaches were presented in the literature for the modified LuGre model [100, 140], bilinear model with hysteresis corrected using neural network [145] or the Bouc-Wen model [129]. The latter paper presents online identification in the case of concurrent execution of the H_∞ control.

Generally, all papers presented in the literature related to the online identification of the MR damper and its inverse model, especially those mentioned above, require measurements of force generated by a MR damper. It is a significant limitation since contrary to the inertial sensors which can be easily fixed with the vehicle body and underbody parts, the force sensors requires modification or even redesigning construction of the vehicle suspension system and, especially, construction of shock-absorbers.

A new approach was proposed for online identification in [66], which requires only inertial measurements of the vehicle response. Since such measurements are commonly used by the classical vibration control, their application in the MR damper identification do not generate any additional costs. The proposed algorithm was initially introduced for the quarter-car model and extended to the half-car model with vibration decoupling in [67]. Moreover, since the applied MR damper model based on tanh function is significantly nonlinear and identification is performed indirectly based on inertial measurement, the evolutionary optimization algorithm was used for parameter estimation. In summary, the presented identification approach allows for adjusting the inverse model

not only to the instantaneous road conditions but also for detecting failures in the MR damper operation.

Since the proposed algorithm is executed separately for the front and rear vehicle part, it is especially recommended for vehicles which exhibit significant vibration decoupling between their front and rear parts. According to [99], it is a very common feature of commercial road vehicles. Thus, the presented algorithm is meant to be a promising idea which can be applied for such vehicles. For the purpose of further simulation studies presented in the dissertation, the half-car model with vibration decoupling was applied, which was defined in Subsection 4.1.3.

A part of the simulation environment, which is dedicated to the controller, consists of the classical Skyhook-1DOF dedicated to the quarter-car model and two additional modules related to the identification algorithm. The main module of the identification algorithm represents an optimization evolutionary algorithm and the second module is responsible for estimation of immeasurable components of vehicle body acceleration (see Figure 6.11). Similarly as for direct adaptive methods, parameter γ_{th} of the inverse Tanh model is neglected in the further analysis.

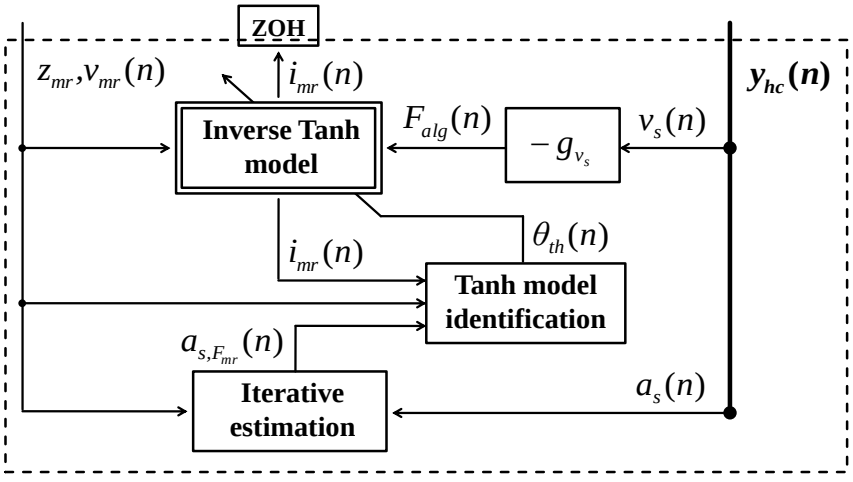

Figure 6.11: SH1 control including algorithm of inverse Tanh model adaptation

6.4.2 SH1 control for multiple-road-bump excitation

The half-car model was subjected to the multiple-road-bump excitation. Such road excitation origins in the single-road-bump excitation defined in Chapter 2 and previously used within the analysis presented in Subsection 5.3.5. Herein, the single road bump

was multiplied in order to simultaneously apply a road excitation of bump type and an excitation which is continuous and allows for execution of adaptive identification methods. An example of simulation of the multiple-road-bump excitation is presented in Figure 6.12a.

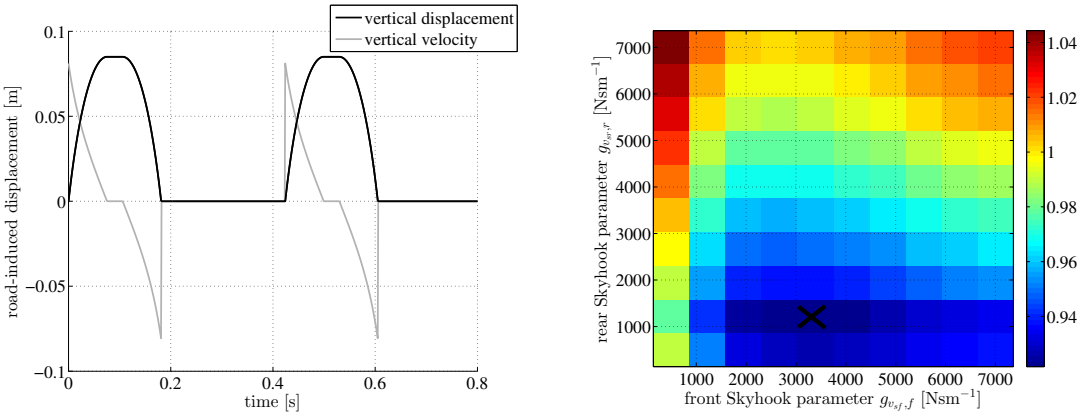

(a) (b)

Figure 6.12: Optimization of SH1 control for the decoupled half-car model subjected to the multiple-road-bump excitation: a) simulation of the road excitation for vehicle speed of 3 ms^{-1}, b) standard deviation of the averaged body acceleration $NI_{a_{s,avg}}$ for different control parameters

Vibration decoupling performed for the half-car model assures that dynamic analysis of the front and the rear vehicle part can be performed separately as for the quarter-car model. Meanwhile, analysis of the coupled quantities of the vehicle body motion (i.e. heave and pitch) is still possible as for the classical half-car model. Since identification procedures related to the quarter-car model are used, application of the SH1 for separate control of suspension quarters was the most suitable. Different configurations of the SH1 control were defined with parameters $g_{v_{sf},f}$ and $g_{v_{sr},r}$ related to the front and the rear suspension part, respectively (see Subsection 5.2.2).

Optimization of the SH1 control was performed for parameters $g_{v_{sf},f}$ and $g_{v_{sr},r}$ varying from 500 to 7000 Nms^{-1}. The optimization was performed using $NI_{a_{s,avg}}$ quality index, i.e. standard deviation of the averaged vehicle body acceleration normalized with respect to the results obtained for the passive uncontrolled vehicle suspension (see Subsection 5.3.5). The optimization space is presented in Figure 6.12b. The minimum value is equal to 0.92 which reflects values of $g_{v_{sf},f}$ and $g_{v_{sr},r}$ equal to 2800 and 1300 Nms^{-1}, respectively.

6.4.3 Estimation of immeasurable signals of quarter-car model response

Using only inertial measurements was an additional requirement for the identification algorithm. Thus, the component of the vehicle body response needs to be evaluated, which is dependent only on the MR damper force. Acceleration of the front or the rear vehicle body part denoted as a_{sf} or a_{sr}, respectively, was selected from the set of kinematic quantities since they are directly related to force generated by MR dampers, see Equations (4.2)-(4.3) in Chapter 4. The aim of the estimation algorithm is to obtain the component of acceleration a_{sf} or a_{sr} dependent on the force F_{mr} generated by the MR damper, which are denoted as $a_{sf,F^*_{mr,f}}$ and $a_{sr,F^*_{mr,r}}$, respectively.

In order to apply the proposed method, the vehicle body acceleration and velocity of damper piston need to be measured. Besides, evaluation of the models of primary and secondary signal paths requires the vehicle model (excluding the MR damper model) to be known, i.e. its stiffness and damping parameters as well as masses of the body and underbody parts. Taking into account that the vehicle model (except the MR damper model) is linear, it can be decomposed for the vehicle body acceleration into the primary and secondary signal path. The decomposition is performed with respect to two road-induced velocity excitations v_{rf}, v_{rr} and two force excitations $F^*_{mr,f}$, $F^*_{mr,r}$ related to the front and the rear vehicle part and influenced by the output dynamics $H_{F_{mr}}$ of the MR damper model (see Subsection 3.3.1).

For the half-car model, four signal paths would be distinguished for each acceleration signal a_{sf} and a_{sr}, i.e.: primary and secondary signal paths for the front vehicle part defined using transfer functions denoted as $T_{v_{rf},a_{sf}}$, $T_{v_{rr},a_{sf}}$, $T_{F^*_{mr,f},a_{sf}}$, $T_{F^*_{mr,r},a_{sf}}$ and signal paths for the rear vehicle part denoted as $T_{v_{rf},a_{sr}}$, $T_{v_{rr},a_{sr}}$, $T_{F^*_{mr,f},a_{sr}}$, $T_{F^*_{mr,r},a_{sr}}$. Since the half-car model with vibration decoupling is used, the coupled transfer functions can be neglected, i.e. $T_{v_{rr},a_{sf}}$, $T_{F^*_{mr,r},a_{sf}}$ and $T_{v_{rf},a_{sr}}$, $T_{F^*_{mr,f},a_{sr}}$ are close to zero. Apart from vehicle body acceleration, similar analysis can be done for vehicle body velocity v_{sk} as well as velocities of damper pistons $v_{mr,k}$ which are used in further analysis. Herein, symbol k denotes a certain quarter of the half-car model.

Decomposition of the k quarter of the half-car model ($k \in \{f, r\}$) into primary and secondary signal paths performed for a_{sk}, v_{sk} and $v_{mr,k}$ as well as estimation procedure are presented in block diagram in Figure 6.13. The algorithm is executed counter-clockwise for the initial value of $a_{sk,F^*_{mr,k}}$ equal to zero. Models of the primary and

the secondary signal paths are organized in pairs which include their direct or inverted representation. As a result two coupled models are constituted: $T_{a_{sk},v_{mr,k}}$ arising from $T_{v_{rk},v_{mr,k}}$ and inverted $T_{v_{rk},a_{sk}}$ as well as $T_{v_{mr,k},v_{sk}}$ arising from $T_{F^*_{mr,k},v_{sk}}$ and inverted $T_{F^*_{mr,k},v_{mr,k}}$. Such configuration allows for cancellation of unstable poles of the neighbouring discrete-time inverted models.

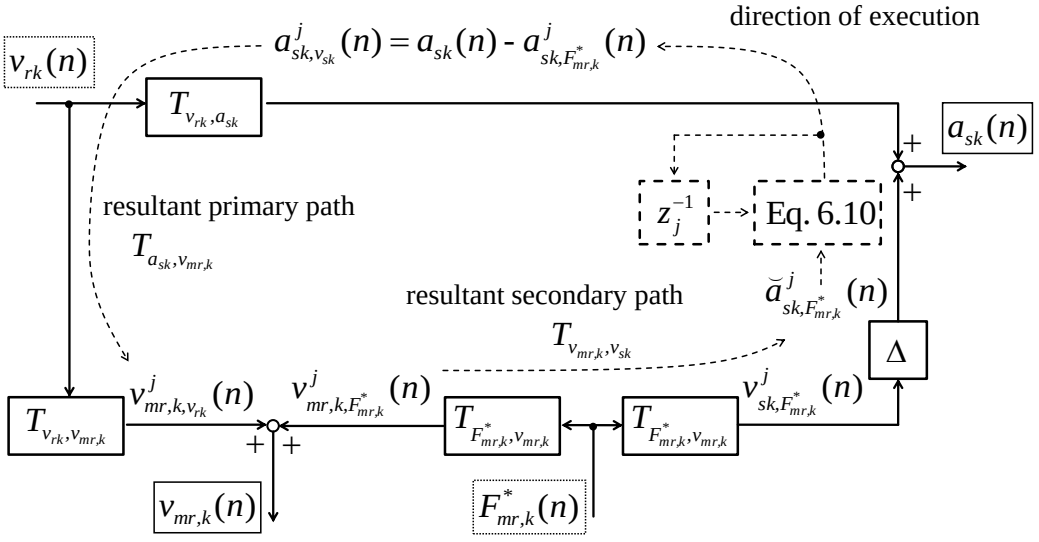

Figure 6.13: Block diagram for estimation of immeasurable signals (k denotes f - front or r - rear vehicle part)

Within further iterations $a^j_{sk,v_{sk}}$ is obtained by subtracting estimated $a^j_{sk,F^*_{mr,k}}$ from the measured sample a_{sk}. The superscript j indicates the number of the current iteration. Next, an estimate of $v^j_{mr,k,v_{rk}}$ is evaluated using the resultant primary path model $T_{a_{sk},v_{mr,k}}$. The $v^j_{mr,k,F^*_{mr,k}}$ is obtained by subtracting the estimate $v^j_{mr,k,v_{rk}}$ from the measured sample $v_{mr,k}$ and processed using the resultant secondary path model filter $T_{v_{mr,k},v_{sk}}$. Consequently, it is differenced resulting in an estimate of acceleration denoted as $\breve{a}^j_{sk,F^*_{mr,k}}$, which is a preliminary result of the current iteration. The final result of the loop $a^j_{sk,F^*_{mr,k}}$ is calculated by low-pass filtration using the previous value $a^{j-1}_{sk,F^*_{mr,k}}$ and the current one $\breve{a}^j_{sk,F^*_{mr,k}}$ according to the following relation:

$$a^j_{sk,F^*_{mr,k}} = (1-\mu_e)\cdot a^{j-1}_{sk,F^*_{mr,k}} + \mu_e \cdot \breve{a}^j_{sk,F^*_{mr,k}} \quad \text{for} \quad \text{abs}(\breve{a}^j_{sk,F^*_{mr,k}} - a^{j-1}_{sk,F^*_{mr,k}}) > \delta_e, \quad (6.10)$$

where the stop condition is indicated during the estimation process using $\delta_e = 10^{-5}$ and the adaptation step $\mu_e = 0.01$. Symbol z_j^{-1} denotes a delay operator with respect to iteration number j.

Results of the estimation procedure given as values of $a_{sf,F^*_{mr,f}}$ and $a_{sr,F^*_{mr,r}}$ for the front and the rear half-car model part, respectively, are shown in Figure 6.14. They were compared with the appropriate reference signals which were obtained by filtration of immeasurable, but available in simulation, forces $F^*_{mr,f}$ and $F^*_{mr,r}$ using transfer functions of the force-related secondary signal paths $T_{F^*_{mr,f},v_{sf}}$ and $T_{F^*_{mr,r},v_{sr}}$, respectively. The results indicate high accuracy of the estimation algorithm for both vehicle parts.

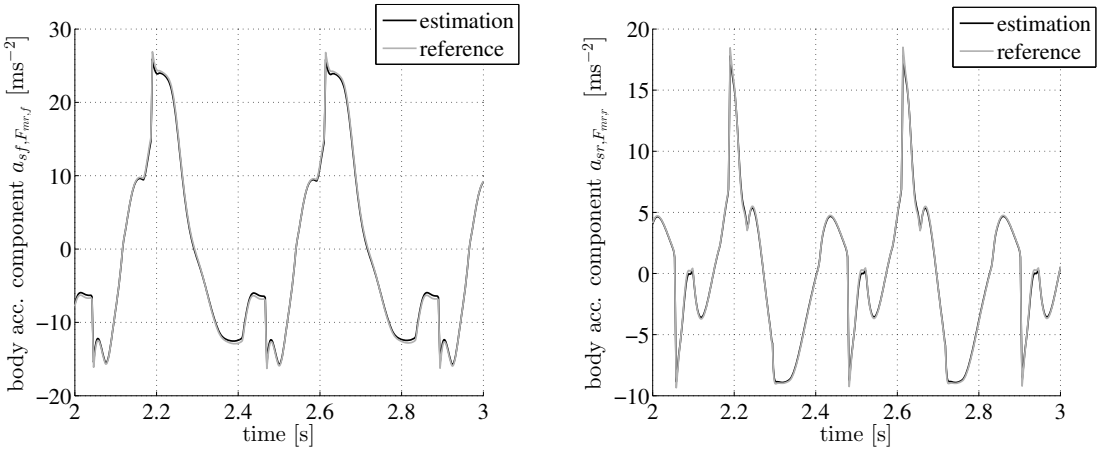

Figure 6.14: Performance of the iterative algorithm for estimation of the vehicle body acceleration components dedicated to: a) the front and b) the rear vehicle parts

6.4.4 Evolutionary algorithm for MR damper model identification

Estimation of the Tanh model parameters is the main task of the identification module. However, it operates on response forces generated by Spencer-Dyke model, since it was applied in the vehicle model as a reference MR damper model. Block diagram for the Tanh model identification is presented in Figure 6.15. It shows a quarter k of the simulated vehicle model which mainly includes a part of the linear half-car model and the nonlinear Spencer-Dyke model (see Subsection 4.2.1). Force $F_{mr,k}$ generated by the Spencer-Dyke model is influenced by the MR-damper-related model of output dynamics $H_{F_{mr}}$ and results in $F^*_{mr,k}$. Estimate of the component of the vehicle body acceleration $a_{sk,F^*_{mr,k}}$ is obtained using model of the secondary signal path $T_{F^*_{mr,k},a_{sk}}$. Besides, for the sake of simplification of further analysis, a damper-related transfer function $T_{F_{mr,k},a_{sk}}$ was defined as a composition of the $H_{F_{mr}}$ and the $T_{F^*_{mr,k},a_{sk}}$ transfer functions.

Similar signal paths were constructed within the controller starting from the Tanh model generating $\hat{F}_{mr,k}$ and including transfer function $T_{F_{mr,k},a_{sk}}$ resulting in an estimate

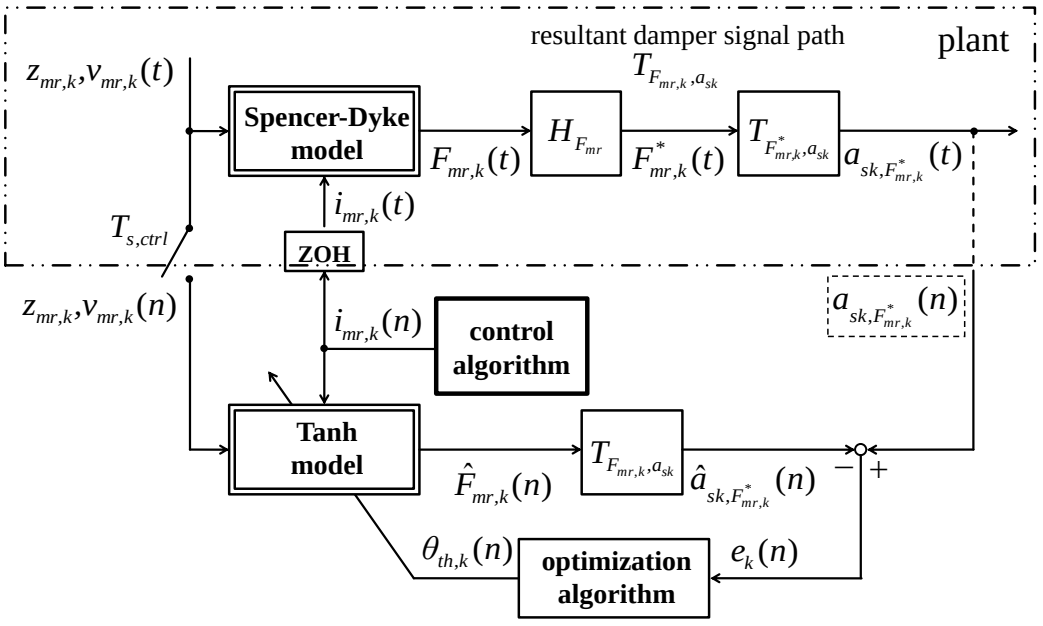

Figure 6.15: Block diagram for identification of Tanh model (k denotes f - front or r - rear vehicle part)

$\hat{a}_{sk,F^*_{mr,k}}$ according to the following formula:

$$\hat{a}_{sk,F^*_{mr,k}}(n) = T_{F_{mr,k},a_{sk}} \cdot \hat{F}_{mr,k}(\theta_{th,k}(n), z_{mr,k}(n), v_{mr,k}(n)), \tag{6.11}$$

where $\theta_{th} = [\alpha_{th,0}, \alpha_{th,1}, \beta_{th}, k_{th}, c_{th,0}, c_{th,1}]$ are being estimated. Both $a_{sk,F^*_{mr,k}}$ and its estimate $\hat{a}_{sk,F^*_{mr,k}}$, which is given by the controller module for iterative estimation, are used for evaluation of an error signal e_k. The error signal is included in the identification-related quality index which is to be minimized within the identification procedure and it is defined as follows:

$$J_{F_{th}} = \sqrt{\sum_{n=1}^{N} [a_{sk,F^*_{mr,k}}(n) - \hat{a}_{sk,F^*_{mr,k}}(n)]^2}. \tag{6.12}$$

Choosing the appropriate optimization algorithm needs to take into consideration the complexity and nonlinearity of both the Spencer-Dyke and the Tanh models which are used for evaluation of quality index $J_{F_{th}}$. Moreover, it was indicated that shape of the solution space defined by $J_{F_{th}}$ with respect to Tanh model parameters is complex. Despite the fact it represents the uni-modal shape in macroscopic scale, further analysis revealed fluctuations of the $J_{F_{th}}$ with respect to parameters. Features mentioned above

are shown in Figure 6.16 by values of $J_{F_{th}}$ evaluated with respect to $\alpha_{th,1}$ for the front vehicle part.

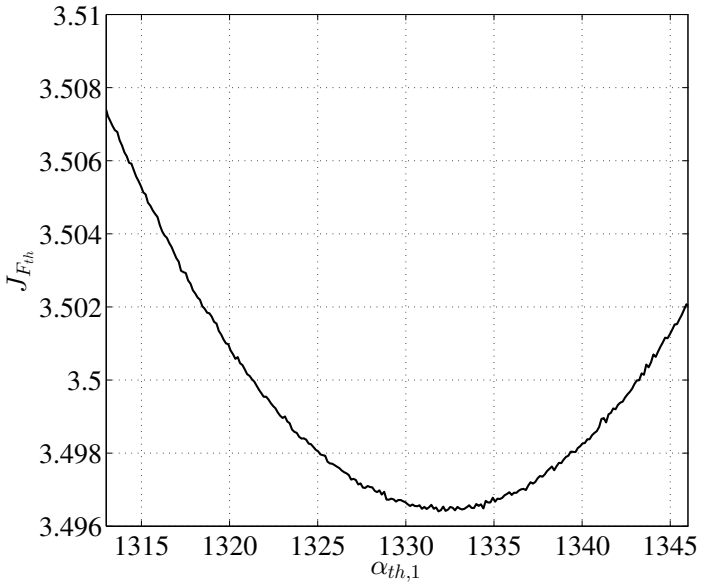

Figure 6.16: Fluctuations of the solution space evaluated using $J_{F_{th}}$ quality index for the parameter $\alpha_{th,1}$ of the Tanh model

As a result of analysis, the stochastic optimization of $J_{F_{th}}$ was applied using evolutionary optimization algorithm (see e.g. [36]). Generally, parameters of the Tanh model can be identified online for the identification algorithm operating on limited number of samples. In the analysed case the length of the identification time window was equal to 10 s. After a certain number of samples were taken, the optimization algorithm was launched as well as parameters of the Tanh models, which are used for inverse modelling in the front and rear vehicle part, were updated and applied for control within the next identification period. The applied evolutionary algorithm was operating on a population of 100 optimization candidates. Furthermore, quality of identification process depends of selected crossover and mutation operators of the evolutionary algorithm. As a result of crossover operation the child candidate obtained based on two parents candidates is located close to the parent with better value of quality index in the line containing both parents. In the case of the mutation operator a random value generated according to the uniform distribution with zero mean value is added to the child candidate.

6.4.5 Vibration control using adaptive inverse MR damper model

Single experiment consists of 3 phases, i.e. initial simulation, further MR damper model identification and second simulation performed for the updated inverse model. In the case of both simulations 10 seconds of the half-car model response to the multi-road-bump excitation is generated while the vehicle model is controlled by the optimized SH1 algorithm. During each initial experimental case the applied Tanh inverse model was deteriorated by multiplying its parameters by a deterioration rate denoted as η_{th} selected from a set $\eta_{th} \in \{ 0.25, 0.5, 0.75, 2, 3, 4 \}$.

At the beginning of the identification phase, the estimation of the component $a_{sk,F_{mr,k}}$ is performed for the front and rear vehicle parts. Next, simulated and estimated data are used for identification of Tanh model, separately for both vehicle parts. Due to the complexity of the identification solution space (see Figure 6.16) and as a result of application of the stochastic optimization method, slightly different results of consecutive executions of identification algorithm were obtained. Thus, the evolutionary algorithm was launched 30 times for each case distinguished by η_{th} in order to statistically analyse its performance.

Finally, within the last phase simulations were performed for the half-car model taking into consideration all sets of updated Tanh model parameters. Quality of vehicle body vibration control was validated for simulation results obtained in the initial and second phase using the $NI_{a_{s,avg}}$ quality index (i.e based on the normalized standard deviation evaluated for the averaged vehicle body acceleration).

Statistical analysis of results take advantage of the mean values and the 3σ deviations evaluated for the values of quality index $NI_{a_{s,avg}}$, which were obtained for all considered η_{th}. Comparison between control quality values obtained for initially deteriorated and corrected inverse model are presented in Figure 6.17. It is shown that in the case of consecutive iterations the quality of vibration control is in majority improved in comparison to that obtained for the initial inverse models. Only sporadic cases reveal further deterioration of the vibration control which is visible for η_{th} varying from 0.75 to 2. Such observations are confirmed by an analysis performed for mean values and 3σ deviations which indicate that the majority of identification executions significantly improves vibration control quality in the case of all values of η_{th}. The algorithm can be

executed iteratively for more time periods which would allow for further inverse model adaptation and improvement of vibration control quality.

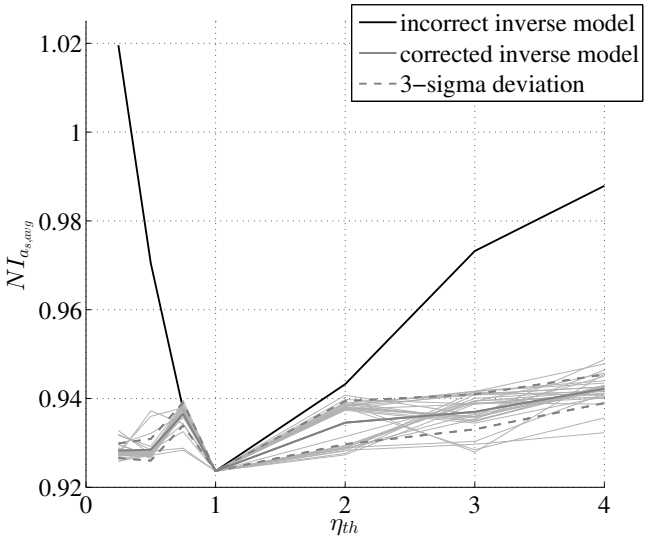

Figure 6.17: Influence of initial inaccuracy and further identification-based corrections of the inverse Tanh model on the quality of vibration control

6.5 Summary

Adaptive control is favoured for its scalability to different controlled objects. It is especially recommended in applications of vibration control for road vehicles, where parameters of both vehicle vibration model and of automotive MR dampers are time-varying, depending on passengers and ambient conditions. Modification of the well-known and robust multi-channel FxLMS control was proposed in order to control semiactive devices, strictly MR dampers. Results were evaluated for the proposed adaptive FxLMS control of the vehicle suspension model with MR dampers. The adaptive algorithm was validated in frequency domain for different road classes. Besides, analysis based on road holding and suspension deflection versus ride comfort diagrams was performed. It was indicated that the performance of the FxLMS algorithm strongly depends on the considered road class, where better performance was achieved for larger amplitudes of road-induced excitation. It was also shown that significant improvement of road holding and suspension deflection can be reached using FxLMS algorithm simultaneously retaining the level of ride comfort.

Moreover, a proposition was given which deals with the inverse model adaptation while control algorithm is being executed and it requires no force measurements. Such algorithm belongs to the group of indirect adaptive methods and consists of two components, i.e. procedure of iterative estimation of immeasurable signals as well as Tanh model identification using evolutionary optimization. Since the algorithm is executed separately for each quarter of the vehicle, it is recommended to be applied for vehicles which exhibit significant vibrations decoupling between front and rear parts. It was shown that inaccuracy of the inverse model can be significantly compensated by introducing its corrections during vehicle ride. In conclusion, both direct and indirect adaptive methods, which face the problem of varying road conditions, vehicle and MR damper parameters as well as control goals changing during ride, allow for improvement of vibration control quality.

Chapter 7

Vibration control of the experimental off-road vehicle

Experimental validation plays a key role in synthesis of a control algorithm and its application using a target controller. Due to inaccuracy of the vehicle vibration model, despite the validation of control algorithms in simulations, they need to be additionally tested and adjusted after implementation. Road experiments allow for checking if the control algorithm is applicable for a real-time suspension control. Experimental validation of the vibration control system can give a final confirmation if the analysed control approach is successful or it shows phenomena which have not been taken into account.

7.1 Studies on the experimental set-up

All road experiments were performed using a real-size off-road vehicle manufactured by ATV-Sweden of type Allroad 500. It is 2 metres long, over 1 metre wide and 1 metre high as well as it is commercially available on the market which allows the presented control system for being directly applied in typical road vehicles (see Figure 7.1).

The experimental vehicle is equipped with a suspension control system involving measurement and control parts. The control part includes four automotive MR dampers (manufactured by Lord Corporation). Construction of the vehicle suspension system consists of four independent parts which allows for controlling all MR dampers separately.

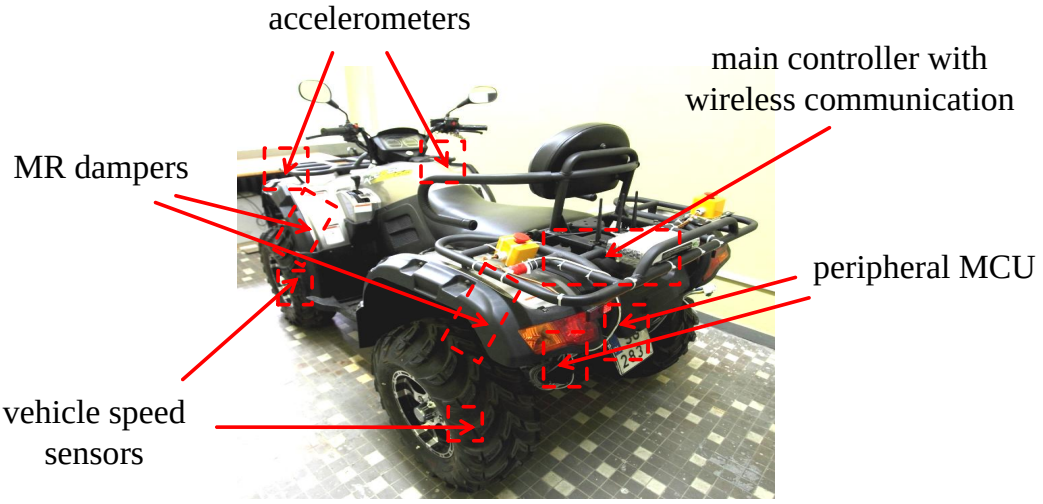

Figure 7.1: Suspension control system based on automotive MR dampers installed in the experimental off-road vehicle

Numerous sensors included in the measurement part as well as wireless access to the controller using a supervisory unit allows for tracking vehicle motion in real time.

Performing experiments dedicated to the vehicle vibration control is demanding. Ensuring repeatable conditions requires both dedicated platform for generation of different types of road-induced excitation as well as a specialized laboratory where local conditions can be stabilized and made independent from weather conditions. Furthermore, large masses are a characteristic feature of road vehicles and require high power to be used by mechanical exciters. Finally, dynamics of off-road vehicles is complex. Numerous significantly nonlinear phenomena, e.g. tyre loss of traction, limits of suspension deflection, varying position of passengers or varying ambient conditions contribute to the overall non-stationarity of the target object.

7.1.1 Topology of the measurement and control system

Presented suspension control system is organised in three layers, i.e. a supervisory layer, main control layer and peripheral control layer (see Figure 7.2 and Section 5.1). Four peripheral MCUs (Measurement and Control Units) which belongs to the lower control layer are responsible for measurement and control for the quarter of the vehicle. The MCUs collect measurement data transferred from accelerometers located in the vehicle body part and in the vicinity of a wheel, from a vehicle speed sensor as well as data transferred from the additional sensor measuring the MR damper control current.

In the case of accelerometers the measurement data are sampled with frequency of 400 or 500 Hz depending on the system configuration while the vehicle speed sensor allows for lower sampling frequency equal to 100 Hz. Unfortunately, the road-induced excitation is not known nor measured by a scanning device as assumed in simulations, and can only be indirectly estimated based on the motion of wheel axles.

All measurements taken in the vehicle body part can be related with each other assuming that bending of the vehicle body is negligible. Furthermore, speed measurement taken for all four vehicle wheels are also related with each other. Such redundancy of sensors can be used, e.g., for validation of vehicle body sensors, improvement of immeasurable quantities estimation as well as for detection of wheel loss of traction or corrections of the vehicle speed indication.

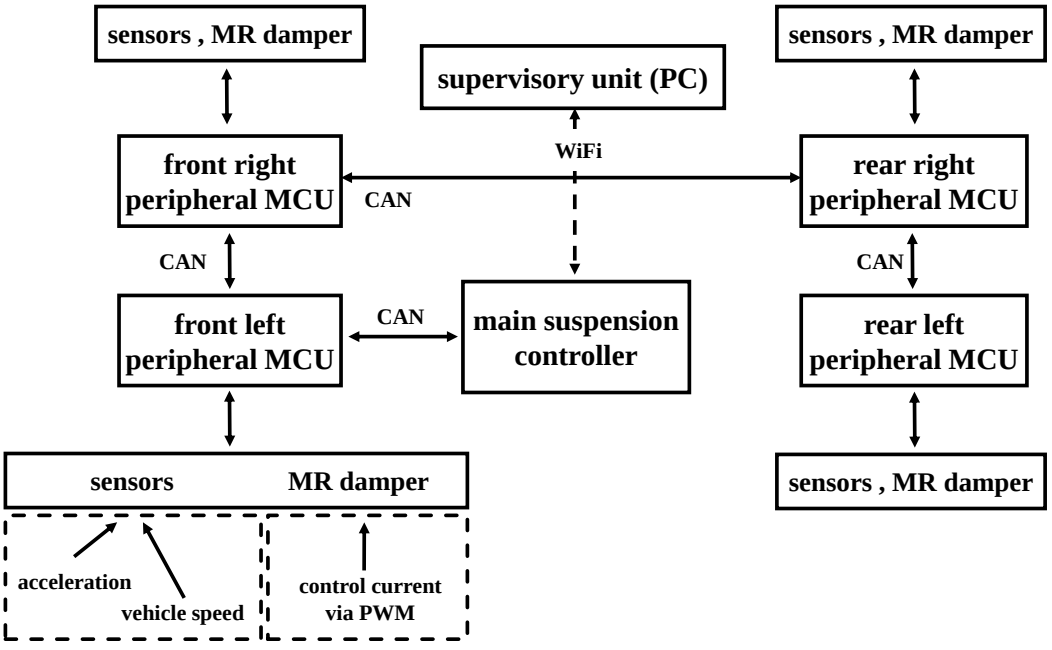

Figure 7.2: Topology and components of the suspension control system

Measurement data are transferred from MCUs to the main suspension control via CAN bus. Control algorithms related to both vibration control and MR damper control layers are located in the main controller rather than in the supervisory unit due to their significant time and computation requirements. Resultant values of control currents are transferred to selected MCU and consequently used for control of MR dampers.

Process of measurement and control tracking can be inspected in the supervisory unit. It is possible to check if experiments are valid just during their performing. After the experiment is finished, all measurements and debug data are transferred to the

supervisory unit which is used for their further processing and analysis.

7.1.2 Single-bump excitation during road experiments

Experimental analysis was performed using only a single-road-bump excitation due to difficulties related to generation of the other, e.g. continuous excitation. The single road bump belongs to the group of impulse excitation and induce simultaneously all vibration modes of the vehicle. Dominant modes, i.e. related to vibrations of vehicle body and wheels, are mainly revealed. During experiments the bump excitation was generated using a wooden beam, 85 milimetres high and wide as well as 2 metres long (see Figure 7.3). The beam was fixed with concrete blocks which allowed for retaining its position unchanged over consecutive rides. The modelling approach used for such bump excitation was presented in Chapter 2.

Figure 7.3: Single-road-bump excitation of the experimental vehicle

7.1.3 Sources of measurement noise

Vibrations of vehicle wheels and body covered by frequency range from 0.5 to 30 Hz (see Table 1.1) are desired by the suspension controller while vibrations outside that range are treated as a disturbance. The engine and tyres of the experimental vehicle are main sources of measurement noise. Some rotational energy of the engine is converted into vibrations, propagate to acceleration measurement points and influences measurements. The engine-induced measurement noise is significant, since it allows for tracking the vehicle engine speed based on only acceleration measurements taken in the vehicle body part which was shown in [80] by application of the adaptive LMS algorithm.

The experiments were performed for unmoving and moving vehicle. In order to capture features of vibrations generated by vehicle engine, its speed was set on the following revolutions per minute: 2700, 3000, 3300, 3600, 4000, 4300. Due to safety issues road experiments were performed for vehicle speed up to 30 kmh^{-1} (8.5 ms^{-1}) which is related to the range of engine speed up to 4300 revolutions per minute (72 revolutions per second).

Acceleration measurements were taken for the vehicle body and underbody parts during the experiments. It was stated based on the frequency domain analysis that obtained resonant frequencies are consistent with the vehicle speed shown in the vehicle dashboard. Exemplary temporal PSD for vehicle engine equal to approximately 3800 was presented in Figure 7.4. It can be noticed that both the fundamental frequency component (marked by gray dots) located at 64 Hz and the second component located at 128 Hz are significant as well as the third one located at 192 is still noticeable. Such measurement signal interference requires application of the higher sampling frequency in order to meet the Nyquist-Shannon sampling theorem.

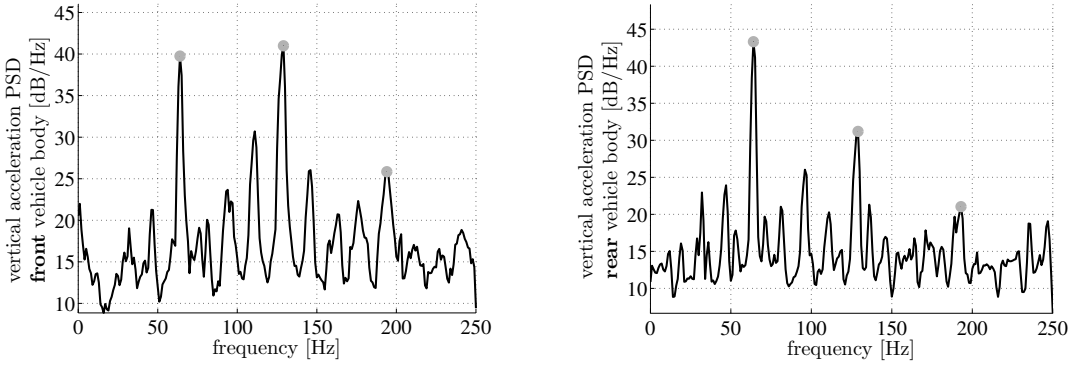

(a) (b)

Figure 7.4: Harmonic components of vehicle engine-induced measurement noise and engine speed of 3800 rpm analysed in frequency domain based on acceleration measurements: a) front and b) rear vehicle body parts

Experiments performed for moving vehicle revealed second dominant source of undesired vibrations generated by tyre thread where size of thread in the case of off-road vehicles is significant. Several experiments were performed for different values of vehicle speed while acceleration measurements taken in the vicinity of wheels were analysed for each experiment. Results showed that frequency of fundamental component of tyre-induced vibrations is directly dependent on vehicle speed (see Figure 7.5).

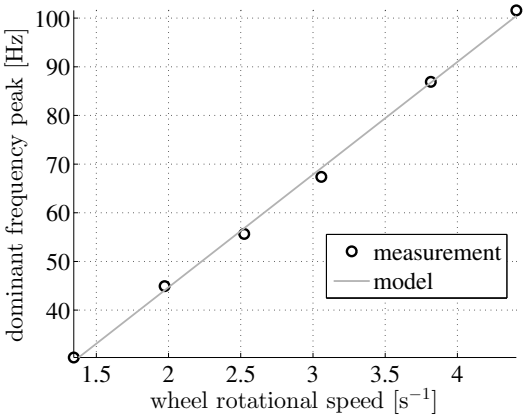

Figure 7.5: Relation between fundamental frequency of tyre-induced noise and rotational speed of wheel for different vehicle speed values

Besides, it was stated for harmonic analysis and confirmed based on observations of the tyre that a single revolution of wheel consists of approximately 23 thread pulses. Results for both unmoving and moving vehicle were compared in Figure 7.6 in order to indicate two sources of measurement noise.

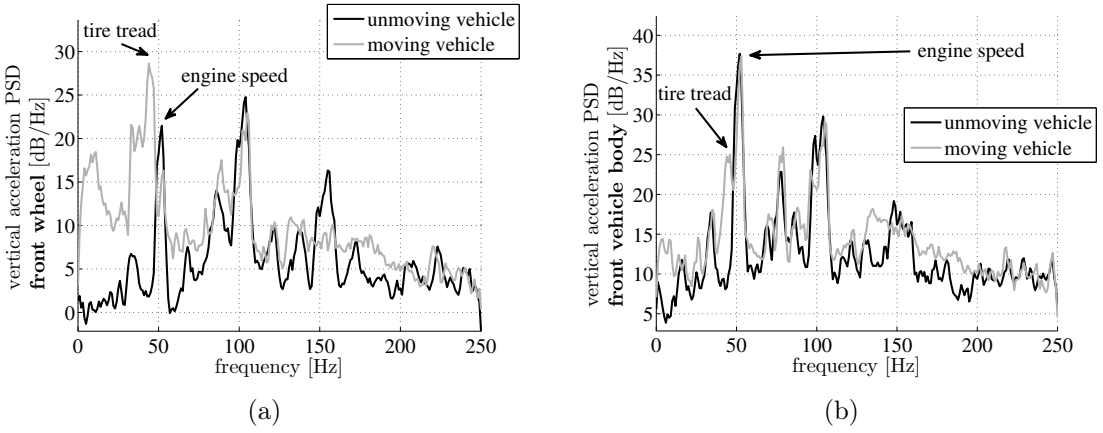

Figure 7.6: Vehicle engine- and tyres-induced noise in frequency domain based on acceleration measurements taken for engine speed of 3000 rpm: a) front vehicle wheel, b) front vehicle body part

7.2 Analysis of the vehicle vibrations

Automotive MR dampers installed in the experimental vehicle give the possibility to examine dynamics for different values of suspension damping parameters by simply changing control currents. It is possible to check how varying suspension damping parameters influences the ride comfort and driving safety issues.

The analysis presented for the experimental vehicle and the road bump excitation was performed based on acceleration measurement obtained in selected parts of the vehicle body and underbody. Finally, ride comfort indices were evaluated, based on RMS and maximum value of different acceleration quantities according to Equations (2.7) and (2.10), respectively, and compared for different current values. However, due to the measurement noise and since velocity quantities are also used in the analysis, the data preprocessing is required.

7.2.1 Measurement data preprocessing

Several kinematic quantities describing motion of the vehicle were used, i.e. vertical and angular pitch velocities and accelerations of the vehicle body parts as well as similar measurements of wheels vibrations. Thus, the goal of preprocessing algorithms is to improve quality of available acceleration measurement and to estimate velocity signals. The following is involved: conversion and space transformation of acceleration measurement, compensation of an acceleration offset induced by the gravitational acceleration, estimation of velocity signal and evaluation of vehicle body pitch-related signals.

Acceleration measurements are available in the form of three-axis components given for 8 measurement points located in the vehicle body and underbody parts. In order to obtain vertical acceleration the measurements are transformed using orientation matrices which describe position of the each accelerometer with respect to the vehicle-related coordinate system. Since only vertical acceleration signals were needed, the transformation is performed according to the following formula:

$$a_k = \boldsymbol{r}_{\boldsymbol{k}}^{\boldsymbol{acc}} \cdot \begin{bmatrix} a_{k,x} \\ a_{k,y} \\ a_{k,z} \end{bmatrix}, \tag{7.1}$$

where a_k denotes resultant vertically oriented acceleration for a certain acceleration measurement point numbered by k. Symbol $\boldsymbol{r}_{\boldsymbol{k}}^{\boldsymbol{acc}}$ denotes a part of complete orientation matrix, which is related to the vertical direction. Symbols $a_{k,x}$, $a_{k,y}$, $a_{k,z}$ denote acceleration taken for x, y and z directions of the sensor-related coordinate system, respectively.

An offset value of acceleration measurement a_k was removed using a digital first order highpass filter, as follows:

$$\hat{a}_k = 0.999 \cdot \frac{1 - z^{-1}}{1 - 0.999 z^{-1}} a_k, \tag{7.2}$$

where $\hat{a}_k$ denotes vertical acceleration signal with filtered offset value.

It was previously stated based on measurement noise analysis that both tyre-thread- and engine-induced vibrations are outside the 30 Hz frequency band which is considered for vibration control. Thus, it was proposed to apply lowpass filter with a cutoff frequency equal to 30 Hz in offline analysis. Results presented in Figure 7.7 were generated for the experimental vehicle traversing the obstacle while MR dampers were uncontrolled. It was indicated that application of the lowpass filter significantly improves quality of acceleration data which is required to analyse the bump response.

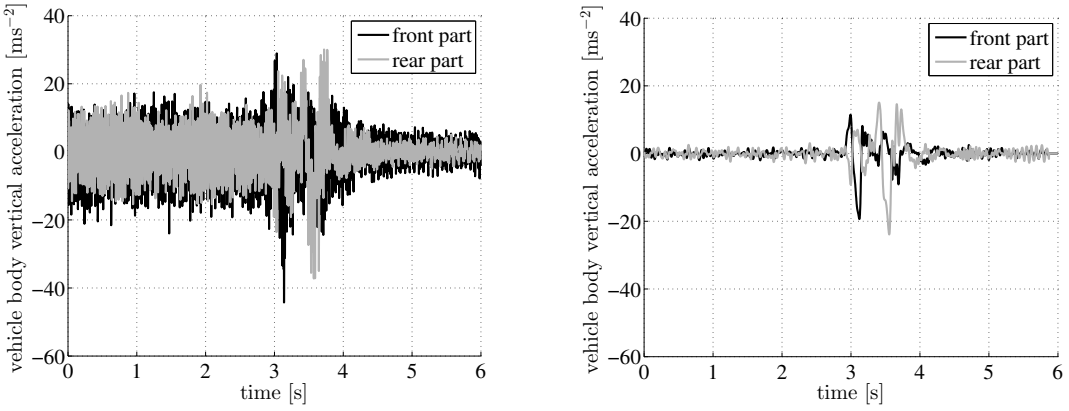

Figure 7.7: Improving quality of measurement using preprocessing algorithms for single-road-bump excitation: a) before and b) after filtration

Velocity signals can be estimated based on acceleration (with or without lowpass filtering) as follows:

$$\hat{v}_k = \frac{1}{1 - 0.99 z^{-1}} \hat{a}_k, \tag{7.3}$$

where $\hat{v}_k$ denotes velocity signal estimated for certain measurement point k. Finally, the pitch acceleration $\hat{\epsilon}_{sp}$ and velocity $\hat{\omega}_{sp}$ are evaluated using $\hat{a}_f$, $\hat{a}_r$ and $\hat{v}_f$, $\hat{v}_r$, i.e. signals estimated for the front and rear vehicle body parts, respectively, as follows:

$$\begin{aligned} \hat{\epsilon}_{sp} &= \frac{1}{L}(\hat{a}_{sr} - \hat{a}_{sf}), \\ \hat{\omega}_{sp} &= \frac{1}{L}(\hat{v}_{sr} - \hat{v}_{sf}). \end{aligned} \tag{7.4}$$

Main disadvantage of the proposed lowpass filter is significant delay time which disqualifies its application in real-time vibration control. However, experiments performed using the suspension control system indicated that the integration by itself filters out the high frequency measurement noise in a very efficient manner. Thus, in real-time control, the lowpass filter was not included in control algorithms which was based on velocity signals. Furthermore, estimation of displacement signals was neglected due to the significant measurement noise. It was concluded that future studies will require extension of the measurement part with suspension displacement sensors.

7.2.2 MR dampers supplied by constant current

Series of road experiments with constant current supplying MR dampers were performed for single-road-bump excitation assuming 10 different current values varying from 0 to 0.66 A. It is difficult to meet repeatability over consecutive experiments, e.g. results depend on both vehicle speed, direction of obstacle traversing, position of the driver. Thus, experiments for a certain current value were performed 10 times and the most similar 4 were chosen according to the fitness index, based on MSE. After the each experiment, position of the obstacle and concrete blocks were checked in order to obtain repeatability as much as possible.

Collected signals were averaged resulting in 10 smoothed cases related to each current value. Described operations were executed for all measurement and estimated signals from velocity to acceleration for all measurement points. Exemplary time diagrams of estimated and averaged velocity obtained for uncontrolled suspension MR dampers are presented in Figure 7.8.

Results present vertical velocity of wheels and vehicle body taken in the front and rear vehicle parts. It can be noticed that the time delay between front and rear vehicle excitation is equal to 0.44 s while, according to the approval documents of the experimental vehicle, the distance between axles is equal to 1.29 m. Thus, the vehicle speed was estimated at the level of 2.9 ms^{-1}, i.e. approximately 10 kmh^{-1}, which is consistent with the values indicated by available vehicle speed sensors.

Furthermore, it is shown for both front and rear vehicle parts that rising time of wheel velocity is much greater than rising time of vehicle body velocities which is caused

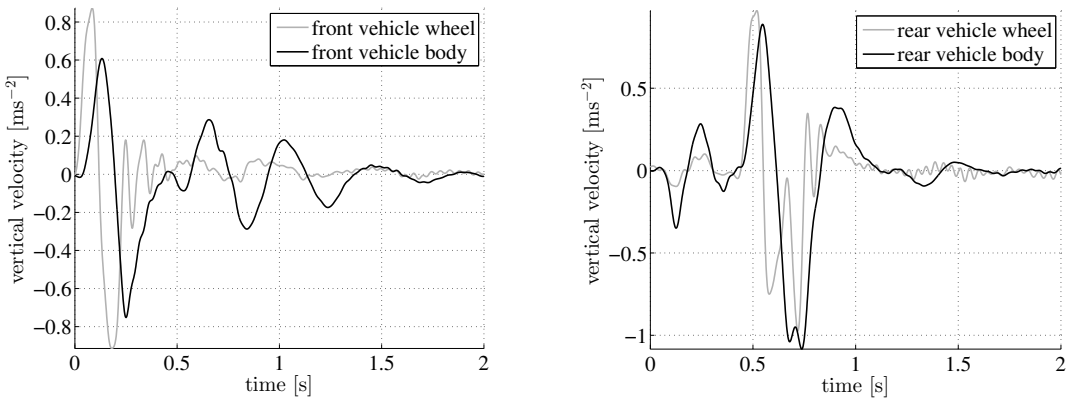

(a) (b)

Figure 7.8: Estimated vertical velocity signals for the front and rear part of vehicle body and wheels for uncontrolled MR dampers: a) front and b) rear vehicle parts

by differences between parameters of tyres and the vehicle suspension where the latter one exhibits low damping and long time decay. Finally, for all performed experiments nonlinear phenomena were clearly revealed, i.e. tyre loss of traction and elongation constraints of shock-absorbers, which is recommended to be taken into account in future models of vehicle vibrations.

7.2.3 Analysis of ride comfort

The ride comfort issue was analysed for the experimental vehicle according to the standard deviation of averaged body acceleration $\hat{I}_{a_{s,avg}}$ as well as maximum absolute acceleration values $\hat{A}_{a_s}$. Both quality indices were normalized with respect to the results obtained for passive suspension and denoted as $NI_{a_{s,avg}}$ and NA_{a_s}, respectively (see definition in Subsection 5.3.5). Such quality indices were evaluated for the each control current value based on measurements of acceleration averaged over consecutive vehicle rides (see Figure 7.9).

Diagram of $NI_{a_{s,avg}}$ shows deterioration of the ride comfort for the increasing control current. Despite the fact that a result obtained for control current equal to 0.07 A presents an exception, it still offers worse performance in comparison to that obtained for uncontrolled MR dampers. Given conclusions are consistent with those presented based on $NI_{a_{s,avg}}$ for simulation-based research (see Figure 5.18 in Chapter 5), where it was shown that higher control currents cause the vibrations of wheels propagate to the vehicle body parts. Such observations were qualitatively confirmed by the driver of the

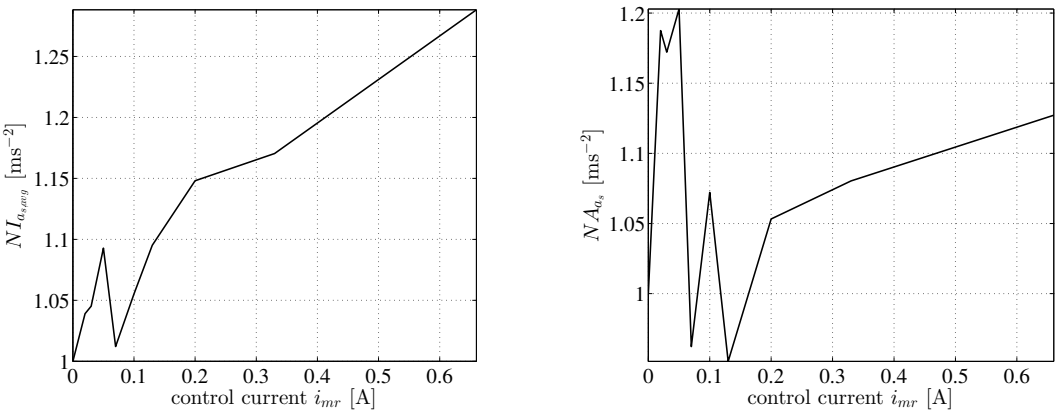

(a) (b)

Figure 7.9: Ride comfort evaluated for passive suspension using different indices based on vehicle body acceleration: a) standard deviation of averaged acceleration, b) acceleration maximum value

experimental vehicle. In the case of NA_{a_s} variation of results is more significant but still better results were obtained for lower control currents while the majority of worse ones were obtained for higher currents.

Additionally, time diagrams of results obtained for the averaged body acceleration $a_{s,avg}$ as well as for the vehicle body pitch acceleration ϵ_{sp} are presented in Figure 7.10 for boundary values of control current equal to 0 and 0.66 A. Previous conclusions about deterioration of ride comfort for increasing control current are confirmed.

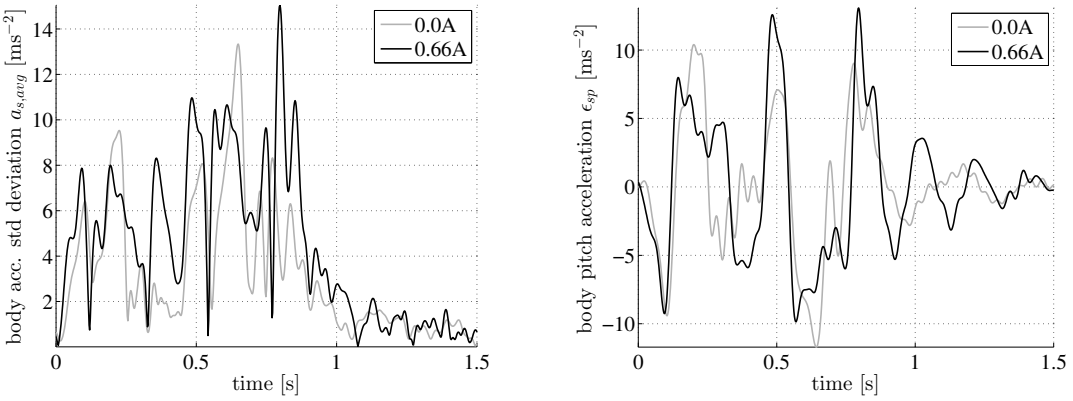

(a) (b)

Figure 7.10: Results of vibration control quality for different values of control current: a) standard deviation of averaged vehicle body acceleration, b) vehicle body pitch acceleration

7.3 Control of the suspension system

Two main approaches of semiactive suspension control using Skyhook algorithm were validated during road experiments, i.e. separate control related to quarter-car model and control of vehicle body pitch velocity. The algorithms are denoted as SH1-$g_{v_{sf},f}$,$g_{v_{sr},r}$ (or single parameter is used in case of parameters equality) and SH2-pitch-$g_{\omega_{sp}}$ (defined in the following section), where $g_{\omega_{sp}}$ is the parameter of the SH2-pitch algorithm. For detailed description of the algorithm parameters see Subsection 5.2.2. Furthermore, for separate Skyhook control two MR damper control approaches were examined, i.e. continuous (SH1) and on-off (SH1-onOff-i_{mr}^{max}, where i_{mr}^{max} is the parameter of the algorithm denoting the maximum control current). For continuous control approach the Tanh inverse model was applied. Similarly as was tested in simulation, the parameter γ_{th} of the inverse model, which is related to the damper piston acceleration, was zeroed.

Results for each experimental case were obtained several times and the final were evaluated by averaging the most similar ones according to the MSE-based fitness index. Comparison is presented in time domain as well as based on quality indices related to ride comfort issue. Commonly, the normalized standard deviation of averaged vehicle body acceleration $NI_{a_{s,avg}}$ and vehicle body pitch acceleration $NI_{\epsilon_{sp}}$ (defined in the following section) were applied as well as the normalized maximum value of vehicle body acceleration NA_{a_s} was used.

7.3.1 Separate Skyhook control of suspension parts

For the purpose of analysis of separate Skyhook algorithm and its implementation in suspension control system, the Equation (5.9) can be reformulated as follows:

$$F_{alg,k} = -g_{v_{sk},k} \cdot \hat{v}_{sk}, \tag{7.5}$$

where $F_{alg,k}$ denotes vertically oriented force desired by SH1 algorithm generated for a quarter of vehicle suspension denoted as k, while $g_{v_{sk},k}$ denotes the control gain. MR dampers installed in the experimental vehicle are leaning with respect to vertical direction which is taken into account in the following:

$$F_{alg,k}^{mr} = (r_k^{mr})^{-1} \cdot F_{alg,k}, \tag{7.6}$$

where $F^{mr}_{alg,k}$ needs to be generated by the MR damper and r^{mr}_{k} describes orientation of the MR damper numbered by k. Finally, control current obtained for the SH1 algorithm can be generated for certain part of the vehicle suspension using inverse Tanh model of the MR damper as follows:

$$i_{mr,k} = i_{mr,th}(F^{mr}_{alg,k}, \hat{v}_{mr,k}). \tag{7.7}$$

It was indicated based on simulation research presented in Chapter 5, that constraints set on $i_{mr,k}$ limiting it to positive values are sufficient for appropriate application of the Skyhook control. Generally, additional switching rule is being proposed in the literature [64] which activates the inverse model only if $v_s \cdot v_{mr}$ is positive. Such modification of the Skyhook control algorithm is defined as follows:

$$i_{mr,k} = \begin{cases} i_{mr,th}(F^{mr}_{alg,k}, \hat{v}_{mr,k}) & \text{for} \quad \hat{v}_{sk} \cdot \hat{v}_{mr,k} > 0 \\ 0 & \text{for} \quad \hat{v}_{sk} \cdot \hat{v}_{mr,k} \leq 0 \end{cases}, \tag{7.8}$$

where MR damper piston velocity v_{mr} can be evaluated as follows:

$$\hat{v}_{mr,k} = (r^{mr}_{k})^{-1} \cdot (\hat{v}_{sk} - \hat{v}_{uk}). \tag{7.9}$$

In order to simplify the SH1, the control current can be switched between only two values resulting in the modified control approach denoted as SH1-onOff and described as follows [122]:

$$i_{mr,k} = \begin{cases} i^{max}_{mr} & \text{for} \quad \hat{v}_{sk} \cdot \hat{v}_{mr,k} > 0 \\ 0 & \text{for} \quad \hat{v}_{sk} \cdot \hat{v}_{mr,k} \leq 0 \end{cases}, \tag{7.10}$$

where i^{max}_{mr} is a parameter of SH1-onOff control and denotes the maximum value of current.

Values of quality index $NI_{a_{s,avg}}$ were evaluated for all cases of SH1 control as well as for the continuous and on/off MR damper control approaches. In the case of continuous control the SH1 with parameter equal to 3000 gave best results while for the on/off control best results were given for a maximum value of current equal to 0.1 A. Time diagrams of vehicle body vertical velocity are presented for the best tuned algorithms in Figure 7.11. Results show worse performance of the on/off control approach in comparison to

the continuous approach which is indicated by greater value of maximum pick-to-pick amplitude.

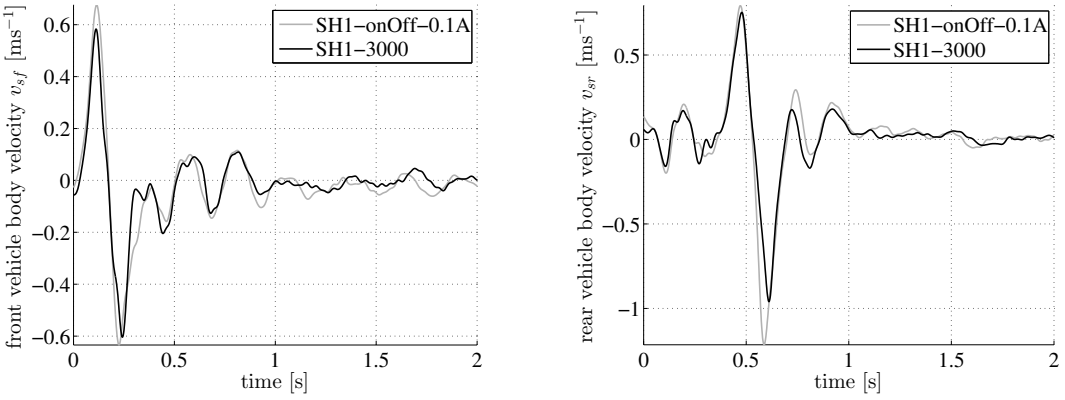

(a) (b)

Figure 7.11: Results based on vehicle body vertical velocity obtained for Skyhook control schemes for continuous and on-off MR damper control approaches: a) front and b) rear vehicle parts

7.3.2 Skyhook control of the pitch vibrations

Multi-dimensional nature of the experimental object offers wide spectrum of possible applications and control goals. Since multiple MR dampers can be utilized in multiple combinations in order to meet a single control goal, other goals can be simultaneously taken into account during control synthesis. Optimization of efficiency of forces generation by MR dampers or minimization of resultant power consumed by the suspension control system are examples of such additional goals.

The aim of the Skyhook control for a half-car model was to minimize vibrations of the vehicle body pitch acceleration. Thus, it is stated that the following standard deviation of the vehicle body pitch acceleration response to single-road-bump excitation is used for validation of the control scheme:

$$\hat{I}_{\epsilon_{sp}} = \sqrt{\frac{1}{N}\sum_{n=1}^{N}\{\epsilon_{sp}(n)\}^2}, \tag{7.11}$$

while $NI_{\epsilon_{sp}}$ denotes $\hat{I}_{\epsilon_{sp}}$ normalized with respect to results obtained for passive suspension with uncontrolled MR dampers. The following pitch related control scheme SH2-pitch was synthesized assuming that all control currents are equal to each other.

Such feature simplifies the control scheme since only a single current value needs to be evaluated and transferred to all MCUs. The algorithm take advantage of the vehicle body pitch velocity signal ω_{sp}, as follows:

$$M_{alg} = -g_{\omega_{sp}} \cdot \hat{\omega}_{sp}, \tag{7.12}$$

where M_{alg} denotes a resultant moment of force desired to be generated by MR dampers while g_{ω_s} denotes a control gain.

Position of the gravity centre of the experimental vehicle body is not known exactly. Thus, it is assumed for the SH2-pitch that $L_f = L_r = 0.5 \cdot L$. Furthermore, it is stated that due to the symmetrical road bump excitation piston velocities of right and left MR dampers are similar, i.e. $\hat{v}_{mr,fr} = \hat{v}_{mr,fl} = \hat{v}_{mr,f}$ and $\hat{v}_{mr,rr} = \hat{v}_{mr,rl} = \hat{v}_{mr,r}$. Such assumption simplifies the experimental vehicle to the half-car model, where the desired control forces correspond to the front and rear vehicle parts. Finally, the inverse model was applied based on the Tanh Equation (3.10). Additionally, due to the noise of the piston acceleration measurements $\hat{a}_{mr}$, the parameter γ_{th} of the inverse model was neglected resulting in the following modification:

$$F_{mr,th} = -\left(\alpha_{th,0} + \alpha_{th,1}\sqrt{i_{mr}}\right)\tanh(\beta_{th} v_{mr}) - \left(c_{th,0} + c_{th,1}\sqrt{i_{mr}}\right) v_{mr}, \tag{7.13}$$

which can be reformulated for the purpose of further control derivation as follows:

$$F_{mr,th} = F_{th,0} + F_{th,1} \cdot \sqrt{i_{mr}}. \tag{7.14}$$

Both control goals related to vibration mitigation and algorithm simplification can be met if instantaneous states of MR dampers allow generating forces consistent with those desired by the control scheme defined by Equation (7.12) in both front and rear vehicle parts. In such a case the inverse MR damper model can be formulated involving the model reformulation (7.14) and the assumption about the equality of currents as follows:

$$i_{mr,th,\varphi_{sp}}(M_{alg}, \boldsymbol{v_{mr}}) = \left(\frac{-\frac{M_{alg}}{L_{fr}} - r_f^{mr} F_{th,f,0} + r_r^{mr} F_{th,r,0}}{r_f^{mr} F_{th,f,1} - r_r^{mr} F_{th,r,1}} \right)^2. \tag{7.15}$$

Apart from situations when for both front and rear vehicle parts the desired forces can be generated, it also happens that only certain vehicle part can be controlled in a desired

manner or none of MR dampers is able to generate desired control force. All above mentioned cases need to be taken into account in the final switching rule of the SH2-pitch control as follows:

$$i_{mr} = \begin{cases} i_{mr,th,\varphi_{sp}}(M_{alg}, \hat{\boldsymbol{v}}_{\boldsymbol{mr}}) & \text{for} \quad \hat{\omega}_s \cdot \hat{v}_{mr,f} < 0 \ \text{ and } \ \hat{\omega}_s \cdot \hat{v}_{mr,r} > 0 \\ 0 & \text{for} \quad \hat{\omega}_s \cdot \hat{v}_{mr,f} \geq 0 \ \text{ and } \ \hat{\omega}_s \cdot \hat{v}_{mr,r} \leq 0 \\ i_{mr,th}(\frac{M^{mr}_{alg,f}}{L_f}, \hat{v}_{mr,f}) & \text{for} \quad \hat{\omega}_s \cdot \hat{v}_{mr,f} < 0 \\ i_{mr,th}(\frac{M^{mr}_{alg,r}}{L_r}, \hat{v}_{mr,r}) & \text{for} \quad \hat{\omega}_s \cdot \hat{v}_{mr,r} > 0 \end{cases}, \tag{7.16}$$

where

$$M^{mr}_{alg,j} = (r^{mr}_j)^{-1} \cdot M_{alg}. \tag{7.17}$$

In the case of vibration control limited to only certain MR dampers, the control is simplified to the SH1 where desired control force is generated based on desired moment of force M_{alg}.

Three cases of SH2-pitch control were validated, i.e. for parameters equal to 6000, 8000 and 10000, where results for boundary cases are presented in Figure 7.12 in the form of time diagrams of vehicle body pitch velocities. Additionally, it can be stated that $g_{\omega_{sp}} = 6000$ Ns rad^{-1} gives best results with respect to both $NI_{a_{s,avg}}$ and $NI_{\epsilon_{sp}}$ quality indices.

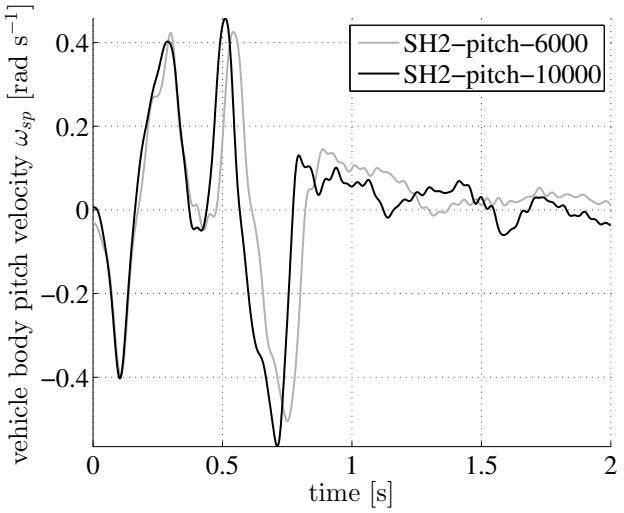

Figure 7.12: Results of vibration control quality based on vehicle body pitch velocity obtained for different parameters of Skyhook algorithm dedicated to pitch control

7.3.3 Comparison of different Skyhook control approaches

The following analysis is performed based on normalized standard deviation and maximum values of the averaged vehicle body acceleration denoted as $NI_{a_{s,avg}}$, NA_{a_s}, respectively (see definition in Subsection 5.3.5), as well as normalized standard deviation of the vehicle body pitch acceleration denoted as $NI_{\epsilon_{sp}}$ (see definition in Subsection 7.3.2). Mainly, three groups of semiactive control algorithms are compared including the Skyhook control with on/off or continuous MR damper control approaches as well as Skyhook control of vehicle body pitch vibrations. Furthermore, the SH1 control schemes with different parameters corresponding to the front and rear vehicle parts were validated. All quality indices were normalized with respect to thosed obtained for a passive suspension system with uncontrolled MR dampers.

Initially, results of the $NI_{a_{s,avg}}$ quality index (i.e. normalized standard deviation of the averaged vehicle body acceleration) was analysed and presented in Figure 7.13. It is shown that simplification of the SH1-onOff algorithm can be applied at the cost of worse performance than obtained for the continuous MR damper control approach. Thus, application of SH1 control is recommended in actual vehicles rather than application of SH1-onOff control.

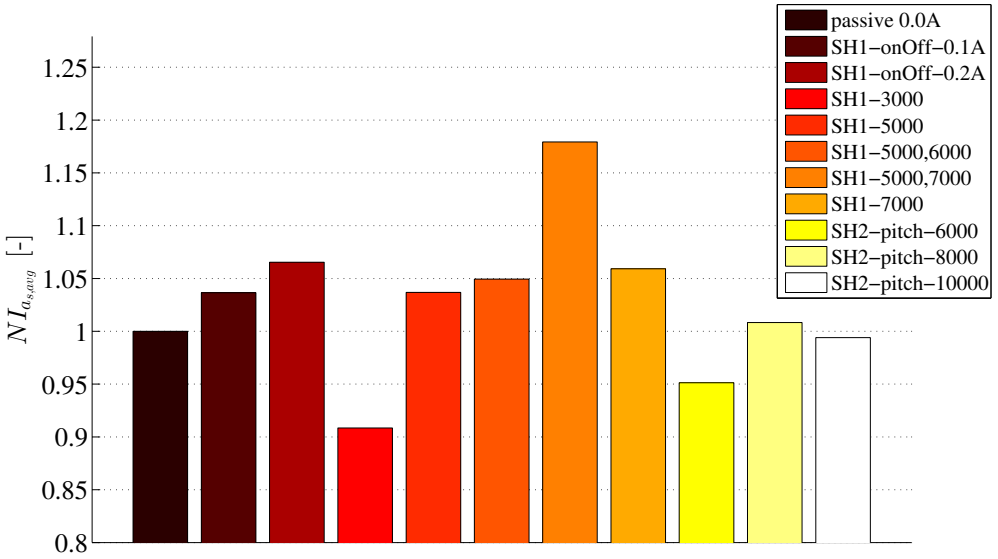

Figure 7.13: Comparison of normalized standard deviation evaluated based on averaged vehicle body acceleration for different semiactive control algorithms

Similar performance with respect to $NI_{a_{s,avg}}$ was obtained for the best cases of both SH1 and SH2-pitch control algorithms, while SH1 with parameter equal to 3000 gives the best results. It improves vibration control by 10 percent in comparison to passive suspension, which is consistent to improvement rates obtained for simulation-based research (see Subsection 5.3.5).

For NA_{a_s} quality index (i.e. normalized maximum value of the vehicle body acceleration), best performance was offered by the SH1 algorithm (see Figure 7.14). Additionally, the SH2-pitch control with parameter equal to 10000 appeared to be the best one in minimization of the maximum values of vehicle body acceleration in comparison to other pitch related algorithms.

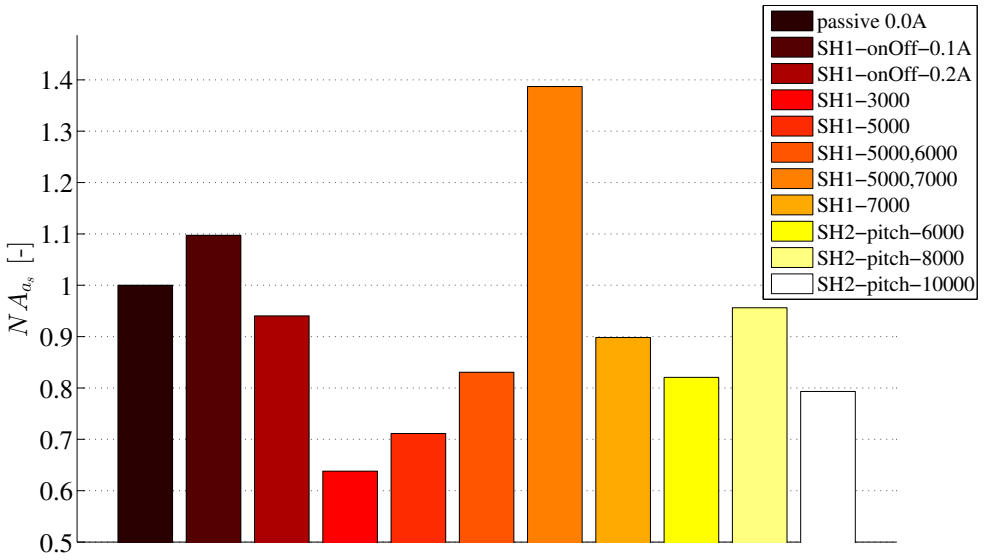

Figure 7.14: Comparison of normalized maximum values of vehicle body acceleration evaluated for different semiactive control algorithms

The $NI_{\epsilon_{sp}}$ quality index is appropriate for validation of semiactive control dedicated to pitch vibrations (see Figure 7.15). It was indicated that SH2-pitch algorithm gives better results in comparison to algorithms from other groups including previously favoured SH1 control.

In conclusion, the SH1 with parameter equal to 3000 offers quite good performance according to all presented quality indices. Finally, it should be noticed how important the appropriate configuration of semiactive control algorithms is. Not only class of a semiactive algorithm needs to be adjusted to its application but also its parameters should be carefully tuned.

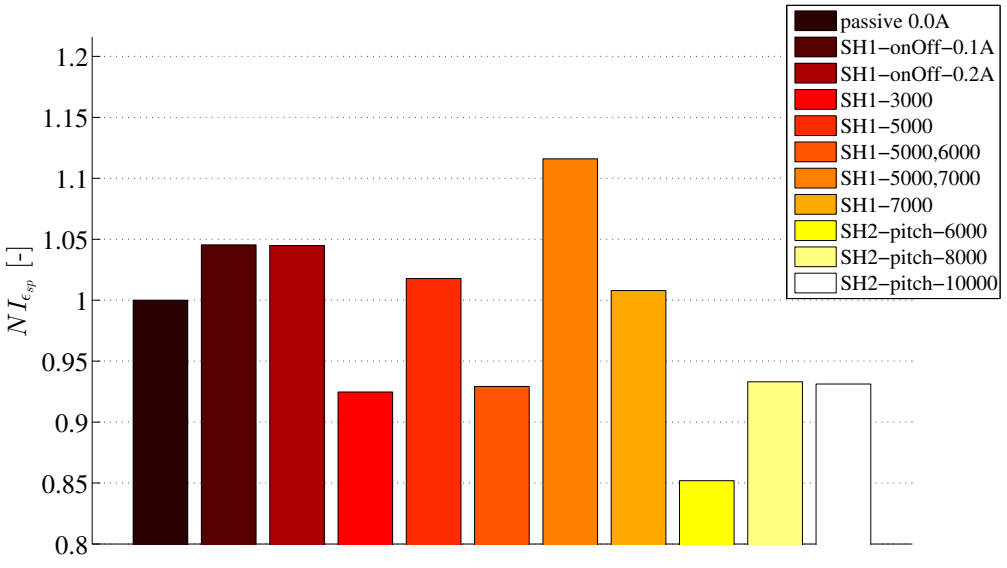

Figure 7.15: Comparison of normalized standard deviation evaluated based on vehicle body pitch acceleration for different semiactive control algorithms

7.4 Summary

Possibility of on-line adaptation of the vehicle suspension allows for significant improvement of the vibration control for different road conditions. The suspension control system was installed and configured for an actual real-sized off-road vehicle which is available on the market. Thus, the proposed solutions can be directly transferred to commercial applications. Semiactive control of vehicle vibrations using MR dampers is challenging due to significant nonlinearities revealed for both the vehicle vibration model as well as for MR dampers. Several problems were solved which are related to tyre-induced and engine-induced measurement noise as well as to other difficulties in experimental studies. It was shown that improvement of vibration control can be reached with respect to different control goals, i.e. related to vertical or angular acceleration, and different on/off or continuous MR damper control approaches.

Chapter 8

Conclusions and perspectives

This dissertation refers control methods dedicated to automotive MR dampers installed in vehicle suspension systems. Significant advantages of MR dampers were confirmed by numerous institutes over the world. Control schemes related to ride comfort and driving safety needs to be applied for varying road conditions, manoeuvres performed by a driver and subjective feelings of passengers whereas possibility of tuning MR dampers during ride is desired. The analysis is focused on improvement of ride comfort which is assessed using acceleration based quality indices while driving safety related issues are simultaneously observed.

MR damper is an example of semiactive device which can only dissipate energy. Analysis of the suspension control system needs to be performed for different classes of road-induced excitations varying from single road bumps to continuous excitation. Commonly, the sinusoidal excitation of different frequencies and amplitudes was used in order to analyse response of complex nonlinear suspension in a wide frequency band.

General model of MR damper can be decomposed into two nonlinear signal paths related to piston velocity and control current. Nonlinearity of the first is revealed in the form of force saturation for greater piston velocities and hysteresis loops for lower velocities. The second is caused by nonlinear relationships between parameters of MR damper model and control current. The Spencer-Dyke model was proposed for simulation-based studies as a reference model while an additionally identified Tanh model was reformulated into an inverse MR damper model, validated and applied in the analysis of semiactive control.

Simulation-based studies were focused on a longitudinal vehicle model, i.e. the 4-DOF half-car model, since road obstacles which are taken into account and construction of the experimental vehicle can be approximately assumed as symmetrical. The half-car model consists of linear part including vehicle body, suspension system and wheels where their stiffness and damping are represented as springs and dampers included in the model. Common nonlinearity of the model is contributed by the Spencer-Dyke model. Furthermore, the control force generated by the MR damper is additionally influenced by the vehicle vibration model, mainly by the damper piston velocity. The resultant vehicle vibration model was validated for different types of excitation while results showed correctness of the simulation environment as well as significant dependence of the vehicle response on road classes.

Generally, three control layers can be distinguished for suspension control systems: optimization layer, vibration control layer and MR damper force control layer which includes the inverse MR damper model. Classical semiactive vibration control is represented by Skyhook control algorithms related to both separate control of each suspension quarter or coupled control of vehicle body vibrations. The LQ control was additionally validated since the Skyhook control has its origin in it. All presented algorithms were optimized with respect to quality indices related to ride comfort.

In the case of adaptive control of MR dampers the direct and indirect approaches can be distinguished. The FxLMS algorithm, which is an example of the direct adaptive control, was applied in the dissertation. Contrary to classical control schemes which have to be optimized before their application, the proposed adaptive algorithm requires only coarse preliminary tuning of its parameters which influence its convergence rate rather than the quality of vibration control. Furthermore, the proposed algorithms allows for improving quality of vibration control for larger amplitudes of road-induced excitation.

It is recommended to identify MR damper model during vehicle ride since MR dampers are sensitive to both their piston motion, degree of wear and tear as well as to ambient conditions. The proposed method, which is an example of the indirect approach, does not require force measurement but takes advantage of kinematic signals of vehicle response which limits the list of required sensors. Application of evolutionary optimization algorithm allows for identifying the most significant parameters of the inverse MR damper model and consequently improve quality of vibration control.

Road experiments were carried out using an off-road vehicle in which original shock-absorbers were replaced by MR dampers. Measurement data generated by numerous sensors installed in the vehicle allow for tracking motion of selected vehicle parts during experiments and are used for generation of control current. Experiments were performed for a single-road-bump excitation while the following control strategies were successfully validated, i.e.: separate Skyhook control of suspension quarter or Skyhook for pitch vibrations of the vehicle body. Results indicated improvement of the vibration control whose rate is similar to that obtained for simulation-based research. Validation performed for different parameters of algorithms showed how important is their optimization. Difficulties related to the optimization process favour future application of adaptive control for the experimental off-road vehicle.

In conclusion, simulation- and experiment-related contributions of the dissertation can be formulated. Developing the idea of vibration control using MR dampers in road vehicles can be presented as a general contribution. The author believes that application of the modified FxLMS algorithm in adaptive control of automotive MR damper model including utilization of road profile obtained in advance is one of main contributions. Furthermore, synthesis of the estimation procedures for online identification of the MR damper using only kinematic quantities were proposed. The author believes that the main and innovative technical contribution of the dissertation was to develop the fully functional suspension control system for an experimental off-road vehicle with MR dampers. Within experimental studies the synthesis, implementation and validation of the selected vibration control algorithms, including different types of the Skyhook algorithm were performed. Furthermore, the MR damper was analysed in details including analysis of the different approaches to modelling of the MR damper behaviour and modelling of the MR damper velocity-force hysteretic behaviour using the transfer function with desired phase characteristics.

Future studies of semiactive suspension systems can be focused on two main directions of research. Initially, the current control system is to be developed and extended with additional sensors, e.g. suspension deflection sensors which generate reliable measurement of MR damper relative displacement. Additionally, gyroscopes can be used for measuring orientation of the vehicle body. Further research can be carried out in the field of scalable adaptive control dedicated not only to the analysed experimental vehicle suspension, but also to other types of road vehicles. Second direction of the future

research is dedicated to the control of driving safety. MR dampers create new possibility of suspension configuration targeted on preventing skidding or vehicle rollover during dangerous manoeuvres. Deteriorated ride comfort leads to inconvenience of passengers while deterioration of driving safety can lead to much more critical severe injuries of passengers. Thus, further research related to driving safety of MR damper based suspension control is particularly desired.

Bibliography

[1] M. Ahmadian. On the isolation properties of semiactive dampers. *Journal of Vibration and Control*, 5:217–232, 1999.

[2] M. Ahmadian and J. Gravatt. A comparative analysis of passive twin tube and skyhook mrf dampers for motorcycle front suspensions. In *SPIE 2004 Smart Structures and Materials/NDE*, San Diego CA, USA, March 2004.

[3] M. Ahmadian and X. Song. Non-parametric model for magneto-rheological dampers. In *Proceedings of 17th biennial conference on mechanical vibration and noise, ASME DETC*, Las Vegas, Nevada, USA, 12-14 September 1999.

[4] N. Alioua, A. Amine, and M. Rziza. Driver's fatigue detection based on yawning extraction. *International Journal of Vehicular Technology*, 2014:1–7, August 2014.

[5] L. Alvarez and R. Jimenez. Real-time identification of magneto-rheological dampers. In *IEEE Conference on Decision and Control*, pages 1017—-1022, Las Vegas, USA, 10-13 December 2002.

[6] K. J. Astrom and B. Wittenmark. *Adaptive control, second edition.* Dover Publications, Mineola, New York, USA, 2008.

[7] S. Bhave. *Mechanical vibrations, theory and practice.* Dorling Kindersley (India) Pvt. Ltd., licensees of Pearson Education in South Asia, New Delhi, India, 2010.

[8] S. Bhowmik. *Modelling and control of magnetorheological damper: real-time implementation and experimental verification, PhD dissertation.* Denmark University of Technology DTU, Lyngby, Denmark, October, 2011.

[9] M. Bitaraf and S. Hurlebaus. Semi-active adaptive control of seismically excited 20-story nonlinear building. *Engineering Structures*, 56:2107–2118, 2013.

[10] M. Bitaraf, S. Hurlebaus, and L. R. Barroso. Active and semi-active adaptive control for undamaged and damaged building structures under seismic load. *Computer-Aided Civil and Infrastructure Engineering*, 27:48–64, 2012.

[11] R. Bouc. Forced vibrations of a mechanical system with hysteresis. In *Proceedings of the 4th Conference on Nonlinear Oscillations*, Prague, Czech Republic, 1967.

[12] J. Brownlee. *Clever algorithms, nature-inspired programming recipes.* www.CleverAlgorithms.com, noncommertial share, Melbourne, Australia, 2011.

[13] A. E. Jr. Bryson and Y.-C. Ho. *Applied optimal control: optimization, estimation and control.* Hemisphere Publishing Corporation, USA, 1975.

[14] T. Butz and O. von Stryk. Modelling and simulation of electro- and magnetorheological fluid dampers. *Journal of Applied Mathematics and Mechanics ZAMM*, 82 (1):3–20, January 2002.

[15] P. Carlbom and M. Berg. Passengers, seats and carbody in rail vehicle dynamics. *Vehicle System Dynamics*, 37:290–300, 2002.

[16] A. Carullo and M. Parvis. An ultrasonic sensor for distance measurement in automotive applications. *IEEE Sensors Journal*, 1(2):143–147, August 2001.

[17] C. Cempel. *Wibroakustyka stosowana.* Wydawnictwo Naukowe PWM, Warsaw, Poland, 1989.

[18] S. Cetin, E. Zergeroglu, S. Sivrioglu, and I. Yuksek. Adaptive control of structures with MR damper. In *18th IEEE International Conference on Control Applications, Part of 2009 IEEE Multi-conference on Systems and Control*, Saint Petersburg, Russia, 8-10 July 2009.

[19] S. Cetin, E. Zergeroglu, S. Sivrioglu, and I. Yuksek. A new semiactive nonlinear adaptive controller for structures using MR damper: design and experimental validation. *Nonlinear Dynamics*, 66:731–743, 2011.

[20] Y. Chen, Z.-L. Wang, J. Qiu, and H.-Z. Huang. Hybrid fuzzy skyhook surface control using multi-objective microgenetic algorithm for semi-active vehicle suspension system ride comfort stability analysis. *Journal of Dynamic Systems, Measurement, and Control*, 134(4):041003, July 2012.

[21] S.-W. Cho, J.-H. Koo, J.-S. Jo, and I.-W. Lee. Vibration control of a cable-stayed bridge using electrorheological induction based sensor integrated MR dampers. *Journal of Mechanical Science and Technology*, 21(6):875–880, June 2007.

[22] Y. Cho, B. S. Song, and K. Yi. A road-adaptive control law for semi-active suspensions. *KSME International Journal*, 13(10):667–676, 1999.

[23] S.-B. Choi and S.-S. Han. H_∞ control of electrorheological suspension system subjected to parameter uncertainties. *Mechatronics*, 13:639–657, 2003.

[24] S.-B. Choi, S.-K. Lee, and Y.-P. Park. A hysteresis model for the field-dependent damping force of a magnetorheological damper. *Journal of Sound and Vibration*, 245(2):375–383, 2001.

[25] Lord Corporation. RD-8040-1 and RD-8041-1 dampers. *Lord Technical Data*, pages 1–2, 2009.

[26] J. de J. Lozoya-Santos, S. Aubouet, R. Morales-Menendez, O. Sename, R. A. Ramirez-Mendoza, and L. Dugard. Hysteresis modelling for a mr damper. In *Proceedings of the 7th EUROSIM Congress on Modelling and Simulation*, Prague, Czech Republic, September 2010.

[27] D. Dieckmann. A study of the influence of vibration on man. *Ergonomics*, pages 347–355, 1957.

[28] X. P. Do, K. Shah, and S.-B. Choi. Damping force tracking control of MR damper system using a new direct adaptive fuzzy controller. *Shock and Vibration*, Article ID 947937, 2015.

[29] X. M. Dong, M. Yu, Z. Li, C. Liao, and W. Chen. A comparison of suitable control methods for full vehicle with four MR dampers, part I: Formulation of control schemes and numerical simulation. *Journal of Intelligent Material Systems and Structures*, 20:771–786, 2009.

[30] H. Du, K. Y. Sze, and J. Lam. Semi-active H_∞ control of vehicle suspension with magneto-rheological dampers. *Journal of Sound and Vibration*, 283:981–996, 2005.

[31] K. Ekkachai, K. Tungpimolrut, and I. Nilkhamhang. A novel approach to model magneto-rheological dampers using EHM with a feed-forward neural network. *ScienceAsia*, 38:386–393, 2012.

[32] M. M. Ferdaus, M. M. Rashid, M. H. Hasan, H. B. M. Yosuf, M. M. I. Bhuiyan, and A. Alraddadi. Temperature effect analysis on magneto-rheological damper's performance. *Journal of Automation and Control Engineering*, 2(4):392–396, December 2014.

[33] H. Gavin, J. Hoagg, and M. Dobossy. Optimal design of MR dampers. In *Proceedings of U.S.-Japan Workshop on Smart Structures for Improved Seismic Performance in Urban Regions*, pages 225–236, Seattle WA, USA, 14 August 2001.

[34] T. Gillespie. *Fundamental of vehicle dynamics*. Society of Automotive Engineers, 1992.

[35] A. Giua, M. Melas, C. Seatzu, and G. Usai. Design of a predictive semiactive suspension system. *Vehicle System Dynamics*, 41(4):277–300, 2004.

[36] D. E. Goldberg. *Genetic algorithms in search, optimization and machine learning*. Addison-Wesley, 1989.

[37] R. B. Gorbet, K. A. Morris, and D. W. L. Wang. Control of hysteretic systems: a state space approach. *Lecture Notes in Control and Information Sciences: Learning, Control and Hybrid Systems*, 241:432–451, 1999.

[38] M. J. Griffin. *Handbook of human vibration*. Academic Press Limited, London, Great Britain, 1990.

[39] R. Guclu and K. Gulez. Neural network control of seat vibrations of a non-linear full vehicle model using PMSM. *Mathematical and Computer Modelling*, 47:1356–1371, 2008.

[40] E. Guglielmino, T. Sireteanu, C. W. Stammers, G. Ghita, and M. Giuclea. *Semiactive suspension control, improved vehicle ride and road friendliness*. Springer-Verlag London Limited, London, United Kingdom, 2008.

[41] K. Gulez and R. Guclu. CBA-neural network control of a non-linear full vehicle model. *Simulation Modelling Practice and Theory*, 16:1163–1176, 2008.

[42] S. Guo, S. Li, and S. Yang. Semi-active vehicle suspension systems with magnetorheological dampers. In *IEEE International Conference on Vehicular Electronics and Safety, ICVES 2006*, pages 403–406, Beijing, China, 13-15 December 2006.

[43] S. Guo, S. Yang, and C. Pan. Dynamic modeling of magnetorheological damper behaviors. *Journal of Intelligent Material Systems and Structures*, 17:3–14, January 2006.

[44] S. Guo, S. Li, and S. Yang. Active suspensions: a reduced-order H_∞ control design study. In *Proceedings of the 15th Mediterranean Conference on Control and Automation*, pages 1–7, Athens, Greece, 27-29 July 2007.

[45] Y. M. Han, S. C. Lim, H. G. Lee, S. B. Choi, and H. J. Choi. Hysteresis identification of polymethylaniline-based ER fluid using Preisach model. *Materials and Design*, 24(1):53–61, February 2003.

[46] F. Havelka and M. Musil. Optimal semi-active preview control of a quarter car model with magnetorheological damper with respect to tire lift off. In *Proceedings of the 18th International Conference on Engineering Mechanics 2012*, volume 175, pages 363–375, Svratka, Czech Republic, 14-17 May 2012.

[47] A. Hać. Suspension optimization of a 2-dof vehicle model using a stochastic optimal control technique. *Journal of Sound and Vibration*, 100(3):343–357, 1985.

[48] A. Hać. Optimal linear preview control of active vehicle suspension. In *29th Conference on Decision and Control*, Honolulu, Hawaii, December 1990.

[49] A. Hać and I. Youn. Optimal semi-active suspension with preview based on a quarter car model. *Journal of Vibration and Acoustics*, 114(1):84–92, 1992.

[50] A. Hać and I. Youn. Optimal design of active and semi-active suspensions including time delays and preview. *Journal of Vibration and Acoustics*, 115(4):498–508, 1993.

[51] G. Heo, C. Kim, and C. Lee. Experimental test of assymetrical cable-stayed bridges using MR-damper for vibration control. *Solid Dynamics and Earthquake Engineering*, 57:78–85, February 2014.

[52] D. Hrovat. A comparison between jerk optimal and acceleration optimal vibration isolation. *Journal of Sound and Vibration*, 112(2):201–210, 1987.

[53] D. Hrovat. Survey of advanced suspension developments and related optimal control applications. *Automatica*, 33:1781–1817, 1997.

[54] D. Hrovat and M. Hubbard. Optimum vehicle suspensions minimizing rms rattlespace, sprung-mass acceleration and jerk. *Journal of Dynamic Systems, Measurement and Control*, 103:228–236, 1981.

[55] D. Hughes and J. T. Wen. Preisach modeling of piezoceramic and shape memory alloy hysteresis. *Smart Materials and Structures*, 6(3):287–300, June 1997.

[56] J.-P. Hyvarinen. *The improvement of full vehicle semi-active suspension through kinematical model.* University of Oulu, Oulu, Finnland, 2004.

[57] ISO. Mechanical vibration and shock - evaluation of human exposure to whole-body vibration. part 1: general requirements. *International Organization for Standarization*, 2631:1978, Geneva, Switzerland, 1978.

[58] ISO. Mechanical vibration - road surface profiles reporting of measured data. *International Organization for Standarization*, 8606:1995(E), Geneva, Switzerland, 1995.

[59] S. Z. Jalilzadeh and M. Asgari. Improving computational load of FxLMS algorithm in multi-channel active noise control by using a modified structure. In *21st International Congress on Sound and Vibration*, pages 1–8, Beijing, China, 13-17 July 2014.

[60] R. N. Jazar. *Vehicle dynamics: theory and application.* Springer Science Business Media, New York, USA, 2008.

[61] H.-L. Ji, J.-H. Qiu, and K.-J. Zhu. Vibration control of a composite beam by an adaptive semi-active method based on LMS algorithm. In *Symposium on Piezoelectricity, Acoustic Waves, and Device Applications, SPAWDA 2008*, Nanjing, China, 5-8 December 2008.

[62] C. D. Jiang, L. Cheng, S. Fengchun, and C. Hongjie. Simulation of road rougheness based on using IFFT method. In *3th World Congress on Software Engineering WCSE*, pages 190–193, Wuhan, China, 6-8 November 2012 2012.

[63] J. A. Joseph and M. J. Griffin. Analytical analysis of human vibration, technical paper. *Journal of Aviation, Space, and Environmental Medicine*, 79(4):390–396, April 2008.

[64] D. Karnopp, M. J. Crosby, and R. A. Harwood. Vibration control using semi-active force generators. *Journal of Engineering for Industry*, 96:619–626, May 1974.

[65] J. Kasprzyk and E. Bielińska. *Identyfikacja procesów: praca zbiorowa.* Wydawnictwo Politechniki Śląskiej, Gliwice, Poland, 2002.

[66] J. Kasprzyk and P. Krauze. Semi-active vibration control with on-line identification of the inverse mr damper model. In *21st International Congress on Sound and Vibration ICSV21*, Beijing, China, 13-17 July 2014.

[67] J. Kasprzyk and P. Krauze. Vibration control for a half-car model with adaptation of the magnetorheological damper model. In *6th International Conference on Modelling, Identification and Control, ICMIC2014*, Melbourne, Australia, 3-5 December 2014.

[68] J. Kasprzyk, K. Plaza, and J. Wyrwał. Identification of a magnetorheological damper for semi-active vibration control. In *International Congress on Sound and Vibration*, Vilnius, Lithuania, 8-12 July 2012.

[69] J. Kasprzyk, J. Wyrwał, and P. Krauze. Automotive MR damper modeling for semi-active vibration control. In *International Conference on Advanced Intelligent Mechatronics*, Besancon, France, 8-11 July 2014.

[70] B. S. Kim, C. H. Chi, and T. K. Lee. A study on radial directional natural frequency and damping ratio in a vehicle tire. *Applied Acoustics*, 68:538–556, 2007.

[71] G. P. A. Koch. *Adaptive control of mechatronic vehicle suspension systems, PhD dissertation.* Technische Universitat Munchen, Lehrstuhl fur Regelungstechnik, Munchen, Germany, February, 2011.

[72] J.-H. Koo, F. D. Goncalves, and M. Ahmadian. A comprehensive analysis of the response time of MR dampers. *Smart Materials and Structures*, 15:351–358, 2006.

[73] P. Kowalski. Pomiar i ocena drgań mechanicznych w środowisku pracy. *Bezpieczeństwo pracy*, 9:1–3, September 2006.

[74] P. Krauze. Adaptive control of magnetorheological quarter-car suspension model using Normalized LMS algorithm. In *15. Międzynarodowe Warsztaty Doktoranckie OWD*, Wisła, Poland, 19-22 October 2013.

[75] P. Krauze. Comparison of control strategies in a semi-active suspension system of the experimental ATV. *Journal of Low Frequency Noise, Vibration and Active Control*, 32(1-2):67–80, 2013.

[76] P. Krauze and J. Kasprzyk. Neural network based LQ control of a semiactive quarter-car model. In *Proceedings of the 18th IEEE International Conference on Methods and Models in Automation and Robotics, MMAR 2013*, pages 189–194, Międzyzdroje, Poland, 26-29 August 2013.

[77] P. Krauze and J. Kasprzyk. Vibration control in quarter-car model with magnetorheological dampers using FxLMS algorithm with preview. In *13th European Control Conference, ECC2014*, pages 1005–1010, Strasbourg, France, 24-27 June 2014.

[78] P. Krauze and J. Kasprzyk. FxLMS algorithm with preview for vibration control of a half-car model with magnetorheological dampers. In *International Conference on Advanced Intelligent Mechatronics*, Besancon, France, 8-11 July 2014.

[79] P. Krauze and J. Kasprzyk. Vibration control for an experimental off-road vehicle using magnetorheological dampers. In *International Conference Vibroengineering 2014*, Gliwice, Poland, 13-15 October 2014.

[80] P. Krauze and P. Kielan. LMS based filtering of engine induced disturbances in a vehicle vibration control system. In *Podstawowe problemy energoelektroniki, elektromechaniki i mechatroniki PPEEm2012*, Gliwice, Poland, 11-13 December 2012.

[81] P. Krauze and J. Wyrwał. Magnetorheological damper dedicated modeling of force-velocity hysteresis using all-pass delay filters. In *18th International Conference on Systems Science ICSS 2013*, Wrocław, Poland, 10-12 September 2013.

[82] R. Krtolica and D. Hrovat. Optimal active suspension control based on a half-car model: an analytical solution. *IEEE Transactions on Automatic Control*, 37(4): 528–532, April 1992.

[83] S. M. Kuo and D. R. Morgan. *Active noise control systems, algorithms and DSP implementations*. Wiley Series in Telecommunications and Signal Processing, A Wiley Inerscience Publication, 1996.

[84] S. Kurczyk and M. Pawełczyk. Fuzzy control for semi-active vehicle suspension. *Journal of Low Frequency Noise, Vibration and Active Control*, 32(3):217–225, 2013.

[85] H. Laalej, Z. Q. Lang, B. Sapiński, and P. Martynowicz. MR damper based implementation of nonlinear damping for a pitch plane suspension system. *Smart Materials and Structures*, 21:1–14, 2012.

[86] J. Lanzendoerfer and C. Szczepaniak. *Teoria ruchu samochodu*. Wydawnictwo Komunikacji i Łączności, Warsaw, Poland, 1980.

[87] A. Lawther and M. J. Griffin. Prediction of the incidence of motion sickness from the magnitude, frequency and duration of vertical oscillation. *Journal of Acoustic Society of America*, 82:957–966, 1986.

[88] R. Lee and F. Pradko. Analytical analysis of human vibration, technical paper. *Society of Automotive Engineers*, 680091:1–15, 1968.

[89] W. H. Li, G. Z. Yao, G. Chen, S. H. Yeo, and F. F. Yap. Testing and steady state modeling of a linear mr damper under sinusoidal loading. *Smart Materials and Structures*, 9:95–102, 2000.

[90] Z. Lijie, Sunxiaolao, and W. Jiong. Study of adaptive control system of magneto-rheological fluid dampers with mechanical properties subject to impact loading. *Advanced Materials Research*, 644:37–41, 2013.

[91] H. Liu, K. Nonami, and T. Hagiwara. Semi-active fuzzy sliding mode control of full vehicle and suspensions. *Journal of Vibration and Control*, 11(8):1025–1042, 2005.

[92] Y. Liu. *Semi-active damping control for vibration isolation of base disturbances, PhD dissertation*. University of Southhampton, Institute of Sound and Vibration Research, Southhampton, Great Britain, December, 2004.

[93] I. Maciejewski. Modelling and control of semi-active seat suspension with magneto-rheological damper. In *Proceedings of the 24th Symposium on Vibrations in Physical Systems*, pages 1–6, Poznań-Bedlewo, Poland, 12-15 May 2010.

[94] J. Marzbanrad, G. Ahmadi, H. Zohoor, and Y. Hojjat. Stochastic optimal preview control of a vehicle suspension. *Journal of Sound and Vibration*, 275:973–990, 2004.

[95] M. E. McCauley, J. W. Royal, C. D. Wilie, J. F. OHanlon, and R. R. Mackie. *Motion sickness incidence: exploratory studies of habituation pitch and roll, and the refinement of a mathematical model, Technical Report No. 1732-2.* California University, Human Factors Research, California, USA, 1976.

[96] G. M. Mikułowski. *Adaptive impact absorbers based on magnetorheological fluids, PhD dissertation.* Polish Academy of Sciences, Institute of Fundamental Technological Research, Smart Technology Centre, Warsaw, Poland, 2008.

[97] A. Miraliakbari and M. Hahn. Development of a multi-sensor system for road condition mapping. In *International Archives of the Photogrammetry, Remote Sensing and Spatial Information Sciences, ISPRS Technical Commision I Symposium*, volume XL-1, Denver, Colorado, USA, 17-20 November 2014.

[98] M. Mitschke. *Teoria samochodu, dynamika samochodu, napęd i hamowanie.* Wydawnictwo Komunikacji i Łączności, Warsaw, Poland, 1987.

[99] M. Mitschke. *Teoria samochodu, dynamika samochodu, drgania pojazdu.* Wydawnictwo Komunikacji i Łączności, Warsaw, Poland, 1987.

[100] T. Mori, I. Nilkhamhand, and A. Sano. Adaptive semi-active control of suspension system with MR damper. In *9th IFAC Workshop on Adaptation and Learning in Control and Signal Processing*, Saint Petersburg, Russia, 29-31 August 2007.

[101] T. Nabagło. *Synteza układu sterowania semiaktywnego zawieszenia samochodu z elementami magnetoreologicznymi, PhD dissertation.* Cracow University of Technology, Cracow, Poland, 2006.

[102] T. H. Nguyen, N. M. Kwok, Q. P. Ha, J. Li, and B. Samali. Adaptive sliding mode control for civil structures using magnetorheological dampers. In *International Symposium on Automation and Robotics in Construction, ISARC2006*, Tokyo, Japan, 3-5 October 2006.

[103] I. Nilkhamhang, A. Sano, and T. Mori. Robust adaptive approach to semi-active control of suspension systems with MR damper. *Journal of Control, Measurement and System Integration*, 1(1):26–32, 2008.

[104] Z. Ogonowski. Quality control of semi-active systems. In *19th International IEEE/IFAC Conference on Methods and Models in Automation and Robotics, MMAR 2007*, Szczecin, Poland, 2007.

[105] P. M. Pardalos and V. Yatsenko. *Optimization and control of bilinear systems: theory, algorithms, and applications.* Springer, Optimization and its applications, vol. 11, New York, USA, 2008.

[106] K. Plaza. An empirical inverse magnetorheological damper model. In *Proceedings of the 12th IEEE International Conference on Methods and Models in Automation and Robotics, MMAR 2006*, pages 919–924, Międzyzdroje, Poland, 28-31 August 2006.

[107] K. Plaza. True RMS-based inverse MR damper model for a semi-active system. In *Proceedings of the 18th International Conference on Methods and Models in Automation and Robotics, MMAR2013*, pages 212–216, Międzyzdroje, Poland, 26-29 August 2013.

[108] K. Plaza. *Modelling and control for semi-active vibration damping, PhD dissertation.* Silesian University of Technology, Gliwice, Poland, October, 2008.

[109] A. J. Pollock and I. A. Craighead. The selection of a criterion to evaluate ride-discomfort in off road vehicles. In *Proceedings of the 9th Annual Conference of the North East Polytechnics, Mathematical Modelling and Computer Simulation Group, Polymodel 9*, pages 21–31, Newcastle upon Tyne, United Kingdom, 21-22 May 1986.

[110] C. Poussot-Vassal, O. Sename, L. Dugard, P. Gaspar, Z. Szabo, and J. Bokor. A new semi-active suspension control strategy through LPV technique. *Control Engineering Practice*, 16:1519–1534, 2008.

[111] R. S. Prabakar, C. Sujatha, and S. Narayanan. Optimal semi-active preview control response of a half car vehicle model with magnetorheological damper. *Journal of Sound and Vibration*, 326:400–420, 2009.

[112] F. Preisach. Uber die magnetische nachwirkung, zeitschrift fur physik. *Zeitschrift fur Physik*, 94(5-6):277–302, 1935.

[113] G. Priyandoko, M. Mailah, and H. Jamaluddin. Vehicle active suspension system using skyhook adaptive neuro active force control. *Mechanical Systems and Signal Processing*, 23:855–868, 2009.

[114] L. V. V. Gopala Rao and S. Narayanan. Preview control of random response of a half-car vehicle model traversing rough road. *Journal of Sound and Vibration*, 310:352–365, 2008.

[115] Dutch Road Transport Directorate RDW. ATV-Sweden Allroad 500. *EC Type-Approval Certificate*, pages 1–88, 2002.

[116] W. D. Robinson. *A pneumatic semi-active control methodology for vibration control of air spring based suspension systems.* Iowa State University, Ames, USA, 2012.

[117] S. Ryu, Y. Kim, and Y. Park. Robust H_∞ preview control of an active suspension system with norm-bounded uncertainties. *International Journal of Automotive Technology*, 9(5):585–592, 2008.

[118] P. Safapour, H. A. Rahimi, and M. Rafeeian. Adaptive control of base-isolated structures against near-field earthquakes using MR damper. In *International Conference on Advances in Structural, Civil and Environmental Engineering, SCEE2013*, Kuala Lumpur, Malaysia, 4-5 May 2013.

[119] D. Sammier, O. Sename, and L. Dugard. Skyhook and H-infinity control of active vehicle suspensions: some practical aspects. *Vehicle System Dynamics*, 39(4):279–308, 2003.

[120] B. Sapiński. Parametric identification of MR linear automotive size damper. *Journal of Theoretical and Applied Mechanics*, 40(3):703–722, 2002.

[121] B. Sapiński. Analysis of parametric models of MR linear damper. *Journal of Theoretical and Applied Mechanics*, 41(2):215–240, 2003.

[122] B. Sapiński. *Magnetorheological dampers in vibration control.* AGH University of Science and Technology Press, Cracow, Poland, 2006.

[123] B. Sapiński. *Real-time control of magnetorheological dampers in mechanical systems.* AGH University of Science and Technology Press, Cracow, Poland, 2008.

[124] B. Sapiński. Real-time control for a magnetorheological shock absorber in a driver seat. *Journal of Theoretical and Applied Mechanics*, 43(3):631–653, Warsaw, 2005.

[125] B. Sapiński, J. Snamina, Ł. Jastrzębski, and A. Staśkiewicz. Laboratory stand for testing self-powered vibration reduction systems. *Journal of Theoretical and Applied Mechanics*, 49(4):1169–1181, 2011.

[126] S. M. Savaresi, C. Poussot-Vassal, C. Spelta, O. Sename, and L. Dugard. *Semi-active suspension control design for vehicles.* Butterworth-Heinemann, Elsevier, 2006.

[127] M. W. Sayers and S. M. Karamihas. *The little book of profiling, basic information about measuring and interpreting road profiles.* University of Michigan, Michigan, USA, 1998.

[128] M.-S. Seong, S.-B. Choi, and Y.-M. Han. Damping force control of a vehicle MR damper using a Preisach hysteresis compensator. *Smart Materials and Structures*, 18(7):1–13, June 2009.

[129] F. A. Shirazi, J. Mohammadpour, and K. M. Grigoriadis. An integrated approach for parameter identification and semi-active control of MR dampers. In *American Control Conference, ACC2010*, pages 720–725, Baltimore, MD, USA, 2010.

[130] M. Sibielak, W. Rączka, and J. Konieczny. Modified clipped-LQR method for semi-active vibration reduction systems with hysteresis. *Solid State Phenomena*, 177: 10–22, 2011.

[131] M.-H. Sigari, M. Fathy, and M. Soryani. A driver face monitoring system for fatigue and distraction detection. *International Journal of Vehicular Technology*, 2013:1–11, 2013.

[132] C. C. Smith, D. Y. McGehee, and A. J. Healey. The prediction of passenger riding comfort from acceleration data, research report. *University of Texas at Austin*, 16: 1–121, March 1976.

[133] M. C. Smith and F.-C. Wang. Controller parameterization for disturbance response decoupling: application to vehicle active suspension control. *IEEE Transactions on Control Systems Technology*, 10(3):393–407, 2002.

[134] T. Soderstrom and P. Stoica. *Identyfikacja systemów*. Państwowe Wydawnictwo Naukowe, Warsaw, Poland, 1997.

[135] X. Song. *Design of adaptive vibration control systems with application of magneto-rheological dampers*. Virginia Polytechnic Institute and State University, Blackburg, Virginia, USA, 1999.

[136] X. Song, M. Ahmadian, and S. C. Southward. Modelling magnetorheological dampers with application of nonparametric approach. *Journal of Intelligent Material Systems and Structures*, 16(5):421–432, May 2005.

[137] B. F. Spencer, S. J. Dyke, M. K. Sain, and J. D. Carlson. Phenomenological model of a magnetorheological damper. *ASCE Journal of Engineering Mechanics*, 123: 230–238, 1997.

[138] S. Sulaiman, P. M. Samin, H. Jamaluddin, R. A. Rahman, and M. S. Burhaumudin. Groundhook control of semi-active suspension for heavy vehicle. *International Journal of Research in Engineering and Technology*, 1(3):146–152, 2012.

[139] M. D. Symans and M. C. Constantinou. Semi-active control systems for seismic protection of structures: a state-of-the-art review. *Engineering Structures*, 21: 469–487, 1999.

[140] T. Terasawa and A. Sano. Fully adaptive vibration control for uncertain structure installed with MR damper. In *American Control Conference, ACC2005*, Portland, OR, USA, 8-10 June 2005.

[141] O. J. Tobias and R. Seara. Leaky-FxLMS algorithm: stochastic analysis for gaussian data and secondary path modeling error. *IEEE Transactions on Speech and Audio Processing*, 13(6):1217–1230, November 2005.

[142] F. Tyan, Y.-F. Hong, S.-H. Tu, and W. S. Jeng. Generation of random road profiles. *CSME:B04-0001*, pages 1373–1377, 2006.

[143] E. R. Wang, X. Q. Ma, S. Rakhela, and C. Y. Su. Modelling the hysteresis characteristics of a magnetorheological fluid damper. *Proceedings of the Institution of Mechanical Engineers, Part D: Journal of Automobile Engineering*, 217(7):537–550, 2003.

[144] F. Weber, C. Boston, and M. Maślanka. An adaptive tuned mass damper based on the emulation of positive and negative stiffness with an MR damper. *Smart Materials and Structures*, 20:1–11, 2011.

[145] W. Wei and X. Pinqi. Adaptive control of helicopter ground resonance with magnetorheological damper. *Chinese Journal of Aeronautics*, 20:501–510, 2007.

[146] Y.-K. Wen. Method for random vibration of hysteresis systems. *Journal of the Engineering Mechanics Division*, 102(2):249–263, March/April 1976.

[147] N. M. Wereley and L. Pang. Nondimentional analysis of semi-active electrorheological and magnetorheological dampers using approximate paralled plate models. *Smart Materials and Structures*, 7:732–743, 1998.

[148] N. M. Wereley, L. Pang, and G. M. Kamath. Idealized hysteresis modeling of electrorheological and magnetorheological dampers. *Journal of Intelligent Material Systems and Structures*, 9(8):642–649, August 1998.

[149] www.bwigroup.com.

[150] www.delphi.com.

[151] www.dynatest.com.

[152] www.en.wikipedia.org/wiki/Cadillac_Seville.

[153] www.en.wikipedia.org/wiki/Range_Rover_Evoque.

[154] www.lord.com.

[155] www.northerntool.com/shop/tools/product_17807_17807.

[156] www.seriouswheels.com/cars/top Ford-EX-Concept-Vehicle.htm.

[157] Z. Xie, P. K. Wong, J. Zhao, T. Xu, K. I. Wong, and H. C. Wong. A noise-insensitive semi-active air suspension for heavy-duty vehicles with an integrated fuzzy-wheelbase preview control. *Mathematical Problems in Engineering, Hindawi Publishing Corporation*, 2013:1–12, 2013.

[158] T. Yamada, T. Ito, and A. Ohya. Detection of road surface damage using mobile robot equipped with 2D laser scanner. In *Proceedings of the 2013 IEEE/SICE*

International Symposium on System Integration, Kobe International Conference Center, Kobe, Japan, 15-17 December 2013.

[159] G. Yang, H. J. Jung, and B. F. Spencer Jr. Dynamic model of full-scale MR dampers for civil engineering applications. In *Proceedings of the U.S.-Japan Workshop on Smart Structures for Improved Seismic Performance in Urban Regions*, 14 August 2001.

[160] G. Yang, B. F. Spencer, J. D. Carlson, and M. K. Sain. Large-scale mr fluid dampers: modelling and dynamic performance considerations. *Engineering Structures*, 24:309–323, 2002.

[161] S. Yang, S. Li, X. Wang, F. Gordaninejad, and G. Hitchcock. A hysteresis model for magneto-rheological damper. *International Journal of Nonlinear Sciences and Numerical Simulation*, 6(2):139–144, 2005.

[162] H. Yarmohamadi. *Advances in heavy vehicle dynamics with focus on engine mounts and individual front suspension, PhD dissertation.* Chalmers University of Technology, Goteborg, Sweden, 2012.

[163] A. S. Yildiz, S. Sivrioglu, and E. Zergeroglu. Adaptive control of semiactive quarter car model with MR damper. In *9th Asian Control Conference, ASCC2013*, Instanbul, Turkey, 23-26 June 2013.

[164] S. Yong, G. Zhiyuan, G. Shouwei, Y. Jincong, and Z. Xiaojin. FxLMS algorithm based multi channel active vibration control of piezoelectric flexible beam. In *8th World Congress on Intelligent Control and Automation*, pages 4845–4850, Jinan, China, 6-9 July 2010.

Appendix A

Specification of the applied automotive MR dampers

MR damper is widely applied for control of vehicle suspension systems. Its typical construction is based on cylindrical housing filled with MR fluid (see Figure A.1a). MR fluid belongs to the group of intelligent materials. It is a composition of magnetically polarizable particles suspended in non-magnetic carrier fluid, e.g. mineral oil, synthetic oil or glycol [124].

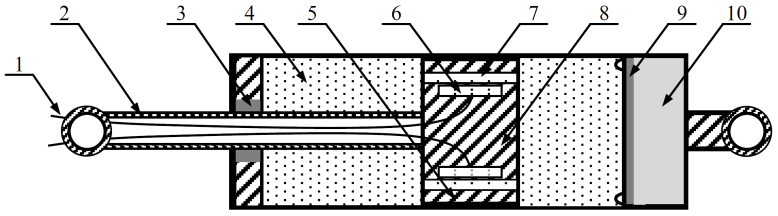

(a) Construction of automotive MR damper presented in [81]: 1 - coil wires, 2 - piston rod, 3 - bearing and seal, 4 - MR fluid, 5 - ring, 6 - coil, 7 - orifice, 8 - piston, 9 - diaphragm, 10 - gas accumulator

(b) Automotive MR damper manufactured by Lord Corporation

Figure A.1

During operation of the MR damper, the MR fluid is flowing through the piston gaps, where electric coils are located. Control current which supplies the coils induces magnetic field and, consequently, modifies properties of MR fluid. Particles of MR fluid are polarized and form chain-like structures along the magnetic field lines and perpendicularly to the direction of suppressed fluid flow, which occurs through the piston gaps.

Two types of MR dampers manufactured by Lord Corporation, i.e. RD-8040-1 and RD-8041-1 (see Figure A.1a), are installed in the experimental vehicle. Most important parameters of the applied MR dampers are listed in Table A.1 according to the specification [25].

Table A.1: Selected properties of MR dampers [25] installed in the experimental vehicle of types RD-8040-1 and RD-8041-1 manufactured by Lord Corporation

Type of MR damper	RD-8040-1	RD-8041-1
Mechanical properties		
Stroke	55 mm	74 mm
Maximum length	208 mm	248 mm
Body diameter	42.1 mm	
Shaft diameter	10 mm	
Electrical properties		
Input current	<1 A (continuous for 30 s), <2 A (intermittent)	
Input voltage	<12 V (DC)	
Resistance	5 Ω (ambient temperature), 7 Ω (71 °C)	
Operating properties		
Tensile strength	<8896 N	
Damper force (Peak to Peak)	>2447 N (0.05 ms^{-1}, 1 A), <667 N (0.2 ms^{-1}, 0 A)	
Response time	<15 ms	
Operating temperature	<71 °C	

Both types of MR dampers differ in the stroke equal to 55 mm or 74 mm and, consequently, in the maximum length equal to 208 mm or 248 mm for the RD-8040-1 or RD-8041-1, respectively. Other mechanical properties, including body diameter and shaft diameter are similar for both dampers.

The dampers can be controlled by a limited current value: not greater than 1 A continuously for 30 s and not greater than 2 A intermittently where input voltage

is limited to 12 V DC. The resistance of the electric coils varies with respect to the temperature of the damper housing from 5 Ω for ambient temperature to 7 Ω for 71 °C.

According to the given operating properties, maximum tensile strength of both dampers should be not greater than 8896 N. Manufacturer states that Peak-to-Peak amplitude of the minimum force possible to be generated by the damper is not smaller than 2447 N for the relative piston velocity equal to 0.05 ms^{-1} and the input current equal to 1 A. The maximum force generated by the damper is equal to 667 N for piston velocity equal to 0.2 ms^{-1} and control current equal to 0 A. Results of experiments which were presented in the dissertation showed that maximum Peak-to-Peak amplitudes of forces varied from 640 N to 3715 N for control current varying from 0 A to 1.33 A (see Figure 3.1). Generally, the minimum force is recommended to be as small as possible and the maximum force should as great as possible which makes the limits presented in the specification are confirmed by the experimental results.

The MR dampers exhibit the response time not greater than 15 ms according to the specification. Furthermore, it is recommended not to overheat MR damper during its operation over 71 °C, where such requirement was met during the identification experiments. Finally, information about hysteretic behaviour of the MR damper are omitted in the specification while such feature can be clearly indicated in the MR damper response (see Section 3.2).

Appendix B

Specification of the experimental all-terrain vehicle

The experimental vehicle of type ATV-Sweden 500 Allroad (see Figure B.1) is the key element of the vehicle suspension control system. Four original shock-aborbers located in the front and rear suspension parts were replaced with MR dampers of type RD-8040-1 and RD-8041-1, respectively.

Figure B.1: The experimental vehicle ATV-Sweden Allroad 500

Selected properties of the vehicle, which are listed in Table B.1 according to the approval certificate [115], were divided into three groups: vehicle dimensions, engine properties and operating properties.

Table B.1: Selected properties of the experimental vehicle ATV-Sweden Allroad 500 according to [115]

Vehicle dimensions	
Length: 2.18 m	Width: 1.17 m
Height: 1.23 m	Weight: 337 kg
Axles distance: 1.29 m	Wheel distance: 0.92 m
Front overhang: 0.44 m	Rear overhang: 0.39 m
Engine properties	
Engine type: 4-stroke	Number of cylinders: single
Engine capacity: 500 cc (0.5 l)	
Operating properties	
Maximum speed: 70 kmh^{-1}	Drivetrain: 2- or 4-wheel-drive
Construction of suspension system: independent for each wheel	

The vehicle is 2.18 m long, 1.17 m wide and 1.23 m high; it weighs 337 kg. It is equipped with the 4-stroke petrol engine including single cylinder. The detailed description of the engine operation was presented in Subsection 7.1.3) which deals with the analysis of significant engine-induced deterioration of measurement quality. The independent suspension of each wheel which allows for separate vibration is the another characteristic feature of the vehicle.

Appendix C

Mathematical description of the 4-DOF half-car model

The half-car model presented in Figure C.1 is considered in the dissertation. The vehicle body is modelled as a 2-dimensional beam of length denoted as L_{fr}. Subscripts f and r denote the front and rear parts of the vehicle, respectively. The vehicle body beam exhibits the following features: the center of gravity whose distances from the ends are L_f and L_r, the mass of the vehicle body m_s and the moment of inertia about the pitch axis denoted as I_{sL}. The sprung and unsprung parts of the vehicle are denoted using subscripts s and u, respectively.

Additional masses moving only vertically, denoted as m_{uf}, m_{ur}, are included in the model. They are related to the vehicle front and rear wheel. Vehicle body mass and wheel masses are connected by linear springs k_{sf}, k_{sr} and viscous dampers c_{sf}, c_{sr}, which stands for the front and rear parts of the vehicle suspension system, respectively. Road-induced kinematic excitation influences the half-car model via springs k_{uf}, k_{ur} and dampers c_{uf}, c_{ur}, which are related to parameters of tyres and are connected to the front and rear wheel masses. Since it was assumed that pitch angle varies in small range, the trigonometric relationships of half-car model description were neglected.

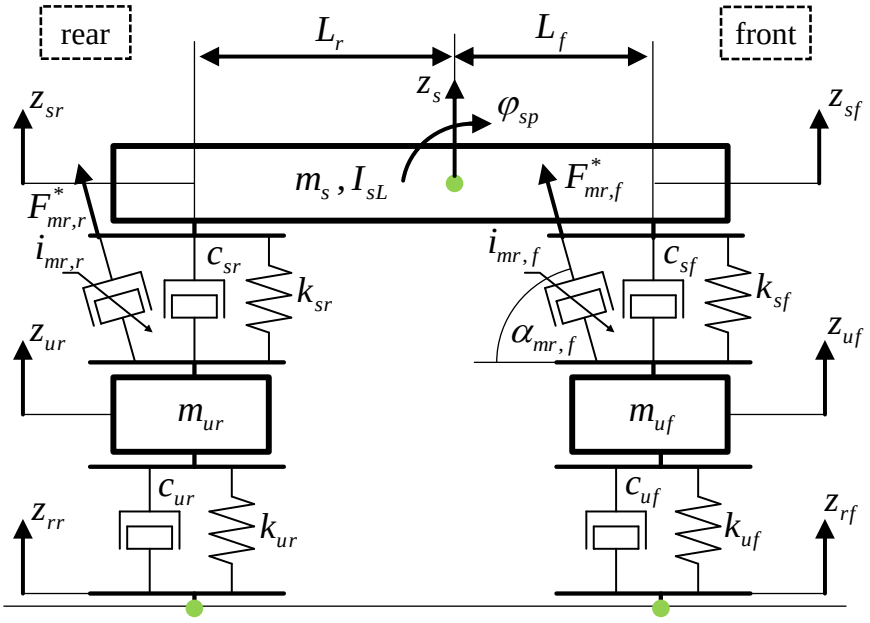

Figure C.1: Half-car model of vehicle vibration model with 4 DOFs including suspension MR dampers

C.1 Equations of dynamics

Derivation of a mathematical description of the half-car model was based on the Euler-Lagrange equations of the second kind:

$$\frac{d}{dt}\left(\frac{\partial L}{\partial \dot{\boldsymbol{q}}_{\boldsymbol{hc}}}\right) - \frac{\partial L}{\partial \boldsymbol{q}_{\boldsymbol{hc}}} + \frac{\partial \Re}{\partial \dot{\boldsymbol{q}}_{\boldsymbol{hc}}} = \boldsymbol{F}_{\boldsymbol{hc}}, \tag{C.1}$$

where the vector of generalized coordinates is denoted as $\boldsymbol{q}_{\boldsymbol{hc}}$ and the vector of generalized forces is denoted as $\boldsymbol{F}_{\boldsymbol{hc}}$. They are expressed as follows:

$$\boldsymbol{q}_{\boldsymbol{hc}} = \begin{bmatrix} z_s \\ \varphi_{sp} \\ z_{uf} \\ z_{ur} \end{bmatrix}, \quad \boldsymbol{F}_{\boldsymbol{hc}} = \begin{bmatrix} F^*_{mr,f}\sin(\alpha_{mr,f}) + F^*_{mr,r}\sin(\alpha_{mr,r}) \\ -L_f F^*_{mr,f}\sin(\alpha_{mr,f}) + L_r F^*_{mr,r}\sin(\alpha_{mr,r}) \\ -F^*_{mr,f}\sin(\alpha_{mr,f}) \\ -F^*_{mr,r}\sin(\alpha_{mr,r}) \end{bmatrix}, \tag{C.2}$$

where vehicle body heave displacement and pitch angle are denoted as z_s and φ_{sp}, respectively. Forces generated by MR dampers for the front and the rear vehicle part are denoted as $F^*_{mr,f}$ and $F^*_{mr,r}$. Additional inclination of MR dampers is considered in the half-car model by introducing angles $\alpha_{mr,f}$ and $\alpha_{mr,r}$. Symbols z_{uf} and z_{ur} denote vertical displacements of wheels.

The Rayleigh dissipation function, which is included in the Euler-Lagrange equations (C.1) was denoted as $\Re$. After including relationships for vertical displacements of the vehicle body z_{sf} and z_{sr}, which were defined in Equation (4.6), the $\Re$ can be defined by the following formula:

$$\begin{aligned}\Re =&\frac{1}{2}c_{sf}(v_s - L_f\omega_{sp} - v_{uf})^2 + \frac{1}{2}c_{sr}(v_s + L_r\omega_{sp} - v_{ur})^2\\ &+\frac{1}{2}c_{uf}(v_{uf} - v_{rf})^2 + \frac{1}{2}c_{ur}(v_{ur} - v_{rr})^2\end{aligned} \tag{C.3}$$

. Furthermore, the Euler-Lagrange equations include the Lagrangian denoted as L:

$$L = T - V, \tag{C.4}$$

where T and V denote the total kinetic and potential energy of the system, respectively. The total kinetic energy is described by the following formula:

$$T = \frac{1}{2}m_s v_s^2 + \frac{1}{2}I_{sL}\omega_{sp}^2 + \frac{1}{2}m_{uf}v_{uf}^2 + \frac{1}{2}m_{ur}v_{ur}^2. \tag{C.5}$$

The potential energy is expressed as follows:

$$\begin{aligned}V =&\frac{1}{2}k_{sf}(z_s - L_f\varphi_{sp} - z_{uf})^2 + \frac{1}{2}k_{sr}(z_s + L_r\varphi_{sp} - z_{ur})^2\\ &+\frac{1}{2}k_{uf}(z_{uf} - z_{rf})^2 + \frac{1}{2}k_{ur}(z_{ur} - z_{rr})^2.\end{aligned} \tag{C.6}$$

For the considered half-car model and assuming the given description of the total kinetic energy (C.5), total potential energy (C.6) and the Rayleigh dissipation function (C.3), the Euler-Lagrange equations given in Equation (C.1) can be simplified into the following:

$$\frac{d}{dt}\left(\frac{\partial T}{\partial \dot{\boldsymbol{q}}_{\boldsymbol{hc}}}\right) + \frac{\partial V}{\partial \boldsymbol{q}_{\boldsymbol{hc}}} + \frac{\partial \Re}{\partial \dot{\boldsymbol{q}}_{\boldsymbol{hc}}} = \boldsymbol{F}_{\boldsymbol{hc}}, \tag{C.7}$$

where their consecutive components are obtained as follows:

$$\frac{d}{dt}\left(\frac{\partial T}{\partial \dot{\boldsymbol{q}}_{\boldsymbol{hc}}}\right) = \begin{bmatrix} m_s a_s \\ I_{sL}\epsilon_{sp} \\ m_{uf}a_{uf} \\ m_{ur}a_{ur} \end{bmatrix}, \tag{C.8}$$

$$\frac{\partial V}{\partial \boldsymbol{q_{hc}}} = \begin{bmatrix} k_{sf}(z_s - L_f\varphi_{sp} - z_{uf}) + k_{sr}(z_s + L_r\varphi_{sp} - z_{ur}) \\ -L_f k_{sf}(z_s - L_f\varphi_{sp} - z_{uf}) + L_r k_{sr}(z_s + L_r\varphi_{sp} - z_{ur}) \\ -k_{sf}(z_s - L_f\varphi_{sp} - z_{uf}) + k_{uf}(z_{uf} - z_{rf}) \\ -k_{sr}(z_s + L_r\varphi_{sp} - z_{ur}) + k_{ur}(z_{ur} - z_{rr}) \end{bmatrix} \tag{C.9}$$

and

$$\frac{\partial \Re}{\partial \dot{\boldsymbol{q}}_{\boldsymbol{hc}}} = \begin{bmatrix} c_{sf}(v_s - L_f\omega_{sp} - v_{uf}) + c_{sr}(v_s + L_r\omega_{sp} - v_{ur}) \\ -L_f c_{sf}(v_s - L_f\omega_{sp} - v_{uf}) + L_r c_{sr}(v_s + L_r\omega_{sp} - v_{ur}) \\ -c_{sf}(v_s - L_f\omega_{sp} - v_{uf}) + c_{uf}(v_{uf} - v_{rf}) \\ -c_{sr}(v_s + L_r\omega_{sp} - v_{ur}) + c_{ur}(v_{ur} - v_{rr}) \end{bmatrix}. \tag{C.10}$$

As a result, the equations of dynamics are evaluated for the half-car model in the following matrix form:

$$\boldsymbol{M} \cdot \ddot{\boldsymbol{q}}_{\boldsymbol{hc}} + \boldsymbol{C} \cdot \dot{\boldsymbol{q}}_{\boldsymbol{hc}} + \boldsymbol{K} \cdot \boldsymbol{q}_{\boldsymbol{hc}} = \boldsymbol{u}_{\boldsymbol{hc}}, \tag{C.11}$$

where the separated equations of dynamics, which are presented in the dissertation in (4.2) - (4.5), can be obtained based on Equation (C.11). The symbol $\boldsymbol{u_{hc}}$ denotes vector of excitation forces for the half-car model, which is expressed as follows:

$$\boldsymbol{u}_{\boldsymbol{hc}} = \begin{bmatrix} F^*_{mr,f}\sin(\alpha_{mr,f}) + F^*_{mr,r}\sin(\alpha_{mr,r}) \\ -L_f F^*_{mr,f}\sin(\alpha_{mr,f}) + L_r F^*_{mr,r}\sin(\alpha_{mr,r}) \\ -F^*_{mr,f}\sin(\alpha_{mr,f}) + k_{uf}z_{rf} + c_{uf}v_{rf} \\ -F^*_{mr,r}\sin(\alpha_{mr,r}) + k_{ur}z_{rr} + c_{ur}v_{rr} \end{bmatrix}. \tag{C.12}$$

Besides, the mass $\boldsymbol{M}$, stiffness $\boldsymbol{K}$ and damping $\boldsymbol{C}$ matrices, which are required by the matrix Equation (C.11), are defined by the following:

$$\boldsymbol{M} = \begin{bmatrix} m_s & 0 & 0 & 0 \\ 0 & I_{sL} & 0 & 0 \\ 0 & 0 & m_{uf} & 0 \\ 0 & 0 & 0 & m_{ur} \end{bmatrix}, \tag{C.13}$$

$$\boldsymbol{K} = \begin{bmatrix} k_{sf} + k_{sr} & -L_f k_{sf} + L_r k_{sr} & -k_{sf} & -k_{sr} \\ -L_f k_{sf} + L_r k_{sr} & L_f^2 k_{sf} + L_r^2 k_{sr} & L_f k_{sf} & -L_r k_{sr} \\ -k_{sf} & L_f k_{sf} & k_{sf} + k_{uf} & 0 \\ -k_{sr} & -L_r k_{sr} & 0 & k_{sr} + k_{ur} \end{bmatrix} \tag{C.14}$$

and

$$\boldsymbol{C} = \begin{bmatrix} c_{sf} + c_{sr} & -L_f c_{sf} + L_r c_{sr} & -c_{sf} & -c_{sr} \\ -L_f c_{sf} + L_r c_{sr} & L_f^2 c_{sf} + L_r^2 c_{sr} & L_f c_{sf} & -L_r c_{sr} \\ -c_{sf} & L_f c_{sf} & c_{sf} + c_{uf} & 0 \\ -c_{sr} & -L_r c_{sr} & 0 & c_{sr} + c_{ur} \end{bmatrix}. \tag{C.15}$$

C.2 Evaluation of the state-space representation

For the purpose of the simulation-based studies, the matrix Equation (C.11) can be reformulated into the following state-space representation:

$$\dot{\boldsymbol{x}}_{\boldsymbol{hc}} = \boldsymbol{A}_{\boldsymbol{hc}} \cdot \boldsymbol{x}_{\boldsymbol{hc}} + \boldsymbol{B}_{\boldsymbol{hc}} \cdot \boldsymbol{u}_{\boldsymbol{hc}}, \tag{C.16}$$

where matrices $\boldsymbol{A}_{\boldsymbol{hc}}$ and $\boldsymbol{B}_{\boldsymbol{hc}}$ are defined by the following:

$$\boldsymbol{A}_{\boldsymbol{hc}} = \begin{bmatrix} \mathbf{0} & \mathbf{1} \\ -\boldsymbol{M}^{-1}\boldsymbol{K}_{\boldsymbol{hc}} & -\boldsymbol{M}^{-1}\boldsymbol{C} \end{bmatrix}, \quad \boldsymbol{B}_{\boldsymbol{hc}} = \begin{bmatrix} \mathbf{0} \\ \boldsymbol{M}^{-1} \end{bmatrix} \tag{C.17}$$

and the vector of state variables $\boldsymbol{x}_{\boldsymbol{hc}} = [\boldsymbol{q}_{\boldsymbol{hc}} \quad \dot{\boldsymbol{q}}_{\boldsymbol{hc}}]^T$.

The second component of the Equation (C.16), i.e. the excitation vector $\boldsymbol{u}_{\boldsymbol{hc}}$ can be further decomposed into two parts which are related to the kinematic and force excitation signals. Such transformation is required in order to evaluate the LQ controller (see Subsection 5.2.1). The modified state matrix equation is of the following form:

$$\dot{\boldsymbol{x}}_{\boldsymbol{hc}} = \boldsymbol{A}_{\boldsymbol{hc}} \cdot \boldsymbol{x}_{\boldsymbol{hc}} + \boldsymbol{B}_{\boldsymbol{hc,F}} \cdot \boldsymbol{F}^*_{\boldsymbol{mr}} + \boldsymbol{B}_{\boldsymbol{hc,r}} \cdot \boldsymbol{u}_{\boldsymbol{r}}. \tag{C.18}$$

The output matrix equation is defined for the half-car model as follows:

$$\boldsymbol{y}_{\boldsymbol{hc}} = \boldsymbol{C}_{\boldsymbol{hc}} \cdot \boldsymbol{x}_{\boldsymbol{hc}} + \boldsymbol{D}_{\boldsymbol{hc,F}} \cdot \boldsymbol{F}^*_{\boldsymbol{mr}} + \boldsymbol{D}_{\boldsymbol{hc,r}} \cdot \boldsymbol{u}_{\boldsymbol{r}}. \tag{C.19}$$

The state equation (C.18) depends on state-related matrix $\boldsymbol{A}_{\boldsymbol{hc}}$ and matrices denoted as $\boldsymbol{B}_{\boldsymbol{hc,F}}$, $\boldsymbol{B}_{\boldsymbol{hc,r}}$ related to the control forces and kinematic road-induced excitation signals,

respectively. They are defined by the following:

$$\boldsymbol{B_{hc,F}} = \begin{bmatrix} \sin(\alpha_{mr,f}) & \sin(\alpha_{mr,r}) \\ -L_f \sin(\alpha_{mr,f}) & L_r \sin(\alpha_{mr,r}) \\ -\sin(\alpha_{mr,f}) & 0 \\ 0 & -\sin(\alpha_{mr,r}) \end{bmatrix} \tag{C.20}$$

and

$$\boldsymbol{B_{hc,r}} = \begin{bmatrix} & & \mathbf{0} & & & \\ & & \mathbf{0} & & & \\ k_{uf} & c_{uf} & 0 & 0 & 0 & 0 \\ 0 & 0 & 0 & k_{ur} & c_{ur} & 0 \end{bmatrix}. \tag{C.21}$$

Herein, vectors of force and kinematic excitation signals are formulated as follows:

$$\boldsymbol{F^*_{mr}} = \begin{bmatrix} F^*_{mr,f} \\ F^*_{mr,r} \end{bmatrix} \tag{C.22}$$

and

$$\boldsymbol{u_r} = \begin{bmatrix} z_{rf} & v_{rf} & a_{rf} & z_{rr} & v_{rr} & a_{rr} \end{bmatrix}^T. \tag{C.23}$$

The matrices $\boldsymbol{C_{hc}}$, $\boldsymbol{D_{hc,F}}$ and $\boldsymbol{D_{hc,r}}$, which are included in the output matrix equation (C.19), are defined in such a way to make all signals, which are necessary for the simulation-based analysis, be included in the vector of output variables $\boldsymbol{y_{hc}}$. Thus, the $\boldsymbol{y_{hc}}$ consists of the following:

$$\begin{aligned} \boldsymbol{y_{hc}} = & \\ & \big[\boldsymbol{x_{hc}}^T, \\ & a_s, \epsilon_{sp}, \\ & v_{sf}, v_{sr}, a_{sf}, a_{sr}, \\ & z_{usf}, z_{usr}, z_{ruf}, z_{rur}, \\ & z_{mr,f}, z_{mr,r}, v_{mr,f}, v_{mr,r}, a_{mr,f}, a_{mr,r}\big]^T. \end{aligned} \tag{C.24}$$

The symbols a_s and ϵ_{sp} stand for the second derivative of z_s and φ_{sp}, respectively. Velocities and accelerations of the front and rear vehicle body parts are denoted as v_{sf} , v_{sr} and a_{sf}, a_{sr}, respectively. Furthermore, suspension and tyres deflections are denoted

as z_{usf}, z_{usr} and z_{ruf}, z_{rur}. Finally, relative displacements, velocities and accelerations of the front and rear MR dampers pistons are denoted as $z_{mr,f}$, $z_{mr,r}$ and $v_{mr,f}$, $v_{mr,r}$ as well as $a_{mr,f}$, $a_{mr,r}$. The latter signals are evaluated taking into consideration the inclination angles in the form of $\sin(\alpha_{mr,f})$ and $\sin(\alpha_{mr,r})$.